INFORMATION TO USERS

This manuscript has been reproduced from the microfilm master. UMI films the text directly from the original or copy submitted. Thus, some thesis and dissertation copies are in typewriter face, while others may be from any type of computer printer.

The quality of this reproduction is dependent upon the quality of the copy submitted. Broken or indistinct print, colored or poor quality illustrations and photographs, print bleedthrough, substandard margins, and improper alignment can adversely affect reproduction.

In the unlikely event that the author did not send UMI a complete manuscript and there are missing pages, these will be noted. Also, if unauthorized copyright material had to be removed, a note will indicate the deletion.

Oversize materials (e.g., maps, drawings, charts) are reproduced by sectioning the original, beginning at the upper left-hand corner and continuing from left to right in equal sections with small overlaps.

ProQuest Information and Learning
300 North Zeeb Road, Ann Arbor, MI 48106-1346 USA
800-521-0600

UNIVERSITY OF ALBERTA

LONG TERM PERFORMANCE OF DEVON GEOGRID REINFORCED CLAY EMBANKMENT

BY

SAMAN ZARNANI 

A thesis submitted to the Faculty of Graduate Studies and Research in partial fulfillment of the requirements for the degree of Master of Science

in

Geotechnical Engineering

DEPARTMENT OF CIVIL AND ENVIRONMENTAL ENGINEERING

Edmonton, Alberta

Spring 2005

ABSTRACT

A research program was established in 1986 on the use of geogrids in a fine-grained cohesive soil to reinforce the steep slopes of a test embankment. The test fill is 12 m high with 1:1 side slopes and has four sections: three are reinforced with different geogrids and the fourth is unreinforced for comparison purposes.

Instrumentation was installed to measure the performance of the soil and geogrid layers. The instrumentation applied to the geogrid layers includes electrical wire resistance and inductance coil strain gauges and thermocouples. Horizontal and vertical extensometers, horizontal and vertical inclinometers and pneumatic piezometers were installed in the embankment and foundation soil to monitor its behavior.

Measurements of the instruments were taken in 2003, fifteen years after the completion of the embankment and they were compared to the last set of measurements taken in 1990. The long term performance of the embankment and instrumentation was investigated.

ACKNOWLEDGEMENTS

This research was conducted under the supervision of Dr. J.D. Scott and Dr. D.C Sego. I would really like to thank them for their most valuable guidance and support during this research.

I wish to acknowledge the technical assistance from Gerry Cyre who really put too effort in doing the field work and his valuable experience was very helpful for the field work. The help of other technologists in the Department of Civil and Environmental Engineering, University of Alberta, is also acknowledged.

A special appreciation to my wife, Maria, that her love, patience and continuous support made the academic learning easier and the life more enjoyable to me.

To my mother and father, I dedicate this thesis. Without their love and encouragement fro a further education, my achievement so far would not have been possible.

Table of Contents

List of Tables

Page

- **Chapter 2. History of Devon Test Fill**

- **Chapter 3. Thermocouples**

- **Chapter 4. Strain Gauges on Geogrids**

- **Chapter 8. Comparison between different measurements**

List of Figures

Page

- **Chapter 2. History of Devon Test Fill**

- **Chapter 3. Thermocouples**

- **Chapter 4. Strain Gauges on Geogrids**

- **Chapter 5. Inclinometers-Horizontal and Vertical**

- **Chapter 6. Extensometers-Horizontal and Vertical**

- **Chapter 7. Piezometers**

Chapter 1. Introduction

1.1 General

Alberta Transportation with the Geotechnical Engineering Group at the University of Alberta established a research program in 1986 on the use of geogrids in a fine-grained cohesive soil to reinforce the steep slopes of a test embankment. The test fill is located near Devon, approximately 30 km south west of Edmonton, Alberta, Canada. The test fill is 12 m high with 1:1 side slopes and has four sections: three are reinforced with different geogrids and the fourth is unreinforced for comparison purposes.

The objectives of the test fill based on the project proposal were: 1) to evaluate the current methods at that time for designing fills using geogrids for reinforcement, 2) to compare the performance of three different geogrid materials, 3) to evaluate the field performance of the compacted fill and its foundation soils, 4) to evaluate the field construction procedures involved in constructing geogrid reinforced slopes and 5) the test fill would be beneficial for predicting the field behavior of compacted embankments and reinforced fills.

Intensive instrumentation was installed to measure the performance of the soil mass and the individual layers of geogrid. The instrumentation applied to the geogrid layers includes electrical wire resistance strain gauges (EWR), inductance coil strain gauges and thermocouples. The main goal of this instrumentation was to measure the strains of the geogrid layers and the temperature at the strain gauge locations. The temperatures were measured to account for any temperature effect on the measured geogrid strains. Another goal of the construction of the test fill was to evaluate how the geogrid layers reinforced the soil mass. Hence measurements of the

soil deformation and the pore water pressure response provided information related to understanding this performance. Horizontal and vertical extensometers, horizontal and vertical inclinometers and pneumatic piezometers were installed in the embankment soil and vertical extensometers, vertical inclinometers and pneumatic piezometers were also installed in the foundation soil to monitor its behavior.

1.2 Objective of Thesis

The first objective of the thesis research was to perform field work to locate and refurbish the instruments about 13 years after the last set of field measurements. The field work consisted of locating all the instruments and access tube ends, excavate the sloughed soil which had buried the tube ends and expose the tubes, locating the piezometer leads, refurbishing the connection boxes for reading strain gauges and thermocouples and leveling surveying the horizontal inclinometer tube ends to determine their elevations.

The second objective of the thesis was to read all the instruments still functioning to determine the deformation patterns in the soil and the geogrids 16 years after the end of construction.

The third objective was to evaluate the long-term performance of the soil instrumentation and geogrid instrumentation in the test embankment. The various soil and geogrid instruments, which had been installed 18 years earlier, were refurbished and new sets of measurements were taken for each instrument. The past readings up to 1990 were available and by comparing them to the new sets of readings, an evaluation of the long-term performance and reliability of the instruments was obtained.

The fourth objective of the research was to collect the previous and new data from the instrumentation and document it for a case history, now in its 16th year of service life.

The fifth objective was to document the present state of the instrumentation and upon completion of the field work, to preserve the leads, tubes and connection boxes for future research.

1.3 Scope and Organization of Thesis

Separate chapters present the long-term performance of each type of instrument. The evaluation of the long-term strain of the geogrids, test embankment and foundation soil is also included.

In Chapter 2 a brief history of the test fill is given. The background of the fill, geogrid reinforcement and instrumentation design, construction procedure and fill and foundation soil properties are discussed. Each of the next chapters covers individual instruments.

Chapter 3 is on the thermocouples. A general description of the instrument is given and the method of installation is discussed. The past readings are presented and then the chapter proceeds with the present status of the instrumentation and the new readings.

A description of and the installation method for the Electrical Wire Resistance Strain Gauges are given in Chapter 4. By comparing the changes of strains between new readings and past readings from the EWR strain gauges, the long-term performance of the gauges have been evaluated. Also Bison gauge measurements up to 1990 are presented since the readout device did not work during the 2003 field measurements

and no new measurements could be carried out. The field correlation between EWR strain gauges and Bison strain gauges are presented.

Horizontal and vertical inclinometers have been studied separately in Chapter 5 to evaluate the long-term performance of the instruments during this long period of service. In Chapter 6 the same study has been performed on the vertical and horizontal extensometers and the new sets of measurements carried out in 2003 are compared with the last set of field measurements in 1990. The long-term performance of the pneumatic piezometers is reviewed in Chapter 7. In Chapter 8 some comparison of different measurements are made and references are given on the surveying, which was performed along with the instrumentation readings in 2003 and 2004. Finally the entire thesis is summarized and concluded in Chapter 9.

Chapter 2. History of Devon Test Fill

2.1 Background Information

Use of geosynthetic material to reinforce slopes is a relatively new technique and it was first used about 3 decades ago. Soil reinforcement is gaining the interest of geotechnical engineers and is being used in design. Its advantages are reduced costs and ease of use, coupled with simplicity (Johnes, 1985). To achieve a better understanding of the performance of geogrids in a cohesive soil, Alberta Transportation with the University of Alberta established a research program on their use in a fine grained cohesive soil to reinforce steep slopes of a test embankment. The test fill is located near Devon, approximately 30 km south west of Edmonton, Alberta, Canada. The test embankment is 12 m high with 1:1 side slopes and has four sections: three are reinforced with geogrids and the fourth is left unreinforced for comparison purposes. The plan view of the Devon test fill is illustrated in Figure 1.

The objectives of the test fill based on the project proposal were: 1) to evaluate the current methods at that time for designing fills using geogrids for reinforcement, 2) to compare the performance of three different geogrid materials, 3) to evaluate the field performance of the compacted fill and its foundation soils, 4) to evaluate the field construction procedures involved in constructing geogrid reinforced slopes and 5) the test fill would be beneficial for predicting the field behavior of compacted embankments and reinforced fills. The slopes were designed to have a low factor of safety to ensure that the geogrids would strain and the tensile resistance of the geogrids would be mobilized. To ensure that lateral strains in soil would occur, only three primary geogrid layers were installed at 2 m vertical spacing. This layout of geogrid layers in the slope allowed it to deform while maintaining overall and local stability of the slope (Liu, 1992).

The construction of the test fill started in the summer of 1986 and required two years to complete. Prior to fill construction a number of boreholes were drilled into the foundation soils and Shelby tube samples and auger samples were taken for soil identification and laboratory testing. Some block samples were also extracted from the foundation soil. Soil instruments were then installed in the foundation and the initial values for reference were measured. Four concrete survey monuments were constructed, one adjacent to each section of the test fill. In addition a deep benchmark was installed into the bedrock.

Figure 2 shows that the fill was constructed in three stages. The site and foundation preparation was started on June 8, 1986 with grading the site to the 702 m level. On September 4, 1986 fill placement started. The soil was hauled from the borrow area at the nearby highway cut by scrapers and compacted using a large four wheel compactor. A small dozer and compactor were used along the edge of the slopes and near the vertical instrumentations. The fill was placed and compacted in lifts between 0.15 and 0.4 m. Field density tests (nuclear and in-situ methods) were carried out during construction and the water content of the soil was monitored. The water content of the soil in the borrow area was higher than the recommended water content range. Hence before compacting the soil, it was spread and left to lose moisture via evaporation. When the fill reached 1 m it was leveled and the bottom primary geogrid layer was laid out. More soil was placed and compacted on top of the this reinforcing layer until the embankment reached the 3m height when the construction was stopped due to the onset of freezing temperatures, on October 23, 1896. Horizontal instruments and one layer of secondary geogrid reinforcement were placed at the 2m level during the first construction season. Tertiary grids were also placed at a 0.33 m spacing.

The construction was resumed on August 30 1987. Some soil affected by freeze-thaw and drying was removed and then an additional 3m of fill was placed. The middle and the top primary reinforcement geogrids were placed at the 3 and 5 m level following the previously outlined procedures prior to shut down on November 3, 1987. In addition, soil instrumentation and secondary reinforcement were placed at the 4m level. The construction of the test embankment continued the following summer. An additional 6m of soil was added to complete the 12 m fill by October 29, 1988. Six layers of secondary reinforcement geogrids were placed during the 1988 summer construction. Due to the rainy weather and construction delays, the top 6m of fill was placed with higher moisture contents than the design values. Also the lifts were thicker than used in the lower 6 m of the fill. The top 6 m of the embankment had a water content about 3 to 5% higher than the lower half of the fill (Liu, 1992). Variation in the water content due to rain and limited compaction along the edge of the slopes caused reduced uniformity and consistency in the properties throughout the fill.

Some surface erosion control materials were put on the slope surfaces during the fall 1988 and the spring of 1989.

Table 1 summarizes the important dates in the history of the Devon test embankment and the information in this table will be used throughout the entire thesis.

2.2 Geogrids in the Test Fill

The primary use for a geogrid is to reinforce or add resistance to the soil; applications are many including strengthening reinforced walls, pavements and highways, construction of earth walls, reinforcing embankment and earth dams and for landslide repair. Three types of high

tensile strength geogrids were used as reinforcing materials in the test fill: Tensar SR2, Signode TNX5001 and Paragrid 50S. From the manufacturer's specifications the properties of the geogrids are summarized in Table 2. Some wide strip tests were also carried out before the grids were placed into the fill and these results are shown in Figure 3.

Tensar SR2 grid is a uniaxially oriented geosynthetic grid which was manufactured by Tensar Corp. It is one of the most widely used geosynthetics for reinforcement purposes. At the beginning of the manufacturing process uniform holes are punched into a plain sheet of high-density polyethylene material and then stress is applied to the punched sheet, which causes the holes to elongate and create rib shaped members along the sheet. This process requires a draw ratio of 8:1 and the high-density polyethylene material is stretched into a post yield state. The structure of optimized nodes and ribs has significant influence on the load transfer from the soil. The strong interlocking action between the ribs applies confinement to the lateral displaced soil. With loading applied, the soil particles settle within the evenly distributed mesh thus spreading the load evenly within the geogrid.

Generally polymer materials have molecular chains distributed randomly with similar properties in all directions. Special molecular orientation is achieved by stretching the polymer which increases the tensile strength in the oriented direction.

This orientation provides the following benefits to the Tensar geogrid: polymer strength is increased and forms the mesh structure with nodes. The orientation confines the inter displacement of the molecular chains, resulting in improvement to its tensile modulus. Orientation reduces the future strain under long-term loading. Hence the molecular structure of the material will be highly elongated and as a result of all these processes, the

resistance to creep will be increased in the final product. It has high strength and modulus. This type of uniaxial geogrid is best used for application with the major principal stress direction known, with the longitudinal members oriented in the same direction as the major principle stress.

Signode TNX5001 is a rectangular shape grid, which was manufactured by the ITW Signode Corp. This grid was made by ultrasonically bonding longitudinal and transverse polyester strips. Like the Tensar uniaxial grids, this grid is also used when the major principle stress direction is known. Production of this grid was halted shortly after the fill was constructed.

The third geogrid used was Paragrid 50S, which is a square shaped grid. It was marketed by Mirafi Inc. This grid is made from high-tenacity polyester filaments, which are held together by a polypropylene sheet. The grid shape was formed by heating the longitudinal and transverse strips creating melt bonded polypropylene joints. Unfortunately this grid had manufacturing defects and according to the laboratory tests, it was found that some of the high strength fibers in the tension members were weakened or damaged at the joints. Possibly this damage was caused by overheating the polypropylene sheet during the bonding process.

Other than the above primary reinforcing materials, Tensar SR1 and SS1, Signode TNX250 and Paragrid 5T grids were used in the three reinforced sections of the test fill as the secondary reinforcing materials to provide additional reinforcement against shallow slope failures. These secondary geogrids were not instrumented and detailed discussion on the properties of the secondary reinforcing materials is beyond the scope of this thesis. A typical cross section and layout of primary and secondary geogrid layers in the reinforced slopes is illustrated in Figure 4. Some tertiary reinforcing grids were also placed every 0.33 m between

secondary and primary geogrids only in the bottom 3 m of the fill during the first construction stage. They were 1.5 m long fiberglass grids and they were installed in order to protect the slope surfaces from heavy equipment during the construction process and sloughing caused by the freeze-thaw cycles. As the contractor had fallen behind the schedule to complete the test embankment, the owner required that the placement of these tertiary geogrids be dispersed with in the top 9 m of the fill.

2.3 Properties of Soils

The detailed properties of the foundation and fill soils were studied by Hofmann (1989). Drained and undrained triaxial compression tests were carried out on compacted samples of the soil used to construct the fill and on the Shelby tube and block samples obtained from the foundation soils. The main results of Hofmann's studies are summarized in the following sections and details of the laboratory testing can be found in Hofmann (1989).

2.3.1 Properties of the Foundation Soil

Details of the bedrock and surficial geology in the Devon area are given by Gabert (1968). The bedrock in the area is the lowest member of the upper Cretaceous Edmonton Formation with alternating bentonitic carbonaceous shales and light grey sandstones containing coal seams. The deposits above the bedrock consist of three major geological units. The soil immediately above the bedrock is sand and gravel, deposits of the North Saskatchewan River. It was overlain by glacial basal till. This till is composed of materials from large granite boulders to fine silty clay and is heavily over consolidated. A glaciofluvial deposit, well-bedded silts, sands and gravels, was sandwiched between till sheets as the glacier retreated and advanced. This was then overlain by the glaciolacustrine

sediments of Lake Edmonton. These sediments range from well bedded sand, silt and clay to till-like materials deposited by melting of ice floating in Lake Edmonton. The geological history of the glaciolacustrine deposit suggests that the soil is normally consolidated. The upper layer of sediments at the location of the test fill, however, may have become over consolidated as sand dunes formed and moved across the area after Lake Edmonton was drained when the glaciers blocking the north drainage receded.

Boreholes were drilled at the test fill site using a wet rotary drilling rig which allowed Shelby tube samples, 73 mm in diameter by 610 mm long to be taken. A typical borehole profile of the foundation soils is given in Figure 5. The upper most 4.6 m of soil consist of brown sandy silt to silty clay with some grey pockets. Block samples were taken from this layer of soil at a depth 4.5 m below the ground surface. The average SPT (Standard Penetration Test) blow count in the upper soil, Figure 6, indicates that the material is of medium consistency. The variation of water content with depth suggests the presence of a desiccated crust near the surface. The ground water table is 5m below the ground surface. This upper soil is underlain by a stiff to very stiff clay till which is heavily over consolidated. The till is then underlain by very dense sand beyond a depth of between 9 and 10 m from the ground surface. From the geological profile of the surficial sediments, it was obvious that the deformation of the foundation soils due to the construction of the test embankment would mainly occur in the glaciolacustrine deposits. Therefore, the studies focused on the upper most silt or silty clay.

The upper soil has average water content of 32%, liquid limit of 37.2% and plastic limit of 23.9%. The dominant particle size of the soil is silt while the clay sizes are only 10 to 20%. According to the results of the X-ray diffraction tests, the clay fraction contains up to 50% illite and up to 60% montomorillonite. Field observation in two test pits indicated vertical

fissures at a spacing of 10 to 15 cm and horizontal fissures at a spacing of about 15 cm. The former seems to be related to some degree of stress relief and the later associated with the nature of the lacustrine deposit.

Consolidation tests on the foundation soil were conducted using a floating ring oedometer, 25.4 mm high by 63.5 mm in diameter. The tests were carried out on both block samples and Shelby tube samples. The specimens were subjected to a load sequence, which was carefully chosen such that the estimated preconsolidation stress of approximately 350 to 500 kPa could be well defined. A seating load of 5 kPa was applied to each specimen before the dial gauge was set to zero and the specimen was then loaded to the in situ vertical effective stress. The specimens were allowed to consolidate or swell for 24 hours under each load increment. The vertical strains of each specimen versus time were plotted as log-time and square-root-time consolidation curves and the time to complete 90% of the primary consolidation were obtained. Due to the fact that the immediate deformation and the primary consolidation of the specimens took place within several minutes after each load, the log-time consolidation curves were essentially straight lines, which indicated secondary consolidation. Thus, it was only possible to determine the coefficient of consolidation, c_v, from the square-root-time plots for each load step. Moreover, it was difficult to calculate c_v from the consolidation curves at low normal stresses and the accuracy of the calculated c_v is questionable.

The results of the consolidation tests of the upper foundation soil are summarized in Table 3. It was observed that the primary consolidation was complete within several minutes. The consolidation of the foundation soil would occur as the embankment was constructed slowly. In other words, high excessive pore water pressures would not be expected to develop in the foundation soil.

Based on the above consolidation characteristics, consolidated undrained triaxial tests with pore pressure measurements were conducted on saturated soil specimens, 76 mm long by 38 mm in diameter, obtained from both block and Shelby tube samples. Backpressure of 300 kPa and 400 kPa were used respectively for the block samples and the tube samples and the specimens were sheared at the displacement rate which gave a strain rate of 5.5% per hour. The specimens showed either a hyperbolic or an elastic-perfectly plastic stress-strain behavior. Therefore, the failure was defined by the maximum principle effective stress ratio. The pore pressures during shearing were positive indicating compression of the soil through out the test. Skempton's pore pressure parameter at failure, A_f, tended to increase from 0.1 under a low confining stress to 0.83 under a stress of 275 kPa. A summary of the results of the consolidated undrained triaxial tests is presented in Table 4.

The results obtained from the consolidation tests carried out on the foundation soil showed that the pre-consolidation stress was approximately 400 kPa. The increase in stress the foundation soil would be subjected to due to the weight of the test embankment was approximately 240 kPa. Therefore Hoffman (1989) concluded that the settlement of the foundation soil due to the weight of the overlying test fill was not expected to be large. In fact settlement due to primary consolidation under a 12 m high embankment was calculated to be only about 35 mm based on the coefficient of recompression measured on the Shelby tube foundation soil samples.

2.3.2 Properties of the Fill Soil

To meet the design requirement that the fill soil deforms sufficiently to induce strain in the geogrids, the upper most foundation soil, silty clay,

which is relatively soft, in the test site area was selected as the material to construct the embankment. In order to characterize the physical properties and the stress-strain behavior of the fill material, large bag samples were removed from the borrow area. During the construction of the embankment, Shelby tube samples, 25.4 mm in diameter and a large bag sample were removed from the compacted lifts of fill to determine the properties of the soil actually placed during the construction.

The Atterberg limits and grain size distribution for the fill soil are shown in Table 5. Even though the plastic index and percentage of clay sized particles of the soil from the borrow site are higher than the values of the soil from the test fill, both soils are classified as inorganic clays or silty clays of low to medium plasticity, according to the Unified Soil Classification System. Compaction tests of the fill material were conducted by Bobey (1988) using both the kneading and the dynamic methods. The two compaction methods resulted in essentially the same relationship between dry density and water content. The compaction curves of the fill material were established using the kneading method and are shown in Figure 7. The optimum water content is 20.5% and the maximum dry density is 1.68 g/cm^3.

In order to determine how the strength and stress-strain behavior of the fill soil varies with changes in water content and density, unconfined compression tests of compacted fill soil samples were conducted on specimens with a water content ranging between 14% and 22% and a dry density between 1.49 and 1.68 g/cm^3. The specimens were prepared using kneading compaction technique. Two 38 mm outer diameter Shelby tubes were pushed into each compaction sample mould and specimens were extruded. The stress-strain curves from the unconfined compression tests vary from one specimen to others as the water content changes. The specimens compacted at water contents less than 18% exhibited brittle

stress-strain curves, while the specimens compacted at water contents higher than 18% showed a slightly plastic stress-strain behavior until the maximum shear stress was reached at larger strains and then gradually dropped off. Again, to satisfy the design requirement that the fill deforms extensively without undergoing shear failure, it was decided that the fill soil had to be compacted wet of its optimum water content of 20.5%.

The variation of the maximum undrained shear strength with changes of water content is illustrated in Figure 8. The maximum shear strength of the soil increases with increasing water content up to about 16.5% and then decreases rapidly with further increase in water content. According to the variation in the undrained shear strength, the water content for field compaction was specified at between 22% and 24% (dry density ranging from 1.66 to 1.59 g/cm^3) such that the corresponding undrained shear strength would be between 60 and 40 kPa yielding a factor of safety against a shear failure in the 12 m high embankment, immediately after construction, of slightly greater than 1.0.

The variation of moisture content at different elevations inside the bottom 6 m of the fill is illustrated in Figure 9. Figures 10, 11 and 12 present the variation in the dry density and moisture content for the fill soil between 0 to 2 m, 2 to 4 m and 4 to 6 m elevation respectively. The field moisture contents and dry densities were collected from the files of the nuclear density tests during the embankment construction. For Figures 10 and 11, the weights of the microwave dried samples were used to calculate the field moisture content but for Figure 12 these values were not available and the nuclear values are shown. These figures show the scatter of density and moisture content in the fill and indicate that the fill soil would have a large variation in its stress-strain properties. As shown in Figure 8, the variation in moisture content has a considerable effect on the

unconfined shear strength. The range of moisture contents indicate that the strength would vary from less than 20 kPa to over 200 kPa.

Unconsolidated undrained triaxial compression tests were conducted on Shelby tube specimens obtained from the compacted fill in the field to determine the variability of the actual shear strength throughout the embankment. The specimens were taken from the bottom 3 m of the compacted fill soil at different locations and elevation levels. Some specimens were saturated using a backpressure to examine the effect of the saturation on the undrained shear strength of the fill soil. The specimens were sheared at a rate of 0.76mm/min. The results of the unconsolidated undrained triaxial tests are compared in Table 6. The undrained shear strengths of the unsaturated samples, subject to the same confining stress, showed a considerable amount of scatter, indicating the importance of moisture control in the fill construction to maintain homogeneous shear strength within the test embankment. The tests conducted on the back pressure saturated specimens showed that neither the undrained shear strength nor the stress-strain behavior was affected by saturation; most likely due to the fact that the average degree of saturation of the soil compacted in the field is 92%.

Unconsolidated undrained triaxial tests were also conducted on laboratory compacted samples prepared from the fill soil. The soil was compacted using the standard kneading method at water contents between 22% and 24% and test specimens were extruded from 38 mm diameter Shelby tubes which had been pushed into the compaction sample mould. The specimens were saturated under a backpressure of 600 kPa and were sheared at a displacement rate of 0.76 mm/min. The specimens tested under confining stresses of 80, 160 and 240 kPa showed approximately the same stress-strain behavior, deviator stresses increasing with strain to large strain values. This stress-strain behavior of

the fill soil indicates that the test fill slopes may deform considerably in their undrained state before consolidation commences.

Consolidated undrained triaxial compression tests with pore pressure measurements were conducted on the fill soil to evaluate the pore pressure response during shear. The specimens were prepared, at average water content of 24%, in the same manner as those prepared for the unconfined compression tests. The specimens were allowed to saturate under a backpressure of 400 kPa for 24 hours prior to consolidation. The consolidation phase under a predetermined stress gave an average t_{90} of 55 minutes and an average coefficient of consolidation of 4.14×10^{-3} cm^2/s. Once primary consolidation was complete the specimens were sheared at a displacement rate of 0.15 mm/min without allowing drainage while the internal pore pressures were recorded. Failure of the specimens was defined by the maximum principle stress ratio.

Table 7 summarizes the results of the consolidated undrained tests. The stress-strain curves generally showed a strain-hardening behavior. There was an initial steep portion in each stress-strain curve, which gave a high tangent modulus; beyond about 2% strain, the stress rose slowly with increasing strain to failure. Peaks in the deviator stress of the specimens consolidated above 150 kPa could be observed in the stress-strain curves. The stress-strain curves of the samples consolidated at stresses less than 150 kPa, however, did not exhibit a peak in the deviator stress even up to 24% strain. Corresponding to the stress-strain curves, the pore pressures in the specimens rose sharply below 5% strain and then slowly decreased with increasing strain throughout the rest of the test. The pore pressures developed during shearing increases with increases in confining stresses. Skempton's pore pressure parameter at failure, A_f, increased

approximately linearly from about 0.02 to 0.5 with increasing confining pressure.

The results of the consolidated undrained tests were interpreted using the total and effective stress p-q plots and the strength parameters were obtained. The total and effective stress friction angles calculated from the slope of the K_f lines were 17.6° and 28° respectively; the cohesive strength ranges from 23 to 24 kPa in terms of total stress and from 8 to 14 kPa in terms of effective stress.

To evaluate the long-term stress-strain behavior of the fill soil, consolidated drained triaxial tests were carried out. The soil was compacted at average water content of 21%, which was 2% lower than that used for the consolidated undrained tests but close to the placement water content of the bottom 3 m of soil in the embankment. The specimens were prepared in the same manner as those prepared for the unconfined compression tests, saturated with a back pressure of 600 kPa, consolidated under different cell pressures and then sheared slowly under drained conditions while volume change measurements were recorded. The stress-strain curves of the consolidated drained tests appear to be hyperbolic, again indicating a stress-hardening behavior. The curves of volume change versus axial strain show that the specimens first contracted and then dilated at high strains. This behavior agrees well with the pore pressure response in the consolidated undrained tests. The results of the drained tests represented in the total/effective stress p-q plot and the strength parameters were obtained from the K_f line .The effective stress friction angle ranges from 27° to 28° and the cohesive strength varies from 23 to 27 kPa.

Based on all the above test results a short term stability analysis of the embankment was conducted by Hoffman (1989) assuming that the top 6

m of fill would be placed quickly on the existing consolidated 6 m high embankment. The short term analysis was conducted in terms of effective stress such that pore pressures could be considered. The critical slip circle established for a fill height of 12 m was also determined and the short term factors of safety for different fill heights and various shear strength parameters were also calculated. A factor of safety greater than 1 was determined for a fill height of up to 10 m when high r_u values were used. Similar calculations using lower r_u values showed that failure is pending at a fill height of 12 m. The analysis conducted for variations in the shear strength parameters showed that the factor of safety was most sensitive to changes in the cohesive strength, while variations in the friction angle had little effect. Since the critical failure surface always passed through the fill soil, varying the shear strength parameters of the foundation soil had no influence on the factor of safety.

A long term stability analysis was also conducted by Hoffman (1989) assuming that the excess pore pressures in both the fill and foundation soils would have dissipated to zero. The long term factors of safety were calculated for different fill heights and cohesive strength values. All the properties obtained by different tests mentioned previously were used to conduct these analyses. As for the results for the short term calculations the critical slip surface passed through the toe of the slope. Therefore changes in the shear strength parameters of the foundation soil had no influence on the factor of safety. The calculations also showed that the long term factor of safety was greater than 1 even for a fill height of 12 m and an effective cohesive strength of only 10 kPa for the fill soil.

Comparison of the long and short term factors of safety showed that the conditions immediately after construction, before the excess pore pressures had had a chance to dissipate, were the most critical. Hence, provided that the pore pressures were monitored during the placement of

the last few meters of the fill and that critically high excess pore pressures were allowed to dissipate, both the short and long term stability of the embankment should have been adequate. The lower factors of safety calculated for the short term analysis showed that the shear stresses in the embankment, and therefore the rate of shear strains which took place, would be greater immediately after construction.

A finite element analysis was conducted by Hoffman (1989) in order to predict the horizontal strains which might occur in the unreinforced slope of the test fill. The study was intended to model the long term conditions of the embankment. Hence it was assumed that the excess pore pressures had dissipated completely. The results showed that a maximum horizontal strain of 2% would occur at an elevation of between 5 and 6 m in the 12 m high slope. Compressive strains were shown along the slope face which penetrated as much as 2 m in to the slope along the lower half of the embankment. Although the soil being used to build the test embankment was quite deformable, the horizontal strains predicted by finite element analysis were small. The results also showed that the grids were not anchored in a zone of negligible horizontal soil strain. They therefore would not be completely effective in reducing the lateral deformation of the embankment. However, although the geogrids may not be long enough to resist horizontal strains completely, they were sufficiently long to prevent a pullout failure. The geogrids were designed to extend at least 4 m beyond the critical failure circle determined from limit equilibrium analyses.

2.4 Geogrid Instrumentation

In order to achieve the main objective of the construction of the test embankment which was to evaluate the current methods at that time for designing fills using geogrids for reinforcement and to compare the performance of three different geogrid materials and to measure the stress

transfer between the soil and the geogrids during the construction time and service time, intensive instrumentation program was performed. The instrumentation on the geogrid layers includes electrical wire resistance strain gauge, inductance coil strain gauges and thermocouples. The main goals of these instruments were to measure the micro and macro strains on the geogrid layers and also measure the temperature variation at the locations where the strains were measured in order to account for any temperature effect on the measured strains. The following chapters will discuss the details of this instrumentation and their results separately. The layout of the geogrid instrumentation is illustrated in Figure 13.

2.5 Fill and Foundation Instrumentation

Another main goal of the construction of this test fill was to evaluate the field performance of the compacted fill and its foundation soils. Hence measurements of the soil deformation and the pore water pressure response could provide valuable information about the understanding of this performance. Horizontal and vertical extensometer, horizontal and vertical inclinometers and pneumatic piezometers were installed in the fill soil and vertical extensometers and inclinometers plus pneumatic piezometers were also installed in the foundation soil. Field surveys were also carried out during and after the fill construction as part of the field instrumentation to assist in understanding the readings from instruments. The layout of the instrumentation in the test fill and foundation is illustrated in Figure 14. Two sections of instrumentation are in the embankment, the north section, as shown in Figure 14, between the Tensar geogrid and the Paragrid geogrid and the south section between the unreinforced slope and the Signode geogrid. These instruments and their results will be discussed in detail in separate chapters.

2.6 Field work carried out in 2003 and 2004

Different sets of instrument measurements were carried out during and after the embankment construction until 1990. No measurements were taken after September 1990. The first steps for the field work in 2003 was identifying the location of buried instruments and access tubes under the soil and refurbishing and cleaning them. In total about 80 trips were made to the site including all the clean up activities and taking the measurements. The field work started with removing debris with a backhoe. All the access tubes buried beneath debris were excavated in order to expose them. Some connection boxes were also buried which were cleaned up as well. A typical view of a connection box with different plugs for measuring different instruments is shown in Figure 15. The next step was cleaning all the connection boxes and all the connectors and plugs were washed and brushed in order to remove any dirt. All the horizontal access tubes of inclinometers and extensometers were washed out by using pumped water and a stiff plastic hose and the dirt inside the access tubes was all washed out. Unfortunately the horizontal access tubes at 6 m elevation were badly damaged during the third construction stage and it was not possible to push the hose through the access pipes. The vertical access tubes at the toe of the slopes were also washed with pumped water and all the dirt collected at the bottom of the vertical access tubes was washed out as well. But the vertical access tubes at the crest of slopes could not be washed due to the highly deformed shape of the access tubes. Some pictures of the slope sections before and after clean up activities are presented in the following chapters showing more details of the refurbishment carried out to retrieve the instruments. After the completion of the required field measurements in 2004, an attempt was made to protect the instruments for further field measurements in future. The door of the connection boxes including the plugs for EWR strain gauges, Bison inductance coil strain gauges and thermocouples were all

closed in order to prevent any contact with outside environment. The piezometer leads which were lying on the ground were collected and put in plastic bags tightened with tape in order to protect the leads from soil. The access tube ends for vertical and horizontal extensometers and inclinometers were covered with plastic bags in order to make a temporary cap preventing any debris getting into the access tubes. It is suggested that for taking any new field measurements in future all the access tubes for inclinometers and extensometers be washed and all the plugs in the connection boxes be cleaned before taking any readings.

Table 1. Important dates in Devon test embankment history

Date	Elapsed time in years	Stage of construction
23-Oct-1986	0.08	Fill height reached 3 m-First construction stage
30-Aug-1987	0.93	Second construction stage started
3-Nov-1987	1.11	Fill height reached 6 m-Second construction stage
10-Aug-1988	1.88	Third construction stage started
29-Oct-1988	2.1	Fill height reached 12 m-End of construction
15-Jan-1990	3.34	Last set of measurements for EWR strain gauges
30-Jul-2003	16.86	First set of measurements in 2003, 14.76 years after construction completed

Table 2. Physical Properties of Geogrids (from Bobey, 1988)

Geogrid		Tensar SR2	Signode TNX5001	Paragrid 50S
Type of Polymer		High Density Polyethylene	Polyester	Polyester Polypropylene
Structure		Uniaxial Grid	Rectangular Grid	Square Grid
Junction Type		Planar	Welded	Welded
Weight (g/m)		930	544	530
Open Area (%)		55	58	78
Aperture Size (mm)	MD	99.1	89.7	66.2
	CMD	15.2	26.2	66.2
Thickness (mm)		T 1.27	T 0.75	T 2.50
		A 4.57	J 1.50	J 3.75
Color		Black	Black	Yellow

Note:
MD: Machine Direction, CMD: Cross Machine Direction
T: Tension Member, A: Anchor Member, J: Joint

Table 3.Results of Consolidation Tests on Upper Foundation Soil (from Hofmann, 1989)

Parameters	Stress Range (kPa)	Block Sample	Tube Sample
P' (kPa)	---	458	417
C_c	800-1600	0.535	0.344
C_r	20-500	0.053	0.015
t_{90} (min)	500	1.96	0.84
	800	2.43	1.24
C_v (cm/s)	500	0.01	0.024
	800	0.008	0.018
M_v (m/kN)	500	1.61E-04	8.36E-05
	800	1.41E-04	9.23E-05
K (cm/s)	500	1.57E-07	1.98E-07
	800	1.03E-07	1.55E-07

Table 4.Summary of Consolidated Undrained Triaxial Test Results on Upper Foundation Soil (from Hofmann, 1989)

Specimen Type		c (kPa)	φ(°)	c' (kPa)	φ'(°)
Block	Range	25-26.7	13-13	23-25.3	24-24.8
	Design	25	13	23	24
Tube	Range	10-11.6	15-18	6-16.5	24.4-33
	Design	10	15	6	33

Table 5.Summary of Atterberg Limits and Grain Size Distribution of Fill Soil (from Hofmann, 1989)

Soil Sample	W%	Wl%	Wp%	Ip%	Sand%	Silt%	Clay%
Borrow site	---	42.3	20.7	21.6	28	44	28
	---	40	19.6	20.4	25	43	32
	---	40	19.2	20.8	---	---	---
Test Fill	---	33.3	18.1	15.2	22	60	18
	---	---	---	---	23	57	20
	20	37.4	20.9	16.5	5	73	22
	19.1	34.5	23	11.5	20	62	18
	---	---	---	---	20	61	19

Table 6.Unconsolidated Undrained Triaxial Test Results on Shelby Tube Samples of Fill Soil (from Hofmann, 1989)

Sigma3 (kPa)	Sr<100%		Sr=100%	
	σ_1-σ_3 (kPa)	ε_f (%)	σ_1-σ_3 (kPa)	ε_f (%)
0	166	12.7	—	—
80	182	15	235	20.7
160	178	15	244	16.4
240	244	14	274	15
	271	21.7	—	—

Table 7. Consolidated Undrained Triaxial Test Results on Fill Soil (from Hofmann, 1989)

Cell Pressure (kPa)	W%	Sr%	σ1-σ3 (kPa)	$(\sigma'1/\sigma'3)_f$	U_f (kPa)	ε_f(%)	A
25	21.3	94.7	100	5.46	2.4	3	0.024
50	25.1	92.7	104	3.81	12.6	6.1	0.121
75	24.3	94.5	125	3.6	27	7	0.216
100	23.6	90.6	143	6.02	71.7	4.4	0.501
125	23.7	87.7	165	3.4	56	13.7	0.339
150	23	99.1	187	3.37	71	7	0.38
175	22.9	92.9	211	4.26	110.3	5.2	0.523
200	23.1	90.9	230	3.36	102.7	10.1	0.446
203	22.5	94.9	258	2.3	91	11	0.353

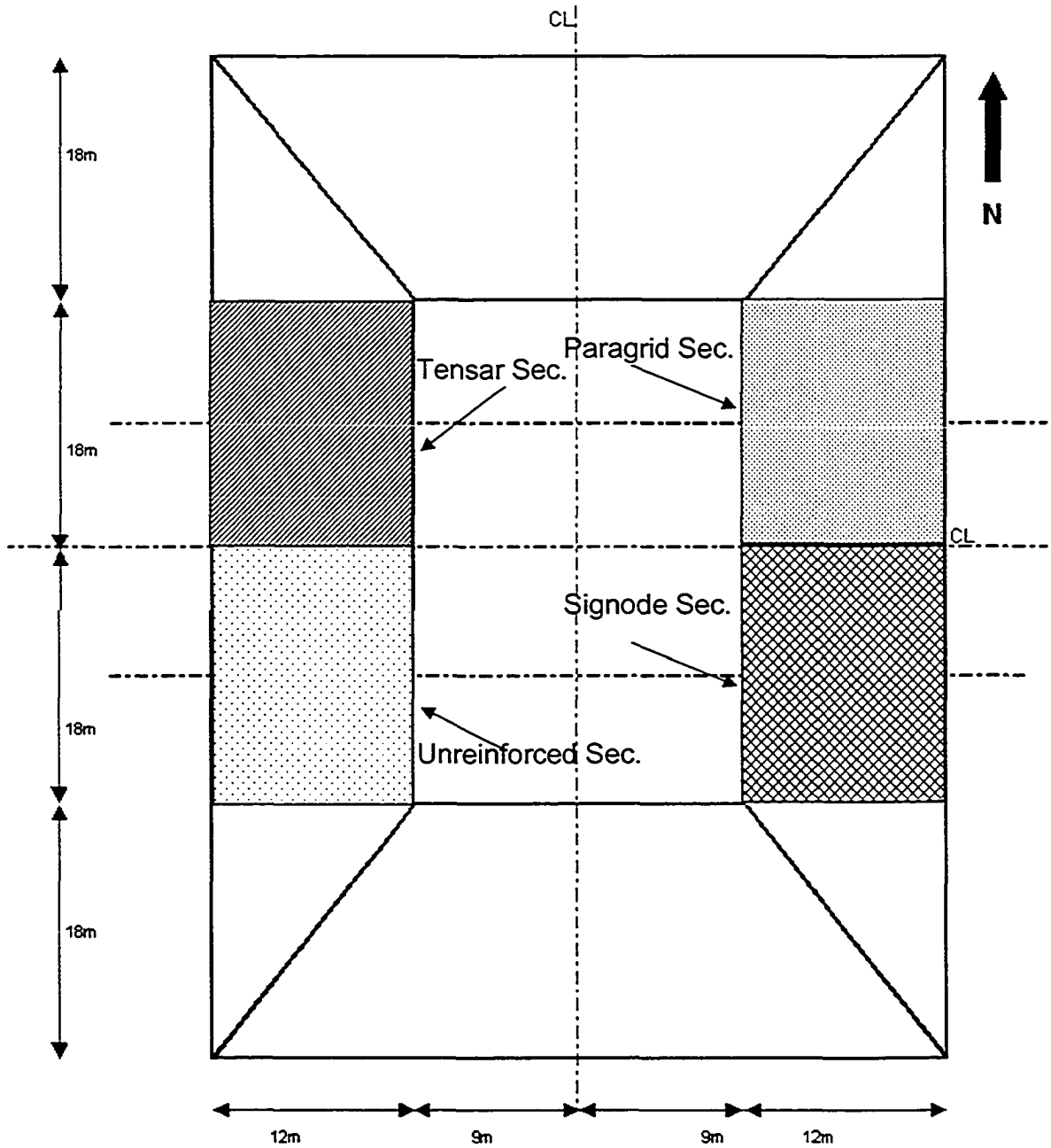

Figure 1.Lay out of the Devon Test Fill

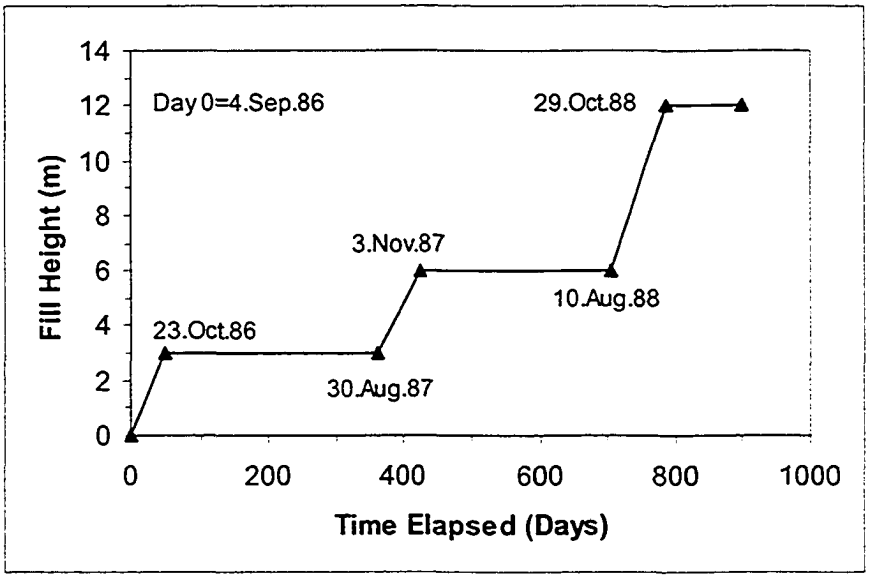

Figure 2.Construction Schedule of Devon Test Fill

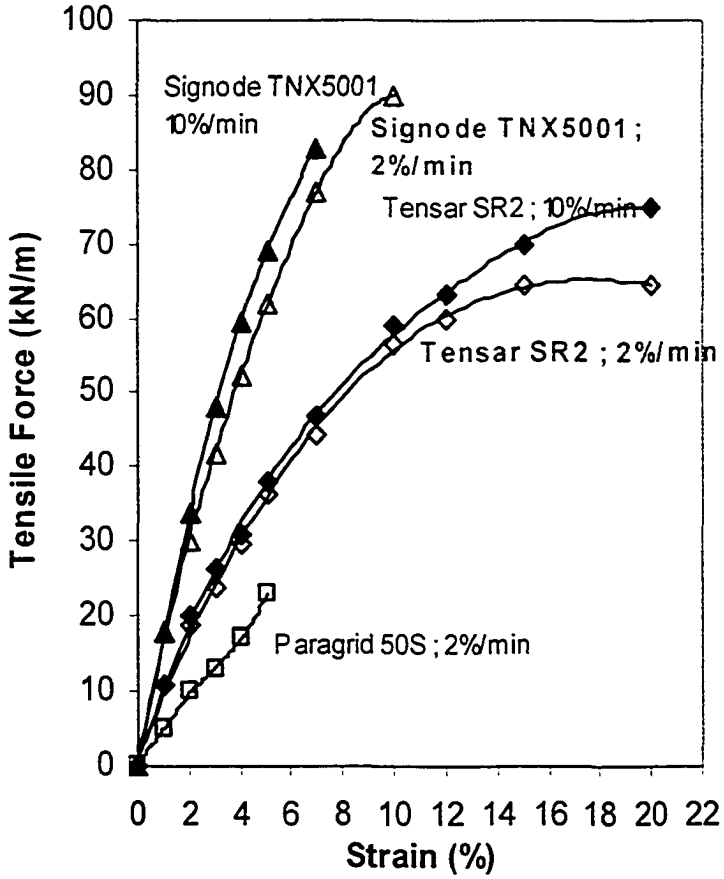

Figure 3. Tensile test results on geogrids

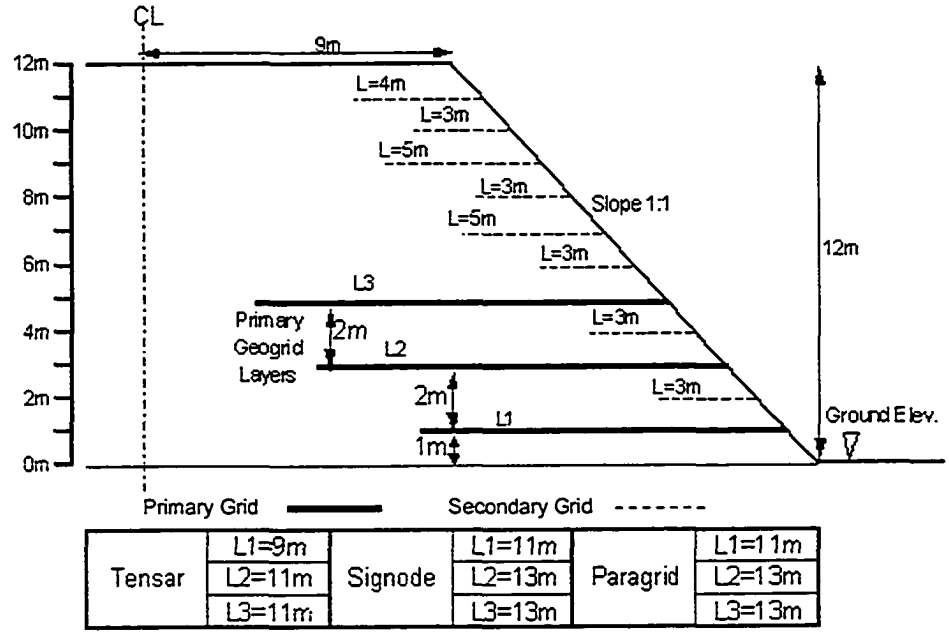

Tensar	L1=9m	Signode	L1=11m	Paragrid	L1=11m
	L2=11m		L2=13m		L2=13m
	L3=11m		L3=13m		L3=13m

Figure 4.Layout of Geogrids in Devon Test Fill

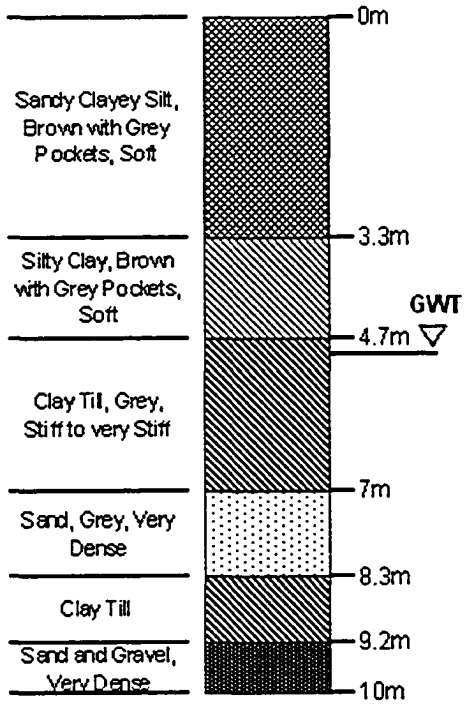

Figure 5.Typical Profile of Foundation Soil (modified from Hofmann, 1989)

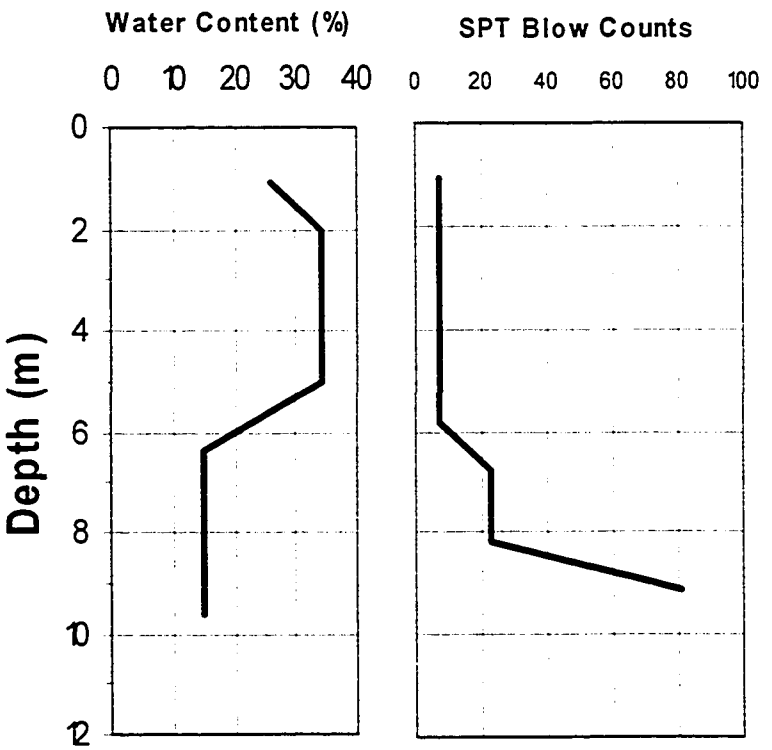

Figure 6. Profile of SPT blow count and water content variation in foundation soil (modified from Hofmann, 1989)

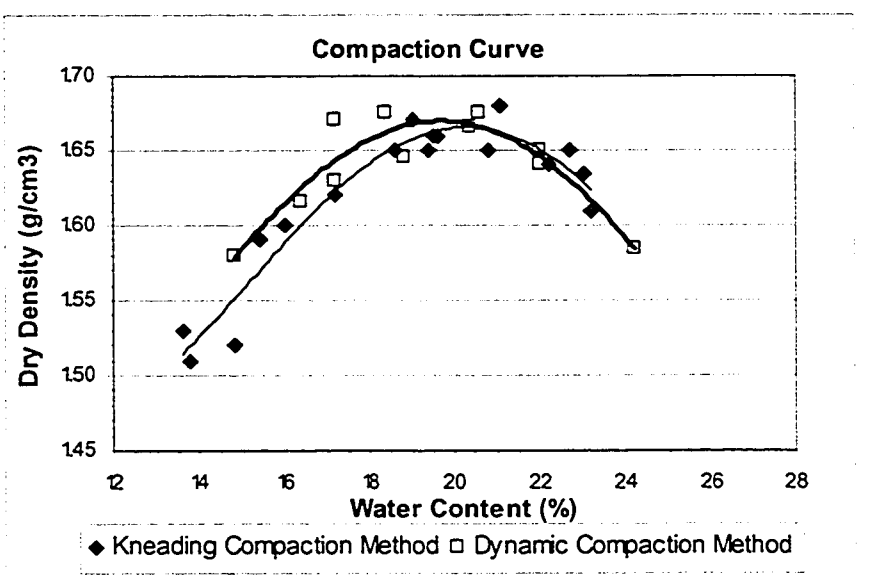

Figure 7. Compaction curves of fill soil (modified from Hofmann, 1989)

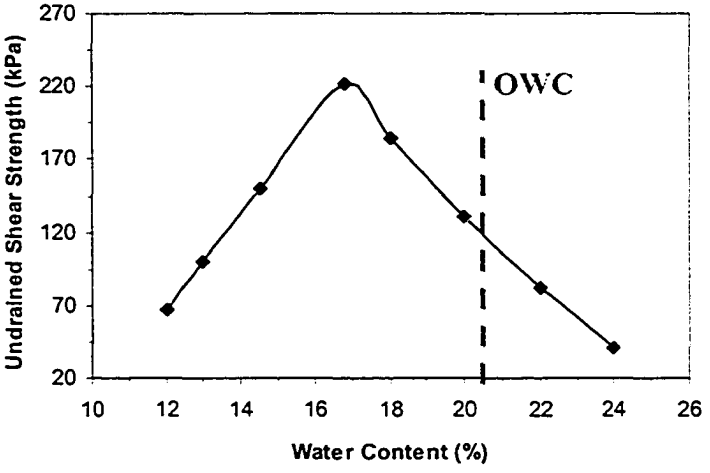

Figure 8. Effect of water content change on maximum undrained shear strength of fill soil

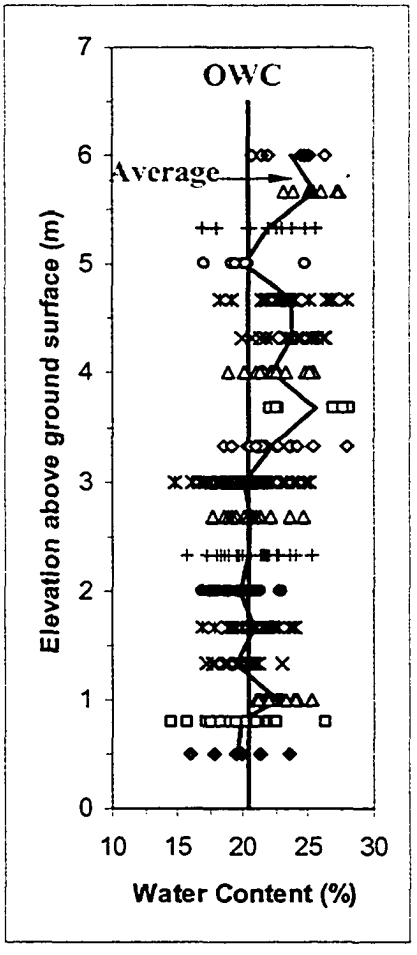

Figure 9. Water content change in bottom 6 m of fill soil, range and average

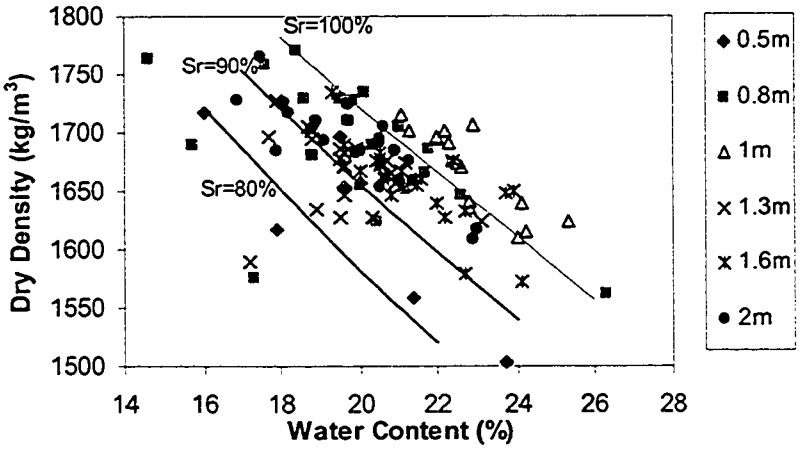

Figure 10. Water content versus dry density variation-0 to 2 m elevation inside fill

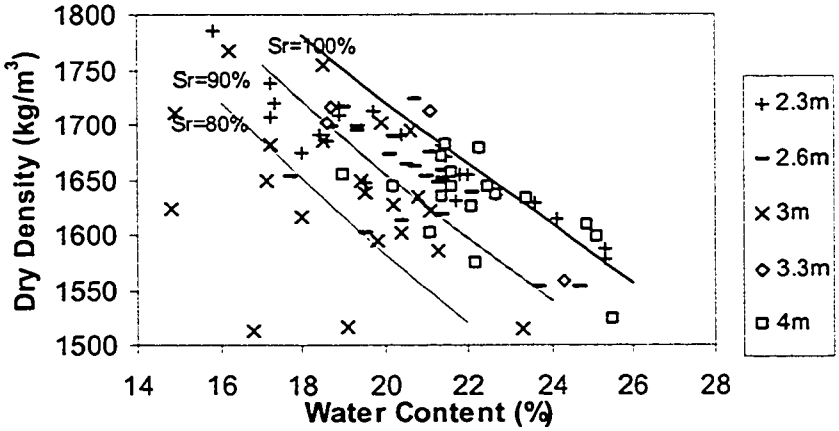

Figure 11. Water content versus dry density variation-2 to 4 m elevation inside fill

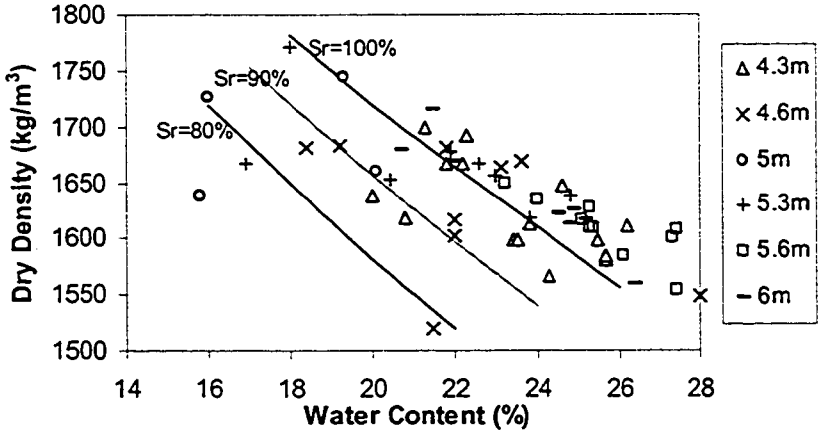

Figure 12. Water content versus dry density variation-4 to 6 m elevation inside fill

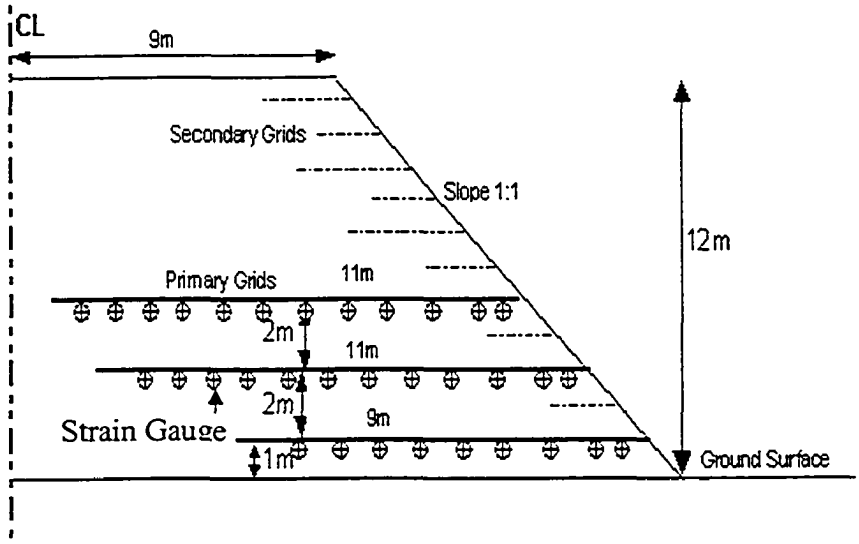

Figure 13. Geogrid instrumentation Layout in Reinforced Slope

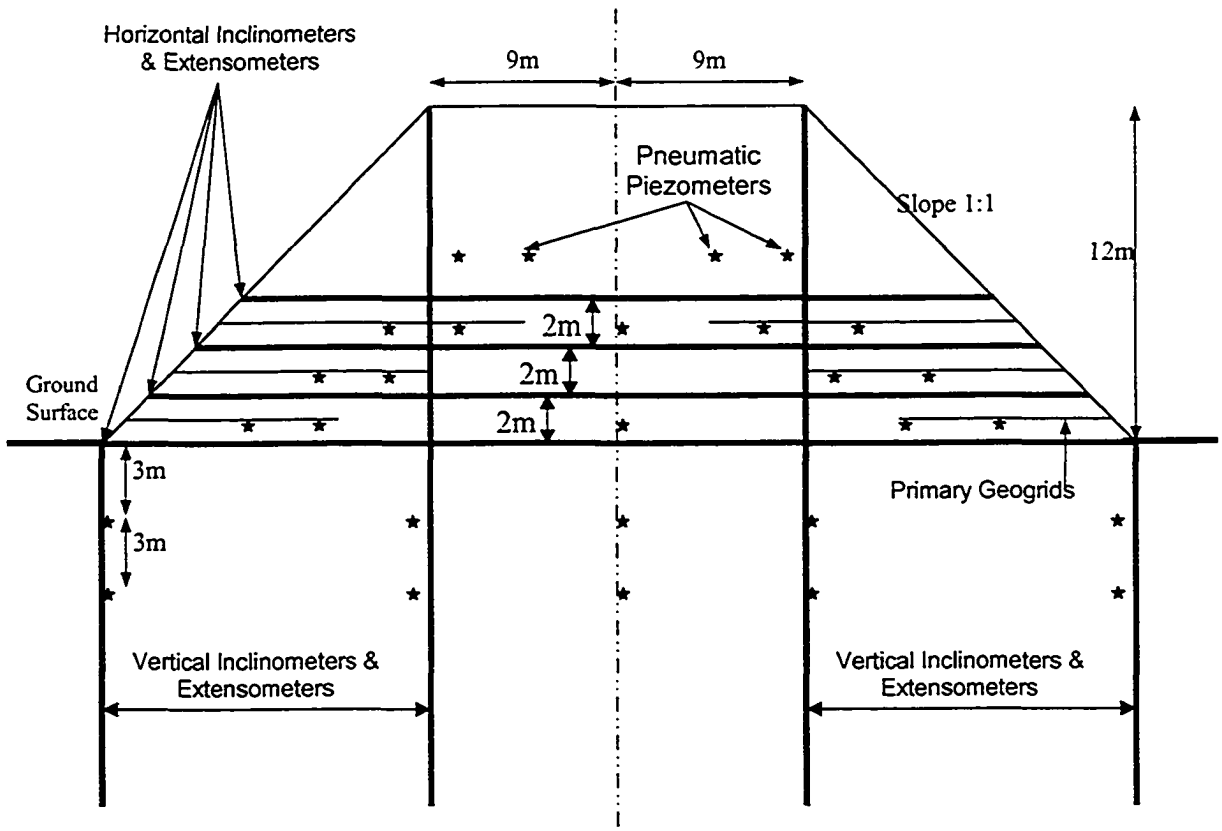

Figure 14.Instrumentation Layout in the Foundation and Fill Soil

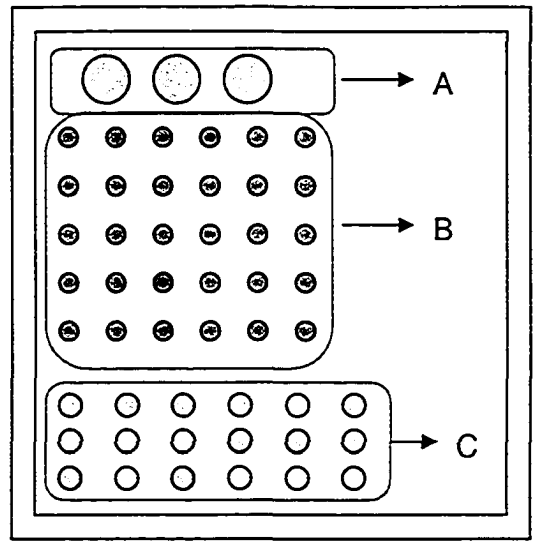

Figure 15. Front view of the connection box with different plugs; A=Thermocouples, B=EWR strain gauges, C=Bison strain gauges (number of plugs may vary for "B" and "C")

Bobey, L. W. M. (1988). "Soil-Geogrid Interfacial Shear Strength." M.Sc. thesis, Department of Civil Eng., University of Alberta, Edmonton, Alberta, 176 p.

Gabert, G. M. (1968). "The geology and hydrology of the surficial deposits in the Devon area, Alberta." B.Sc. Thesis, University of Alberta.

Hofmann, B. A. (1989). "Evaluation of the soil properties of the Devon test fill." M.Sc. thesis, Department of Civil Eng., University of Alberta, Edmonton, Alberta, 325 p.

Johnes, C. J. F. P. (1985). "Earth reinforcement and soil structures." Butterworth Advanced Series in Geotechnical Engineering, Butterworth and Co. (Publishers) Ltd.: 183.

Liu, Y. (1992). "Performance of Geogrid Reinforced Clay Slopes." PhD. Thesis, Civil Engineering Dept., University of Alberta, 406 p.

Liu, Y., Scott, J. D. and Sego, D.C. (1992). "Geogrid Reinforced Clay Slopes in a 12m High Test Fill." Geosynthetics Case Studies Book for North America, CGS, NAGS 2.

Chapter 3. Thermocouples

3.1. Introduction

Detailed observations of temperature in reinforced soil structures are rarely reported. This may be attributed to the fact that, over the usual temperature range associated with civil engineering structures, the stress-strain properties of steel reinforcement are not significantly affected. This can be contrasted with geotextiles whose properties may be affected over quite small temperature ranges (Murray and Farrar, 1988). In addition to that, the predominant factor influencing the aging of polymers appears to be temperature. The chemical reactions and physical reactions such as creep or structural change are accelerated as the temperature increases. Consequently a full and accurate knowledge of the insitu temperature is of major importance (Segrestin and Jailloux, 1988). Since the mechanical properties of the geogrid vary with temperature, to understand the effect of temperature variation on different types of geogrids and also on the measured strains with EWR strain gauges, a thermocouple was installed at the same location as EWR strain gauges inside the fill in order to measure the insitu temperature. These temperature variations were then multiplied by the coefficients of thermal expansion of geogrids to calculate the thermal strain induced in the geogrids by the temperature change within the test fill.

In this chapter the long term performance of the T-type thermocouples used in Devon test embankment are discussed by presenting the measurements carried out in 2003 and comparing them with the pattern of heat flow measured in 1990.

3.2. Literature review on temperature measurements in reinforced soil

In most reinforced soil projects using geosynthetic materials knowing the soil and geosynthetic temperature variation is a key point to better understand the behavior of the geosynthetic reinforcement material. Any comparison between the field and laboratory data of the load-strain-time behavior of polymeric materials must address the range of temperature over which the data are recorded. Fannin (1994) reviews the results of the temperature variation in a sloped reinforced soil wall with a 4.8 m height in Norway measured using thermistors placed in the backfill material at different elevations. The maximum and minimum soil temperatures that were recorded show a variation between –0.5°C and 18°C. This variation is attributed to seasonal changes in air temperature, which occurred over a period of five years. The upper part of the structure is reported to be warmest in summer and coolest in winter. The maximum values show a moderate decrease with distance from the face of the structure and indicate a thermal gradient in the soil that was not evident for the minimum temperatures. A mean annual temperature between 6°C and 8°C was recorded at all locations in the soil and is taken as the characteristic temperature influencing the behavior of the geogrid. Fannin (2000) discusses measurements from the same project and indicated that a sinusoidal relationship between soil temperature and time of year existed. A decrease occurs in the amplitude of seasonal temperature fluctuations, and a lag exists in the time to maximum amplitude, with increasing distance from the face of the structure. This behavior is similar to that reported by Murray and Farrar (1988) for a wall composed of concrete facing panels and metallic reinforcement and by Valestad (1996) for a steep slope with flexible facing units and geogrid reinforcement.

Segrestin and Jailloux (1988) studied a theoretical approach using one and two-dimensional calculations of the distribution and evolution of temperatures inside a soil mass, which was confirmed by in situ temperature measurements, recorded using thermocouples. This study reveals that soil temperatures are constant only at a great depth (more than about 10 m). At this depth it equals the average annual air atmospheric temperature for the geographical site. It also indicated that geogrid reinforcements in soil are subject to ongoing temperature variations and for those reinforcements used in retaining walls the temperature variation is greater near the wall face. The effect of the daily temperature variation combined with the effect of solar radiation is felt as deep as half a meter and it is in the zone behind the wall facing where the loads in the reinforcements are high. This study also shows that the reinforcement may be subject to large variations in temperature, and that the higher seasonal temperatures, although lasting only for a few months of the year, produce ageing much greater than deducted from the average yearly insitu temperature.

Murray and Farrar (1988) discussed the temperature distribution measured using thermocouples in a full-scale study of a reinforced earth retaining wall, 7.9 m high, over a seven-year period. In the paper it is mentioned that in order to avoid damage, the thermocouple leads were installed in a shallow trench excavated in the compacted layer of fill at the required level. Each thermocouple sensor was located about 30 cm to one side of the trench. The paper concludes that after an initial 3 months period, the temperatures within the reinforced fill followed an annual cyclic pattern. The walls facing north and at a depth of about 0.3 m had measured temperatures that were close to the ambient air temperature. With depth the amplitudes of the annual temperature cycles reduced and the time lag increased.

In another study by Buttry *et.al* (1996) thermistors were installed at different levels in a segmental retaining wall 3.5 m high in Wisconsin. It showed that the soil temperatures tracked the seasonal air temperature variations although there was a lag in the response time and temperature amplitudes were smaller in the soil than in the air. It was expected that the heat would flow from the deeper soil toward the surface during the colder months and that the soil would be warmer than the air. Conversely during the warmer months heat would flow from the surface into the soil and the soil would be cooler than the air.

Benson *et.al* (1996) also reported the measurements of temperature with type "T" thermocouples installed beneath the insulation liner in a landfill in southeastern Michigan. The temperatures at each thermocouple station were monitored with a data acquisition. Temperature measurements were made hourly at all thermocouple locations.

In another study by Brandon *et.al* (1996) in a geosynthetically stabilized secondary road test sections, type "T" thermocouples were also installed in the pavement subgrade layer at a depth of 15.2 cm below the surface. The thermocouple was placed in an excavated hole, and the subgrade material was backfilled and compacted over it. The construction of temperature sensors consisted of a twisted, welded pair of T-type thermocouple wire. After the wire pair was welded, the exposed end was surrounded by 0.64 cm (inside diameter) copper tubing. Approximately 8 months after the initial construction 15 out of 17 thermocouples were still functioning with a survivability of about 88%.

3.3. Description of thermocouples, readout device and connection box

The thermocouples used for this project were T-type thermocouple wires, which were coated wires of copper and constantan (copper and nickel). The copper wire is the positive lead and the constantan wire is the negative lead. The accuracy for this type of thermocouple is 1.0°C or 0.75% above 0°C (whichever is greater) and 1.0°C or 1.5% below 0°C (whichever is greater). This type of thermocouple can measure temperatures varying in the range of –270°C to 400°C. The thermocouples were installed at the location of each EWR strain gauge to measure the temperature inside the fill at that specific location. The readout device is a Fluke 2175A digital thermometer, which reads the temperature to the tenth of a degree Celsius. The thermocouple leads terminated in a connection box were also used to take the temperature readings.

3.4. Location and Method of installation

As mentioned before the thermocouples were installed at the location of the EWR strain gauges. In the Tensar reinforced bottom layer, 1 m from ground surface, the thermocouples were installed at 0.5 m, 1 m and with 1 m intervals up to 7 m from the slope face and another one at 8.5 m from the slope face. In the Tensar reinforced middle layer and top layer, 3 m and 5 m from ground surface respectively, the thermocouples were installed at 0.5 m, 1 m and with 1 m intervals up to 9 m from the slope face and another one at 10.5 m from the slope face. In the Signode and Paragrid reinforced sections at the bottom layer, 1 m from ground surface, the thermocouples were installed at 0.5 m, 1 m and with 1 m intervals up to 7 m from the slope face and two at 8.5 m and 10.5 m from the slope face. In the Signode and Paragrid reinforced sections in the middle and top layers, 3 m and 5 m from ground surface respectively, the

thermocouples were installed at 0.5 m, 1 m and with 1 m intervals up to 9 m from slope face and two at 10.5 m and 12 m from slope face.

The method used for installation of thermocouples in this project was as follows: (1) The thermocouple wires were cut to the same length and then the outer insulation that surrounds the wires are removed, (2) The insulation from each of the two wire ends were cut off about 10 mm and then the wires are twisted together, (3) The twisted end was then sealed and for the final insulation heat shrink FIT 300 was used; then this end was installed in its proper location adjacent to the EWR strain gauges, (4) the wire ends on the other side were cut as mentioned before and they were ready to be soldered onto the thermocouple plug, (5) the thermocouple plug can accommodate a maximum of 12 thermocouples; it has 24 metal connectors. Each of the connectors on the plug has a letter corresponding to that connector as shown in Figure 1, (6) the thermocouple readout box which was connected to the thermocouple plug on the connection box can read up to 12 thermocouples; each thermocouple is read in succession using the dial marked 1 to12, (7) Table 1 shows the letters on the thermocouple plug that correspond to each dial number on the thermocouple readout box; each dial number has two corresponding letters, i.e. if a thermocouple wire pair are soldered on letters J and K of the thermocouple plug, then the temperature will be read on dial 5 on the thermocouple readout box, (8) the thermocouple plug was then mounted in the thermocouple plug holder, and then the holder was fixed to the electrical board.

3.5. State of Instruments in 2003

The same readout box was used as for previous readings. The readout connection boxes for the three reinforced sections were covered with soil from surface sloughing. Figures 2, 3 and 4 illustrate a view of the

northeast, northwest and southeast-reinforced slopes respectively in 2003 with buried connection boxes. The connection boxes had shifted and moved with the soil movements but almost all the cable connections from the thermocouples to the connection box were functioning properly. Only some soil removal and cleanup was carried out around the connection boxes with a backhoe and shovel and all the connection plugs were cleaned with a brush and washed to make a good connection between the plug and the connector. Figures 5, 6 and 7 show the condition of the northeast, northwest and southeast readout boxes after cleaning and removing the surrounding soil.

The readout device could also measure the surrounding air temperature, which is a good indication of the proper functioning of the readout device.

3.6. Previous Readings

Each time that the EWR strain gauges were read the thermocouples were also read to measure the insitu temperature at EWR strain gauge locations. At each reinforced section after installing the geogrid and thermocouples, the temperatures along the geogrid were measured and considered as the initial temperatures; then for calculation of the temperature induced strains, the temperature difference from the initial temperature was calculated and multiplied by the thermal expansion coefficient of the geogrids. The initial temperatures at the time of geogrid installation for different layers were as follows: Tensar bottom layer, 11.3°C at 23 September,1986; Tensar middle layer, 17.2°C at 1 September, 1987; Tensar top layer, 8°C at 23 October, 1987; Signode bottom layer, 12.9°C at 23 September, 1986; Signode middle layer, 15.8°C at 4 August, 1987; Signode top layer, 5°C at 23 October, 1987; Paragrid bottom layer, 11.3°C at 24 September, 1986; Paragrid middle layer, 12.6°C at 22 August, 1987 and Paragrid top layer, 2°C at 14 October, 1987.

As a sample, Figures 8, 9 and 10 show the temperature variation along the Tensar middle layer during different reading times in 1987, 1988 and 1989 respectively. Figure 8 illustrates the temperature variation at 4 different reading times after installation of the geogrid layer. As the fill height increases and more fill is placed over the geogrid layer the temperature variation decreases and the temperature reaches a constant value at some distance from the slope face. The two last readings show that the ambient temperature is lower than the temperature inside the fill so the heat flows outward. The first four plots in Figure 9 measured in May, June, August and September 1988 show that the heat flow is from outside inward, because the outside temperature is warmer than the temperature inside of the fill but this trend changes during the fall and winter. In November 1988 as the temperature gets cooler the heat flow changes its direction and it flows from inside of the fill with higher temperatures towards the outside of the slope. Also it can be observed that deep within the fill, at 10.5 m from slope face, the temperature variation at different times is considerable. This might be because of the low height of fill material placed over the geogrid layer, but as the fill height increases and more fill is placed, it acts like an insulation material and reduces the heat exchange between the geogrid and the outside temperature, which is shown in Figure 10. In this figure the temperature inside the fill is almost unchanged during all measurements. In this Figure different trend of temperature variation along the geogrid for various times exists because of the variation in heat flow discussed for Figure 8.

3.7.2003 Readings

Figure 11 shows the temperature variation along the same grid layer in 1990 and 2003. A temperature variation of around 5°C at the end of the grid, 10.5m from slope face, exists which shows that the temperature at

this location has changed during this period. The same pattern of heat flow with different warm and cool readings can be observed. The same plots for other geogrids at different elevations and different times are presented in Appendix A.

3.8. Summary and Conclusions

In general the recovery of the temperature measuring system at Devon test fill was successful. The readout device, connection boxes and thermocouples all have functioned properly since their installation time. Only two thermocouples out of 97 failed which gives a survival rate of about 98% and shows that the installation procedure for these thermocouples was successful. The plots of temperature variation along geogrids at different elevations and different times also show that the heat flow inside the test embankment changes its direction at different times based on cool and warm temperature outside of the fill. When the outside temperatures are cool the temperature inside the fill causes heat flow towards the outside. But in warmer seasons the heat flow is from outside towards inside of the fill. The temperature variation close to the slope face is high and gets less as the distance from the slope face increases towards inside of the fill and far within the fill it reaches a steady state temperature where there is almost no temperature change along the geogrid. This distance differs because of the amount of fill over the thermocouple acting as an insulating material and also the temperature at that time of the year. Figure 12 shows the maximum variation of temperature along the geogrid layers versus distance from the slope face. As the distance into the slope increases the maximum variation of temperature along the geogrid layer decreases. It is maximum close to the slope face because of the high temperature exchange between the air and the fill and as the distance into the fill increases the fill acts as insulation and reduces the temperature exchange and heat transfer between air and

the fill soil at that location. But still some 4°C to 5°C maximum temperature variation is observed from about 6 m from the slope face up to 12 m from the slope face.

Figure 13 presents the approximate time lag of temperature change in days versus distance from the slope face. It is confirmed that as the distance from the slope face increases the time required for temperature change based on air temperature variations is increased. This time lag is about 25 days at 1 m from the slope face and reaches about 210 days at 10.5 m from the slope face.

Table 1.Corresponding thermocouple plug letters to dial numbers on temperature readout box

Dial # on Readout Box	Corresponding plug letters
1	A , B
2	C , D
3	E , F
4	G , H
5	J , K
6	L , M
7	N , P
8	Q , R
9	S , T
10	U , V
11	W , X
12	Y , Z

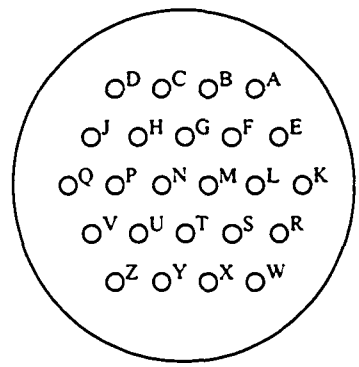

Figure 1. Back view of thermocouple plug

Figure 2. North-East section of test fill before cleanup

Figure 3.North-West section before cleanup

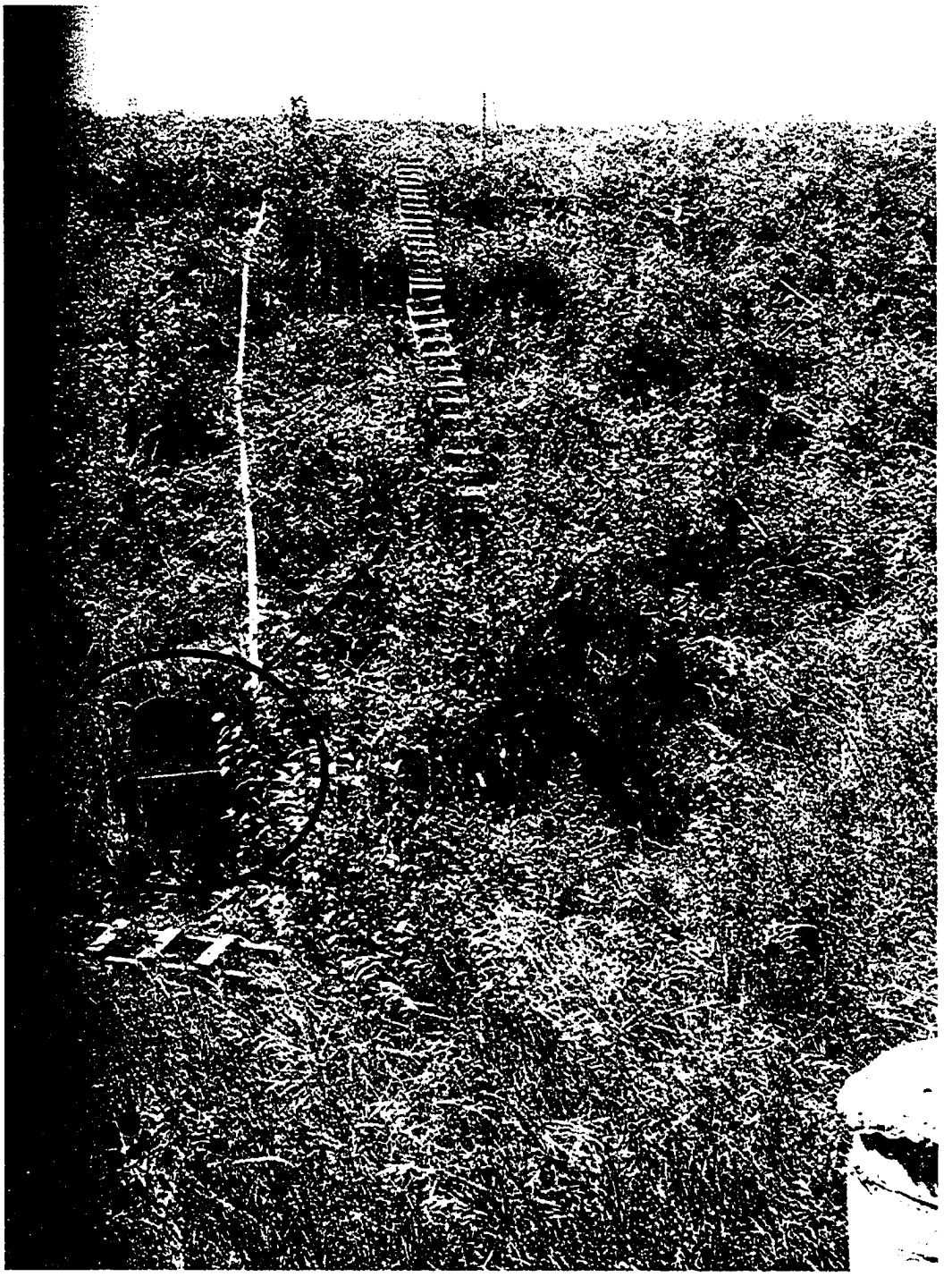

Figure 4.South-East section before cleanup

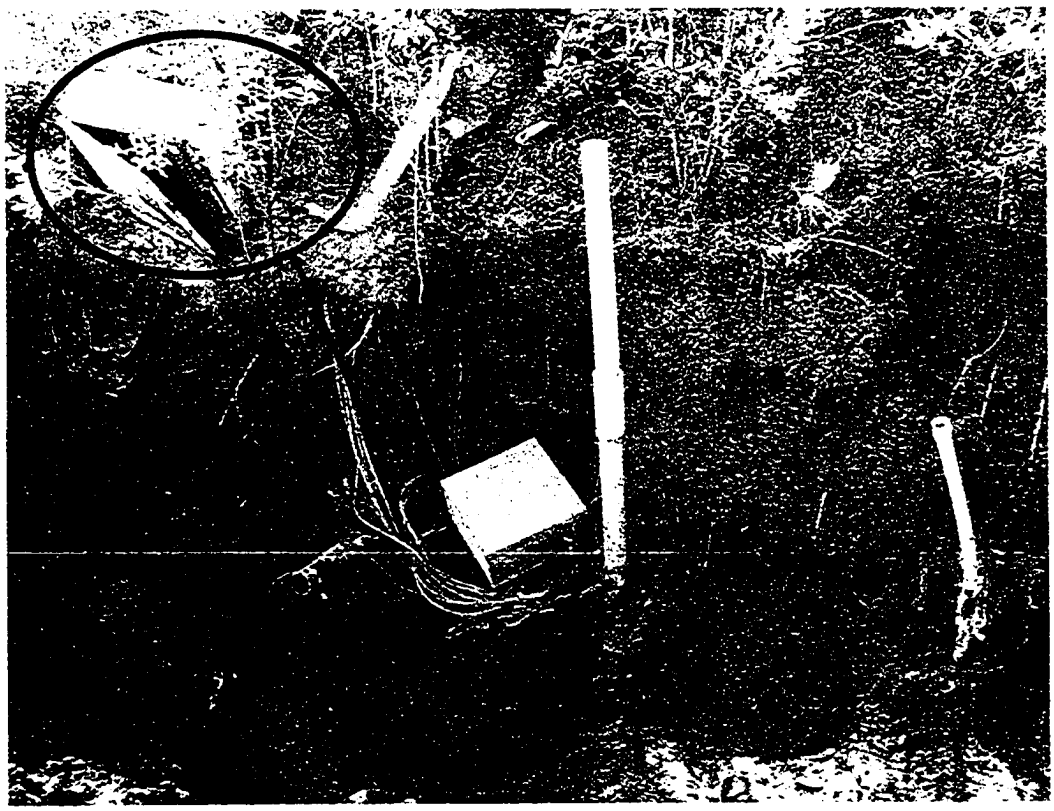

Figure 5.North-East section after cleanup

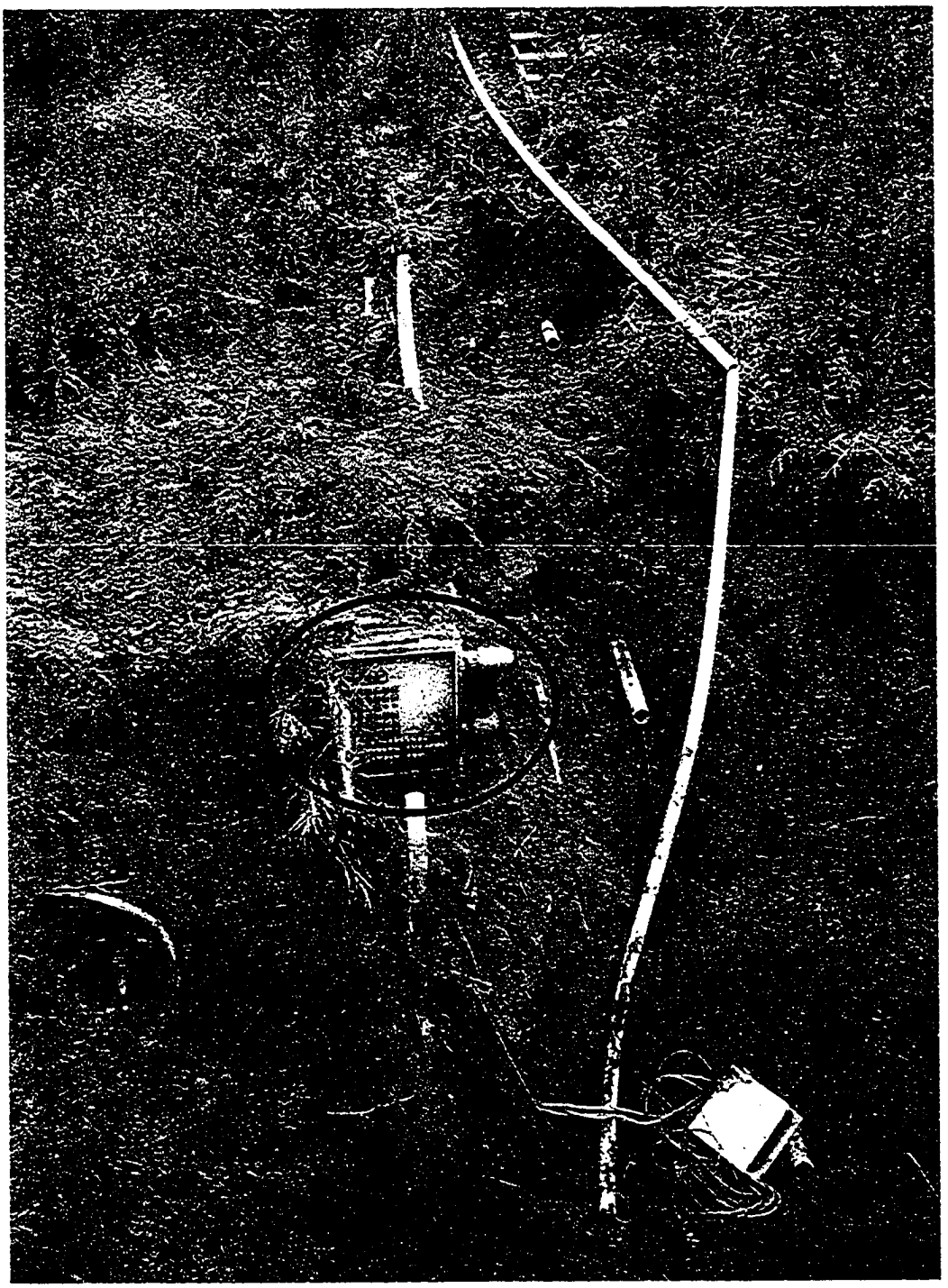

Figure 6.North-West section after cleanup

Figure 7.South-East section after cleanup

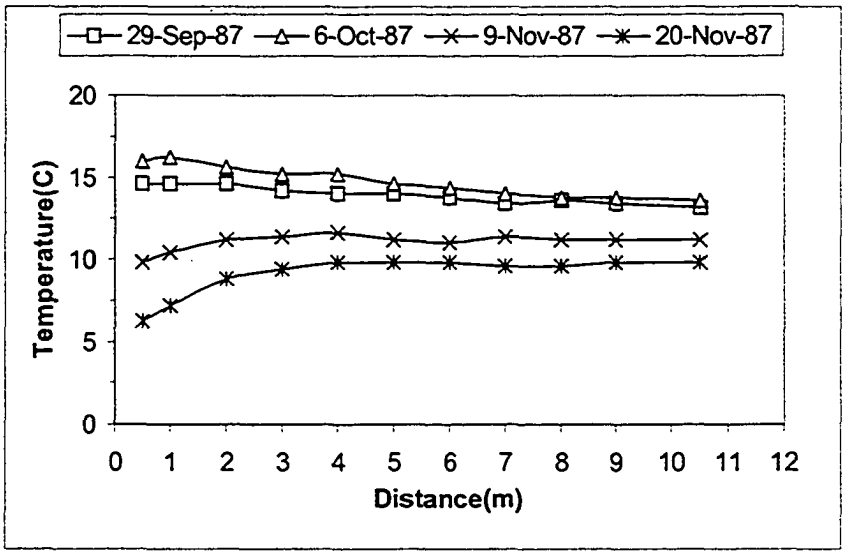

Figure 8. Temperature variation with time and distance, Tensar middle layer, 1987

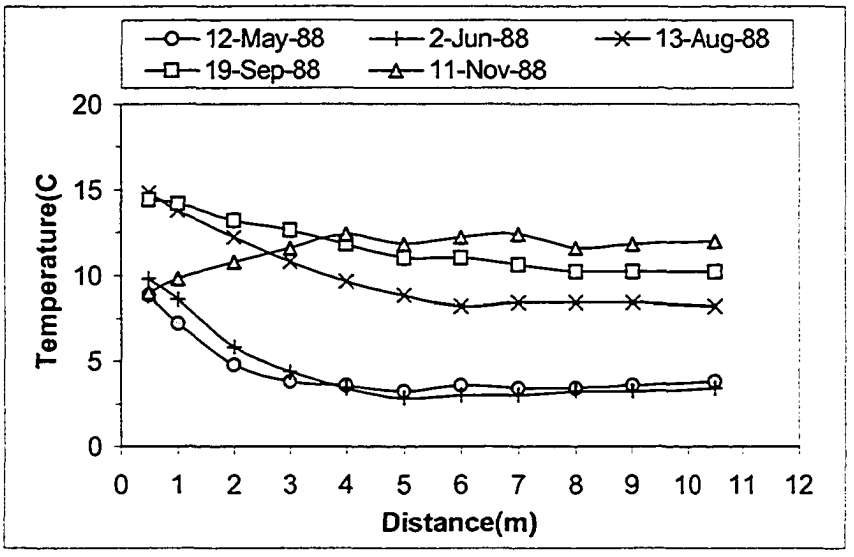

Figure 9.Temperature variation with time and distance, Tensar middle layer, 1988

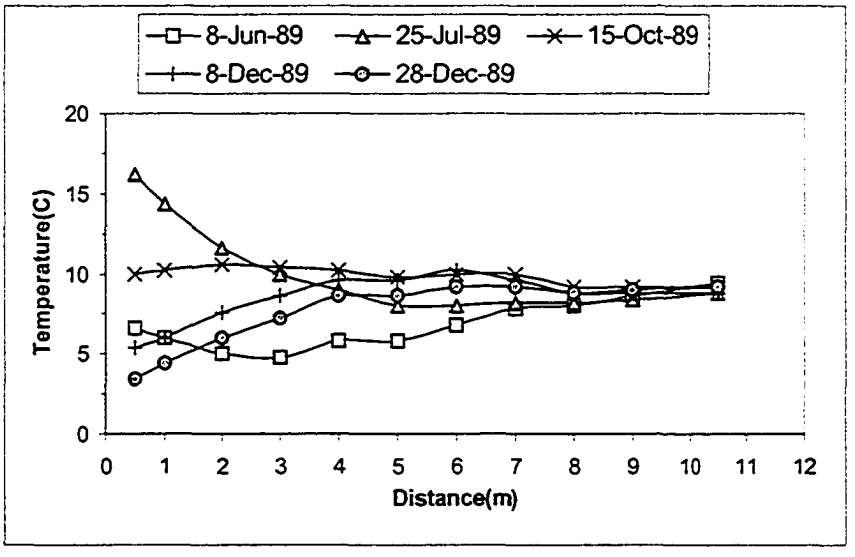

Figure 10.Temperature variation with time and distance, Tensar middle layer, 1989

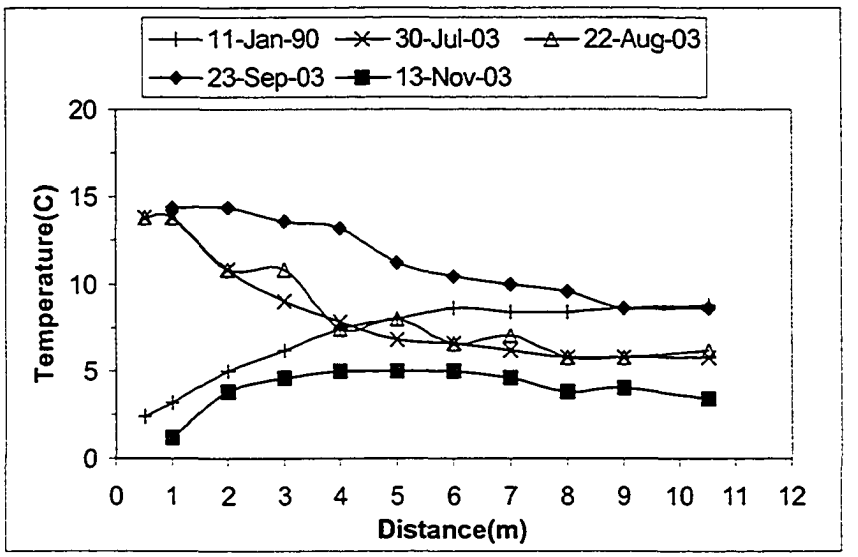

Figure 11.Temperature variation with time and distance, Tensar middle layer, 1990 and 2003

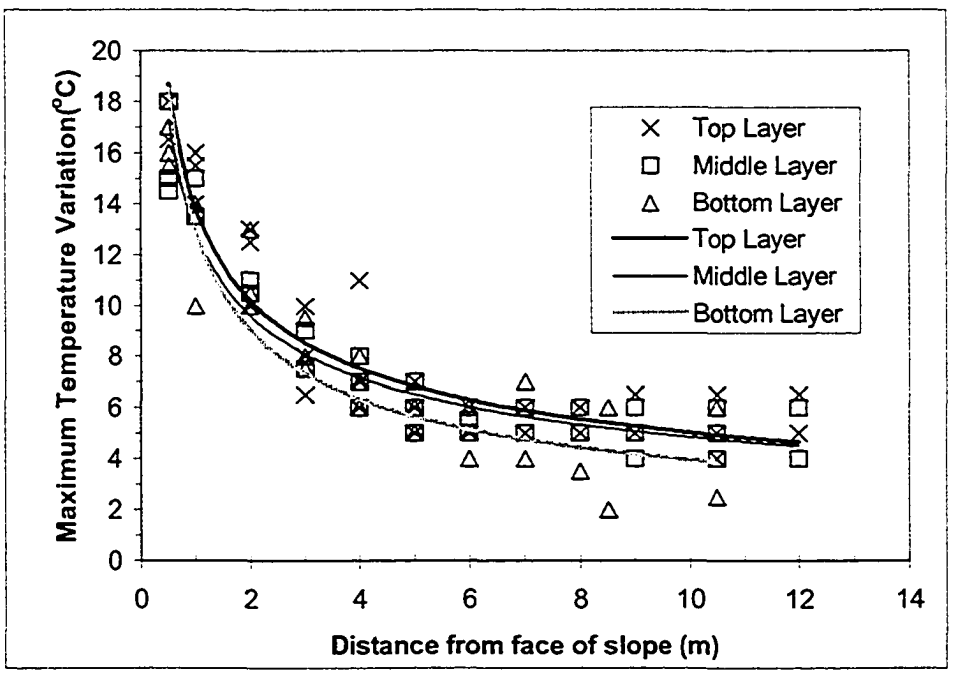

Figure 12.Maximum temperature variation along geogrids

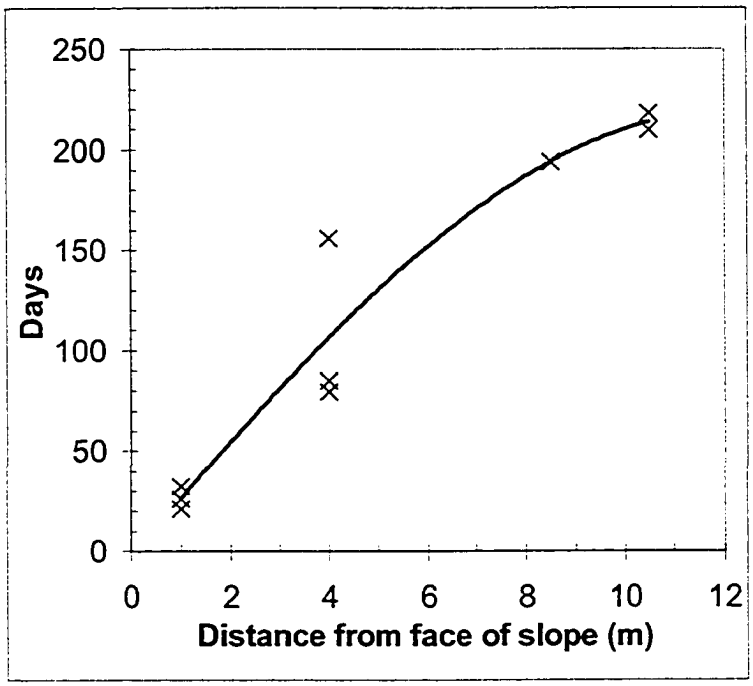

Figure 13.Time lag of temperature change

Benson, C.H., Olson, M.A. and Bergstorm, W.R. (1996). "Temperatures of Insulated Landfill Liner", Transportation Research Record, No.1534, pp.24-31.

Brandon, T.L., Al-Qadi, I.M., Lacina, B.A. and Bhutta, S.A. (1996). "Construction and Instrumentation of Geosynthetically Stabilized Secondary Road Test Sections", Transportation Research Record, No.1534, pp.50-57.

Buttry, K.E., McCullough, E.S. and Wetzel, R.A. (1996). "Temperatures and Related Behavior in Segmental Retaining Wall System", Transportation Research Record, No.1534, pp.19-23.

Fannin, R. J. (1994). "Field Observations on the Load-Strain Time Behavior of Geogrid Reinforcement." Canadian Geotechnical Journal, Vol.31, No.4, pp.564-569.

Fannin, R. J. (2000). "Long-Term Variation of Force and Strain in a Steep Geogrid-Reinforced Soil Slope." Geosynthetics International, Vol.8, No.1, pp.81-96.

Liu, Y. (1992). "Performance of Geogrid Reinforced Clay Slopes." PhD. Thesis, University of Alberta: 406.

Murray, R.T. and Farrar, D.M. (1988). "Temperature Distribution in Reinforced Soil Retaining Walls", Geotextiles and Geomembranes, Vol.7, No.1, pp.33-50.

Segrestin, P. and Jailloux, J.M. (1988). "Temperature in Soils and Its Effect on the Ageing of Synthetic Materials." Geotextiles and Geomembranes, Vol.7, Nos.1&2, pp.51-69.

Valestad, J. (1996). "Long-Term Behavior of a 13 m High Reinforced Steep Slope", Geosynthetics: application, design and construction, de Groot, M.B., den Hoedt, G., and Termaat, R.J., Editors, Balkema, Proceedings of the First European Geosynthetics Conference EUROGEO 1, Maastricht, Netherlands, Sep. 1996, pp.399-404.

Chapter 4. Strain Gauges on Geogrids

4.1 Introduction

In order to monitor the performance of the Devon test embankment extensive field instrumentation was used. Electrical Wire Resistance (EWR) strain gauges and inductance coils (Bison strain gauges) were used in the Devon test embankment to measure the strains developed in the geogrids. The EWR strain gauges were glued to the longitudinal members of the geogrids placed in the test embankment. The EWR strain gauge measurements in 2003 and the long term performance of the gauges are discussed in this chapter. Bison inductance coil strain gauges were fastened to the geogrids to measure global strains. Readings on these gauges up to 1990 are presented. Since the readout device did not work during the 2003 field investigation, no measurements could be carried out. The field correlation between the EWR strain gauges and the Bison strain gauges up to 1990 is presented.

4.2 Literature review on EWR strain gauges installed on polymeric material

Use of EWR strain gauges for measuring strains and equivalent stresses in geogrid members are quite common. Fishman *et.al* (1993) discusses the field behavior of an instrumented geogrid soil reinforced wall with height of 4.72 m in which Tensar SR2 geogrids were used as reinforcement. Resistance strain gauges and inductance coils were fastened to geogrid reinforcement to measure the strains therein at different depths inside the wall and also different elevations. Instrument readings were taken during construction of the wall and at intervals throughout a period of one year after the construction of the wall. Temperature compensation was provided for resistance strain gauges and

no significant or consistent fluctuations with temperature variation throughout the year were observed. Creep effects were not apparent for 1-year period during which readings were taken. The effects of creep may have been masked by temperature effects. However, the level of tension in the geogrids may be low enough so that creep effects can be insignificant. Strains induced by compaction during the construction were not included and the strains presented are only the strains resulted by the subsequent placement of lifts over the geogrids after compaction of the first lift. The results indicated that the tensile strains in the geogrids were in the range of 0.3% to 0.8%, corresponding to 3.28 to 8.75 kN/m load in the geogrids. Comparing this load to the maximum tensile strength of the geogrids, which was 79 kN/m, the grids were only loaded to between 4% and 11% of the ultimate strength. At this low load level, significant creep was not expected. Based on the design equation used in this project, the maximum tensile forces in the geogrids were calculated, which was then converted to strains. Computed maximum strains were compared with measured maximum strains in the geogrids. It appeared that the process of compaction did not induce some additional strain; roughly between 0.1% and 0.2%. Results presented for geogrids located at the lower elevations of 0.15 and 0.46m showed that the strain measurements taken during the early stages of construction when the height of fill over the grids was low were relatively close to those predicted by the design formula. As construction proceeded and the height of fill over geogrid layers increased, strains predicted by the design methods were higher than from measurements. Results for geogrids located at higher elevations showed that the measurements were in good agreement with predicted strains throughout the construction process, indicating closer agreement.

Bonaparte *et.al* (1989) reported use of reinforced soil buttress to stabilize a high natural slope with a height of about 34 m. The soil buttress was built using compacted onsite fill (primarily shale) reinforced with layers of

Tensar UX1600 uniaxial geogrid. Geogrid strains were measured at three elevations in the fill. At each elevation, strain gauges were placed on both the top and bottom sides of the geogrids to evaluate not only extension, but also bending. There was no clear indication of geogrid bending from the strain gauge results. Measured strains were low, with the maximum strain less than 0.4%, and the average strain in the range of 0.2%, or less. From the results, it appeared that most of the strain occurred during the construction stages. The reported measurements cover about a year since starting the construction, which was also about 7 month after the end of construction.

Kenneth *et.al* (1996) discussed the behavior of a 3.5 m high segmental retaining wall which was reinforced with three different geosynthetic materials: geotextile, rigid geogrid and flexible geogrid. Foil strain gauges were bonded to the ribs of rigid geogrid. Two gauges were mounted at each location, one on the top of the rib and the other on the bottom. In this pattern the strains due to bending canceled, and the gauges measured axial deformation. Seven gauge locations were installed originally but after 5 years following construction only six were still working. Calibration of the strain gauge system was done in the laboratory. The geogrid specimen used was 480 mm long and included four junctions and three sets of ribs, and the width was 188 mm and included nine ribs. Gauges were mounted on the top and bottom of the center rib to match the field installation. The specimen was loaded in tension, and gauge readings, which represent localized strain in the ribs, were recorded. At the same time corresponding determinations of average strain over a repeating length of one rib and one junction were made. The strains in the geogrid increased as the wall height increased during construction. At the end of construction in December 1993 the strain readings leveled out and remained constant or increased slowly over a period of 6 months. In April 1994 strain readings increased significantly at all 6 gauge locations and continued increasing

through the summer months and into October 1994. During this same period the normal force between facing units decreased significantly. Also during this period the wall facing moved outward approximately 2 mm. These 3 observations-geogrid strain increases, a reduction in normal force between facing units and outward movement of the wall- all indicated that the backfill was moving and settling to reach a more stable condition. These processes appeared to have been initiated in April during the spring thaw, when any ice in the backfill was melting and the soil may had been temporarily wet. Average strains recorded since the beginning of the project vary from 0.25% to 0.45%, which were equivalent to 4.6 and 8.2 mm of elongation in the embedded geogrid length of 1.83 m. These compared favorably with the measured horizontal wall movements of 2 to 9 mm.

In another study by Brandon *et.al* (1996) in geosynthetically stabilized secondary road test sections where geotextiles and geogrids were placed on top of the subgrade layer, the pavement test sections were heavily instrumented. Strain gauges were installed directly on the geogrid and geotextile. Measurements Group foil-type strain gauges were used to monitor the changes in horizontal strain at the bottom of the geotextile. The foil strain gauges, 10.2 cm in length, were attached to the underside of the geotextile along the gauge lengths with Measurement Group M-Bond epoxy-type adhesive. A layer of Teflon tape was secured over the gauge assembly. The gauges were then coated with Measurements Group J-2 protective coating over the Teflon type; this was followed by a layer of aluminum foil and then RTV silicon to protect the gauge assembly from environment effects. The aluminum foil was placed wrinkled to accommodate any extension that might occur in the geosynthetics. The use of aluminum foil and Teflon type would minimize potential hard spots that may develop on the gauge assembly.

Texas Measurements foil-type strain gauges were used to monitor the changes in horizontal strain at the bottom of the geogrid. These strain gauges consisted of a foil-type strain gauge 2.5 cm long with three lead wires. The foil strain gauges were attached to the underside of the geogrid and were protected in the same manner as the geotextile strain gauges. Calibration factors for the strain gauges installed on the geosynthetics were provided by the manufacturer and were verified through tensile strength testing of instrumented geosynthetic samples. Approximately 8 months after the initial construction the geotextile strain gauges had a survivability rate of 6% with 1 gauge functioning out of 18 gauges and for geogrid strain gauges, 28% with 5 gauges functioned out of 18 gauges.

Bartlett et.al (2001) discusses the strain gauge attachment to geotextiles being used to reinforce the embankments and MSE walls for a reconstruction project. High strength woven geotextile was used to improve the global stability of some embankment and wall systems during rapid, undrained loading conditions. In some locales as many as three layers of geotextile (730 kN/m ultimate strength; 292 kN/m allowable strength) were used to guard against development of shear failure in the foundation. Laboratory tests showed that the high-strength geotextile fabric would fail at approximately 15% strain. Final embankment heights and geometries were designed to limit the strain developed in the geotextile layers to about 5% allowable strain. In the instrumented areas only about 2% strain developed in the geotextile at a final height of 16 m, suggesting that not all the allowable strain in the geotextile had been fully mobilized. As a result of these favorable data, the geotextile reinforcement in subsequent design and installation was reduced by about 33%.

In a comprehensive study by Bathurst *et.al* (2001) full-scale performance testing of reinforced soil retaining walls were studied through heavily instrumented reinforced soil segmental retaining walls. The modular facing

units were a solid masonry block with a continuous concrete shear key. An extruded biaxial polypropylene (PP) geogrid reinforcement was used in walls 1 to 4 and wall 5 incorporated a knitted uniaxial PVC-coated polyester (PET) geogrid. Each layer of reinforcement had a total length of 2.52 m measured from the front of the facing. The PP geogrid used in the tests had the advantage that it could be easily instrumented using foil strain gauges bonded directly to the surface of the longitudinal members. Bonding the strain gauges to the PET geogrid was accomplished using a special technique developed at RMCC. For measurement redundancy, strain gauges were attached at nominally identical distances behind the facing column on different parallel longitudinal members of the reinforcement. Experience has shown that the local strain recorded by the strain gauges may not be the same value as the average strain recorded over a gauge length that captures many geogrid apertures (Bathurst 1991, Bathurst and Allen 2002). Hence each combination of gauge type, bonding method and geogrid type must be individually calibrated in order to determine the relationship between local strain and global strain using in-isolation index tensile and creep tests. This is particularly important since reinforcement tensile forces inferred from strain readings must be global values for back analysis purposes. The strain gauge measurements showed that the strains were generally low (less than 1%) but that they are nevertheless, largest at the connections and tend to dissipate rapidly along the length of the reinforcement. The peak strain occurred in a reinforcement layer, which was at an elevation corresponding to about ½ the total height of the wall, 3.6 m. Also a relatively large jump in the magnitudes of strain could be seen during the application of surcharge load. The multiple peaks in the distribution of reinforcement strains in some results during surcharge load might be due to retrogressive failure of the soil in the active zone (i.e. a family of failure surfaces propagating down and back into the reinforced soil zone with increasing surcharge load).

Wu and Helwany (1996) studied a performance test for assessment of long-term creep behavior of soil-geosynthetic composites. They developed a special test configuration and loading mechanism and used a polypropylene heat-bonded non-woven geotextile to reinforce the soil mass inside the testing apparatus. The soil confines the geotextile at both the top and the bottom. Upon the application of a sustained vertical surcharge to the top surface of the reinforced soil unit, the geosynthetic reinforcement and its confining soil will deform interactively over time. Thus there will be a reciprocated restraining effect on deformation between the geosynthetic reinforcement and the soil. To monitor the behavior of the long-term performance tests, high elongation strain gauges were used to measure the strain distribution along the geotextile. In these tests only the ends of each strain gauge were glued to the geotextile to avoid local stiffening of the geotextile by the adhesive (Billiard and Wu, 1991). For the clay-backfill test, the strain gauges were covered with a mixture of wax and petroleum jelly to protect the gauges from soil moisture. The wax and petroleum jelly mixture was very flexible and nearly impermeable. To evaluate the validity of this procedure, a uniaxial tension test was performed on a 305 mm by 51 mm geotextile specimen on which five strain gauges were mounted and covered with the protective mixture. The gauge factors determined from these strain gauges were nearly identical to those without the protective mixture. A total of 15 strain gauges were mounted on the geotextile along its length in the sand-backfill test, whereas 10 strain gauges were used in the clay-backfill test. In both tests the strain gauges were mounted on the geotextile along its length in two parallel lines to provide redundant strain gauge readings. The final results of the tests showed that although the initial responses of the two sets were comparable (3.5% and 4.0% strains at the center of the geotextile; 1.0% and 1.3% near the extremities of the geotextile, for the sand-backfill test and second-stage clay-backfill tests respectively), subsequent time-

dependent deformation of the two tests was very different. The time dependant deformation of the confining soil played a very important role in the long-term creep behavior of the geotextile, indicating that it can be misleading to evaluate the long-term creep potential of a GRS structure based on the results of element creep tests performed on the geotextile alone. In the sand-backfill test, the soil had a tendency to deform at a slower rate than the geotextile and the element creep test overestimated the strain by a factor approximately 4 at the time equal to 30 days. On the other hand in the clay-backfill test the soil had a tendency to deform at a faster rate than the geotextile and the element creep test underestimated the strain by a factor of about 2.5 at the time equal to about 2 days.

In a study by Toriihara *et.al* (1994) on the construction of a final deposition site of general waste, an embankment which consists of a fill dam with a height of 15 m, length of 150 m and width of 120 m and a steep slope embankment 25 m high with a slope ratio of 1:1. Uniaxial geogrids were used as the reinforcing material with a length of approximately 10 m with 1 m vertical spacing. Measurements of tensile strain distribution of geogrids were implemented on the two sections of the project. Two or three layers of the geogrids in the whole height of the embankment were instrumented and along each seven strain gauges were installed. Measurements were carried out once a day during construction once a week after completion of the embankment. Tensile strain distribution was angular and the maximum tensile lines by connecting the peaks comparatively match with the slip surface that is the minimum safety factor according to circular slip calculation without reinforcing material. The maximum strain measured was about 0.3% but when converted into stress it becomes about 14% of the permissible tensile strength of 21.6 kN/m in the geogrid taking creep into consideration. Generally tensile strains increased as the as the height of embankment increased after laying. It might be noted that with exception to some gauges, the strain

settled close to a fixed value with in a comparatively early stages. Tensile strains near the slope actually tended to decrease as the construction of the embankment progresses to a certain extent. This tendency was also observed from other reinforcing material for measurement purposes and was believed to be due to settling of the embankment from the weight of the upper fill and slight loosening of the geogrid on the slope portion.

A major research project on the behavior of reinforced soil was sponsored by the United States Department of Transportation, Federal Highway Administration (FHWA) to develop comprehensive guidelines for evaluating and using soil reinforcement techniques in the construction of retaining walls, cut slopes and roadway embankments. Part of the results of this study was reported by Christopher *et.al* (1994). The field portion of the project consisted of constructing eight reinforced soil walls, each 10.7 m long and 6.1 m high, and four reinforced soil steep slopes, each 15 m long and 7.6 m high. The walls and slopes were heavily instrumented so that their performance could be evaluated in terms of the design model. Reinforcements selected were representative of the generic reinforcement types in use at the time of the study. Specifically they were: metal strips, metal grids, polymeric geogrids, woven geotextiles and non-woven geotextiles. Three types of soil were selected for the structures to represent the range of backfill material recommended by FHWA. The gravely sand, silt and cobbles were used as backfill material. Field performance of the structures was evaluated from the instrumentation installed in them. The locations of the instruments were based on the anticipated stress distribution and deformation response of a reinforced soil structure. Gauges were concentrated across zones of anticipated maximum stress. Bonded resistance gauges glued to the reinforcements were used to measure local reinforcement strain. Each measurement point consisted of two gauges, one mounted on the top and the other on the bottom of each reinforcement. Each gauge was read independently to

evaluate possible bending and for redundancy. For extensible reinforcements, gauge selection was based on tension-strain calibration tests using both unconfined wide strip tension tests and in-soil pullout tests. For the wide strip test, the strain in the extensible reinforcements, as measured with extensometers over the clamped length, was compared to the strain gauge measurements. Before final selection gauges and adhesives were modified until a match in strain response was obtained. The in-soil strain response was then evaluated by performing pullout tests with the selected gauges installed on the reinforcement. Bonded resistance gauge type 6/120 LY61 from Hottinger-Baldwin and M-Bond 200 adhesive from Micro Measurements Inc. were used for gauges installed on ribbed metal strips, extruded geogrid, welded strand geogrid and bar mat. Hottinger-Baldwin type 10/120 LD20 gauges and AE15 adhesive from Micro Measurements were used on non-woven geotextile, welded strand geogrid and woven geotextile. In most cases the gauges were bonded directly to the reinforcement. All gauges were double sealed with highly extensible bonding and water proofing sulfide sealants prior to transportation to the field site. Special application procedures were developed for gauging the non-woven geotextile materials to reduce the influence of the gauge on the elongation of the parent material. In this method small metal tabs were first glued to the ends of the strain gauge. The tabs were then glued to the geotextile. The strain gauge area was therefore not directly attached to the reinforcement reducing the potential for the glue and the gauge to stiffen the geotextile. The output strain was a measure of the relative movement between the two attached points. Initial readings were taken when the gauged reinforcement was in place with some backfill (one layer or less before compaction) providing anchoring. As anticipated, the reinforcement strains indicated a relationship between reinforcement stiffness and the magnitude of the maximum tension in the reinforcement. The location of peak strains was somewhat distorted by anomalies in gauge readings (i.e. the malfunction of a single gauge point

had a significant influence on the peak strain location). Even so, the data tended to support a log spiral distribution of the peak strains. Distortion of the data was somewhat overcome in the evaluation of tension in the reinforcement by using the incremental strain values and correcting the measurements for obvious anomalies. The results for the embankment slopes showed that the magnitude of measured strains in both the 1H:1V slopes and the 1H:2V slopes respectively were similar for the geogrid and geotextile reinforcements. The maximum strains were on the order of 0.7% for both materials in the 1H:2V slopes and 0.3% for the flatter 1H:1V slopes. This was somehow anticipated as the modulii of the geogrid and geotextile reinforcement was similar. The location of peak strains measured in each slope reinforcement layer showed that the locus of peak strains fell very close to the critical surface (surface of maximum reinforcement tension) defined by the rotational stability method used in the design. The results also tended to confirm that the location of peak strains were further from the face for the flatter slopes as was predicted by the rotational stability method.

Zanzinger and Gartung (1992) executed a model test on a sand-geogrid-wall with a face inclined at 85° height 3.7 m, length 2.8 m and depth of model 4.3 m. The well-compacted sand was reinforced by 7 layers of PVC-coated PET-grid-fabric. The retaining structure was loaded to failure under earth pressure induced by a strip footing. The extensive internal and external instrumentation gave a complete record of the deformation and load bearing behavior of the model throughout the test. The geogrid consists of a woven polyester-yarn fabric (PET) coated by PVC. The PVC coating protects the high-strength PET-fibers against chemical, biological and other environmental influences, it fixes the knots where wrap and weft yarns are crossing, and it facilitates handling and installation of the geogrid without mechanical damage to the sensitive PET-fibers. The tensile strength of the geogrid is 64.7 kN/m in wrap and 32.4 kN/m in weft

direction at failure strains of 12.9% and 12.2% respectively. Thirty strain gauges were attached to the PVC-surface of the geogrid. Previous investigations had shown that the strain of the PET-strings could be measured correctly in this way. So the tensile forces within the geogrid layers could be deducted directly from the strain gauge measurements, which were fed into a computer like other electrical signals. After placement and compaction of the bottom layer of sand of 50cm thickness, the first geogrid with strain gauges attached to it was installed. Sand filled jute sacks were used to form the face of the retaining structure. The sand layer of 51 cm thickness was placed in two lifts and compacted by a vibrating steel plate. The anchoring part of the geogrid of 1.3 m length was carefully wrapped around the jute sacks. Three loading cycles were carried out: 200 kN, 800 kN and 1450 kN, which brought the system to failure. From strain measurements and distributions at different levels and locations the failure surface was sketched and it agreed very well with the assumptions made for the limit state analysis based on the kinematical element method of two rigid blocks. As one might expect, the geogrid reinforcements experienced only very small strains arrest horizontal earth pressure conditions (less than 0.1%) but during yielding of the structure, near the failure zone on the geogrid, the measured maximum strain of 1.2% was observed.

In order to better understand the behavior of reinforced structures and the development of slip surfaces and the tensile forces acting in the reinforcements, a vertical retaining wall, 4 m high and 10 m long was constructed by reinforcing the back fill with geogrids. Data related to reinforcement strains and loads are reported by Carrubba *et.al* (1999). The wall was built using two different reinforcement geogrids. One section was 5 m in width and was reinforced with high-density polyethylene (HDPE) uniaxial oriented extruded geogrids. The second section was also 5 m in width and was reinforced with polypropylene (PP) biaxially oriented

extruded geogrids. Since geogrids with different strengths were used in the designs, the vertical spacing and reinforcement lengths of two sections were different. HDPE geogrids were each 2 m long and were installed at 0, 1.3 and 2.9 m elevation. PP geogrids were each 2.4 m long and were installed at 0, 0.8 and 2.4 m elevation. The fill soil (clayey gravel) was compacted in layers of 0.3 m thick using a vibrating roller (80 kN). The geogrids were instrumented with self-temperature compensated strain gauges length of 5 mm and a maximum strain of 10% with a measurement accuracy of 0.5%. The strain gauges were glued to the geogrid ribs with cyanoacrylate adhesive using a multi-step method. This procedure allows the measurement of geogrid strains up to 10%, over a period in excess of two years and during freezing temperatures. Ten strain gauges were installed on each reinforcement layer at a spacing of about 0.2 m. The strain gauges were protected with silicon rubber and with a 0.10m-thick sand layer. The effectiveness of this procedure had been demonstrated by the low mortality rate of the sensors (only one out of 63 sensors malfunctioned). The electrical connection was made using a three wires Wheatstone quarter bridge. The strain gauges were connected to an automatic data acquisition unit, which was capable of recording up to 100 sensors every 15 minutes. The actual recording frequency was reduced to once per day after the construction was completed. Additional specimens of geogrids instrumented with strain gauges, were prepared and tested in the laboratory to provide a basis for calibration and correlation between strain and tensile stress. The development of tensile strain over time was presented in the paper for the geogrid layers. The maximum tensile strain achieved in each reinforcing layer indicated the location where tension was the greatest. Using this information, the location of the internal failure plan can be identified. The two slip surfaces obtained by this analysis were compared with the failure surfaces considered in the design step. This comparison indicated that the reinforcing layers were stressed in a different way. The actual mechanism of failure for HDPE geogrid was

pullout as indicated by low values of measured tensile strains (0.6-1.6%) and the actual failure mechanism for PP geogrid was tensile stress in the upper reinforcing layer as indicated by the high tensile strains measured (about 4.0%).

Montanelli *et.al* (1999) discusses a 15 m high vegetated face reinforced slope, which was built in 1996 to stabilize a landslide situated on the Montone hill in the province of Perugia in Italy. The body of the land slide was completely removed and the existing ground surface was modeled to a maximum height of about 15 m in three 5 m high blocks, at 60° slope separated by two berms. The reinforced slope was built using locally available soils as fill material (a silty soil of lacustrine origin) and HDPE mono-oriented extruded geogrids as reinforcement. The reinforced slope had been instrumented with strain gauges connected to the reinforcing geogrids. Tenax TT060 SAMP HDPE geogrids, having 60 kN/m ultimate tensile strength and 25 kN/m long-term design strength was used as reinforcement. The steep reinforced slope had been built using the Tenax RIVEL System (Rimoldi and Jaecklin, 1996). It consisted in the use of sacrificial steel mesh formworks that helped in the construction of the face slope and obtaining a uniform geometry of the slope. The vegetation of the face was further enhanced by hydro seeding the face at the end of the construction of the reinforced soil structure. The geogrid layers were vertically 0.65 m apart and 3.7 or 7 m long. In order to verify the long-term behavior of the structure the geogrids were instrumented with electrical wire resistance strain gauges. The dimension of the geogrid ribs required the use of strain gauges with very small dimensions (3.18 mm x 2.54mm). The strain gauges were completely encapsulated in polyamide resin for protecting them and to allow for their use in soils. The strain gauges were self-temperature compensated within a range of -20°C up to 60°C and with a strain limit up to 5% of the gauge length. The installation of this kind of gauges on the geogrid ribs was particularly difficult due to their dimension

and their fragility. The strain gauges were electrically connected with a 3 wire quarter bridge system to an automated data acquisition system. First of all the geogrid to be instrumented was prepared in the lab by making it perfectly flat; it was cleaned with alcohol, then the gauge area was abraded with 180 and 400 silicon-carbide paper to increase the roughness. A light flame was quickly passed over the rib to eliminate any residual powder from the abrasion and to increase the number of radicals. A neutralizer was applied to the gauge are, keeping the surface wet by scrubbing it with a cotton tipped applicator not to allow evaporation. Immediately after applying the neutralizer, the residual was removed with a gauge sponge. Then the gauges were glued using a cyanoacrylate adhesive to the ribs, and cured in an oven at 40° C for at least 8 hours. The strain gauges were coated with a layer of silicon rubber to protect and waterproof them. In particular it was very difficult to apply a thin and uniform adhesive layer (due to the non planarity of the surface); then, taking into account the fact that the strain gauges had to be glued on a 10 m long geogrid layer, it was difficult to handle it in all phases (from preparation to transportation on site and installation) with the necessary care. The number of "dead" strain gauges (9 out of 37) could therefore be considered a success. The instrumented geogrids were (from the bottom) the first, third and fifth layers of the first step, with gauges installed each 0.5 m up to 3.5 m from the face; the 7^{th} geogrid from the first step with gauges at each 0.5 m up to 6.5 m from the face; the first and fifth geogrids of the second step, with gauges at 0.5 m, 1.0m and 1.5m from slope face. The geogrids were installed in tension and the strain gauges and cables were covered with 150 mm of fine sand. From the analysis of the measurements, it was possible to see the presence of strain peaks in the strain envelopes, corresponding to a stress concentration in the geogrids. Analyzing the 7^{th} geogrid, it was possible to see an important peak (about 1.7% strain) at 2 m distance from the face, which together with the peak at the face point of the third geogrid, seems to be justified by the circular

surface found during the global stability analysis and passing through the toe of the third geogrid layer. The second peak of the 7th geogrid at 4.5 m from the face, together with the peak of the first geogrid (at 3.5 m from slope face) could belong to the deep-seated failure (intersecting also the upper step), which provided the lowest factor of safety in the design stage. Some of the relatively high strains recorded near the face may be a result of the contractor using a heavy-duty roller too close to the slope face and the consequent face bulging and geogrid tension. Hence the strain gauges readings provided qualitative results, which can be well explained with the global stability analysis.

4.3 Description of EWR strain gauge, readout device and connection box

Electrical wire resistance strain gauges were used to measure the strain variations along the geogrids in Devon reinforced test embankment. The gauges were foil type EWR gauge, code number CEA-13-250UN-350 made by Micro Measurements Group Inc. This gauge is a universal general-purpose strain gauge with constantan grid totally encapsulated in polyimide with large, rugged copper-coated tabs. These gauges function in a temperature range between -70°C to +175°C and a strain range of ±5% strain. Figure 1 shows a typical gauge of this type. This type of strain gauge has a narrow geometry, which is appropriate for installation on narrow geogrid members. The number 13 in the code is the STC number: Self-Temperature-Compensation. An important property shared by constantan strain gauge alloys is their responsiveness to special processing for self-temperature compensation. Self-temperature-compensated strain gauges are designed to produce minimum thermal output (temperature-induced apparent strain) over the temperature range from about -50 deg to +400 deg F (-45 deg to +200 deg C). The S-T-C number is the approximate thermal expansion coefficient in ppm/ deg F of

the structural material on which the strain gauge will display minimum thermal output. In normal practice, the S-T-C number for a constantan gauge is selected to most closely match the thermal expansion coefficient of the test material.

The resistance of the foil in a strain gauge increases with increasing strain and decreases with decreasing strain. This change in resistance is due to a dimensional change in the foil or wire under strain. The change in resistivity in terms of the change in strain is termed the strain sensitivity or gauge factor. The higher the gauge factor, the higher the electrical output and the higher the sensitivity. Gauge factor is defined as the ratio of fractional change in electrical resistance to the fractional change in length:

$$\text{Gauge Factor=F=}\frac{(\Delta R)(L)}{(R)(\Delta L)},$$

ΔR= change in resistance,

R=total gauge resistance,

ΔL= change length of the conductor,

L= total length of the conductor

$$\text{Strain=}\frac{\Delta R}{(R)(F)}$$

The gauge factor for metallic strain gauges are usually around 2 and for this project the gauge factor is 2.092 to 2.120.

The readout system is based on the principle of the Wheatstone bridge; a quarter bridge system was used for this project with a minimum reading of ten micro strain units. The readout box is a P-3500 portable, battery-powered strain indicator made by Micro Measurements Group Inc. The accuracy of the readout device is ±0.05% of reading ±3 micro strain for Gauge Factor settings of 1.000 to 9.900; ±0.05% of reading ±20 micro

strain for gauge factor settings of 1.000 to 9.900 when using X10 multiplier. The sensitivity or resolution of the device is ±1 micro strain at all gauge factor settings and ±10 micro strain when using X10 multiplier.

The wires from the EWR strain gauges run inside the fill and along the slope inside the trenches and PVC pipes towards the electrical box. There are 2½" holes in the electrical box where the wires can enter the box. These holes are located at the bottom of the electrical box. The EWR strain gauge connectors are soldiered on each of the wires (4 per each strain gauge location). The electrical wire resistance gauge connections are inserted into black plastic plugs. The plug has four holes that are numbered 1 to 4. Each color-coded wire must be inserted in its corresponding number on the plug as shown in Figure 2 and Table 1. This order was maintained since the fabricated plug on the strain gauge readout box uses the same order. After all the electrical resistance gauge connectors have been inserted in the plastic plugs, the plugs were fastened to the steel electrical board.

4.4 Location of EWR strain gauges and method of installation

The EWR strain gauges were installed on geogrids to measure the tensile strain and the subsequent stress distribution in the geogrids. The EWR gauges were installed at 0.5 m and 1 m from the face of the slope and then at 1 m intervals along the geogrid. The 1 m spacing was chosen to ensure that the region of larger deformations within the test embankment was monitored. At each location two strain gauges were bonded to the geogrid; one at the top and the other at the bottom of the geogrid longitudinal members. This was to monitor any bending of the geogrid as well as the elongation. In the Tensar, Signode and Paragrid sections at the bottom layer pairs of strain gauges were installed at 0.5 m up to 7 m with 1 m intervals and one at 8.5 m from the slope face. In the Tensar

section in the middle and top layers, pairs of strain gauges were installed at 0.5 m up to 9 m with 1 m intervals and one at 10.5 m from the slope face. In the Signode and Paragrid sections the middle and top layers of the geogrid were instrumented with EWR strain gauges installed at 0.5 m up to 9 m with 1 m intervals and two pairs at 10.5 and 12 m from the slope face. In all geogrids the EWR strain gauges were attached to the longitudinal members of the geogrids. In Signode and Paragrid the longitudinal members or bars have quit consistent cross section along the bars but this is not the case for Tensar geogrid. Its cross section at the bars become narrow towards the mid point in the bars and the middle of the bar has the smallest cross section. Hence the EWR strain gauges were attached to Tensar bars between the midpoint in the bar and the crossing of transverse members and bars, more close to the transverse members.

The process of installing the EWR strain gauges on the longitudinal members of the geogrids consisted of several steps. (1) The location where the gauge was to be installed was sanded, (2) The sanded surface was cleaned with Freon degreaser and it was wiped with MM gauge sponges, (3) The degreaser was cleaned from surface with "M-Prep Conditioner A#MCA-1" and it was wiped off with MM gauge sponges, (4) The conditioner in step 3 was neutralized with M-Prep neutralizer 5 No.MNS-1 and it was wiped off with MM gauge sponges, (5) the back cover of the strain gauge package was cleaned with Freon degreaser, conditioner A and neutralizer S as described in steps 2 through 4, (6) the strain gauge was placed down on the cleaned surface of the back cover described in step 5, (7) 2 inch piece of scotch brand magic transparent tape was placed over the gauge, (8) M-Bond AE-10 (resin/curing agent) epoxy was mixed, (9) back scotch tape was peeled so as to expose the bonding side of gauge and by using a clean glass rod a small amount of epoxy was applied to both the gauge and the geogrid surfaces, (10) the

gauge and tape was replaced onto the geogrid, (11) a finger was rolled over the gauge to spread glue out beneath gauge, (12) the gauge was clamped and it was allowed 24 hours for adhesive to set, (13) the clamp was removed and scotch tape was peeled off carefully, (14) any excess dry epoxy was trimmed from sides of geogrid ribs, (15) M-Flux AR activated resin was applied soldering flux to the gauges, (16) two leads of 7×#40 PVC insulated audio connecting cable were soldered, (17) excess soldering flux was removed with M-lin resin solvent and excess solvent was soaked off with Q-tips, (18) a liberal amounts of M-coat BT air drying nitrite rubber coating was added to surface of the strain gauge, (19) 4 conductor; 7×#30 tin copper "Unreal" cable were attached to the strain gauge pair, (20) all connections between leads on gauge and the Unreal leads were heat shrinked making sure to protect the geogrid from any heat from the heat gun, (21) 2.5cm×2.5cm M-coat FB-2 Butyl rubber general purpose strain gauge protective coating was applied sealing all cracks with silicon adhesive sealant; the Unreal cable is attached to the geogrid by means of 5 cm plastic ties to reduce any strain on the soldered connection.

Pairs of aluminum splints were installed to protect the gauges from damage during transportation and installation of geogrids in the test fill. These splints were removed following the geogrid installation in the field and the gauges were covered with a piece of Styrofoam to protect them from damage during fill placement and soil compaction. More detailed information on gauge selection and attachment procedures are reported by Soderberg (1990).

EWR strain gauges were also attached to short pieces of geogrids following the same procedures as used on the instrumented reinforcement and installed in the fill in the same manner. The purpose of these gauges was to evaluate the influence of the wet soil environment, the soil

confining stresses, the temperature and the readout instrument on the performance of the gauges and to provide correction factors for the geogrid gauges associated with these environmental influences. These dummy gauges were placed at each instrumented geogrid layer at 0.5, 1.0 and 5.0 m from the slope surface. As for the geogrid strain gauges, the first reading following placement of a 15 cm soil layer on the geogrid was taken as an initial reading and is subtracted from all subsequent readings. The dummy gauges were placed adjacent to thermocouples so temperature influences could be evaluated.

4.5 Calibration tests

4.5.1 Calibration tests on EWR strain gauges

Before attaching the strain gauges to the geogrids calibration tests were carried out. The EWR gauges were attached to lengths of geogrids and were loaded under a specific strain rate. The overall geogrid strain was monitored using a vernier between fixed points on the geogrid, which could measure the strain along the entire length of the geogrid. It should be mentioned that in the 1986 files on the EWR strain gauge calibration tests, there were different sets of test results with different strain gauge locations for the Tensar geogrids. These test results showed different correlations between local and global grid strains. It was assumed based on the sketches found in Soderberg (1990), that the EWR strain gauges were attached to the longitudinal members of the Tensar geogrid somewhere between the middle of the rib and the node (the junction of the rib and transverse member of the grid), closer to the node. The EWR measured strain will be different from the global grid strain depending on the EWR strain gauge location. Based on the above location assumption, test results which had similar strain gauge attachment locations were chosen to establish the correlation between the local and global strains in

the Tensar geogrid. Four sets of test results could be identified in the 1986 files and the results are summarized in different plots. In test number 2, it was mentioned that the strain gauges were attached on the grid "ribs" and as shown in Figure 3, the global strain is less than local strain. In test numbers 3 and 5 the gauges were attached to the grid "bars" and the results (Figures 4 and 5) show that the global strain was higher than the local strain. In test number 6, it was mentioned that the EWR strain gauges were attached at the grid "intersections" and again the results show (Figure 6) higher global strains. It should be admitted that the location of the EWR strain gauges are not exactly recorded in the 1986 documents and further investigation on this location is required.

For the Tensar geogrid the tests numbered 5 and 6 showed (Figure 7) that the overall grid strain was higher than the strains measured by the EWR strain gauges. This difference in strain occurs because the longitudinal tension member changes its cross-section along the geogrid. The average of these plots for Tensar geogrid can be used to convert the strains measured by EWR strain gauges to the overall geogrid strains.

Another method to establish a correlation between global and local strain measurements could be relating strains measured in the field by Bison and EWR strain gauges at the same dates and locations. This correlation is presented and discussed in section 4.12 where the measurements of Bison strain gauges are reviewed. The results from correlation between those two strains for Tensar geogrid show that the best fit line for the plotted data points is very close to a 45 ° line. This implies that the strains measured in the field by EWR gauges are very close to the strains measured by Bison gauges. Hence the lab test results for Tensar as discussed previously do not represent the actual correlation which was found based on field measurements and are reported here only for keeping records of those tests.

For Signode, as its longitudinal members have a constant cross section, the location of the gauge attachment on the rib would not affect the correlation between local and global strains. And all the tests were carried out with EWR strain gauges attached to the ribs. The tensile test results in Figure 7 with a gauge length of about 556 mm between jaws and a strain rate of 2 mm/min show that for the Signode geogrid the measured strains from EWR strain gauges were almost the same as the overall grid strain.

No test results were found in the old files regarding the calibration between Paragrid global and local strains.

4.5.2 Recalibration of the EWR strain gauge readout device

In order to overcome any systematic error, the same readout device was used to measure the strains in the EWR strain gauges. Recalibration of the readout device was performed in 2003 to ensure that the new measurements by the same readout device are reliable and comparable to the old measurements. The recalibration of the P-3500 readout device was checked by a 1550 Strain Indicator Calibrator, made by Vishay Instruments, Micro Measurements Group Inc. In an ideal case the readings from P-3500 readout devise should have been identical with the calibrator readings at different levels of strain. The Calibrator strains are plotted against P-3500 measured strains in Figure 8. The 45° line represents the ideal case where the two measured strains are equal. The measured strain line lies beneath the ideal 45° line but it is very close to the 45° line that it is almost not distinguishable. Hence the difference between the measured strains and actual strains is also illustrated in the same plot with dashed line. The P-3500 measured strains are higher than the calibrator measured strains up to about 0.85% strain but after that the P-3500 measured strains are lower than the actual indicator strains.

These differences between measured strains and actual strains increase as the strain increases. The recalibration check was done up to 4% strain and the maximum observed difference was about 0.08% strain less than the actual strain, which is negligible. This confirms that the calibration of the P-3500 readout box used to measure EWR strains was reliable.

4.6 Previous readings of EWR strain gauges

Initial or zero field readings were taken for each gauge immediately after the layer of geogrid was laid out on the test embankment and about 15cm of fill soil had covered the geogrid layer. The initial field reading dates for EWR strain gauges are summarized in Table 2. The differences between the initial readings and the subsequent readings gave the strains, which developed in the geogrids due to loading applied by the embankment soil. At each location the measurements of the top and bottom gauges were averaged. Temperature induced strains were also subtracted from the measured strain in order to omit the influence of thermal strains of geogrids. To do the temperature correction, thermal expansion coefficients of the geogrids were measured through thermal expansion tests conducted in the laboratory before construction of the embankment. EWR strain gauges were bonded to pieces of geogrids in the same way as the instrumented primary geogrid layers for use in the test embankment. Then strains were measured at different temperatures under stress free conditions. Thermal expansion coefficients of the geogrids were calculated to be 0.017, 0.027 and 0.011% strain per °C for the Tensar, Signode and Paragrid geogrids respectively. The measured coefficient of thermal expansion for the Tensar SR2 geogrid was confirmed by the manufacturer. (The thermal expansion coefficient of the strain gauges is one order of magnitude lower than that of geogrids) (Liu, 1992). Temperatures at different strain gauge locations were monitored using a thermocouple during the field measurements as discussed in Chapter 3.

The temperature-induced strains were then calculated as the product of the thermal expansion coefficient of the geogrid and the temperature differences between the time of the reading and the initial temperature at that specific location.

It should be emphasized that all the strain measurements with EWR strain gauges only indicate the local strain values at the strain gauge locations and may not represent the global geogrid strain values. Field readings were taken during and after construction. The number of field measurements for each geogrid layer from 1986 to 1990 is summarized in Table 3.The full detailed discussion of geogrid strain variation over time during the construction and after the construction are discussed by Liu (1992) but in general the EWR strain variation follows the sequence of construction. As each stage of construction is elapsed and a geogrid layer is installed in the fill, the strains show an increase subsequent to fill placement and when the construction had stopped there is a very slight reduction in the geogrid strains. This pattern is repeated for all 3 stages of construction in all geogrids, which reflects the effect of construction activities and also loading of the geogrids with the placement of the additional fill. Some typical results up to 1990 for Tensar geogrid at different layers are presented in Figures 9 to 14. The vertical dashed lines showing the elapsed time in years from the beginning of construction correspond to different stages of construction and consolidation of the test embankment. In some locations where one of the two EWR gauges failed, the representative strain was determined from the sum of the average before failure and the increments of strain measured thereafter in the remaining gauge. These locations will be shown with a small circle on the plots. At these locations the bending of the geogrids also could not be determined. Table 4 shows the number and location of failed EWR strain gauges. In total 198 EWR strain gauges were attached to primary geogrid layers and 30 of them had failed by the 1990 field measurements.

4.7 State of EWR strain gauges in 2003

As mentioned before the surface shallow slope movements and sloughing had moved all the electrical connection boxes and they were almost buried as illustrated in Figures 2, 3 and 4 in chapter 3. Fortunately the movement of the electrical connection boxes had not damaged the EWR strain gauge wire connections and the majority of the connections were functioning properly. During the 2003 field measurements it was found that in total 46 EWR strain gauges had failed which means only 16 EWR strain gauges had failed since the 1990 field measurements. The total survival rate of EWR strain gauges installed on primary geogrids is about 77% which shows that the installation method adopted for this project was successful after 16 years of service life. The clean up of the soil sloughs and removing debris around and over the electrical connection boxes was a difficult task because it was very likely that the connection of the wires to the box would be damaged by the backhoe shovel which was used to clean up the site. But the carefully performed cleaning job did not do any damage to the electrical connection boxes and the wires running through PVC pipes to the boxes. The plugs for EWR strain gauges on the electrical boards were cleaned and washed and all the plugholes were carefully cleaned in order to prevent pushing any dirt into the plugs during the reading when inserting the connector of the readout device. In general the refurbishments of the electrical connection boxes for reading the EWR strain gauges were successfully done. The connection boxes are illustrated in Figures 5, 6 and 7 of chapter 3 after removing the debris and cleaning the electrical connection boxes.

4.8 EWR strain gauge readings in 2003

During the 2003 field measurements, 4 new sets of EWR strain gauge measurements were carried out using the same readout device that was used for previous readings in order to minimize the reading errors. The results of the EWR strain gauges for each geogrid layer are summarized in the following sections. It should be mentioned that all the previous strains were calculated again along with the new field measurements in order to check the method of calculation and initial readings for the new sets of measurements. Also the temperature correction is applied to the measured strains as mentioned before.

4.8.1 Tensar bottom layer

Nine pairs of strain gauges were installed on the bottom primary Tensar geogrid layer at 0.5, 1, 2, 3, 4, 5, 6, 7 and 8.5 m from the slope face. Pair of EWR strain gauges at 0.5 m and one gauge in each pair of EWR strain gauges at 1, 2 and 3 m from slope face were failed till 1990 field measurements. In 2003 measurement the other gauge at 1 m location also was failed. At locations were one gauge had failed the strain at that location was determined as mentioned before. At locations where both gauges failed, strains after failure were estimated based on the strains at the adjacent locations and the ratio of the measured strains at the two locations prior to the failure. The first set of field measurements taken in September 23, 1986, was considered as the initial strain and was subtracted from the strains measured after. Some adjustment was made to initial strains at 8.5 m from slope face because the strains measured after were showing localized compression of the geogrid caused by construction activities. In order to eliminate further negative strains, -0.087 was considered as the initial value. Figure 15 illustrates the variation of strain at different locations and during different times. Figure 16 shows the

entire strain development at various locations along the geogrid layer. Two typical measurements during 2003 field measurements are illustrated in the plots. These measurements illustrate that the trend of strain variation along the geogrid layer is almost same as the previous reading after the end of construction but there is a slight reduction in the amount of strain in comparison to last set of measurements. This reduction is very small from a 4 m location from the slope face towards the end of the geogrid.

4.8.2 Tensar middle layer

Eleven pairs of EWR strain gauges were installed on the middle primary Tensar geogrid layer at 0.5, 1, 2, 3, 4, 5, 6, 7, 8, 9 and 10.5 m from the slope face. No EWR strain gauge was failed on this primary geogrid layer till 2003 measurements and all the strain gauges functioned properly. The set of field measurements taken in September 1, 1987 was considered as the initial strain values. The strain profiles of the geogrid in the Tensar middle layer are illustrated in Figure 17. The development of the tensile strains with in the geogrid at different locations along the geogrid during and subsequent to the construction activities is shown in Figure 18. The 2003 measurement are consistent and show the same tendency of strain variation along geogrid with a slight decrease in strain values at most locations. At some locations close to the slope surface fluctuations of strain occurred which will be discussed later by the effect of temperature corrections.

4.8.3 Tensar top layer

There are 11 pairs of EWR strain gauges installed on Tensar top primary geogrid layer at 0.5, 1, 2, 3, 4, 5, 6, 7, 8, 9 and 10.5 m from the slope face. Three pairs of EWR strain gauge at 0.5, 1 and 3 m locations from the slope face and one gauge at 4 m from slope face failed till 1990. One

gauge was recovered during 2003 measurements and no more EWR gauge was failed between 1990 and 2003. The set of field measurements taken in October 23, 1987 was considered as the initial strain measurements. Figure 19 shows profile of the tensile strain in the top layer of the Tensar geogrid. Diagrams indicating entire strain development at different locations on the geogrid are presented in Figure 20. The reduction of strains as discussed before can also be seen in these plots. The trend of strain variation along the geogrid, however, is identical to the previous strain measurements along the geogrid.

4.8.4 Signode bottom layer

On the instrumented section of bottom layer of Signode primary geogrid nine pairs of EWR strain gauges were installed at 0.5, 1, 2, 3, 4, 5, 6, 7 and 8.5 m from the slope face. Pairs of gauges at 2, 3 and 4 m locations from the slope face and one gauge of each pair at 5, 7 and 8.5 m locations from sloe face failed during and after construction till 1990. One more EWR gauge failed between 1990 and 2003 measurements. The initial strain values were measured in September 23, 1986. The EWR strain gauges at 7 m location functioned but showed unreasonable values during the whole period of measurements. The value of strain measured at this location was dramatically low in comparison to its adjacent locations hence in the final plots the 7 m location results are omitted regarding that this pair of gauges did not functioned properly and strains at this location were estimated by taking average of the strains at the 6 m and 8.5 m locations. Profiles of the strain distribution along the bottom layer of Signode geogrid are shown in Figure 21. The development of strains at different locations along the geogrid layer is illustrated in the strain-time diagrams, shown in Appendix B. In general the same pattern of strain variation is observed for Signode bottom layer. The trend of strain variation along the geogrid layer is consistent with the previous readings

but the strains have reduced in range of 0.2-0.4% at most locations along the geogrid.

4.8.5 Signode middle layer

Along the Signode middle layer geogrid, 12 pairs of EWR strain gauges were installed at 0.5, 1, 2, 3, 4, 5, 6, 7, 8, 9, 10.5 and 12 m from the slope face. One gauge at each location of 1 and 8 m from the slope face failed till 1990 field measurements and no more gauges were failed between 1990 and 2003 field measurements. EWR strain measurements in August 4, 1987 were considered as the initial set of readings for this geogrid layer. Figure 22 illustrates the profiles of strain variation along Signode middle layer at different times and locations. The 2003 measurements did not show any significant changes in the strain profiles except at some locations close to the slope surface which might have been influenced by temperature variations and the applied temperature corrections which will be discussed later. The magnitude of strains, however, shows a slight reduction as was the case for the other geogrid layers. The full development of the tensile strain at locations along the geogrid layer can be observed in the strain-time diagrams in Appendix B.

4.8.6 Signode top layer

Twelve pairs of EWR strain gauges were installed on the top primary reinforcement layer of geogrid in the Signode section at 0.5, 1, 2, 3, 4, 5, 6, 7, 8, 9, 10.5 and 12 m from the slope face. Pair of gauges at 0.5 m and one gauge at 1 m location from the slope face failed during and after construction till 1990. Two pairs of gauges at 6 and 8 m locations from the slope face failed between 1990 and 2003 field measurements. The field measurements in October 23, 1987 were considered as the initial set of readings for these gauges. Figure 23 illustrates the profile of strain

variation along the geogrid at different times. The development of the strain can also be observed in the strain-time diagrams shown in Appendix B. Measurements in 2003 did not show significant changes in the profile of the strains except at the locations near the slope surface where large reductions of tensile strain were observed. At other locations far from the slope surface the reductions of strains were small.

4.8.7 Paragrid bottom layer

Nine pairs of EWR strain gauges were attached to the bottom primary reinforcement layer of Paragrid geogrid at 0.5, 1, 2, 3, 4, 5, 6, 7 and 8.5 m from the slope face. No gauges were failed during and after construction till 1990, but 4 gauges failed between 1990 and 2003 field measurements at 0.5 and 2 m locations from the slope face. The readings in September 24, 1986 after compacting with one pass of packer were considered as the initial set of readings. Figure 24 shows the profiles of tensile strain of the geogrid at different times and locations. The development of the tensile strain at different stages of construction and consolidation is also shown in the strain-time diagrams in Appendix B. The pair of strain gauges at 7 m location shows very different magnitudes of strain in comparison to its adjacent strain gauges hence the results for this particular location are not presented along the other locations. In 2003 measurements the strain variation close to the slope surface were considerable but as the distance from the slope face increased the reduction in strain became less and more consistent with the previous measurements.

4.8.8 Paragrid middle layer

Twelve pairs of EWR strain gauges were installed on the middle primary reinforcement layer of geogrid in the Paragrid section at 0.5, 1, 2, 3, 4, 5, 6, 7, 8, 9, 10.5 and 12 m from the slope face. No gauges failed during and

after construction till 1990 measurements. Pair of gauges at 2 m location from the slope face failed between 1990 and 2003 measurements. Measurements in August 22, 1987 were considered as the initial readings for this set of EWR strain gauges. Figure 25 illustrates profiles of the strain distribution along the middle layer of the Paragrid geogrid at different stages of construction, consolidation and 2003 measurements. The development of the tensile strain at different stages of construction and consolidation is also shown in the strain-time diagrams in Appendix B. The trend for strain distribution along the geogrid in 2003 is identical as the previous measurements made after the construction but again there is a slight reduction in the amount of strain for all locations along the geogrid.

4.8.9 Paragrid top layer

Twelve pairs of EWR strain gauges were installed on the top primary reinforcement layer of geogrid in the Paragrid section at 0.5, 1, 2, 3, 4, 5, 6, 7, 8, 9, 10.5 and 12 m from the slope face. One gauge of each pair of gauges at 0.5 and 1 m locations were failed till 1990 field measurements and between 1990 and 2003 field measurements the other gauge at 1 m location and the pair of gauge at 5 m location from the slope face also failed. Readings in October 14, 1987 were considered as the initial readings for these EWR strain gauges. Figure 26 illustrates profiles of the strain distribution along the top layer of the Paragrid geogrid at different stages of construction, consolidation and 2003 measurements. The development of the tensile strain at different stages of construction and consolidation is also shown in the strain-time diagrams in Appendix B. Identical profiles for tensile strain along the geogrid as 1990 measurements and small reduction in tensile strain values can be observed in the plots.

4.9 Long term performance of dummy EWR strain gauges

As mentioned in section 4.4, eighteen dummy EWR strain gauges were installed at each reinforced section, 3 pairs at each geogrid elevation, at 0.5, 1 and 5 m from the slope face. The purpose of these gauges was to evaluate the influence of the wet soil environment, the soil confining stresses, the temperature and the readout instrument on the performance of the gauges. The temperatures were also measured at each location of dummy gauges in order to check the effect of temperature-induced strains on the strain measurements. In total 54 dummy EWR strain gauges were installed in the fill to monitor for environmental influences on the gauge and by 2003 field measurements only one gauge had failed. The temperature correction procedure mentioned before was also applied to dummy EWR strain gauge measurements.

Figure 27 illustrates a typical profile of the temperature corrected strains at 3 different locations in Tensar bottom layer section. This plot shows that the strain in dummy EWR strain gauges might have fluctuated due to different environmental affects but all three gauges show a consistent profile of strain variation over the lifetime of the project. Figure 28 shows a typical result of a dummy EWR strain gauge variation at Tensar bottom layer 5 m from the slope face. The square data points show the value of strains with out any temperature correction; the triangles show the temperature variation at the reading times and the diamond data points illustrate the strains with temperature correction. As it can be seen, the strain variation without any temperature correction (square points) is very limited and the strain values are all in range of ±0.1% strain during the whole period of measurements. On the other hand the temperature fluctuation is much more considerable at different reading times. When the

temperature correction is applied to the measured strains the temperature corrected strains show a mirror profile of the temperature variation with the same fluctuations observed in temperature variation and the uncorrected strain profile lies somewhere in between those two plots. This is the same condition for all dummy gauges and the strains vary a lot after applying the temperature correction. Figure 29 includes all the dummy EWR strain gauge measurements with out any temperature correction. The strain variations in these dummy gauges are in range of ±0.15% strain. Figure 30 illustrates all the dummy EWR strain gauge measurements with temperature correction. The strain variation for dummy gauges after applying the temperature correction is in range of ±0.30% strain, almost twice as the range of strains without temperature correction. The majority of the dummy EWR strain gauge measurements in 2003 show that there is a reduction in strain in both temperature corrected and without temperature correction measurements.

The results of all dummy EWR strain gauge values for all the geogrids at all locations are presented in Appendix B.

4.10 Long term performance of active EWR strain gauges

By reviewing the 2003 measurements of all geogrids it can be found that all strain measurements (temperature corrected) show a reduction in strain values. Figure 31 illustrates the amount of reduction in strain values between 1990 and 2003 field measurements versus distance from slope face for all geogrids. This figure show that the amount of reduction in strain values are higher close to the slope face and as the distance from the slope face increases the amount of strain reduction decreases. In other words deep into the slope the strain variation between 1990 and 2003 measurements are less than the locations close to the slope. This difference might have been caused by temperature variations and the

temperature correction, which was applied to all strain gauge measurements. The effect of temperature correction is also shown in dummy EWR strain measurements plots. As discussed in temperature measurement chapter, the temperature variation inside the fill also follows the same patter of strain reduction inside the fill (Figure 31). The maximum temperature difference reduces as the distance from the slope face increases. Hence close to the slope face the temperature variation was higher.

From all these active and dummy EWR strain gauge results it appears that geogrid temperature correction is not applicable. The confining stress of the soil must prevent the geogrid from undergoing thermal expansion or contraction and as a result the strain of the geogrid is over or under estimated when a temperature correction is applied. As mentioned before the linear coefficients of thermal expansion of Tensar, Signode and Paragrid are 17×10^{-5}, 27×10^{-5} and 11×10^{-5} per °C. Soils and rocks generally have a linear coefficient of thermal expansion of about 1×10^{-5} per °C, only a small fraction of that of polymers. If no slippage occurs between the soil and geogrid, then the geogrid cannot significantly change length from temperature change. The water in the soil has a volumetric coefficient of thermal expansion of about 21×10^{-5} per °C but the temperature changes occur so slowly that flow of the water into air voids in the unsaturated compacted soil can take place. This volumetric change of the water may have an effect on the pore fluid pressures in the soil but not significantly on the soil volume.

As the geogrids are prevented from undergoing thermal strain by the confining soil, they will develop thermal stresses. The thermal stress, σ_t, can be calculated from the following equation:

$$\sigma_t = \frac{E\alpha}{(1-\nu)}\Delta t \quad \text{kN/m}$$

where E = elastic modulus in kN/m

α = Linear coefficient of thermal expansion

ν = Poisson's ratio

Δt = change in temperature

The elastic moduli for strains below 1% are 1100, 1800 and 500 kN/m for Tensar, Signode and Paragrid respectively. These values were obtained from the tensile force – strain test results shown in Chapter 2. For most polymers, Poisson's ratio is about 0.4. For a temperature change of 18°C (maximum observed temperature variation at 0.5 m from slope face), the thermal stress will vary from 5.6, 14.6 and 1.6 kN/m for Tensar, Signode and Paragrid respectively. The actual thermal stress will depend on the temperature change from the time of installation of a geogrid and could be compressive or tensile.

Hence as the temperature variation in a location along the geogrid is larger the overestimation or underestimation of the thermal strains will become more. Therefore the locations with higher temperature variations (locations more close to the slope face) will show more variation in strain change. This trend can be observed in Figure 31 clearly. Other possible causes for this strain reduction over 13 years period could be creep within the bonding agent between the gauge and geogrid or consolidation and soil strengthening over the time due to pore pressure dissipation allowing the soil to better resist the gravity stresses. These other two possibilities cannot be investigated and confirmed only with EWR strain gauge measurements and more detailed study is required to clarify this reduction.

All the EWR strain measurements presented in this chapter and in the rest of the thesis are temperature corrected and these calculated strains were subtracted from all initial active and dummy strain gauge readings. The reason for making this temperature correction was that at the beginning of this new research in 2003, the objective was to compare the new measurements with the last set of measurements carried out in 1990. As all the EWR strain gauge measurements in Liu's thesis (1992) included the temperature correction, the same procedure was followed to correct all measured strains in 2003. No discussion was presented by Liu regarding the dummy strain gauge measurements but in 2004, all the dummy strain gauge measurements since the beginning of the embankment construction were reviewed and analyzed. As discussed above, it was concluded that the application of the temperature correction to the EWR strain gauge measurements is not necessary and will overestimate or underestimate the actual strain measurements. Liu's thesis also did not consider any correlation between the grid global strains and the local measured EWR strains and there is no discussion on the relation between the measured local strains and the grid overall strains for different geogrids.

4.11 Summary and conclusions of EWR strain gauge measurements

Strains in geogrids in the test fill were measured using electrical wire resistance strain gauges and they measure the strains in longitudinal (tensile) members or ribs of the geogrids. The last set of field measurements after the end of the construction was done in 1990. Four new sets of field measurements were made in 2003. A considerable amount of effort was spent in the field in order to refurbish all the instruments. Due to some soil sloughing and resulting debris, most of the instruments including the EWR strain gauge electrical connection boxes

were buried under soil. All the electrical connection boxes were cleaned and the calibration of the readout box was confirmed. The same readout box was used for the 2003 measurements that was used for the measurements before 1990. A summary of some major findings are presented below:

- In the 2003 field measurements 46 strain gauges out of 198 active EWR strain gauges installed on primary geogrids had failed and 16 of them had failed between field measurements in 1990 and 2003. In total 54 dummy EWR strain gauges were installed on pieces of geogrid following the same procedures as used on the instrumented reinforcement and installed in the fill in the same manner in order to study the effect of the environment on the strain measurements. Fifty-three of these gauges functioned properly during the 2003 field measurements. The survival rate for the 252 active and dummy EWR strain gauges attached to the geogrids is 81%, which shows that the EWR strain gauge installation method used for this project was successful.

- The dummy EWR strain gauge measurements show that before applying any temperature correction to eliminate the temperature induced strain from the measured strains, the strain variation in all dummy gauges are in range of ±0.15% strain during the service life of the project, but when the temperature correction is applied the variations are more scattered and they are in the range of ±0.3% strain. It is argued that if no slippage occurred between the soil and the geogrids (which is the case for this project as will be discussed in chapter 8), geogrids confined with soil would not undergo thermal expansion or contraction from temperature changes. So instead of temperature induced strains, thermal stress or thermal force will occur in the geogrids with the magnitude depending on the elastic properties,

temperature change and linear coefficient of thermal expansion. Therefore the application of temperature correction for eliminating temperature-induced strains from the measured strains used for this project has underestimated or overestimated the final strains.

- The majority of the dummy EWR strain gauge measurements in 2003 show that there is a reduction in strain compared to the previous readings in both temperature corrected measurements and measurements without temperature correction.

- The active EWR strain gauge measurements in 2003 illustrate that the profile of local strain variation along the geogrids are almost identical and follow the same pattern of strain distribution along the geogrids that is similar to the last sets of measurements after the end of the construction but the amount of strains have reduced since the last measurements. The amount of this reduction varies in the range of 0.1% to 0.65% strain along the geogrids but it has a pattern; as the distance from the slope face increases the amount of strain difference, between 1990 and 2003 field measurements increases. This pattern of difference in strain reduction is partially due to the effect of the temperature correction.

4.12 Review of inductance coil strain gauge measurements

4.12.1 Description of Gauge and Installation

Inductance coils, model 4101A, made by Bison Instruments Inc. were used to monitor strains across adjacent transverse members of the geogrids. The coil measures the electromagnetic coupling between two sensors of 5.3 cm in diameter and 0.68 cm in thickness. The coupling is extremely sensitive to axial distance between the sensors; it is capable of

measuring strains from 0.01% to as large as 50%. This range is greater than the working range of the EWR strain gauges and is not influenced by moisture content and temperature variation within the soil, as claimed by the manufacturer. The inductance coils were designed to measure axial strains between two sensors. In other words the pair of disk shaped sensors is designed to be placed in parallel and coaxial orientation separated by a distance over which the strain is averaged. In the case of monitoring the strain in a layer of geogrid, however, the relative transverse movement between the sensors is measured, i.e., the pair of sensors has to be placed approximately in the same plane. To evaluate the accuracy and sensitivity of the inductance coils to the transverse movements, a series of calibration tests were conducted before installing the coils. Figures 32 and 33 show the calibration curves indicating the relationship between the amplitude in the readout indicator and the central distance between two sensors. The calibration tests were conducted on two sets of inductance coils and the results were consistent and repeatable. From these calibration tests it was found that the minimum detectable strain was between 0.02% to 0.05% within the range of working distance between sensors in the test fill.

Inductance coils were attached to the geogrids by plastic bolts placed through the center of adjacent transverse members. They were placed several centimeters from and at the same depth as the EWR strain gauges. Electrical leads were connected after the geogrids were placed in the field. The coils were protected in the field using plywood and Styrofoam. Initial readings were taken immediately after the completion of field installation. Measured amplitudes from the readout indicator were converted into distances between sensors according to the calibration curves. The distances measured thereafter were compared with the initial distances and displacements. Strains developed in the geogrids due to construction and soil strain were then calculated. Between August 1986 to

September 1990 only 10 from a total of 87 inductance coils failed (Martin, 1986 and Liu, 1992).

In the next paragraphs the Bison strain gauge measurements at four different available dates in Liu's thesis (1992) are re-plotted and one of those measurements is compared with EWR strain gauge measurements carried out at a same date. The subsequent calibration plots include only those 4 Bison gauge and the corresponding EWR strain gauge measurements.

4.12.2 State of Readout Instrument in 2003

In order to measure the geogrid strains by inductance coils (Bison gauges) during the 2003 field work, the first step was to check the calibration of the readout device. During the recalibration of the readout device (Bison model 4101) in 2003 it was found that the meter did not travel very smoothly and in some occasions and it became stuck at the far right side of the indicator. So the first part of the calibration which was zero adjustment could not be carried out correctly. Since the manufacture of these readout instruments was halted by the Bison Company several years ago and the company no longer existed, it was not possible to ask for technical support from the manufacturer. The instrument was sent to the Geophysical Instrument Supply Co. (GISCO) in the USA for repair. After the return of the instrument, during calibration the zero adjustment screw at the back of the instrument was used to make the zero adjustment and this time the meter was very sensitive to the screw movements. A very slight touch of screw made the meter jump dramatically to either end of the indicator and it was not possible to adjust it. After contacting GISCO, they mentioned that everything was fine when they checked the instrument before shipping. It was thought that this problem might have been caused by the sensitivity adjustment knob and the technicians at the

University of Alberta checked it and found nothing wrong with the sensitivity knob. An attempt to find a similar readout device also failed. Therefore, due to the malfunction of the readout device, it was not possible to measure the Bison strain gauges and no recent measurements are presented.

4.12.3 Comparison with EWR strain gauges

Figures 34, 35 and 36 present the strain variation in the Tensar bottom, middle and top layers respectively measured by Bison gauges till 1990. All these figures are modified from Liu (1992) and show the measurements up to October 1990. The EWR strain gauge measurement for November 1988 is also shown for each geogrid layer for comparison. In the Tensar bottom layer (Figure 34) the EWR strain gauge and Bison gauge measurement for November 1988 match very well with each other but the peak strain measured by Bison gauge is at 1 m from the slope face and the peak measured by EWR strain gauge is at 3 m location from the slope face. However the magnitudes are similar to each other. At Tensar middle layer, Figure 35, the trends of EWR and Bison gauge measurement in November 1988, show a similar trend with same location of peak strain but the magnitudes of strain measured by EWR strain gauge are higher except in the 3 m distance from the slope face. At Tensar top layer, Figure 36, there is also a good match between EWR and Bison strain gauge measurements in November 1988. The trend of strain variation is almost identical, except between 3 and 5 m location from the slope face where the EWR strain gauge measurements show higher values. The location of the peak strain is similar in both measurements and the magnitude of the peak strain measured by EWR strain gauge is 0.3% strain higher than the strain measured by Bison strain gauge.

Similarly Figures 37, 38 and 39 illustrate the strain variation along the Signode bottom, middle and top geogrid layers respectively with a typical EWR strain gauge measurement in November 1988. In Signode bottom layer, Figure 37, the measurement by EWR strain gauges measured in November 1987 are presented because during November 1988 measurements most of the EWR strain gauges at this layer had failed. The EWR strain gauge measurement shows lower values (0.2 to 1.7% strain) than the measurements by Bison strain gauges. In Signode middle layer, Figure 38, both measurements illustrate a similar trend of strain variation with a same peak strain location and almost identical strain values along the geogrid. But there are some locations between 3 m and 6 m from the slope face where Bison gauge measurements show another small peak which EWR measurement does not show such a peak in strain. In Signode top layer, Figure 39, again the Bison strain gauge measurements shows higher values (0.2 to 0.7% strain) with multiple peaks in strain where the EWR measurement show a very smooth strain variation along the geogrid. If those peak and drop points in Bison strain measurement are ignored, then the trend of strain variation along the geogrid would be identical in both measurements by EWR and Bison strain gauges.

The strain variation measured by the Bison gauges in the Paragrid bottom, middle and top geogrid layers are presented in Figures 40, 41 and 42 respectively and for comparison a typical EWR strain gauge measurement in November 1988 is also shown on each plot. The comparison between EWR and Bison strain gauge measurements in all three grid layers show that Bison gauge measurement have higher strain values than EWR gauge measurements and the magnitudes and locations of the peak strain do not match with each other.

4.13 Field correlation between local and global strains

Despite that there were no inductance coil strain gauge measurements available in 2003, the previous measurements on Nov. 87, Nov. 88 and Oct. 89 were used to establish a correlation between the local strains measured by EWR strain gauges and the global strains measured by inductance coil gauges for each geogrid. These correlations present the actual relationship between local and global strains based on the real field conditions. The EWR gauge readings are temperature corrected but this correction would only give a maximum error of 0.2% strain in the EWR readings. Figures 43, 44 and 45 illustrate these correlations for Tensar, Signode and Paragrid geogrids separately. A best fit line passing through the origin is used to illustrate the dominant relation between EWR and Bison gauge strains.

In Figure 43 which is the correlation for all the Tensar geogrids the two different test results from the previous tensile tests at two different gauge locations are also shown. These test results again show a considerable difference in the correlations fro the different strain gauge locations.

For the Signode geogrids, Figure 44, the field correlation between EWR strain gauge measurements and Bison strain gauges are very close to the tensile test results presented in section 4.5.1 and are very close to the 45° line.

For the Paragrid geogrids, Figure 45, the results show that the Bison global strain values are higher than the EWR strain values. This relationship appears logical due to the defects found at the welded grid junctions. As the welded junctions had defects, the longitudinal members could not be strained enough hence the Bison strain gauge measurements showed higher values than the EWR strain gauge measurements.

Table 1. Corresponding colors and plug numbers for EWR strain gauge plugs

Wire color	Plug Number
Red	1
Black	2
White	3
Green	4

Table 2. Initial field measurement dates for EWR strain gauges installed at different locations

Layer	Bottom	Middle	Top
Tensar	9/23/1986	9/1/1987	10/23/1987
Signode	9/23/1986	8/4/1987	10/23/1987
Paragrid	24-Sep-86, after one pass with packer	8/22/1987	10/23/1987

Table 3. Number of EWR strain gauge measurements till 1990

EWR strain gauge measurements		Tensar	Signode	Paragrid
Layer	Top	16	14	13
	Middle	19	21	19
	Bottom	33	32	31

Table 4. Number of failed active EWR strain gauges during different times

Geogrid	Tensar			Signode			Paragrid		
	Bottom	Middle	Top	Bottom	Middle	Top	Bottom	Middle	Top
Stage 1	1	—	—	4	—	—	0	—	—
Stage 2	2	0	1	0	0	0	0	0	0
Stage 3 till 1990	2	0	6	5	2	3	0	0	2
2003	1	0	-1	1	0	4	4	2	5
Total	**6**	**0**	**6**	**10**	**2**	**7**	**4**	**2**	**7**

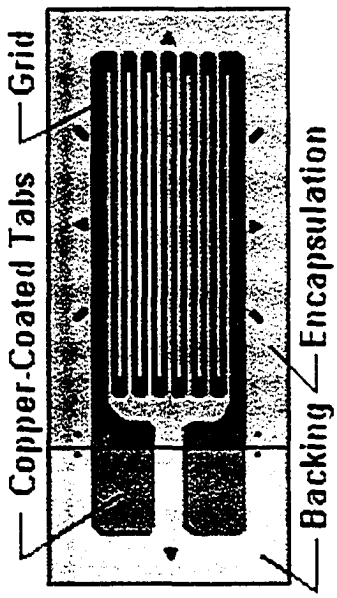

Figure 1. Foil type EWR strain gauge

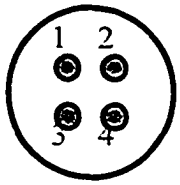

Figure 2. EWR strain gauge plugs at the connection box

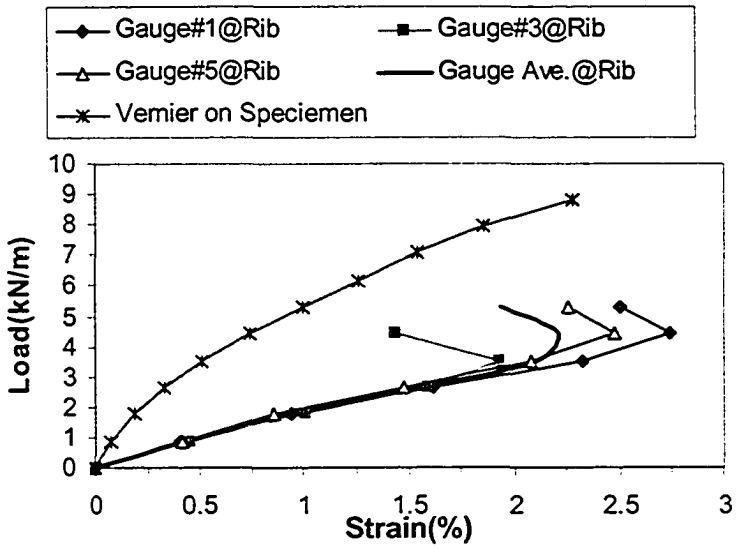

Figure 3. EWR strain gauge calibrations-Tensar test #2, 2 mm/min, gauge length 562 mm, EWR gauges at ribs

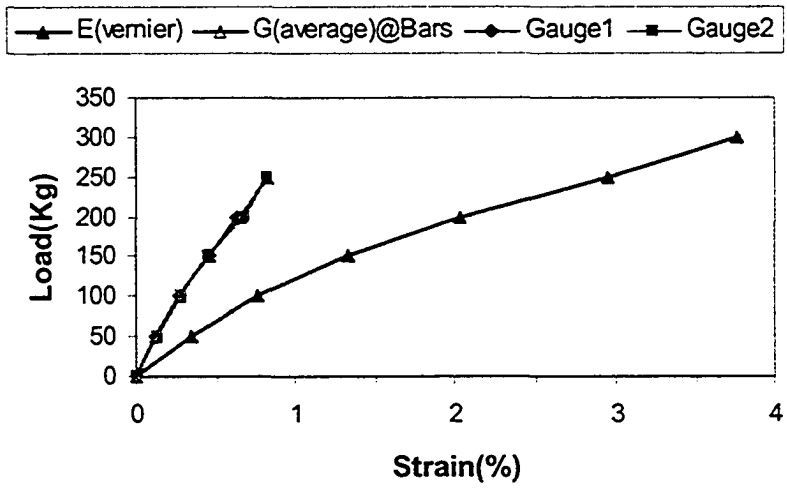

Figure 4. EWR strain gauge calibrations-Tensar test #3, EWR gauges at bars

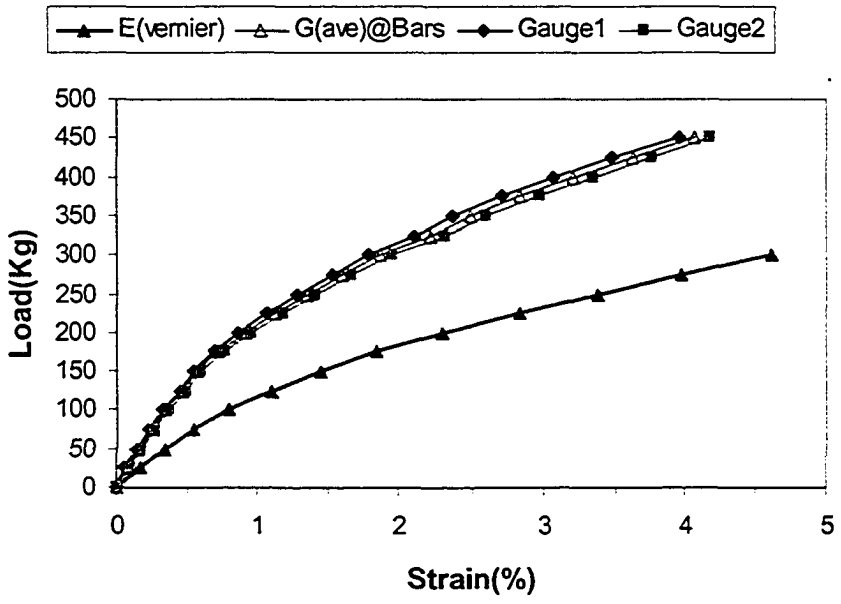

Figure 5. EWR strain gauge calibrations-Tensar test #5, EWR gauges at bars

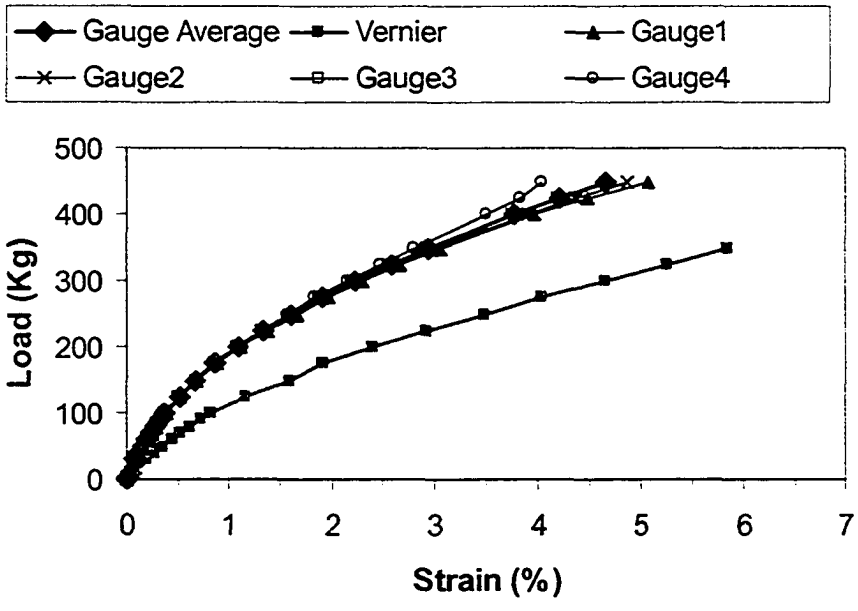

Figure 6. EWR strain gauge calibrations-Tensar test #6, EWR gauges at grid intersections

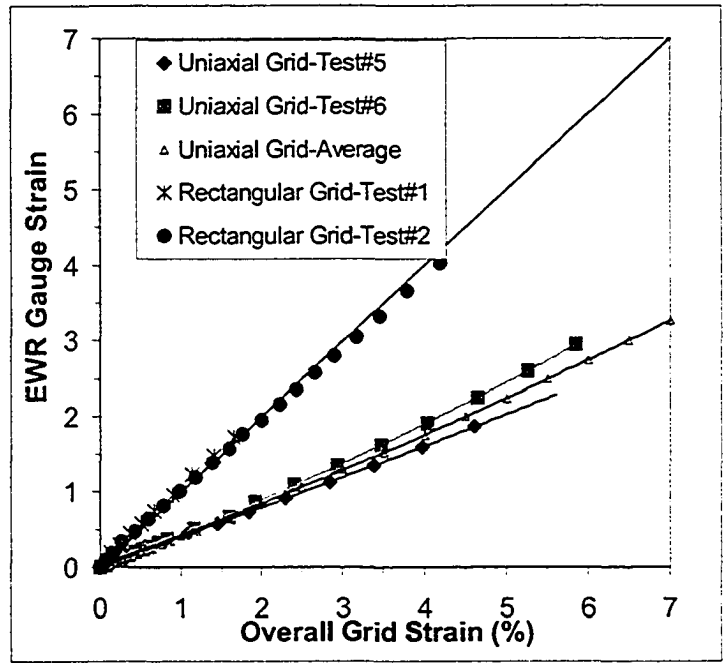

Figure 7. EWR strain gauge calibrations-summary

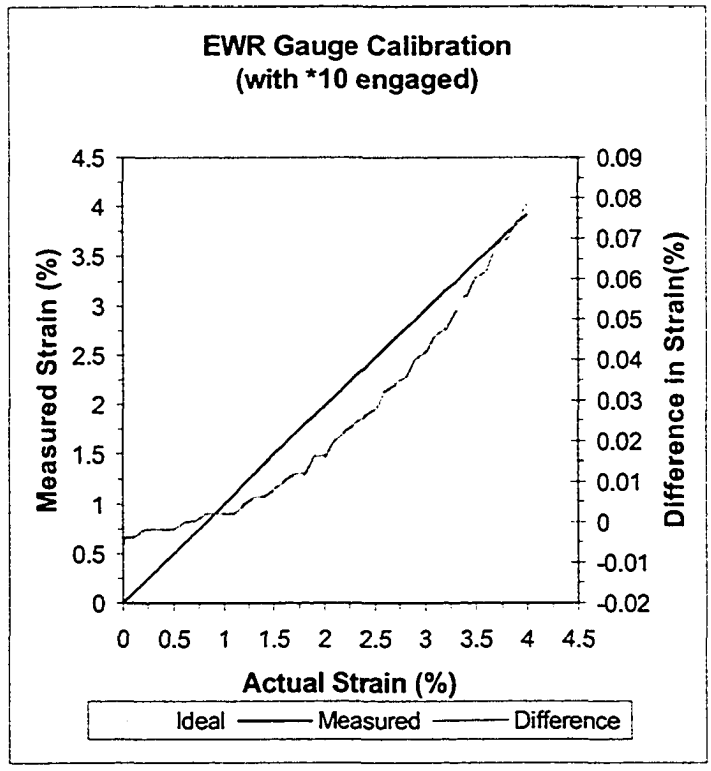

Figure 8. Recalibration check for the P-3500 readout device

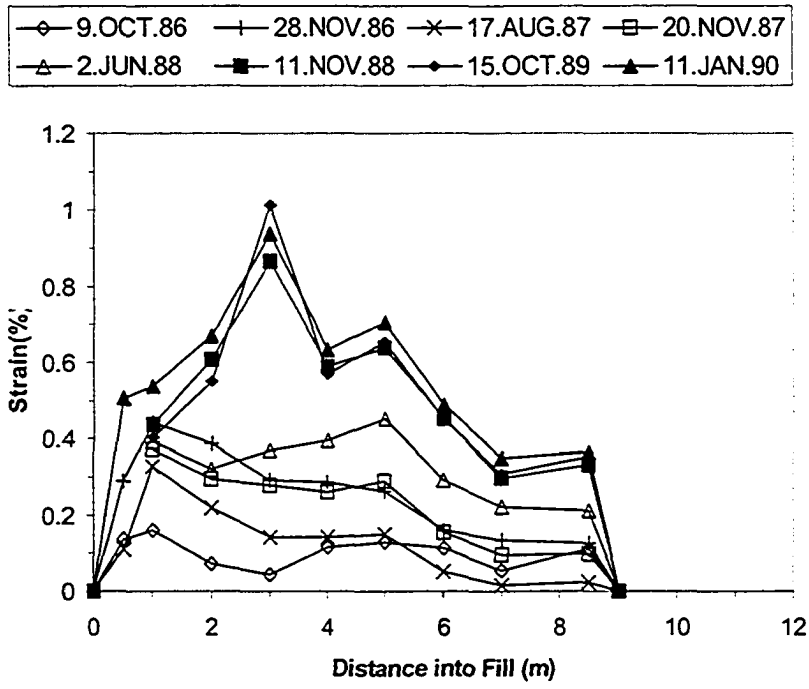

Figure 9. Tensar bottom layer-EWR strain gauge variation till 1990

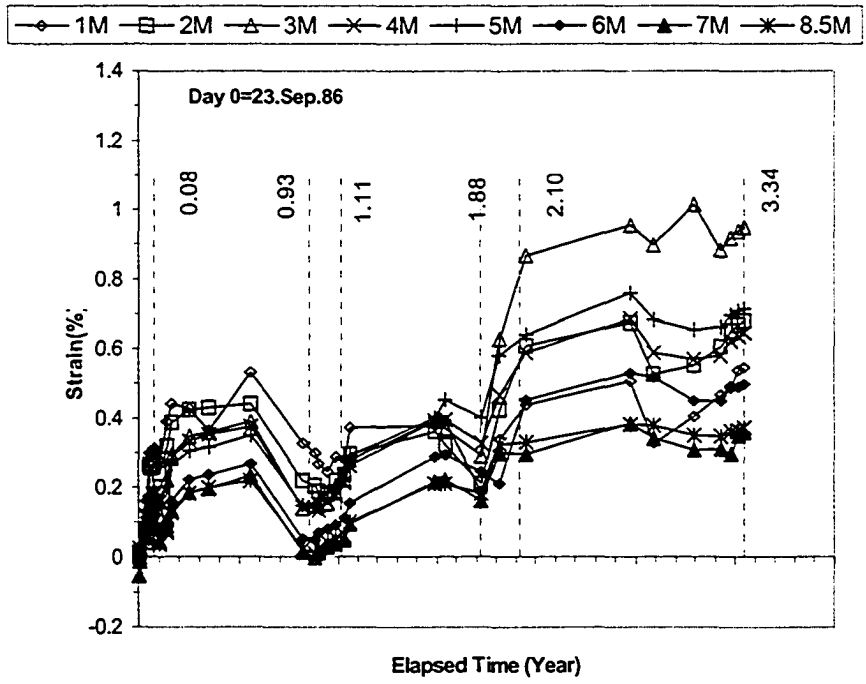

Figure 10. Tensar bottom layer-EWR strain gauge variation till 1990

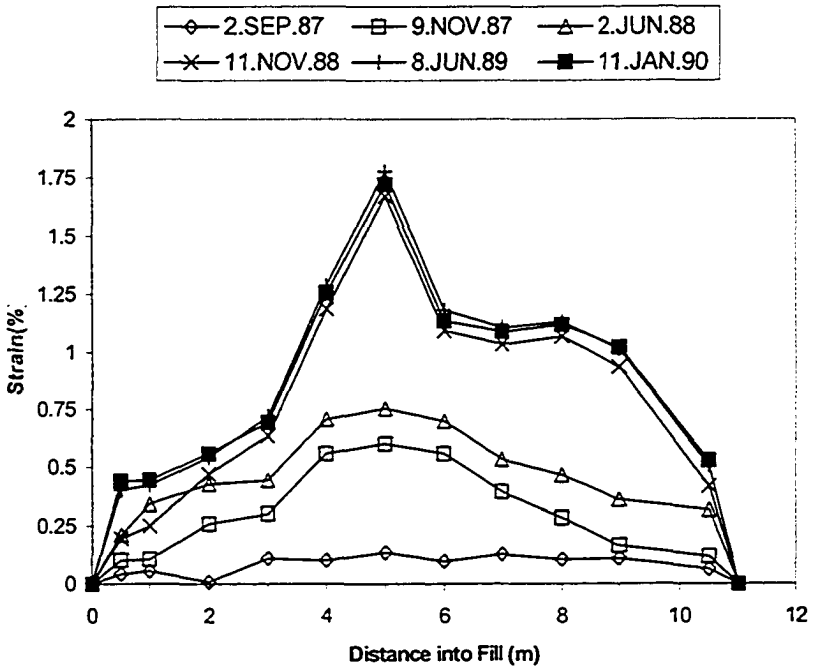

Figure 11. Tensar middle layer-EWR strain gauge variation till 1990

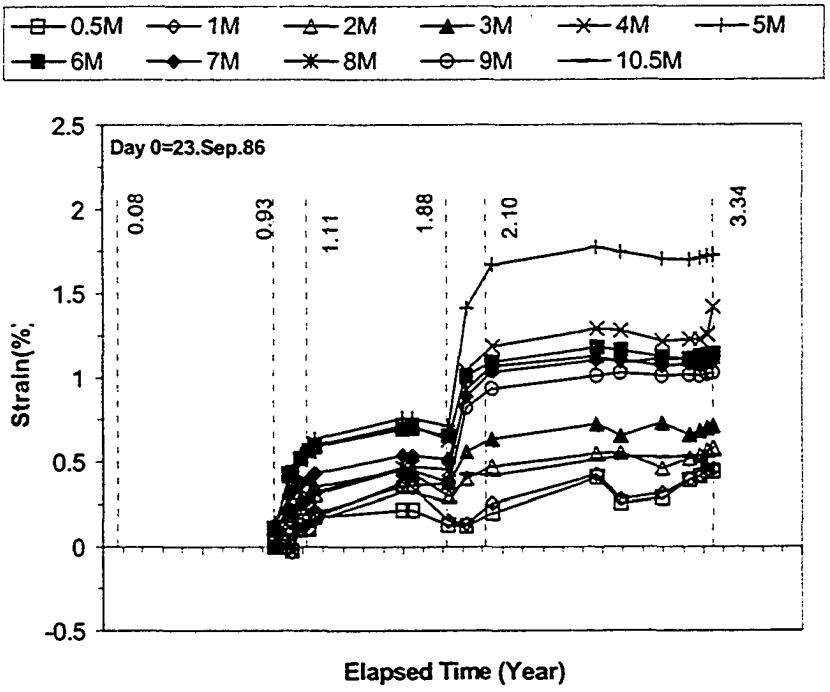

Figure 12. Tensar middle layer-EWR strain gauge variation till 1990

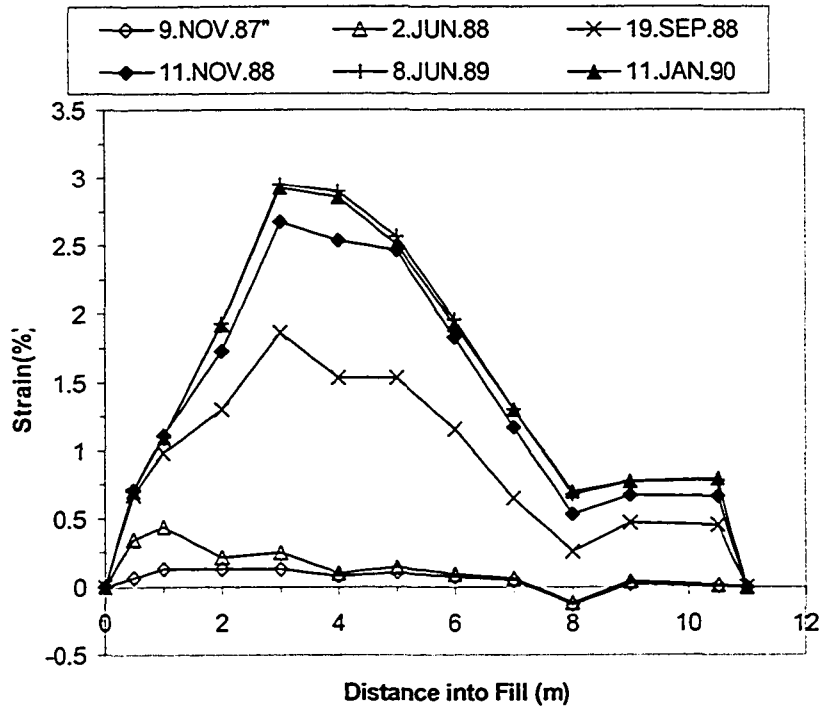

Figure 13. Tensar top layer-EWR strain gauge variation till 1990

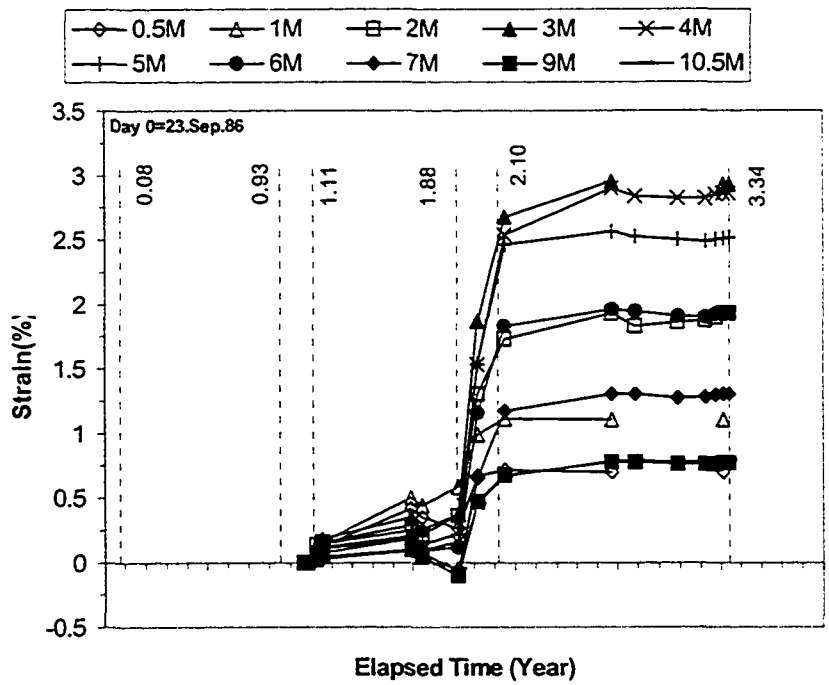

Figure 14. Tensar top layer-EWR strain gauge variation till 1990

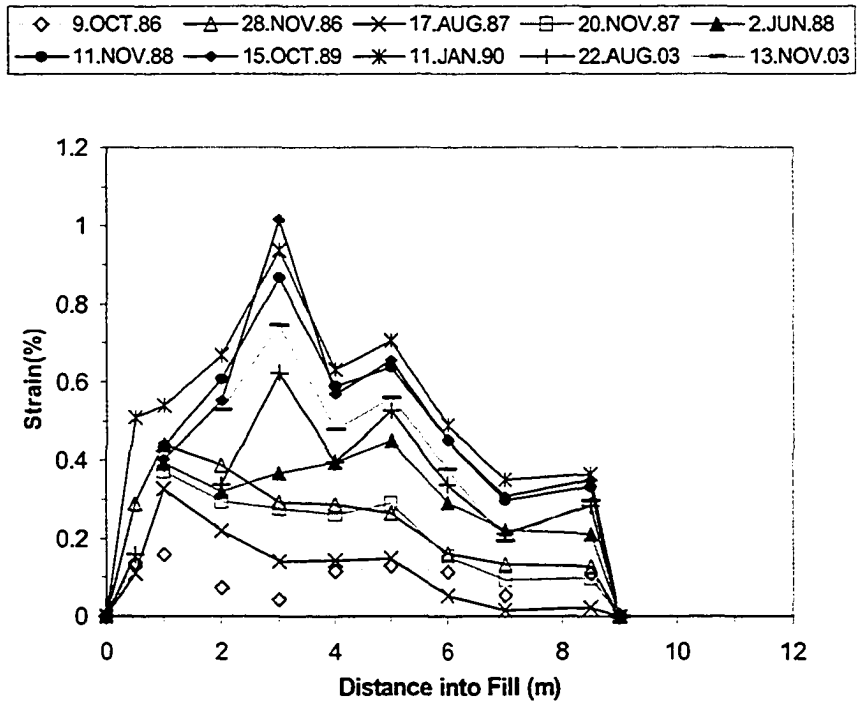

Figure 15. EWR strain gauge variation including 2003 measurements-Tensar bottom layer

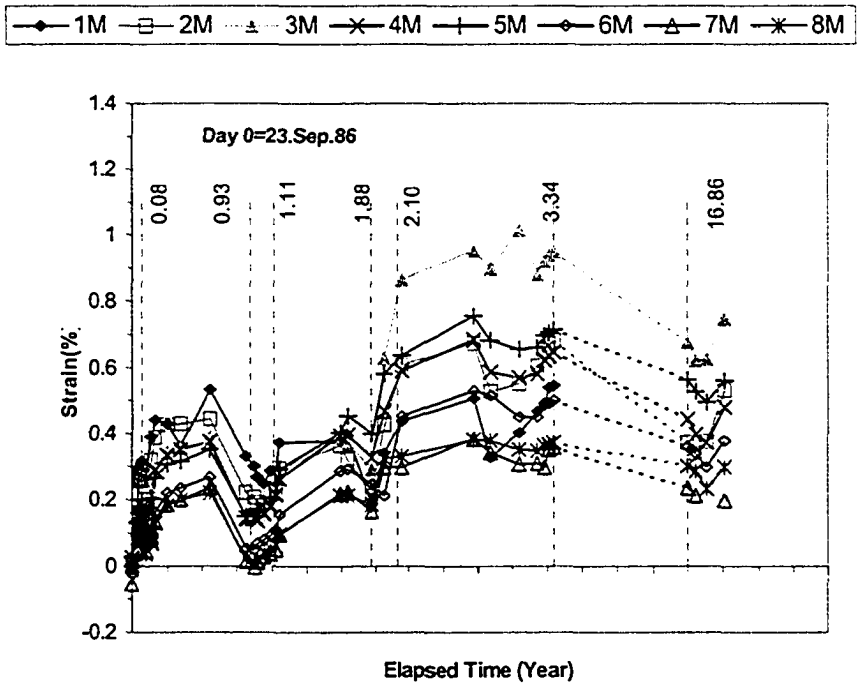

Figure 16. EWR strain gauge variation including 2003 measurements-Tensar bottom layer

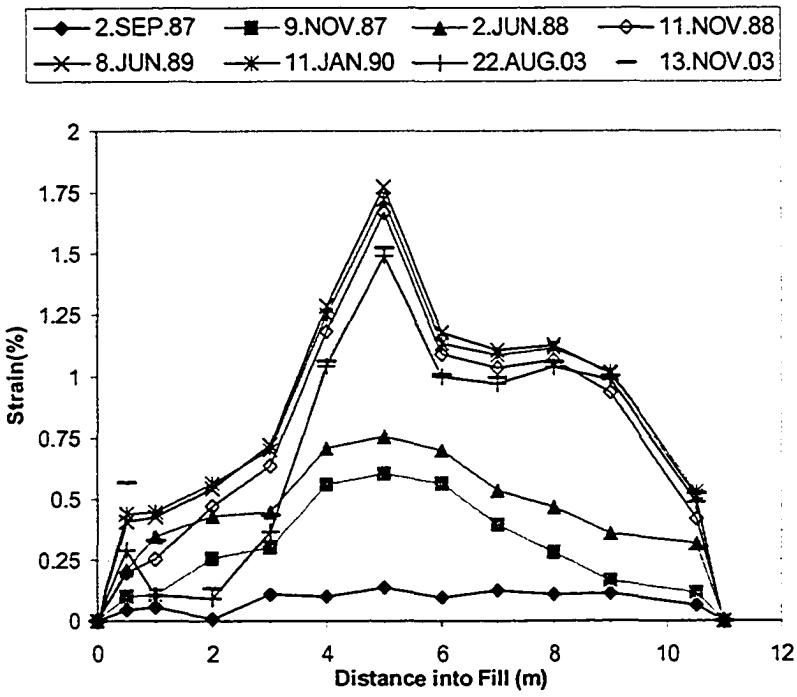

Figure 17. EWR strain gauge variation including 2003 measurements- Tensar middle layer

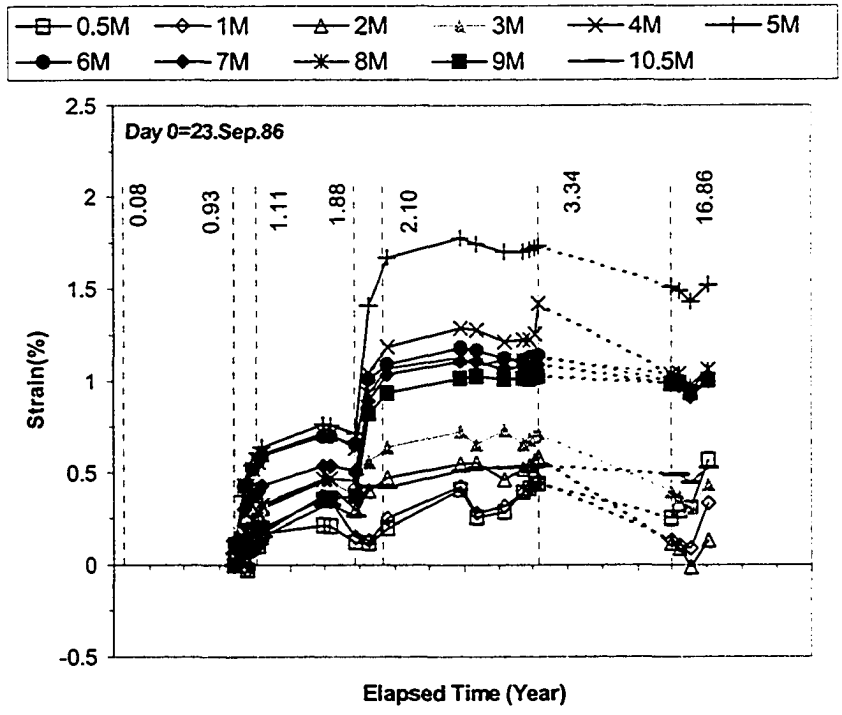

Figure 18. EWR strain gauge variation including 2003 measurements- Tensar middle layer

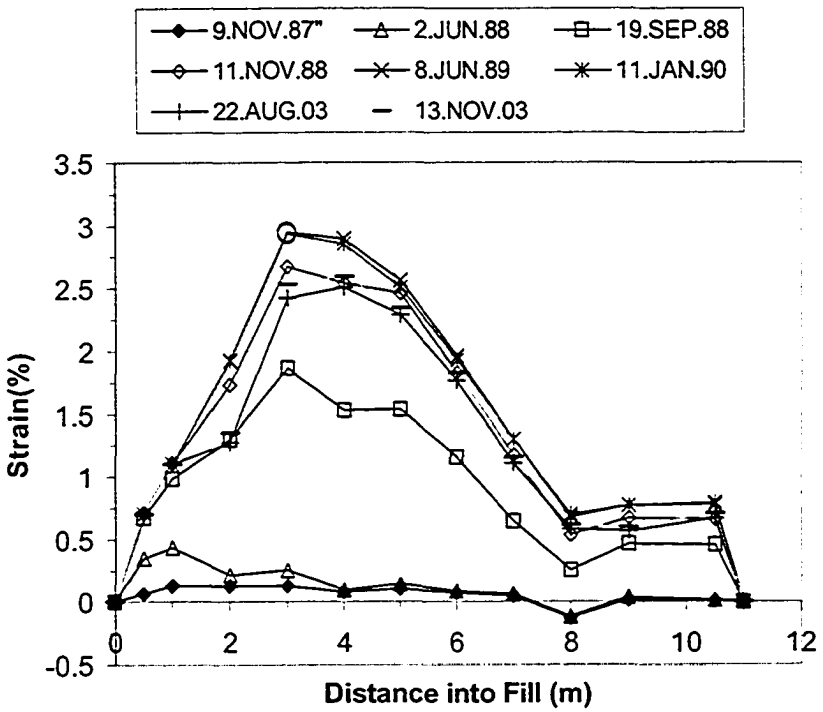

Figure 19. EWR strain gauge variation including 2003 measurements- Tensar top layer

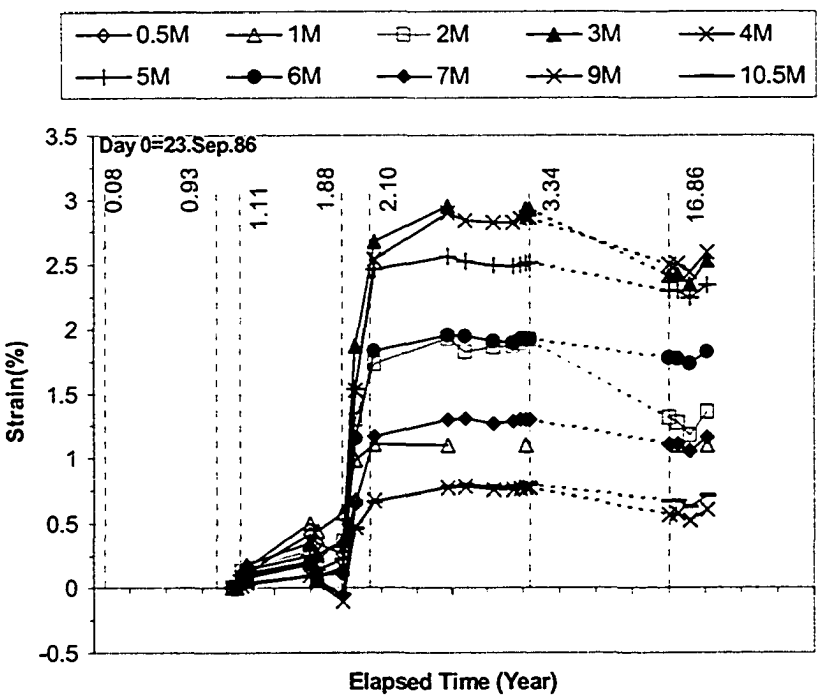

Figure 20. EWR strain gauge variation including 2003 measurements- Tensar top layer

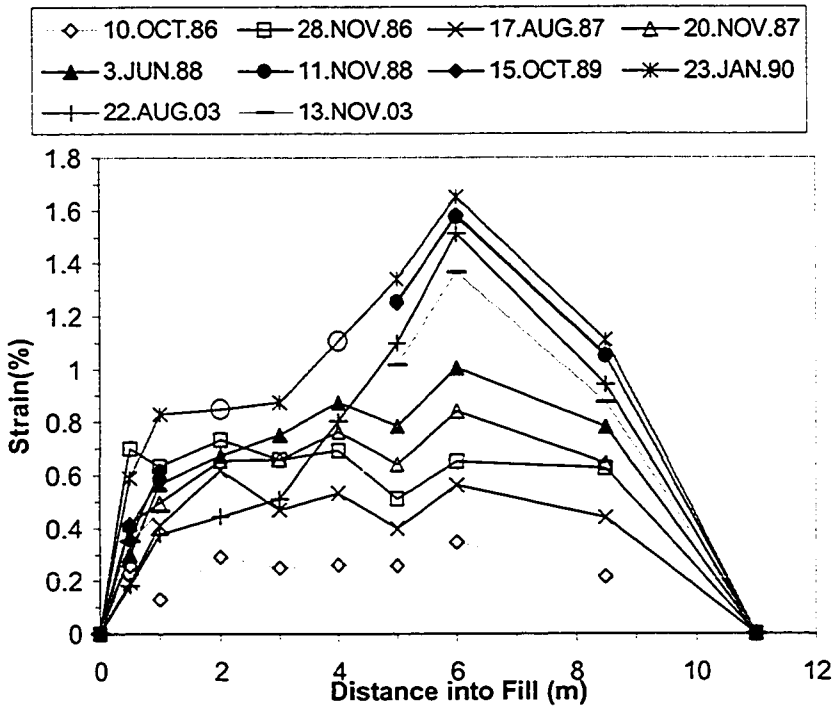

Figure 21. EWR strain gauge variation including 2003 measurements- Signode bottom layer

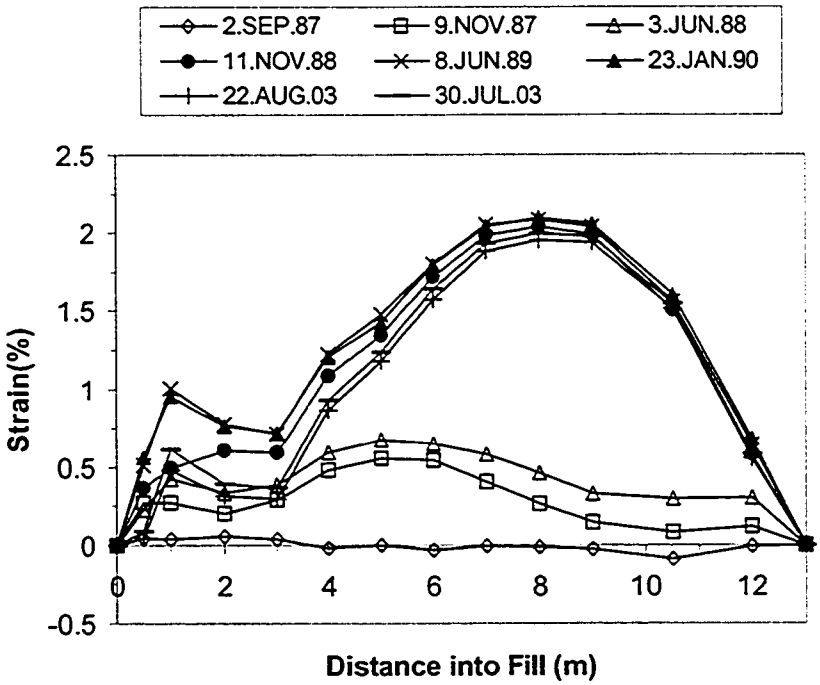

Figure 22. EWR strain gauge variation including 2003 measurements- Signode middle layer

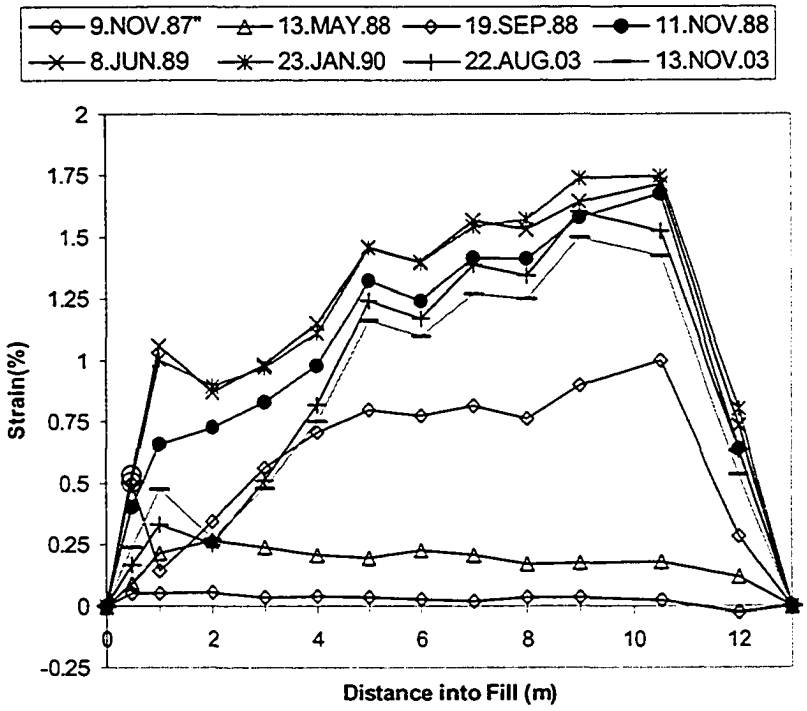

Figure 23. EWR strain variation including 2003 measurements- Signode top layer

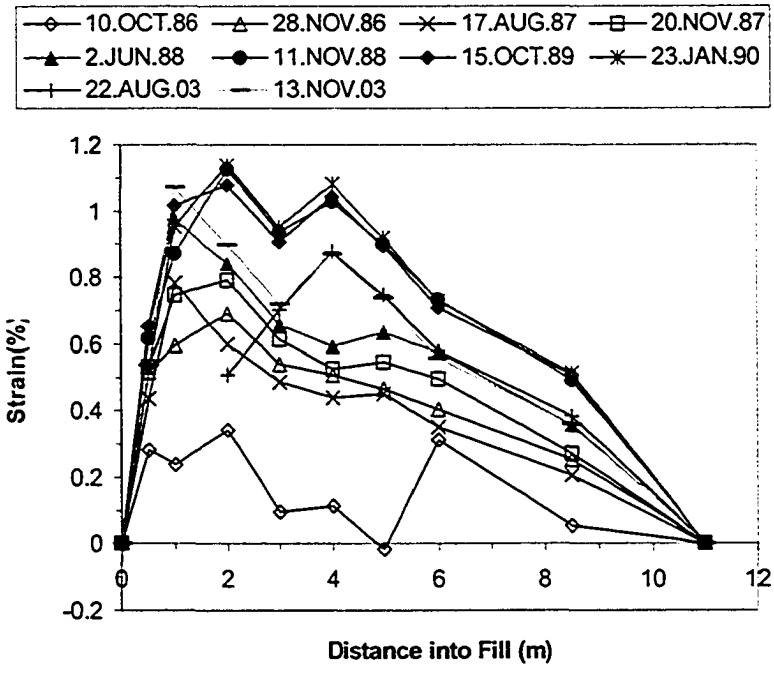

Figure 24. EWR strain gauge variation including 2003 measurements- Paragrid bottom layer

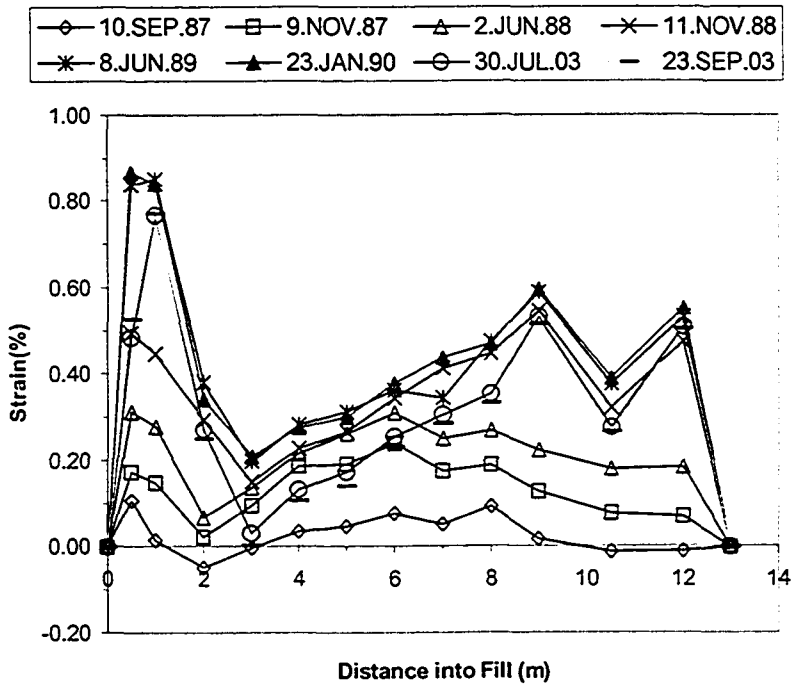

Figure 25. EWR strain gauge variation including 2003 measurements- Paragrid middle layer

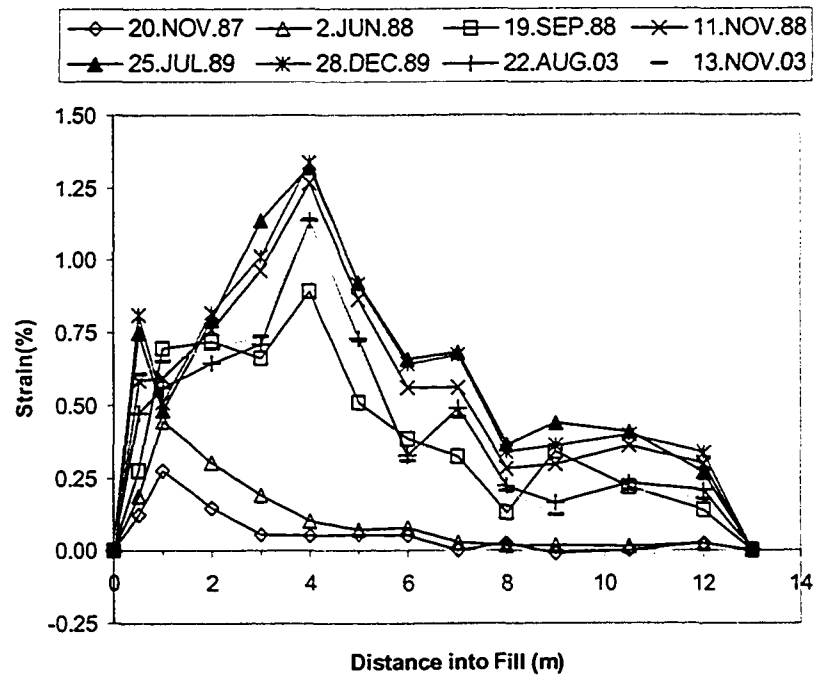

Figure 26. EWR strain gauge variation including 2003 measurements- Paragrid top layer

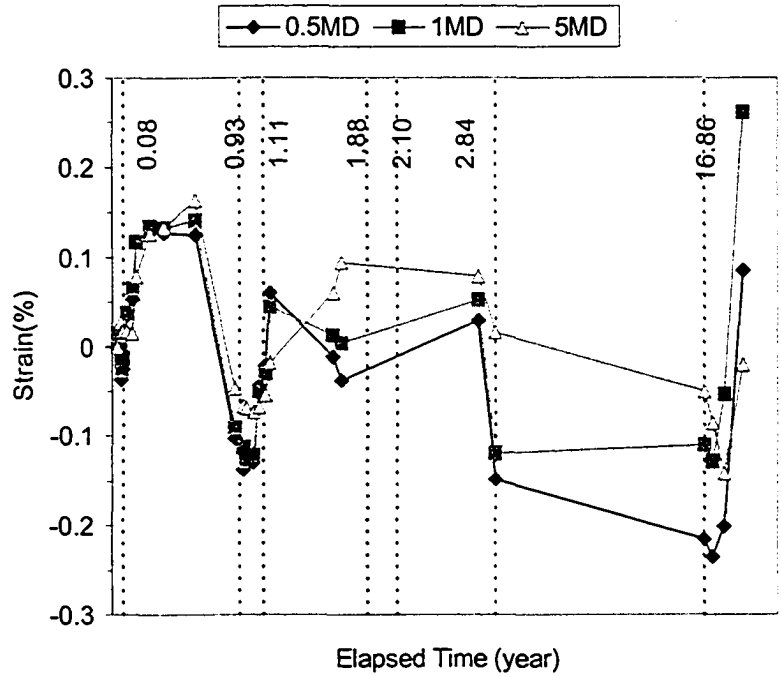

Figure 27. Temperature corrected strain variation in dummy EWR strain gauges- Tensar bottom layer

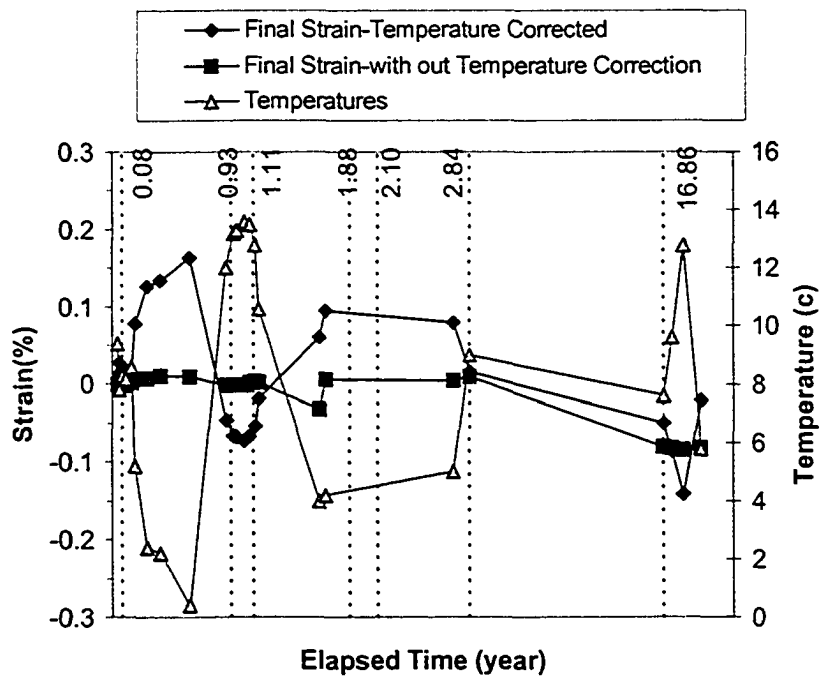

Figure 28. Dummy EWR strain gauge variation- Tensar bottom layer- 5 m from slope face

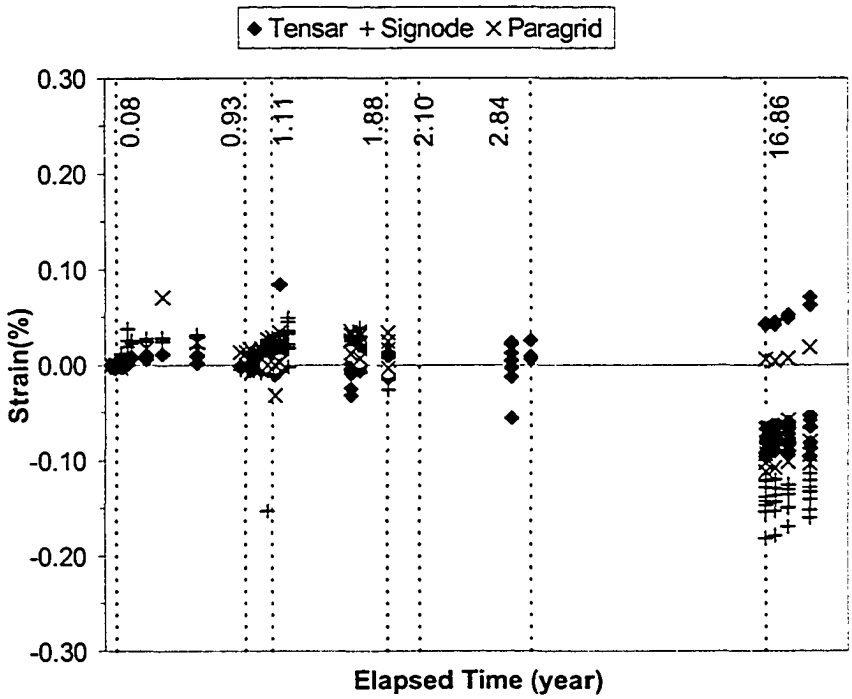

Figure 29. Dummy EWR strain gauge variation for all geogrids- without temperature correction

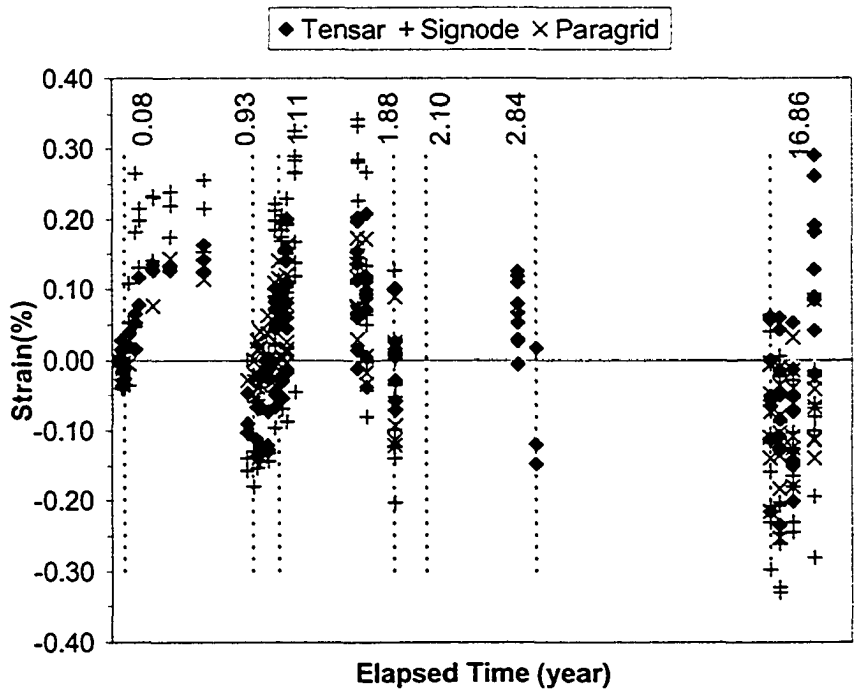

Figure 30. Dummy EWR strain gauge variation for all geogrids- with temperature correction

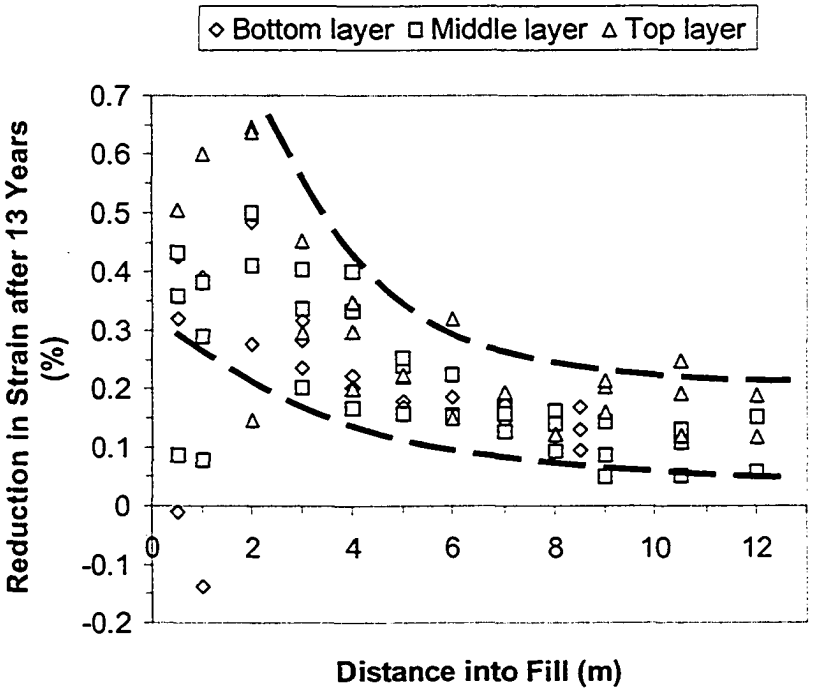

Figure 31. Reduction in EWR strain gauge measurements between 1990 and 2003 field measurements for all geogrids

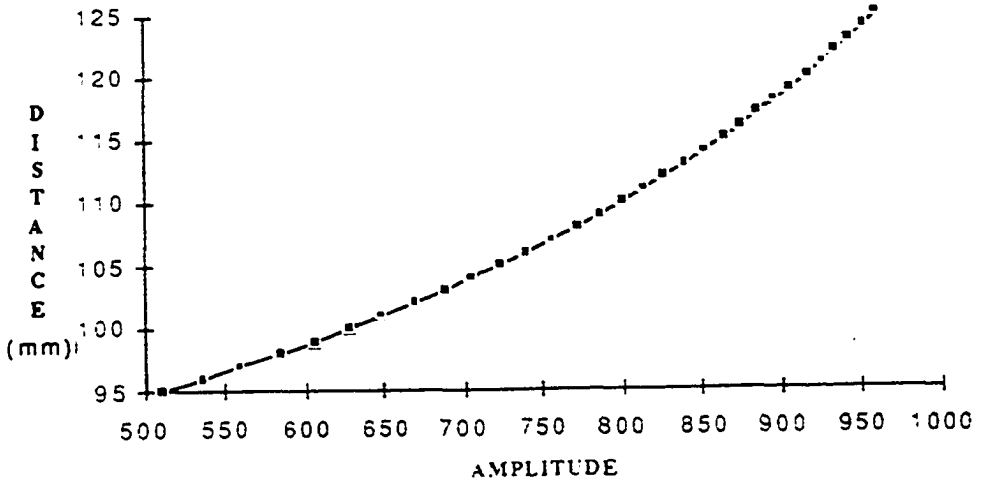

Figure 32. Calibration curve of inductance coils - Range 2 (modified from Liu, 1992)

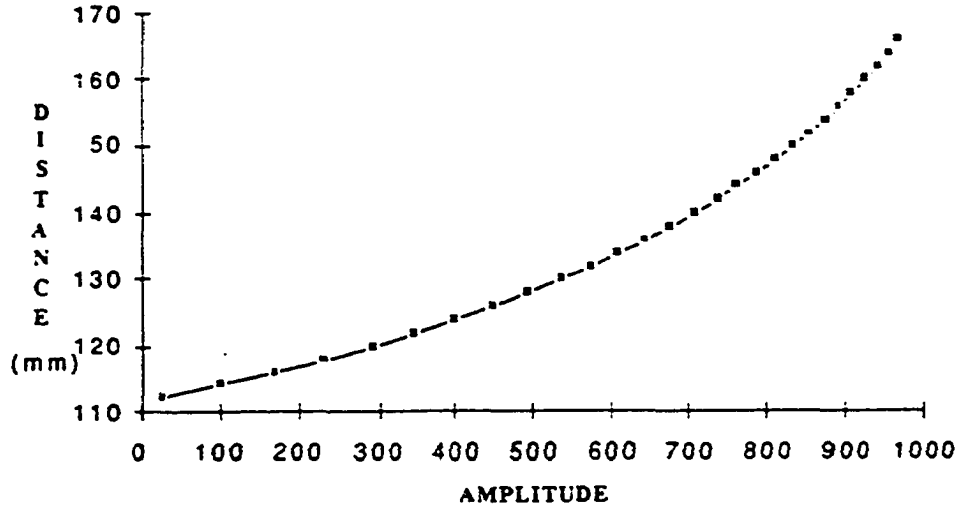

Figure 33. Calibration curve of inductance coils - Range 3 (modified from Liu, 1992)

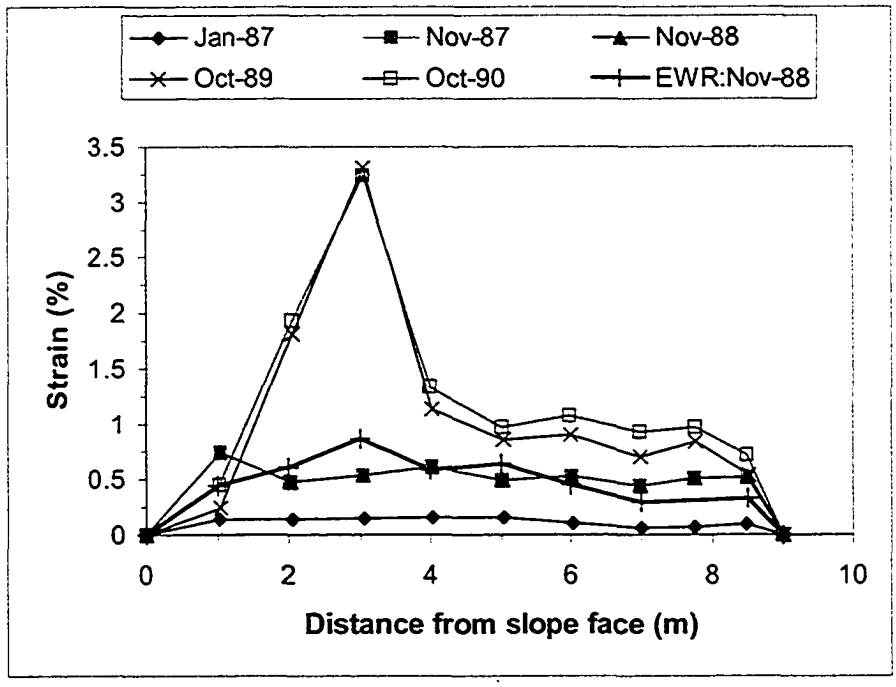

Figure 34. Strain distribution measured by Bison gauges-Tensar bottom layer (modified from Liu, 1992)

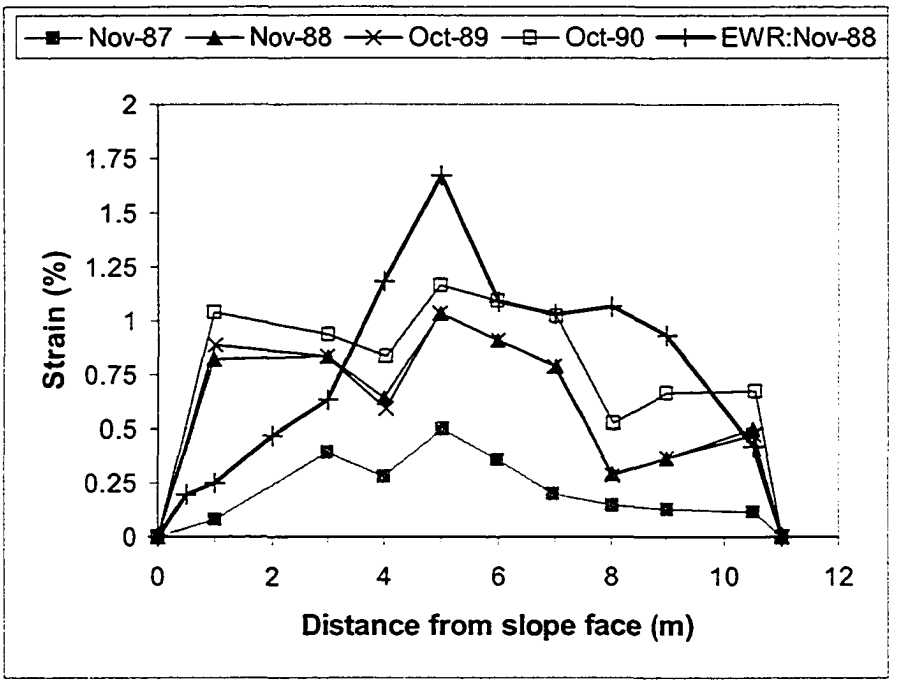

Figure 35. Strain distribution measured by Bison gauges-Tensar middle layer (modified from Liu, 1992)

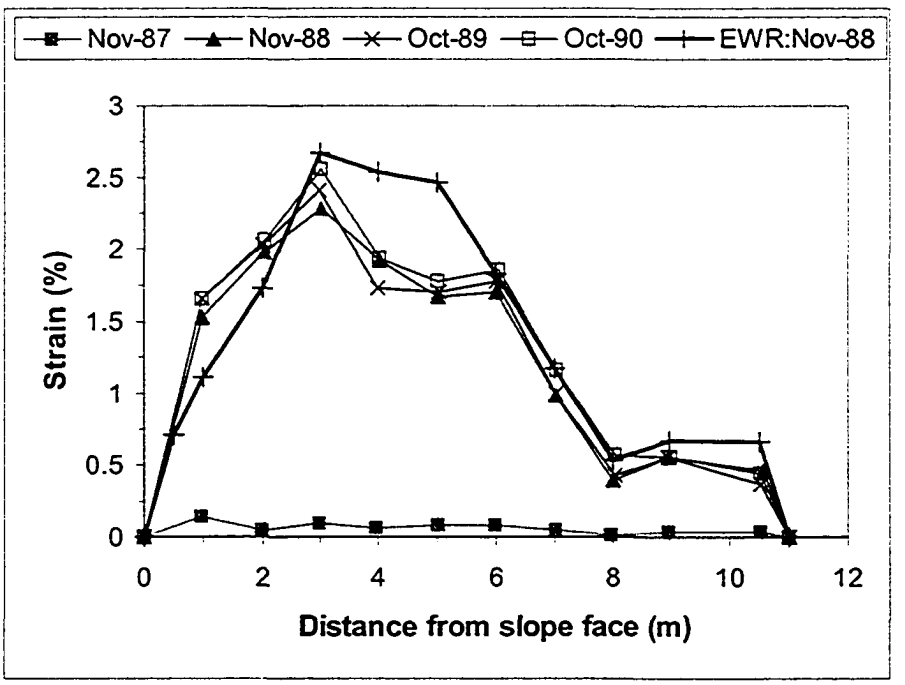

Figure 36. Strain distribution measured by Bison gauges-Tensar top layer (modified from Liu, 1992)

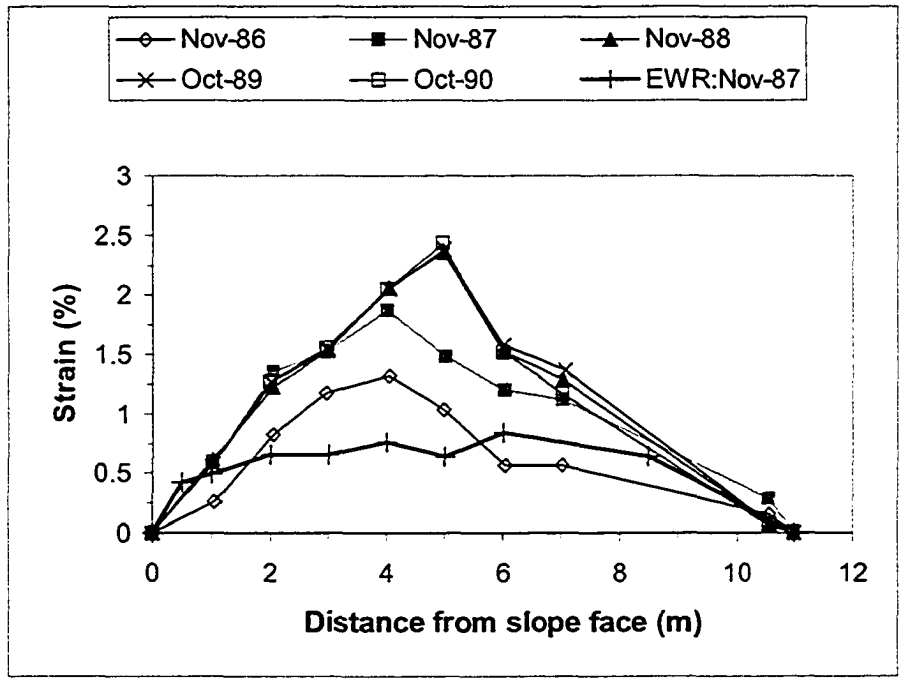

Figure 37. Strain distribution measured by Bison gauges-Signode bottom layer (modified from Liu, 1992)

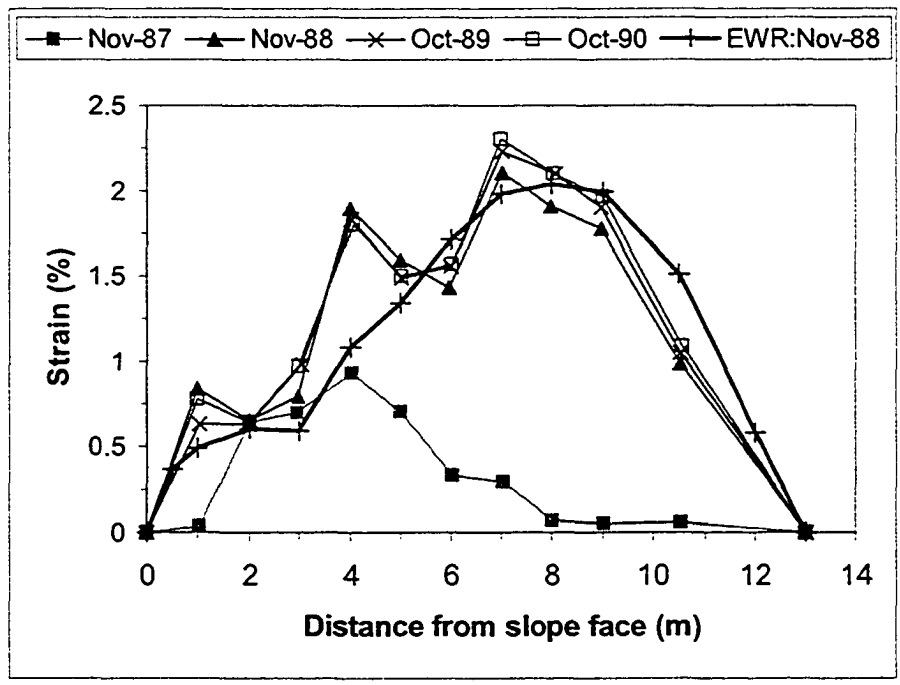

Figure 38. Strain distribution measured by Bison gauges-Signode middle layer (modified from Liu, 1992)

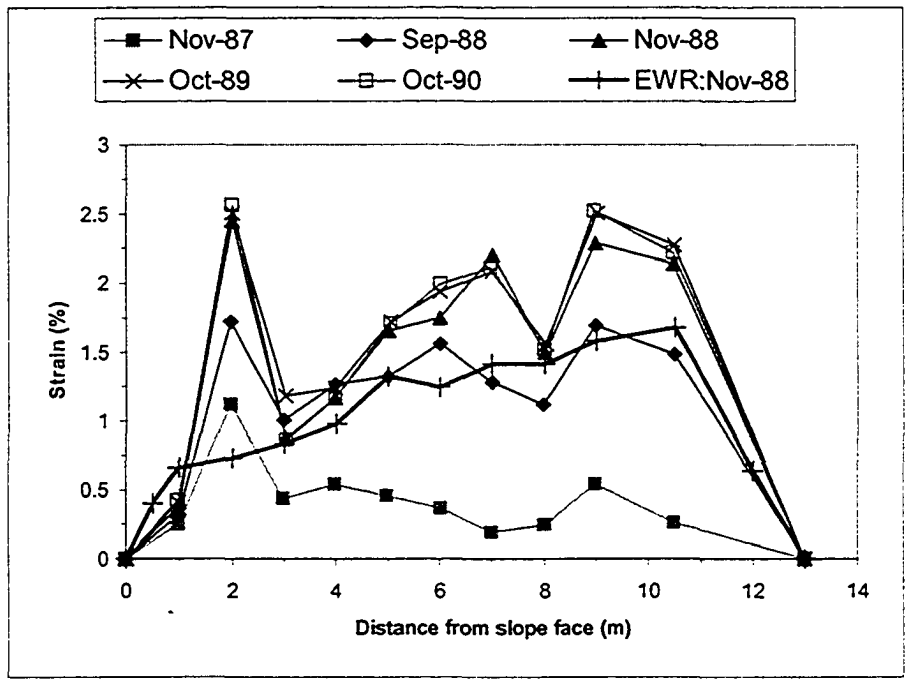

Figure 39. Strain distribution measured by Bison gauges-Signode top layer (modified from Liu, 1992)

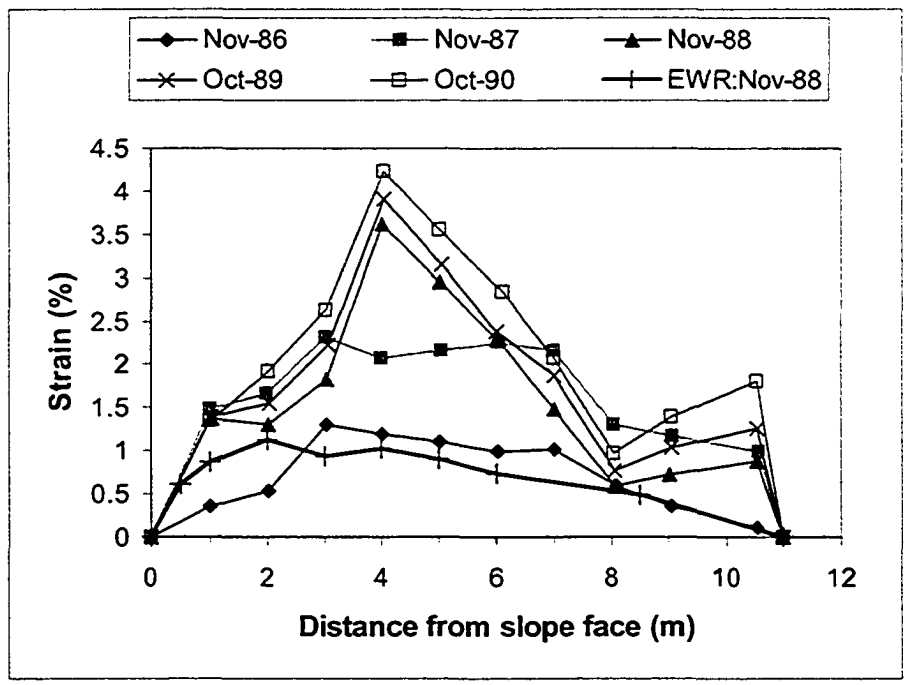

Figure 40. Strain distribution measured by Bison gauges-Paragrid bottom layer (modified from Liu, 1992)

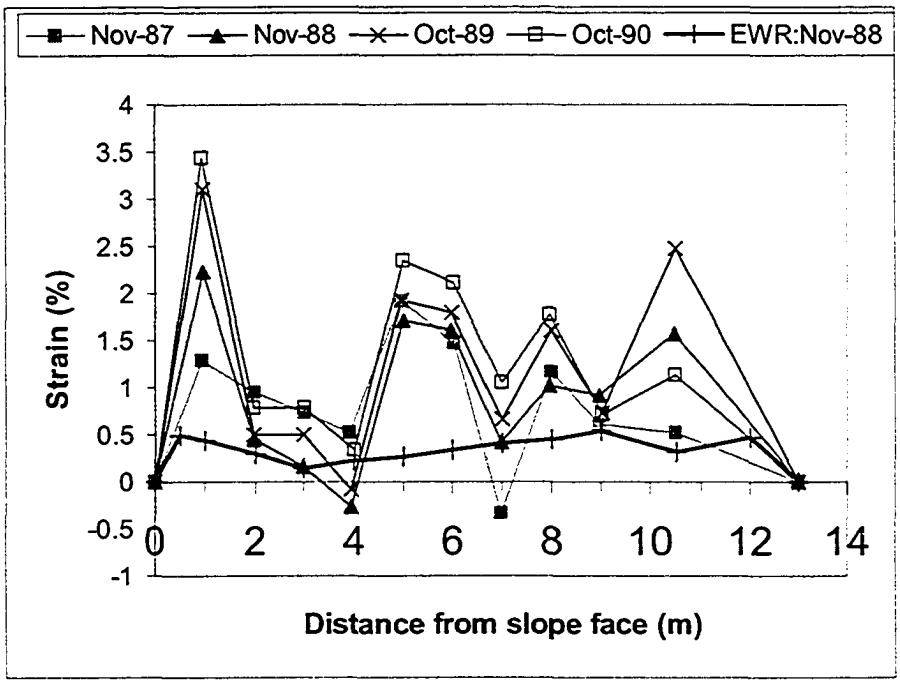

Figure 41. Strain distribution measured by Bison gauges-Paragrid middle layer (modified from Liu, 1992)

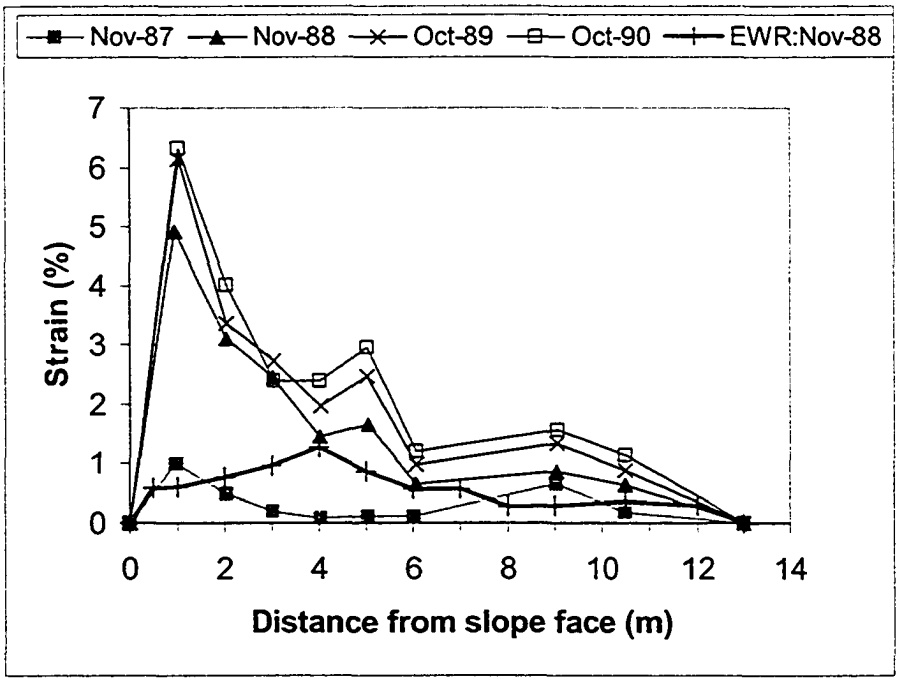

Figure 42. Strain distribution measured by Bison gauges-Paragrid top layer (modified from Liu, 1992)

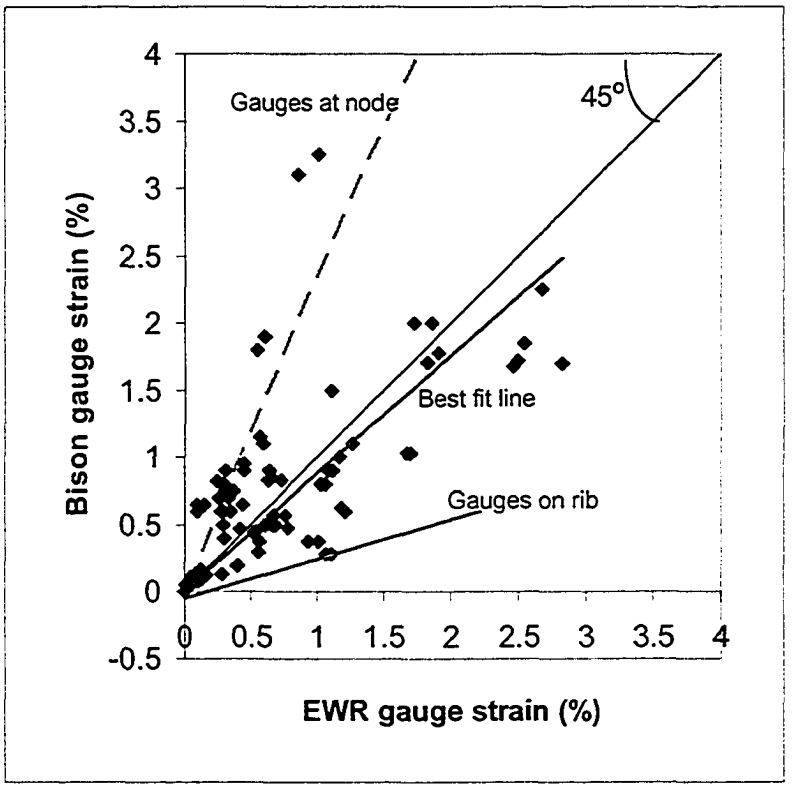

Figure 43. Correlation between EWR strain gauge measurements and Bison strain gauge measurements – Tensar

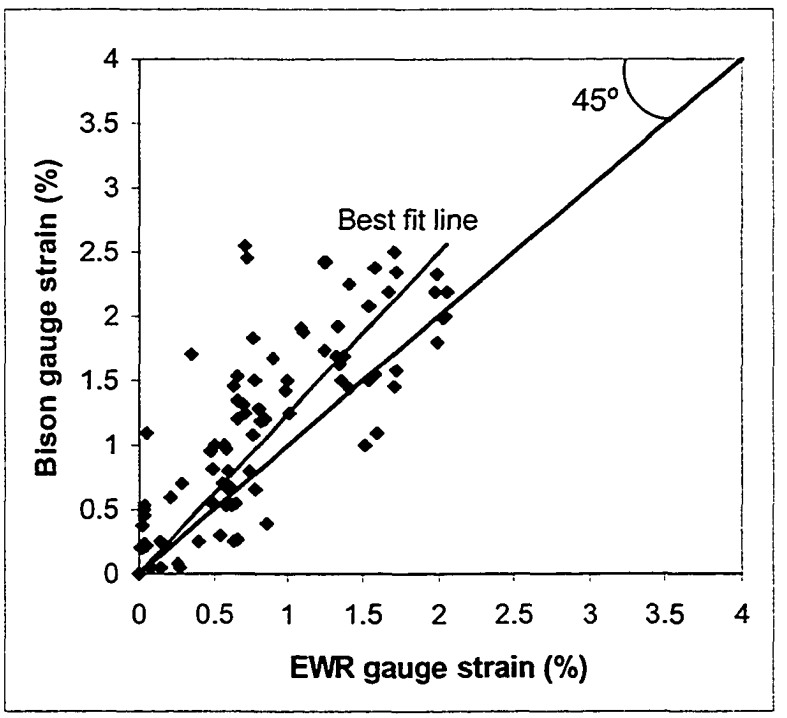

Figure 44. Correlation between EWR strain gauge measurements and Bison strain gauge measurements - Signode

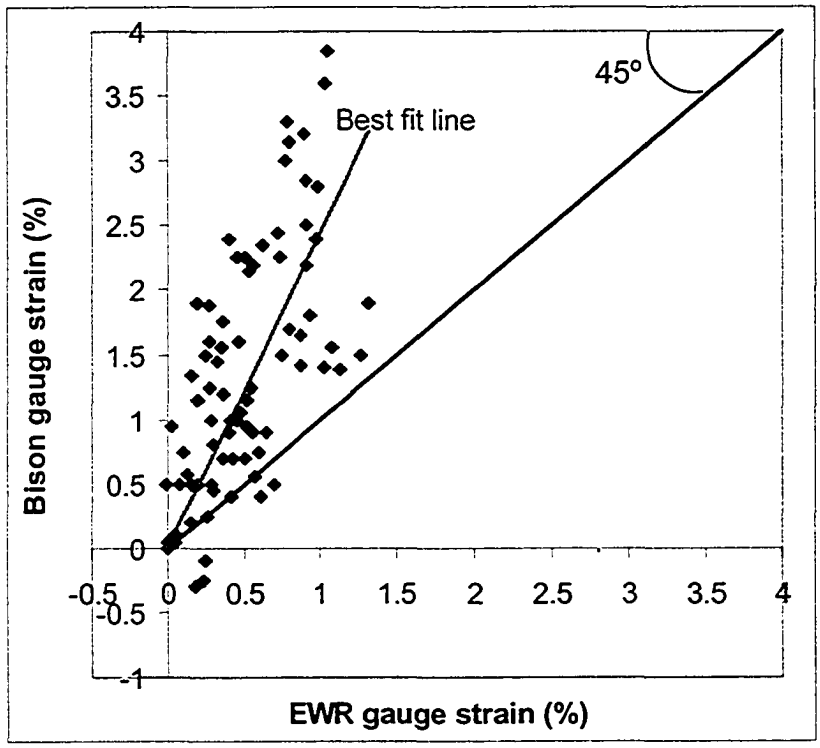

Figure 45. Correlation between EWR strain gauge measurements and Bison strain gauge measurements - Paragrid

Bartlett, S., Monley, G., Soderberg, A. and Palmer, A. (2001). "Instrumentation and Construction Performance Monitoring for I-15 Reconstruction Project in Salt Lake City, Utah", Transportation Research Record, No.1772, pp.40-47.

Bathurst, R.J. (1991). " Case study of a monitored propped panel wall", Geosynthetic-Reinforced soil retaining walls, Proc. of the Int. Symp. Denver, 8-9 August 1991, pp.159-166.

Bathurst, R.J. and Allen, T.M., (2002). " Short term strain and deformation behavior of geosynthetic walls at working stress conditions", Geosynthetics International, Vol.9, No.5-6, pp. 451-482.

Bathurst, R.J., Walters, D.L, Hatami, K. and Allen, T.M., (2001). " Full-Scale Performance Testing and Numerical Modeling of Reinforced Soil Retaining Walls", Landmarks in earth reinforcement: Proceedings of the international symposium on earth reinforcement, Fukuoka, Kyushu, Japan, Nov.14-16, pp.777-799.

Billiard, J.W. and Wu, J.T.H. (1991). "Load test of a large-scale geotextile-reinforced retaining wall", Proceedings of Geosynthetics '91, IFAI, Vol.2, Atlanta, Georgia, USA, February 1991, pp.537-548.

Bonaparte, R., Schmertmann, G.R., Chu, D. and Chouery-Curtis, V.E. (1989) " Reinforced Soil Buttress to Stabilize a High Natural Slope", Proceedings of the Twelfth international conference on soil mechanics and foundation engineering, Rio de Janeiro, 1989, Vol.2, pp.1227-1230.

Brandon, T.L., Al-Qadi, I.M., Lacina, B.A. and Bhutta, S.A. (1996). "Construction and Instrumentation of Geosynthetically Stabilized Secondary Road Test Sections", Transportation Research Record, No.1534, pp.50-57.

Buttry, K.E., McCullough, E.S. and Wetzel, R.A. (1996). "Temperatures and Related Behavior in Segmental Retaining Wall System", Transportation Research Record, No.1534, pp.19-23.

Carrubba, P., Moraci, N. and Montanelli, F. (1999). "Instrumented soil reinforced retaining wall: analysis of measurements", Proceedings of Geosynthetics' 99 conference, Boston, Massachusetts, 1999, Vol.2, pp.921-934.

Christopher, B.R., Bonczkiewicz, C. and Holtz, R.D. (1994). "Design, construction and monitoring of full scale test of reinforced soil walls and slopes", Proceedings of the recent case histories of permanent geosynthetic-reinforced soil retaining walls conference, pp.45-60.
Fishman, K.L., Desai, C.S. and Sogge, R.L. (1993) "Field Behavior of Instrumented Geogrid Soil Reinforced Wall", Journal of Geotechnical Engineering, Vol.119, No.8, pp.1293-1307.

Liu, Y. (1992). "Performance of Geogrid Reinforced Clay Slopes." PhD. Thesis, Civil Eng. Dept., University of Alberta, Edmonton, Alberta: 406p.

Martin, E.D. (1986). "Instrumenting geogrids with Bison gauges." Report for 905 work term, Civil Engineering Dept., University of Alberta, Edmonton, Alberta, 18p.

Montanelli, F., Recalcati, P. and Rimoldi, P. (1999). " An instrumented geogrid reinforced slope in central Italy: field measurements and FEM analysis results", Field instrumentation for soil and rock, ASTM STP 1358, G.N.Durham and W.A.Marr, Eds., American Society for Testing and Materials, West Conshohocken, PA, 1999, pp.16-35.

Rimoldi, P. and Jaecklin, F. (1996). "Green faced reinforced soil walls and steep slopes: the state-of-the-art", Geosynthetics: Applications Design and construction, De Groot, Den Hoedt and Termaat Editors, Balkema, Rotterdam, pp.361-380.

Soderberg, H.C., (1990). "Application of Electrical Wire Resistance Strain Gauges to Plastic Material", M.Eng. Report, Department of Civil Engineering, University of Alberta, Edmonton, Canada, 104p.

Toriihara, M., Matsumoto, S. and Hirama, K. (1994). "Construction and measurement of embankment reinforced with geogrid using in-situ cohesive soil", Proceedings of the recent case histories of permanent geosynthetic-reinforced soil retaining walls conference, pp.295-299.

Wu, J.T.H. and Helwany, A.M.B. (1996). "A performance test for assessment of long-term creep behavior of soil-geosynthetic composites", Geosynthetics International, Vol.3, No.1, pp.107-124.

Zanzinger, H. and Gartung, E. (1992). "Large scale model test for the determination of the structural behavior of a geogrid-reinforced slope" Earth reinforcement practice: Proceedings of the International Symposium on Earth Reinforcement Practice, Fukuoka, Kyushu, Japan, 11-13 November 1992, pp.317-322.

Chapter 5. Inclinometers-Horizontal and Vertical

5.1 Introduction

Monitoring the deformation pattern of the Devon test embankment and the foundation soil is an important component in evaluating the embankment performance. In order to study the deformation pattern of the test fill and the foundation soil horizontal and vertical inclinometers were installed at different locations in the test embankment and the foundation soil. The long term deformation pattern of the test fill will be discussed by comparing the 1990 and 2003 measurements of the horizontal and vertical inclinometers. The long term performance of the instruments is also evaluated.

5.2 Literature review on horizontal and vertical inclinometers used in reinforced soil structures

Instrumentation of an anchored segmental retaining wall is reported by Yoo and Lee (2003). An extensive field monitoring program was implemented for a 7 m high anchored segmental wall to better understand the fundamental behavior of the wall. Two vertical inclinometers were installed at 1.3 and 4.3 m behind the wall facing column for the purpose of monitoring the post-construction lateral soil movements with in the reinforced zone. The inclinometers (ACE Model INC 1410) were a vibrating wire type with a maximum range of ±10°. Shielded cables having a diameter of 6.4 mm with PVC jacket were used to collect the data. Casings were first grouted in predrilled holes in the foundation prior to backfill placement; the bottom of the casings was located 0.5 m below the base of the leveling pad, which was 1 m below the ground surface. Zero readings were taken after the construction had been completed so the data only represented additional movements after the completion of the

wall construction. Hence movements during the construction are not covered since the inclinometer casings were built up with the fill placement and did not provide a fixed datum over the period of wall construction.

Cantilever type of movements were recorded in the inclinometers during the period of about one month after end of the construction with a maximum lateral movement of approximately 8 and 4 mm at the top of the front and back inclinometers respectively. Those movements imposed an additional lateral soil tensile strain of approximately 0.1% in the upper portion of the soil mass, and this trend was consistent with other measured data showing a slight increase during that period. Such movements that occurred after the completion of the wall construction may have been caused by the heavy rainfalls as well as a redistribution of soil shear stress as tension was mobilized in the anchor bars. No further movements were observed since then, indicating no time-dependant movements.

In a paper by Allen and Bathurst (2002), they reviewed the measurements of more than 10 geosynthetic walls with adequate deformation and strain data to determine long term creep rates. Instrumentation details can be found in the paper by Bathurst *et.al* (2002) for each case history but in general the walls were reinforced with HDPE, PET or PP geosynthetic polymers and the deformations were mainly measured using inclinometers and survey measurements of facings. The data for these case histories were plotted as the wall face post-construction lateral deformations to a function of normalized depth below the wall top.

Three main observations can be made from these results. The post-construction face deformations increase linearly with increasing height above the wall face for half of the studied cases, with the maximum

deformation near the wall top. The post-construction face deformations do not appear to be a function of total wall height, nor do they appear to be a function of wall facing type based on the available database of case studies. Also most of the wall deformations have occurred within 10,000 hours of wall construction.

Bonaparte *et.al* (1989) reports a use of reinforced soil buttress to stabilize a high natural slope with height of about 34 m. The soil buttress was built using compacted onsite fill (primarily shale) reinforced with layers of Tensar UX1600 uniaxial geogrid. Horizontal buttress deformations were monitored using two vertical inclinometers installed at the top of the buttress and 11 m from the base of the buttress. The bottoms of vertical casings were embedded deep enough in the conglomerate and sandstone lying beneath the buttress. Maximum deformations of about 10 mm occurred in the lower portion of the buttress during construction. Post-construction horizontal deformations were small, typically less than 5 mm.

Bartlett et.al (2001) discussed the instrumentation of geotextiles that were used to reinforce the embankments and MSE walls for a reconstruction project. A high strength woven geotextile was used to improve the global stability of some embankment and wall systems during rapid, undrained loading conditions. In some locations as many as three layers of geotextile (730 kN/m ultimate strength; 292 kN/m allowable strength) were used to guard against development of shear failure in the foundation. Near the toe of critical embankments and walls, vertical inclinometer casing was installed to depths of about 25 m below ground surface into the Pleistocene alluvium to monitor horizontal deformation in the Lake Bonneville sediments. The casing consisted of flush-jointed, 69-mm (outside diameter) ABS plastic inclinometer casing placed in a 150-mm bore hole. Two to four telescopic couplings, each able to accommodate up to 150 mm of settlement, were also placed at casing joints to prevent

bending of the casing due to differential settlement within the soil profile. A relatively stiff grout mix of 1:0.28:0.02 water/cement/bentonite ratio was used to seat the casing into the Pleistocene sands. A less stiff grout was used to set the remaining casing. All inclinometer casings were protected from construction activities by locked metal housings. During active fill placement, horizontal displacement rates of 8 to 12 mm per day were measured in the Lake Bonneville sediments in response to embankment loading rates that equaled or exceeded 1 m per day. Although rates of horizontal displacement exceeding 7.6 mm per day were considered to be large by the geotechnical design team, this criterion alone was not necessarily an indicator of pending instability.

A major research project on the behavior of reinforced soil was sponsored by the United States Department of Transportation, Federal Highway Administration (FHWA) to develop comprehensive guidelines for evaluating and using soil reinforcement techniques in the construction of retaining walls, cut slopes and roadway embankments. Part of the results of this study is reported by Christopher *et.al* (1994). The field portion of the project consisted of constructing eight reinforced soil walls, each 10.7 m long and 6.1 m high, and four reinforced soil steep slopes, each 15 m long and 7.6 m high with 1:0.5 slope. The walls and slopes were heavily instrumented so that their performance could be evaluated in terms of the design model. Reinforcements selected were representative of the generic reinforcement types in use at the time of the study. Specifically they were: metal strips, metal grids, polymeric geogrids, woven geotextiles and non-woven geotextiles. Three types of soil were selected for the structures to represent the range of backfill material recommended by FHWA. Gravely sand, silt and cobbles were used as backfill material. Field performance of the structures was evaluated from the installed instrumentation. The locations of the instruments were based on the anticipated stress distribution and deformation response of a reinforced soil structure.

Vertical inclinometers were installed 5.5 m into the ground beneath the structures and were extended up through the reinforced soil section as backfilling processed. In reinforced walls 3 vertical inclinometers were installed, one at the back of the wall face, one at the middle of the reinforcement length and one at the end of the reinforcement length. In reinforced slopes, two vertical inclinometers were installed; one at the crest of the slope and the other 1.5 m from the slope toe.

For all the walls reinforced with steel strips, extruded geogrid (Tensar SR2) and bar mat, the lateral wall movement at the end of the construction was between 0 and 38 mm at the front vertical inclinometer, between 0 and 25 mm at the middle vertical inclinometer and around 5 mm at the back vertical inclinometer. In the wall reinforced with non woven geotextile the lateral movement of the top of the wall at the end of the construction was about 100 mm. In the slopes reinforced with welded geogrid and woven geotextile, the lateral movement of the embankment slopes at the end of the construction was between 0 and 46 mm at the inclinometer 1.5 m from the toe and between 0 and 87 mm at the inclinometer at the crest of the slope. Bending of the inclinometer casing occurred at some walls and only partial monitoring was possible.

The inclinometer data indicated that practically all movement occurred within the reinforced soil sections. It also tended to confirm the face survey movements. With the exception of the wall reinforced with non woven geotextile both the survey and inclinometer data indicate some rotation at the base and a relatively uniform lateral movement of the upper portion of the walls. The relatively large movement in the upper part of the wall reinforced with non woven geotextile was attributed to problems in construction. The magnitude of rotation in the walls appears to be related to both the stiffness of the reinforcement and the type of the backfill

material. Walls reinforced with extensible reinforcements showed the greatest rotation (on the order of 0.8°). The wall constructed with inextensible reinforcement and silt type soil had a similar amount of movement. The less extensible walls experienced a base rotation of the order of 0.3 to 0.4°.

In contrast to the walls, lateral movement of the embankment slopes appeared to increase with embankment height. The lateral movements observed in the geogrid and geotextile slopes for the same slope angle were almost identical, which tends to support the strain observations. The results of this study show that the different reinforcement systems when designed according to a unified approach behave in a similar and predictable manner, provided that the density of reinforcement (amount of reinforcement per area of the reinforced section) is similar. The principle difference in performance can be attributed to the extensibility of the reinforcement.

Design and construction of a geogrid reinforced high embankment with high water content volcanic cohesive soil is discussed by Miyoshi *et.al* (1992). A high embankment, approximately 20 m, was reinforced with geogrids with maximum tensile strength of 10 tf/m. After completion of the embankment a stability berm 4 m in height was placed as a load at the foot of the embankment and the movement of the embankment was observed for 15 months. The embankment was constructed after clearing and removal of any soft layers at the ground surface. Geogrid and drainage sheets were installed at vertical intervals of 5 m and 2.5 m respectively and the latter was arranged in a zigzag pattern.

Two points of the main embankment were selected for monitoring. Two vertical inclinometers were installed in the embankment one across the 5.5 m elevation and the other at 10.5 m elevation. Casing for inclinometers

was installed as the embankment construction progressed. Monitoring with the inclinometer was therefore continuously recorded from the start of the embankment construction. The maximum horizontal deformation at the lower inclinometer was 40 mm just after the completion of the embankment and 170 mm before construction of the stability berm. These measurements indicate that large horizontal deformations occurred after completion of the embankment. The horizontal deformation at the upper inclinometer was smaller (approximately 1/3).

By calculating the deformation vector, it was found that the settlement was larger than the horizontal deformation at the location of the upper inclinometer. It can be assumed, therefore that the stability of the embankment was improved by strength increase due to consolidation. While the settlement was almost equal to the horizontal deformation at the lower inclinometer location, this cannot be assumed to be the result of some improvement of the embankment stability. Horizontal deformation after completion of the stability berm was stable but some settlement occurred. It can be concluded that settlement only occurred in the embankment, while horizontal deformation stopped and the stability of the embankment was improved. Large deformations of the embankment slope can be assumed to have been caused by the effects of settlement and lateral deformations due to the high water content of the volcanic cohesive soil, because neither major scarp nor cracks were observed. It can therefore be concluded that the embankment was stable against sliding.

5.3 Description of the instrument and readout device

5.3.1 Vertical Inclinometers

For vertical inclinometers, a vertical digital biaxial inclinometer, model P/N 50309-E with model 50325-E sensor made by Sinco Slope Indicator Co.

was used. This inclinometer was operated in a 5.9 cm inner diameter casing and was used to monitor horizontal deflections between two pairs of wheels (61 cm) apart in directions parallel and perpendicular to the axis of the embankment. This Digitilt Inclinometer System consists of four units: the movable borehole sensor, the portable digital indicator, the interconnecting electrical cable and the Slope Indicator inclinometer guide casing permanently installed in the embankment. The movable sensor provides an electrical signal proportional to the angle of inclination from its vertical axis. The sensor is supported laterally in the casing by means of guide wheels and is suspended vertically by means of the interconnecting cable. The guide wheels are guided by four longitudinal grooves spaced equally around the inside circumference of the casing to control directional orientation of the measurements. The Digital Indicator displays the angle of inclination from vertical in terms of 2 times the sine of the angle with four significant digits. Resolution is 1 in 10,000 parts over ±30°. The system accuracy for a near vertical (±3°) casing installation is ±6 mm per 30 m. The cable is 0.42 inch OD with six insulated multiple strand, copper conductors and neoprene jacket overall. The length changes when suspended are minimized by use of this cable. The cable is attached to the sensor by means of a waterproof connector. The casing used for this vertical inclinometer in this project is model 51111. The larger diameter (7.2 cm) casing allows a greater range of casing deformation and generally provides higher accuracy. The smaller casing (5.9 cm) is suitable for measuring very small deformations in rock and structures but is generally not suited for soil deformation monitoring.

5.3.2 Horizontal Inclinometers

A horizontal digital uniaxial inclinometer, model P/N 50329, made by Sinco Slope Indicator Co. and operated in a 7.2 cm inner diameter casing which was installed horizontally during the construction, was employed to

measure vertical deflections between two pairs of supporting wheels (61 cm apart). The casing model for horizontal inclinometer is 51103. The components and the measurement system of the instrument are same as the vertical inclinometer discussed in 5.3.1.

5.4 Location of the inclinometers

The layout of the vertical and horizontal inclinometers is illustrated in Figure 14 of Chapter 2. The horizontal inclinometer casings were installed at levels 0 m, +2 m, +4 m and +6 m and run through the whole cross section of the embankment, from west to east. In total 8 horizontal inclinometer casings were installed in the embankment, 4 in the northern section of the embankment at the Tensar and Paragrid reinforced sections and 4 in the southern section of the embankment at the unreinforced and Signode sections. The vertical casings were placed at the toe and at the crest of the slopes in each section of the embankment. In total 8 vertical inclinometers were installed in the test embankment, 4 at the toes and 4 at the crest of slopes at the four sections of the embankment. Each vertical inclinometer casing was installed to a depth 12 m below ground surface to ensure that it was founded in the stiff foundation soil and its bottom would not be displaced by the movements in the embankment and the upper foundation soil.

5.5 Previous readings

5.5.1 Vertical Inclinometer readings

Horizontal movements of the fill and foundation soils along vertical lines beneath the toe and the crest of each test section were monitored in directions parallel and perpendicular to the long axis of the embankment. The slope direction is designated as direction "A" and the direction parallel

to the long axis of the embankment is designated as direction "B" and will be used through out this thesis. In the "A" direction the positive deflections are towards the slope and the negative deflections are away from the slope. In the "B" direction the positive values are in the direction of the axis 90° counter clockwise from the "A+" direction. In other words for the eastern sections of the fill (Signode and Paragrid) the "B+" direction is towards north of the fill and for the western sections (Tensar and unreinforced) the "B+" direction is towards the south of the fill. All measurements were taken from the bottom of a casing to the top and accumulated deflections along the casing were calculated. Field measurements were recorded two times with the pairs of wheels rotated 180°, to eliminate zero errors caused by either the sensor or the indicator. Finally the horizontal displacements at different locations along the vertical alignment were obtained by subtracting the initial configuration of the casing from the measures accumulated deflections.

During the summer of 1988, some severe damage was caused by the construction activities and the vertical casings at the crest of all test sections were blocked when the fill height reached 8 m and no additional measurements were taken. Hence only the horizontal deflections before August 1988 were measured. The casings of the vertical inclinometers at the crest of the slopes were extended during the construction of the fill to allow measurement of the horizontal displacements. Detailed discussions of soil horizontal deformations during construction and after the end of construction till 1990 are reported by Liu (1992) but in general the development of horizontal displacement with the construction activities was obvious. The outward movement increased in the first construction season and ceased following the construction period. It increased again in the second and third construction seasons and remained approximately constant after construction.

The number of field measurements for vertical inclinometers till 1990 is summarized in Table 1 and the initial field measurement dates for vertical inclinometers are listed in Table 2.

5.5.2 Horizontal Inclinometer readings

Relative vertical movements of the fill soil within the test embankment at levels 0, 2, 4 and 6 m above the ground surface were monitored using horizontal inclinometers. During the summer of 1988, some severe damage was caused by construction activities and the horizontal casings at 6 m elevation were blocked when the fill height reached 8 m and no additional measurements could be taken.

The inclinometer was operated in horizontally installed casings. The readings were taken first by inserting the probe from the west end of the casing and pulling towards the east end. Data was recorded for two opposite directions to eliminate zero errors caused by either the sensor or the indicator. To read the opposite direction the sensor was turned end to end from the east side of the embankment and inserted in the casing again in order to travel from east to west. When taking readings, the sensor should be inserted with the fixed wheel down so that that the weight of the sensor is supported by the fixed wheels not the spring-loaded wheels. By traveling through a casing from one side of the embankment to the other side, the probe detected vertical deflections of the casing at intervals of 61 cm. Field readings taken from the digital indicator were converted into deflections between each set of two measuring points.

From comparison of measured configurations of the casing with its original configuration obtained in the first field measurements, accumulated vertical displacement at each point with respect to a reference point along

the casing was calculated. To eliminate systematic errors, field measurements were taken consistently with the indicator connecting to the west end of the inclinometer probe. Therefore the west end of the casing became the reference point. The absolute movement of the datum point was required in order to locate the exact location of the casing in the fill and show the amount of settlement within the test embankment. After comparing different methods of obtaining the absolute movement, it appeared appropriate to use the absolute vertical displacements measured beneath the crest on the west side of the embankment by the vertical extensometers for settlement calculations. Since the vertical extensometer tubes beneath the crest of all test sections were blocked during the 1988 construction, the absolute settlement after completion of the fill could only be evaluated for the profiles based on an elevation leveling survey from a bench mark to the west end of each casing (Liu, 1992).

Readings after May 1988 did not show consistency with the previous measurements and adjustments were applied to the readings after that date. The detailed description of this adjustment is discussed by Liu (1992).

The development of settlements is fully discussed by Liu (1992) for all horizontal casings during construction and after the end of construction till 1990. Typically the vertical displacements increased following construction and subsequent consolidation periods and the displacement due to placement of the fill varied at different locations: near the center there were larger displacements than at locations near the slope surface. At different locations the displacement was developed at different rates and comparatively the differences in the settlement due to consolidation were small.

The number of field measurements for horizontal inclinometers till 1990 is summarized in Table 1 and the initial field measurement dates for horizontal inclinometers are listed in Table 3.

5.6 State of instrument in 2003

As mentioned in previous chapters, surface soil sloughing and some shallow surface movements had caused debris to move to the toe of the slope in almost all sections of the test embankment. This soil had covered the majority of the ends of the casings for horizontal and vertical inclinometers. The first task was to determine the location of buried casings and then to remove the debris without causing serious damage to the access tubes. The clean up was done by a backhoe and shovel and all the casing ends were cleaned from debris. But during the cleanup, breakages of some of the access tube ends were inevitable and hence some sections of the access pipes were cut off and broken. The next step was to clean and wash all the inclinometer horizontal and vertical tubes. A pump and a stiff plastic hose were used to wash inside all the casings. The access tubes for the inclinometers at the +4 m elevation in the Tensar, Paragrid and unreinforced sections were blocked at the time of the 1990 field measurements but after washing the access tubes thoroughly, they became accessible again. The tube ends of the horizontal and vertical inclinometers at different sections of the test fill after the clean-up are illustrated in Figures 1 through 6. The inclinometer tube ends are shown by circles. Figure 1 is at the Tensar section. Figures 2 and 3 are at the Signode section. Figure 4 is at the Paragrid section and Figures 5 and 6 are at the unreinforced section.

5.7 2003 Readings

Two sets of measurements were carried out in 2003 for all horizontal and vertical inclinometers except the ones at the crest. The standard probe could not travel all the way down the access tubes of the vertical inclinometers at the crest of all test sections. A shorter probe, 30 cm long by Sinco Slope Indicator was obtained in order to read these highly deformed access tubes. This short probe traveled about 13.5 m, 11.1 m and 11.7 m down the access tubes of the vertical inclinometers at the crest of the Tensar, Paragrid and unreinforced sections respectively. The instrument got stuck while reading the vertical inclinometer at the crest of the Signode reinforced slope and various attempts to retrieve the instrument failed. Since the probe could not reach the bottom of the vertical inclinometers at the crest where it was considered as the fixed points, it was assumed that at the depths that the probe had reached, no considerable amount of horizontal deflection had occurred. In other words the lowest depth reached by the probe was assumed as the new fixed point for plotting the horizontal deflections in 2003. The horizontal deflection of the vertical inclinometers which had occurred since August 1988 could only be calculated at the elevations where previous initial readings were read.

All the calculations for horizontal and vertical deflections were performed again for the previous readings in order to check the consistency of the method of calculation and to check the choice of the initial sets of readings for the inclinometers. The same instrument and readout device was used through out the measurements so any systematic error caused by using another instrument was eliminated.

During the 2003 field measurements all the previous raw readings on the horizontal inclinometers were also calculated again to check the

calculation procedures. The recalculated results of the previous measurements showed that the profile of settlement was identical to the previous measurements presented by Liu (1992) but the absolute amount of settlement for each horizontal access tube did not match with the amount of settlement based on the assumptions by Liu (1992). In his thesis there was a discussion regarding choosing an appropriate reference point for determining the absolute amount of settlement for each horizontal inclinometer access tube. Following his procedures the calculated results did not match with his data. Finally it was decided to accept the results by Liu (1992) and assume that his calculations were correct. Therefore all the results for the horizontal inclinometers before the 2003 measurements are based on Liu's data.

5.7.1 Vertical Inclinometer at the Toe-Tensar section

The horizontal deformation profiles at the toe of the Tensar reinforced section for the A and B direction are presented in Figures 7 and 8 respectively. The measurements in 2003 are consistent and there is no additional horizontal soil deflection in either the "A" or "B" directions since the last measurements in 1990. Figure 7 shows that the horizontal deflection in the "A" direction is very small (±2 mm) between 8 and 12 m depth below the ground surface but after that the horizontal deflection increases till 2 m depth below the ground surface and reaches about 15 mm at this depth. But the horizontal deflection in the top 2 m increased rapidly to about 57 mm at 1 m depth from the ground surface. This high increase shows that the casing end close to the ground surface has deformed significantly by the fill placement and consolidation of the foundation soil.

While taking the measurements in the field it was found that the grooves inside this vertical inclinometer are not in the slope direction. In other

words the grooves had rotated about 45° clockwise from the slope direction. The high values of horizontal deflections in the "B" which are close to the deflections in the "A" direction, shown in Figures 7 and 8, illustrate this matter. Hence the measured horizontal deflections are not exactly in the direction of the slope and the axis perpendicular to it. Therefore the components of these two deflections should be recalculated in order to know the deflections in the real "A" and "B" directions.

Based on the above argument if the rotated grooves represent A' and B' directions the true horizontal deflections will be: A=A'(Cos45°) + B'(Sin45°) and B=B'(Cos45°) - A'(Sin45°). Hence considering this adjustment the horizontal deflection in the "A" direction is still very small (±4 mm) between 8 and 12 m depth below the ground surface but after that the horizontal deflection increases till 2 m depth below the ground surface and reaches about 17 mm at this depth. But the horizontal deflection in the top 2 m increased rapidly to about 61 mm at 1 m depth from the ground surface. The maximum value of horizontal deflection in "B" direction after above adjustments will be -17 mm, which is 17 mm towards north, at the -1.2 m depth.

5.7.2 Vertical Inclinometer at the Crest-Tensar section

As mentioned before a shorter inclinometer probe (30 cm) was used to read the vertical inclinometers at the crest of slopes. The average of previous measurements with the 60 cm long probe at two adjacent locations was used in order to calculate the measurements at 30 cm intervals. During the 2003 measurements it was not possible to reach the bottom of the inclinometer where it was considered as the fixed reference point. In order to plot the horizontal deflection of the soil, it was assumed that the lowest point that could be reached during the 2003 measurements had not experienced any additional horizontal movement. In other words

the horizontal deflection of the lowest measured point in the vertical inclinometer in 2003 was assumed to be same as the horizontal deflection measured in August 1988, before the placement of the top 6 m of fill. As the lowest point reached in the Tensar section was -2.5 m and as at this depth there was no horizontal deflection up to August 1988, this assumption appears valid. The profile of horizontal deformations in "A" and "B" directions at the crest of the slope in the Tensar section are presented in Figures 9 and 10. The same rotation of inclinometer grooves, as discussed in Section 5.7.1 had occurred at this inclinometer as well. Hence the same adjustments are also applied to all the horizontal deflection values discussed below.

Figure 9 shows that the horizontal deformation in "A" direction in 2003 is almost same as the previous measurement in August 1988 in the foundation soil up to the ground surface. But in the fill there is some inward horizontal deformation till 5 m above the ground surface and above the +5 m elevation the outward horizontal deformation increased very rapidly and reached about 635 mm at 7.6 m level above the ground surface. As there were no initial field measurements available for higher elevations, the profile of the horizontal deformations at elevations higher than 7.6 m above ground surface could not be determined. Since the access tubes for the vertical inclinometers at the crest of all slopes were blocked due to construction activities in the summer of 1988 (third construction stage) there is no measurement available during or after the placement of the top 6 m of soil. Hence there is no previous reading after the end of the construction available to compare the 2003 measurements with. But in general it shows that after the placement of the top 6 m of fill the horizontal outward deformation in the unreinforced portion of the slope above 5 m has increased dramatically. This pattern of horizontal deformation confirms higher horizontal deformations in the top 7 m unreinforced portion of the fill. In Figure 10 the same pattern of horizontal

deformations exists in the "B" direction. The maximum horizontal deflection in the "B" direction after adjustment is about 7 mm at +7.2 m.

5.7.3 Vertical Inclinometer at the Toe-Signode section

Figures 11 and 12 illustrate the horizontal deformation in "A" and "B" directions at the toe of Signode section, 12 deep in the foundation soil. Two measurements were made in 2003 which both show consistent results. There is not any additional horizontal deformation at the toe of this section since the 1990 measurements, except at the end of the access pipe at the ground surface where about 15 mm horizontal deformation in "A" direction has occurred since 1990. This may be due to the clean up activities which might have deformed the access pipe end. The profiles of horizontal deformation in the "A" direction show that there is not any horizontal deformation in the foundation soil between a depth of 12 and 8 m below the ground surface. From the depth of 8 m the horizontal deformation increases almost linearly from 0 mm to about 35 mm at a depth of 1.2 m from the ground surface. Then it suddenly increases to 95 mm close to the ground surface.

5.7.4 Vertical Inclinometer at the Crest-Signode section

While lowering down the small inclinometer probe inside the vertical inclinometer access tube at the crest of Signode section, the instrument got stuck inside the pipe and it was not possible to retrieve the instrument and take it out. Hence no 2003 measurements are available for this vertical inclinometer. Figures 13 and 14 only illustrate 3 measurements made till summer 1988. The discussion for these results can be found in Liu (1992).

5.7.5 Vertical Inclinometer at the Toe-Paragrid section

Two sets of new measurements were carried out in 2003 at the vertical inclinometers at the toe of slope in the Paragrid section. There is not any measurement in 1990 and the last set of previous measurements was in summer of 1988 before the top 6 m of the embankment was constructed. Figures 15 and 16 present the profiles of horizontal deformations at the toe of the Paragrid section in the "A" and "B" directions. The two sets of readings in 2003 are consistent and show that the trend of horizontal deformation is similar to the 1988 measurements but some horizontal deformation developed due to the fall 1988 embankment construction. There is not any horizontal deformation in the "A" direction between 12 and 9 m depth below the ground surface and above that the horizontal deformation increases linearly from zero to around 32 mm at a depth of about 2 m from the ground surface. Then the horizontal deformation increases dramatically from 32 mm at 2 m depth to 91 mm at the ground surface. The difference between the measurements in August 1988 and in 2003 also increases from zero at a depth of 9 m to about 5 mm at the 2 m depth. Again a sudden increase appears between the 1988 and 2003 horizontal deformation measurements with an increase from 5 mm at the 2 m depth to 30 mm at the ground surface.

The same pattern exists in the horizontal deformations in the "B" direction; however the magnitude of deflection in the "B" direction was much smaller than in the "A" direction. The horizontal movement in the "B" direction is of minor significance compared to the movement in the "A" direction.

5.7.6 Vertical Inclinometer at the crest-Paragrid section

For this section the lowest reading in 2003 was approximately at the ground surface. Therefore the horizontal movement from the horizontal

extensometer at the ground surface was used to calculate the location of the vertical inclinometer at the ground surface for the 2003 horizontal deflection calculations. Figures 17 and 18 illustrate the profiles of horizontal deformations at the crest of Paragrid slope in "A" and "B" directions. One measurement in 2003 was made using the small inclinometer probe. It should be mentioned that the small inclinometer probe (30 cm) from Sinco Slope Indicator Co., was a uniaxial inclinometer and for each "A" and "B" direction readings separate measurements have to be taken. So the probe had to be pulled out and inserted again in the vertical access tube for each reading of "A^{+}", "A^{-}" , "B^{+}" and "B^{-}". "A" direction readings were done successfully but for "B" direction readings it was not possible to insert the probe and pass it below a depth of about 8.5 m. Hence measurements in the "B" direction were not possible in 2003.

Figure 17 shows the horizontal deformations in the "A" direction with the 2003 measurement starting close to the ground surface to about +8.5 m in the fill. As there were no initial readings for elevations higher than 8.5 m, no horizontal deformations could be determined for those higher elevations. But the pattern of horizontal deformations in 2003 shows that the deformation increases from 13 mm close to the ground surface to about 460 mm at 8.5 m above the ground surface. Again in the upper unreinforced portion of the Paragrid slope, above +5.2 m the horizontal deformations increase substantially.

5.7.7 Vertical Inclinometer at the Toe-Unreinforced section

Two measurements were made in 2003 at the vertical inclinometer installed at the toe of the unreinforced section. The same rotation of inclinometer grooves as discussed in Section 5.7.1 was observed at this inclinometer as well. Figures 19 and 20 present the horizontal deformation pattern of the foundation at the toe of the slope in the "A" and "B"

directions respectively without any groove rotation adjustments. The previous readings during the construction time in the "A" direction show that after the first construction season the horizontal deformation starts from zero at -12 m depth and reached to about -4 mm (-5 mm before adjustments) at 6 m depth below the ground surface. From this depth to ground surface, the outward horizontal movement of the foundation soil started and reached to about 92 mm (50 mm before adjustments) close to the ground surface. Measurements in 2003 also show the same pattern of horizontal deformation from 12 m depth to 4 m depth below the ground surface but there is a small reduction in range of 1 to 4 mm in horizontal deformation in the mentioned depth. Above 4 m depth, 2003 measurements show a difference from the 1990 measurements. This difference might be caused by debris moving down the slope and pushing the upper portion of the access tube more towards the inside of the fill, or might be caused during clean up activities by pushing from the backhoe shovel displacing the upper portion of the access tube.

In the "B" direction the horizontal deformation is in the range of ±3 mm between 12 m depth and 2 m depth below the ground surface and the 2003 measurements are quite consistent with the previous readings. But above the 2 m depth some outward movement in the "B" direction occurred and increased after each construction season such that it reached to about 25 mm (90 mm before adjustments) near the ground surface. But the 2003 measurements in the top 2 m of the foundation soil indicated that the horizontal deformation was only 5 mm (20 mm before adjustments) at 1.2 m depth.

5.7.8 Vertical Inclinometer at the crest-Unreinforced section

For this section the lowest reading in 2003 was approximately at the ground surface. Therefore the horizontal movement from the horizontal

extensometer at the ground surface was used to calculate the location of the vertical inclinometer at the ground surface for the 2003 horizontal deflection calculations. The vertical inclinometer at the crest of unreinforced section was blocked during the 1988 construction season therefore no measurements after that were available. In 2003 one set of measurements were made using the small inclinometer probe (30 cm) and the horizontal deformation pattern in the unreinforced section could be determined from 1 m above the ground surface to about 7.8 m from the ground surface inside the unreinforced section. Since no initial measurements were made for elevations higher than 7.8 m, the horizontal deformation could not be calculated for the elevations higher than 7.8 although readings were made for those elevations in 2003. Figures 21 and 22 illustrate the horizontal deformation pattern of the vertical inclinometer at the crest of unreinforced section in "A" and "B" directions. Since no measurements were available after the end of construction, 2003 measurements can only be compared with measurements in summer of 1988, before placement of the top 6 m of fill. Measurements in 1986, 1987 and summer of 1988 show that there is almost no horizontal deformation in the foundation soil, but the horizontal deformation started to develop above the ground surface in the fill during different stages of construction. In November 1987, at +5 m elevation, the horizontal deformation reached 35 mm and this increased to 52 mm in August 1988 and in 2003 to 160 mm. Above +5 m elevation, the horizontal deformation increased rapidly and reached about 535 mm at +7.3 m.

Horizontal deformations in the "B" direction in 2003 started to increase from +1 m and reached about 60 mm at +3.5 m as illustrated in Figure 22.

5.7.9 Analyses of the horizontal deflection from vertical for the inclinometers at the crest of slopes

As mentioned in Section 5.7.2, since the inclinometer probe could not reach to the bottom fixed reference point, in order to define the horizontal deflection of the vertical inclinometers at the crest in 2003 some assumptions had to be made. It was assumed that the lowest point that the probe could reach in the vertical inclinometers at the crest had undergone horizontal deflections as discussed in Sections 5.7.2, 5.7.6 and 5.7.8 for the Tensar, Paragrid and unreinforced sections respectively. Another assumption was that the inclinometers were installed as vertically as possible during their installation.

Figures 23, 24 and 25 illustrate the horizontal deflection from vertical in August 1988 and 2003 for the Tensar, Paragrid and unreinforced sections. Figure 23, Tensar section, confirms that the assumptions made that the lowest measured point in the vertical inclinometer in 2003 has not underwent additional horizontal deflection is correct. It also shows that there is a good match between the deflection patterns for elevations higher than 5 m calculated in 2003 and the horizontal deflection pattern from vertical considering the above mentioned assumptions. Therefore the profile of horizontal deflection from vertical for elevations higher that 8 m to the top of the fill can represent a realistic view of the horizontal deflections occurring at those elevations. Any difference between those two profiles could be the horizontal deflections caused by construction activities and equipment. Taking both the "A" and "B" readings into consideration, the inclinometer deflection at the top of the fill is about 0.8 m.

Figures 24 and 25, Paragrid section and unreinforced section respectively, illustrate that there was a large horizontal movement at the ground surface

after August 1988, probably during the third construction stage. This large deflection at the ground surface is probably the reason that even the short inclinometer probe could not pass this depth. The large deformations in the top 6 m of all 3 sections were probably caused by construction equipment during the placing of the fill.

5.8 Horizontal Inclinometers

5.8.1 Tensar section

Two measurements of the horizontal inclinometers at 0, 2 and 4 m levels in the Tensar reinforced section were made in 2003 after washing the horizontal access pipes. Figures 26, 27 and 28 illustrate the pattern of settlement inside the fill at 0 m, +2 m and +4 m. The inclinometer readings give the deformation pattern of the horizontal casing and in order to define the settlement profile, the absolute amount of settlement at the casing reference point should be known as well. In order to determine the amount of absolute settlements, either the casing ends could be surveyed at each reading time or the vertical extensometer settlement data could be referenced. The elevation survey of all horizontal and vertical instruments was carried out in 2003 but unfortunately there was not a well documented history of the initial elevation survey available for the Devon test embankment. Also the elevation of the main bench mark which was used through all the surveying could not be verified and reconfirmed. Hence the use of casing end elevations for determining the absolute amount of settlement for each horizontal inclinometer was not confident enough and the settlement measured by the vertical extensometers installed at the crest of slopes were used to locate the elevation of the casing inside the fill. In the northern reinforced sections of the embankment (Tensar and Paragrid) the settlements defined by the vertical extensometer installed at the crest of the Tensar section were used to determine the elevation of the

horizontal inclinometer casings at the crossing of vertical extensometer and horizontal inclinometer access tube. Figure 26 illustrates the profile of settlement at the ground surface in the Tensar reinforced section. The two measurements in 2003 are quite consistent and show that the fill soil had settled more at the center of the fill. Between the 1990 and the 2003 field measurements the settlement at the center of the fill showed a very small amount of increase (about 4 mm). In other words since 1990 the foundation soil beneath the Tensar reinforced section almost did not settle any more. The settlement profile close to the slope surface showed some amount of heave (maximum of 15 mm). The profile of settlement in 2003 follows the profile of the last set of measurements in 1990.

Figure 27 shows the settlement pattern at 2 m elevation above the ground surface in the Tensar section. The settlement increased from the slope face towards the fill center and the measurements in 2003 illustrated that the settlement beneath the centerline of the fill increased from 330 mm in 1990 to 370 mm in 2003. The pattern of settlement along the casing at this elevation in 2003 was consistent with the previous measurement in 1990.

In Figure 28 the settlement of the fill soil at 4 m elevation above the ground surface is presented. The fill soil settlement close to the center of the fill at this elevation increased about 125 mm between 1990 and 2003 and reached 468 mm. The two measurements in 2003 show consistent settlement patterns at this elevation inside the fill.

5.8.2 Signode section

In order to determine the absolute amount of settlement for the horizontal inclinometer casings in the southern part of the test embankment (Signode and Unreinforced sections), settlements measured by the vertical extensometer at the crest of the Signode reinforced slope were used in

2003 field measurements since the vertical extensometer at the crest of the unreinforced section was not accessible. The reference point was selected to be the crossing point of this vertical extensometer with the horizontal inclinometer casings in the southern half of the test embankment. Figures 29, 30 and 31 illustrate the settlement profile of the Signode section at 0 m, +2 m and +4 m. Two sets of measurements were made in 2003 after washing all the access pipes.

In Figure 29 the settlement pattern of the foundation soil (0 m from the ground surface) is illustrated. The profile showed that after the end of construction, about 15 mm settlement occurred between 1989 and 1990 at the centerline of the fill. The measurements in 2003 are quite consistent and show that only a small amount of settlement, in the range of 8 mm, occurred at the center of the fill since 1990. The settlement at the center of the fill at this elevation reached about 150 mm closer to the slope face the variation of settlement is very small and almost negligible.

The settlement profile of the fill at 2 m elevation above the ground surface is presented in Figure 30. This plot shows that between 1989 and 1990, after the end of the construction, the fill at the centerline settled about 35 mm. The measurements in 2003 illustrate that at this elevation the settlement increased from 190 mm at the centerline in 1990 to about 240 mm. The measurements in 2003 are quite consistent but close to the slope surface there is some variation (about 10 mm) in the two settlement profiles measured in 2003.

The profiles of settlement in the fill at +4 m are shown in Figure 31. Again after the end of construction, between 1989 and 1990 the settlement at the center of the fill increased from 190 mm to 230 mm. The 2003 measurements show that about 85 mm more settlement occurred close to centerline of the fill since 1990. The deformation patterns for the two

measurements in 2003 are consistent and the settlement pattern is similar to the settlement pattern measured in 1990 and before.

5.8.3 Paragrid section

As mentioned before in Section 5.8.1, the absolute amount of settlement in the 2003 measurements was determined by the vertical extensometer installed at the crest of the Tensar reinforced slope. Figures 32, 33 and 34 present the settlement profiles at 0 m, +2 m and +4 m at the Paragrid reinforced section.

Figure 32 illustrates the settlement profile of the foundation soil at 0 m. The two measurements in 2003 are consistent and show that since 1990 a very small amount of settlement (about 5 mm) occurred at the center of the fill. Close to the slope surface and within about 12 m from the slope face there is a difference in the 2003 measurements. They are higher than the 1989 and 1990 measurements. No reason for this difference is obvious but the inclinometer pipe might contain debris which would cause the probe to ride higher.

The settlement pattern of the fill soil at 2 m elevation is presented in Figure 33. The settlement profile at this elevation in 2003 does not follow the pattern of previous measurements. The two measurements in 2003 are consistent but their pattern is different from measurements in 1990 and 1989 at some locations. This may be due to debris in the tube. The settlement close to the slope face might be due to soil movement and sloughing at the slope surface which caused the horizontal casing close to the slope face to bend downward.

As shown in Figure 34, the settlement profiles at +4 m measured in 2003 are quite consistent and follow the pattern of previous settlement profiles.

It illustrates that between 1989 and 1990, 50 mm settlement occurred almost at all locations inside the fill. In 2003 the settlement at the center of the fill increased from 330 mm in 1990 to 450 mm.

5.8.4 Unreinforced section

The absolute settlements of the horizontal inclinometer casings installed in the unreinforced section of the test fill were determined by the vertical extensometer at the crest of the Signode section for the 2003 field measurements. The settlement at the crossing of the vertical extensometer casing and the horizontal inclinometer casings were considered as the reference points for determining the absolute amount of settlements. Figures 35, 36 and 37 illustrate the settlement profile of the horizontal inclinometers installed at 0 m, +2 m and +4 m at the unreinforced section.

The foundation settlement at the ground surface is presented in Figure 35. The two measurements in 2003 are consistent deep inside the fill but there is some difference between the two readings (maximum of 15 mm) close to the slope face. Between the 1989 and the 1990 field measurements about 15 mm settlement occurred at the center of the fill. Only 5 mm of settlement developed after 1990 till 2003 at the centerline of the fill where the settlement reached about 150 mm.

Figure 36 presents the settlement profile of the fill soil at 2 m elevation inside the fill at the unreinforced section of the fill. The fill soil at this elevation settled about 35 mm at the centerline of the fill between 1989 and 1990. The two consistent field measurements in 2003 show that about 50 mm more settlement developed at the center line of the fill at this elevation which increased the total settlement of the center of the fill to

about 260 mm. Within 2 m of the slope surface the casing end moved downward due to the surface sloughing and soil movement.

Figure 37 illustrates the settlement of the fill at 4 m elevation above the ground surface inside the fill. About 40 mm settlement occurred close to the centerline of the slope between 1989 and 1990. Between 1990 and 2003, the settlement increased about 85 mm at that location and reached about 340 mm close to the embankment centerline. The two measurements in 2003 show consistent settlement profiles. Close to the slope surface the pipe end bent downward due to soil movement which can be an indication of some shallow surface failure in the unreinforced slope.

5.9 Long term performance of inclinometers

5.9.1 Long term performance of vertical inclinometers

In 2003, sixteen years after the end of construction of the test embankment, measurements were taken from vertical inclinometers installed at the toe and the crest in all sections of the test embankment. Vertical inclinometers installed at the toe of the slope were all washed and cleaned out so it was possible to reach the bottom of the access pipes. Vertical inclinometers installed at the crest of the slopes were all damaged and blocked during the summer of 1988 construction activities but after washing all the access pipes at the crest of slopes in 2003 and using a small inclinometer probe to pass the bent locations of the pipe, the horizontal deformation pattern could be determined.

The measurements from the vertical inclinometers at the toe of the slopes in the Tensar and Signode reinforced sections showed consistent results in both "A' and "B' directions with the last set of measurements in 1990,

two years after the completion of the test embankment. In the Paragrid reinforced section no measurements were made during or after the 1988 construction season due to the blockage of the access pipe but in 2003 after washing the access pipe readings could be made. The results show that the 2003 measurements in both "A" and 'B' directions are quite consistent in the pattern of horizontal deformation with the 1988 measurements and change in the magnitude of deformation since 1988 was small. This was the case for all other vertical inclinometers at the toe as well. In the unreinforced section of the test embankment there was a small reduction in horizontal deformations inside the foundation soil in the "A" direction but the pattern of horizontal deformation was similar to the last measurement after the completion of the test embankment. In the "B" direction there was almost no change in horizontal deformation between 12 m depth and 2 m depth from the ground surface since the 1990 measurements but in the top 2 m of the foundation soil there was some reduction in the amount of horizontal deformation since 1990 which might be due to clean up activities or soil movements down the slope.

The vertical inclinometers at the crest of slopes were read only once in 2003 with the small inclinometer probe after washing them. No previous measurements were available after the summer of 1988. Since the small probe could not reach the bottom of the inclinometer in the Tensar section it was assumed that the lowest point reached by the small probe had not undergone any additional horizontal deflection since August 1988, and the casing was installed as close as possible to vertical. For the Paragrid and unreinforced sections, the horizontal movements from horizontal extensometers at the ground surface were considered for the lowest point in the vertical inclinometers. The readings at the crest of the Tensar reinforced section in 2003 show that the horizontal deformation increases dramatically from 5 m elevation above ground surface and reaches to 635 mm at +7.6 m in "A" direction after the groove rotation adjustments. The

same increase was also observed for horizontal deformation in "B" direction which increased from 5 m elevation above ground surface and reached to 7 mm at +7.6 m after the groove rotation adjustments. In the Signode reinforced section it was not possible to lower the small inclinometer probe down the vertical inclinometer access pipe and the instrument got stock in the access pipe and it could not be retrieved again. In the Paragrid reinforced section only measurements could be carried out in the "A" direction and the instrument could not be lowered down the access pipe to read the horizontal deflections in the "B" direction. The horizontal deformation pattern in this vertical inclinometer showed that the horizontal deformation picked up close to the ground surface and increased to 460 mm at +7.6 m in the "A" direction. In the unreinforced section the measurement in 2003 illustrated that the horizontal deformation in the "A" direction increased dramatically at +5 m from 160 mm to about 535 mm at +7.3 m.

It was possible to read all vertical inclinometers at the toe of the slopes by washing the vertical inclinometer access tubes and also by using the small inclinometer probe, three vertical inclinometers out of four at the crest of the slopes could also be read and the horizontal deformation profiles were calculated which in all cases gave consistent results with the previous measurements in the test embankment.

5.9.2 Long term performance of horizontal inclinometers

Settlement measurements in 2003, which were made 16 years after the completion of the test embankment were carried out at 0 (ground surface), +2 m and +4 m. The attempt to measure the settlement profile at +6 m failed due to serious damage to the access tubes during the third construction stage, when the top 6 m of fill soil was placed. Some portions of the horizontal inclinometer access tubes at 4 m elevations were also

blocked after the end of construction but they were retrieved after washing and cleaning. This action made the settlement measurements possible at that elevation in 2003. The access tubes at 0 and 2 m elevation from the ground surface were also washed and cleaned thoroughly.

The settlement profiles measured in 2003 at all sections show consistent results and the trend follows the settlement trend measured in 1990, except at the Paragrid reinforced section at 2 m elevation where there is some change in the settlement profile since 1990. This discrepancy can be due to the access tube realignment inside the fill in that section which might have caused realignment of the grooves inside the tube, or it could have been caused by some obstacles inside the grooves and access tube, i.e. soil, pieces of wood or plants. Table 4 summarizes the amount of maximum settlements at different sections and elevations inside the embankment which developed since 1990 until 2003 measurements. Table 5 shows the amount of additional settlement occurred since 1990 field measurements until 2003 at different sections and elevations inside the fill. The 2003 results illustrate that the foundation soil at the ground level settled only about 4 mm to 7 mm since 1990. In other words the foundation consolidation had substantially completed by the 1990 measurements. The settlement in the embankment increased with the increase in elevation. The settlement at 2 m elevation in the embankment increased in the range of 46 mm to 54 mm since 1990 at all 4 sections of the embankment. At +4 m the settlement increase is not similar in all 4 sections. At the southern sections (unreinforced and Signode) the settlement increase since 1990 was very similar at the two sections and was about 78 mm, reaching a maximum of about 352 mm. At the northern sections (Tensar and Paragrid), however, the settlement increase since the 1990 field measurements, which were similar to each other, was about 135 mm and the maximum settlement was about 478 mm. The data from the 0 and 2 m elevations also show that the northern sections settled more

than the southern sections which might have been due to different moisture content or compaction effort during the construction of the embankment or differences in foundation soil properties.

5.10 Summary and Conclusions

After retrieving all the vertical and horizontal inclinometers and washing the access tubes, measurements were made on all the inclinometers in 2003, sixteen years after the end of construction. After washing, the vertical inclinometers at the toe of the slopes were cleaned to the bottom of the access tubes where the tubes were fixed in the stiff foundation soil. Two sets of measurements at vertical inclinometers at the toe were carried out in 2003 and the main findings are:

- The two sets of field measurements revealed consistent results and the deformation profiles matched well which confirmed the repeatability of the measurements.
- In the Tensar and Signode reinforced sections, the 2003 measurements showed the same deformation profile in "A" and "B" directions as the 1990 measurements, except very close to the ground surface where the horizontal deformations were increased probably due to some more surface movement of the soil which pushed the tube ends outwards or due to some clean up activities when the tube ends might had been displaced by the backhoe shovel. These results indicate that no major horizontal deformation occurred at the toe of these sections since 1990. At the Paragrid section there were no 1990 field measurements available to compare with the 2003 measurements but the recent readings showed that the trend of horizontal deformation was similar to the last set of measurements in August 1988 in both "A" and "B" directions. At the unreinforced section, "A" direction, 2003 measurements show that the horizontal deformation decreased

since the 1990 measurements in all locations along the vertical inclinometer access tube in range of 1 to 9 mm. In the "B" direction the horizontal deformation profile remained similar to the 1990 measurement at depths -12 m to -4 m.

The vertical inclinometers at the crest of the slope were read by using a small probe (30 cm long) in order to pass the critical bent locations along the access tubes. The probe worked very well but in the Signode section, it got stuck at the 10 m depth while lowering it down and it was not possible to retrieve the instrument. At the 3 other sections the horizontal fill soil deformation measurements were carried out. However, since the access tubes of the vertical inclinometers at the crest of the slopes were damaged during the 3rd construction stage, no initial readings were available at elevations higher than about 7.5 m from the base of the fill; hence no deformation pattern could be calculated for those locations. The small probe also could not reach the bottom of the access tube at the 12 m depth below the ground surface and in the Tensar section it only reached to 2 m depth below the ground surface and only 1 m above the ground surface in the Paragrid and unreinforced sections. The measured horizontal deformation pattern in "A" direction in 2003 showed that above the +5.2 m the horizontal deformation increased very dramatically such that in the Tensar section it increased from 58 mm (3 mm before adjustments) at +5.2 m to 635 mm (470 mm before adjustments) at +7.2 m, in the Paragrid section it increased from 240 mm at +5.2 m to 470 mm at +7.2 m and finally in the unreinforced section it increased from 185 mm at +5.2 m to 520 mm at +7.2 m. In other words after the placement of the top 6 m of fill the upper 7 m unreinforced portion of each slope section underwent a substantial amount of horizontal deformation which caused critical bends in the vertical inclinometers at the crest of the slopes. The bottom 5 m reinforced portion of the Tensar section experienced a less amount of horizontal deformation in comparison to the other two sections

(unreinforced and Paragrid). Since the Paragrid geogrids had some manufacturing defects in their structure, the behavior of this section was very similar to the unreinforced section as also reported by Liu (1992).

The horizontal inclinometers at 0, +2 m and +4 m elevation were washed thoroughly and the readings in 2003 were made with the same probe as was used in previous measurements. The major findings for the settlement measurements by horizontal inclinometers are:

- The two measurements made in 2003 are quite consistent with each other and the settlement profiles measured in 2003 at all sections show that the trend followed the settlement trend measured in the 1990 field measurements.
- Since the previous leveling survey records were not reliable and the bench mark elevation could not be reconfirmed, the absolute amounts of settlements measured by vertical extensometers at the crest of slopes were used to locate the elevation of the horizontal inclinometers in the fill. For the horizontal inclinometers installed at the northern sections of the embankment (Tensar and Paragrid) the west vertical extensometer at the crest of Tensar reinforced section was used as the reference and for the southern horizontal inclinometers inside the fill, the eastern vertical extensometer at the crest of Signode reinforced section was considered as the reference since the vertical extensometer at the unreinforced section was not accessible.
- At the ground surface the foundation soil did not settle significantly from 1990 to 2003. Only about 6 mm additional settlement occurred close to the center line of the fill in all sections of the fill. At +2 m elevation all sections showed a similar amount of increase in settlement since 1990, in the range of 46 mm to 54 mm. The increase of settlement at +4 m elevation was different for the

northern and southern sections. The maximum settlement in the northern sections increased about 135 mm since the 1990 measurements and the southern sections experienced an increase in maximum settlement of about 78 mm. The data also showed that the maximum amount of settlement at the 0 m, +2 m and +4 m elevations in the northern sections were higher than the maximum settlements at the southern sections. This difference might have been due to having different moisture content or compaction effort during the construction of the embankment and/or a difference in foundation soil properties.

Table 1. Number of inclinometer field measurements till 1990

Instrumentation		Tensar	Signode	Paragrid	Unreinforced
Horizontal Inclinometer	0 m	15	14	15	14
	2m	13	13	13	13
	4m	10	10	10	10
	6m	3	2	3	2
Vertical Inclinometer	Crest	9	10	9	9
	Toe	14	14	9	14

Table 2. Initial field measurement dates of vertical inclinometers

	Toe	**Crest**
Tensar	12-Sep-86	12-Sep-86
Signode	12-Sep-86	12-Sep-86
Paragrid	14-Sep-86	12-Sep-86
Unreinforced	12-Sep-86	14-Sep-86

Table 3. Initial field measurement dates of horizontal inclinometers

Elevation	**North Section**	**South Section**
4m	17-Sep-87	17-Sep-87
2m	22-Oct-86	20-Oct-86
0m	22-Sep-86	20-Sep-86

Table 4. Maximum settlement at different sections and different elevation inside the embankment- Measured at mentioned distances from the slope face.

Settlement (mm)	Tensar		Signode		Paragrid		Unreinforced	
	1990	2003	1990	2003	1990	2003	1990	2003
4 m	343	478	274	349	343	479	273	355
Measure at	11 m		8 m		11 m		13.4 m	
2 m	327	380	214	261	335	389	220	266
Measure at	17 m		14.6 m		18.3 m		17.7 m	
0 m	233	240	147	151	207	213	147	153
Measure at	19.5 m		20.7 m		18.3 m		20.7 m	

Table 5. Additional settlement in mm since 1990 measurements.

	Tensar	Signode	Paragrid	Unreinforced
4 m	135	75	136	82
2 m	53	47	54	46
0 m	7	4	6	6

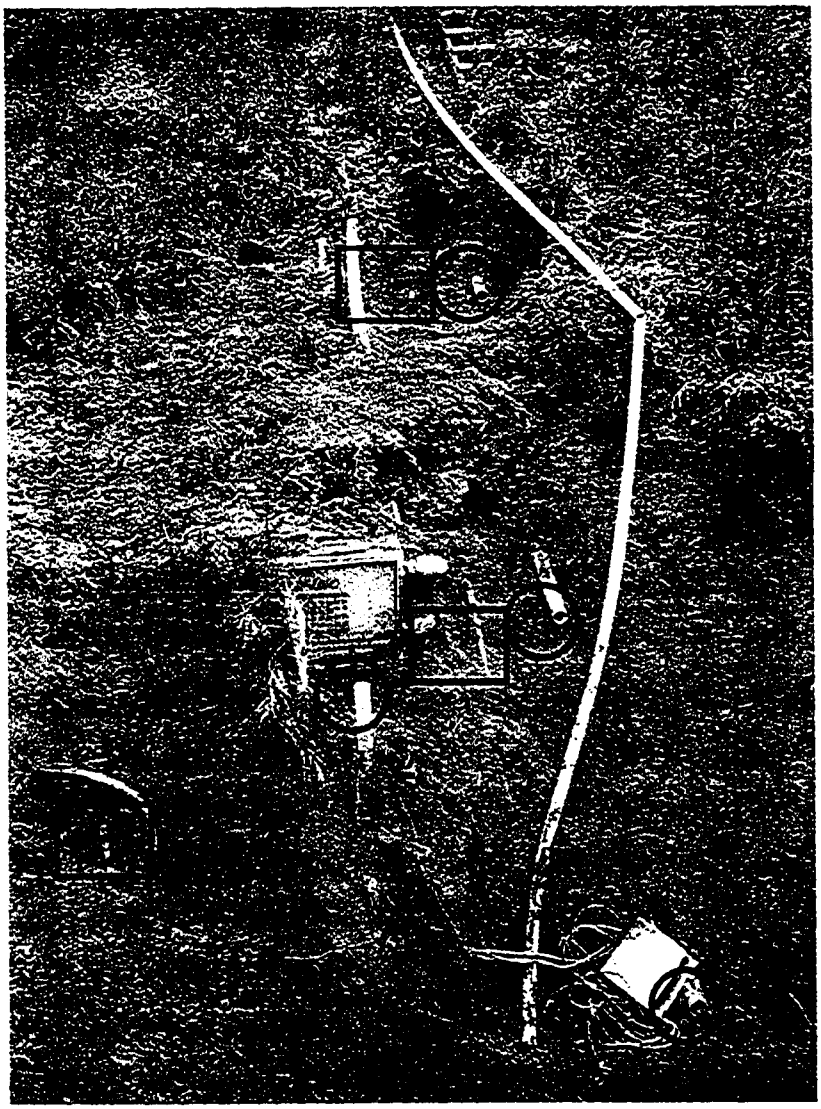

Figure 1. Tensar Section at toe-Access for inclinometer casings (shown by circles)

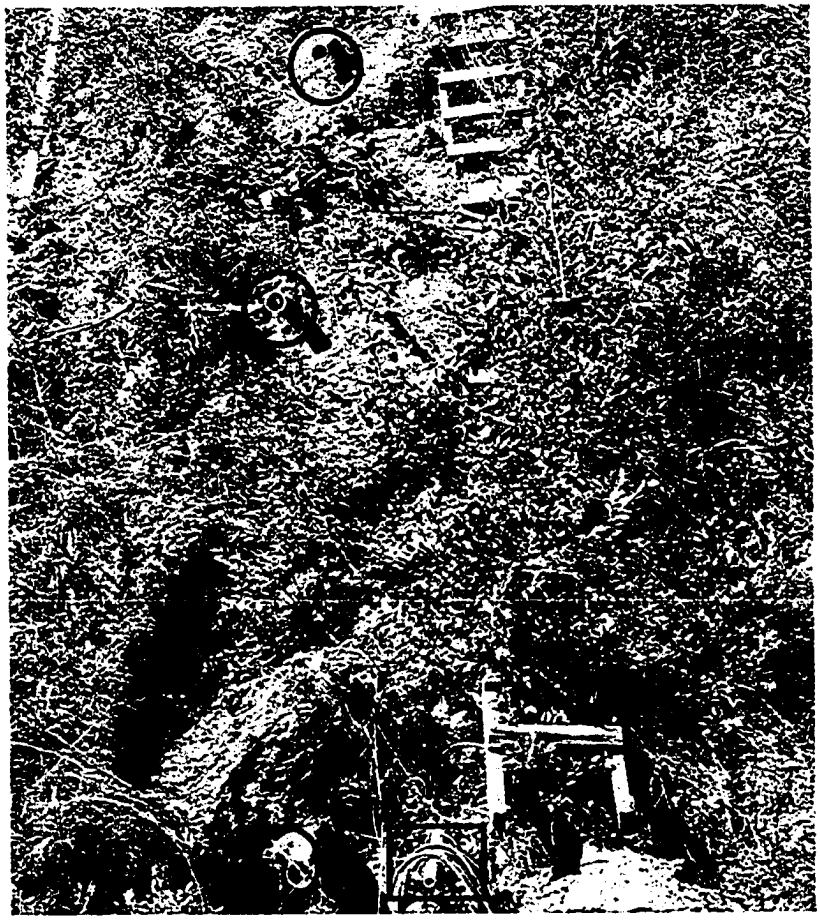

Figure 2. Signode section-Access for inclinometer casings

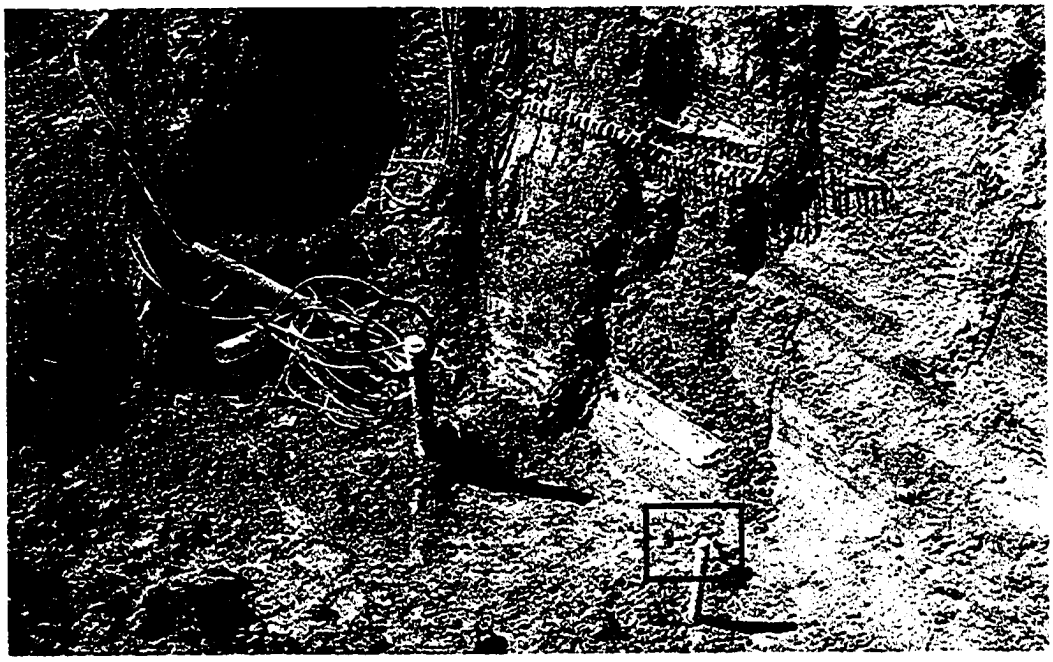

Figure 3. Signode section at toe-Access for inclinometer casings

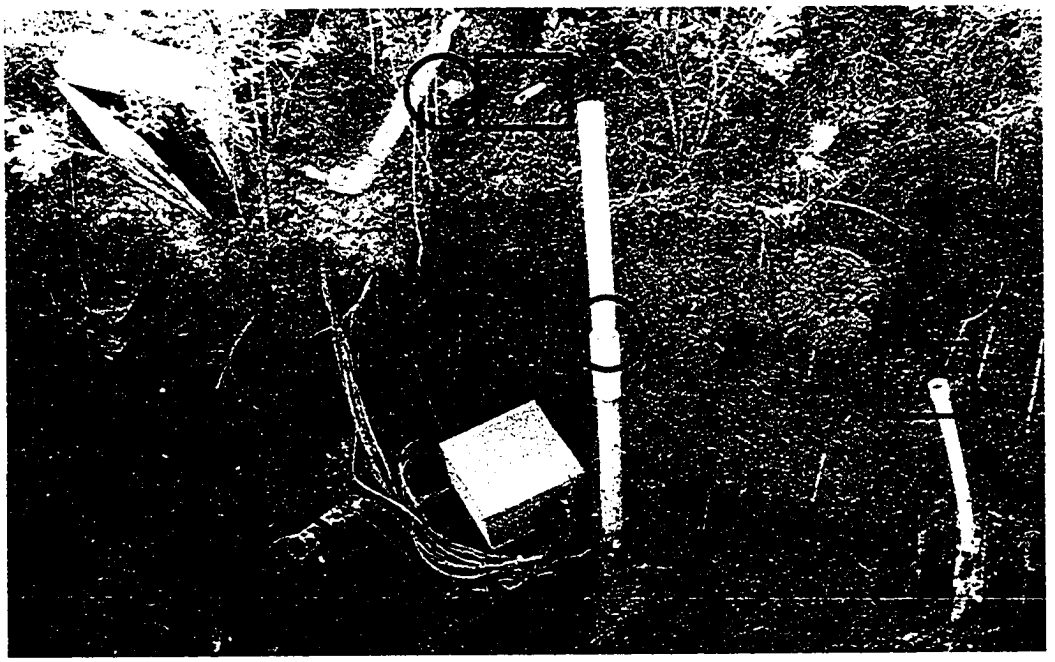

Figure 4. Paragrid section at toe-Access for inclinometer casings

Figure 5. Unreinforced section at toe-Access for inclinometer casings

Figure 6. Unreinforced section at toe-Access for inclinometer casings

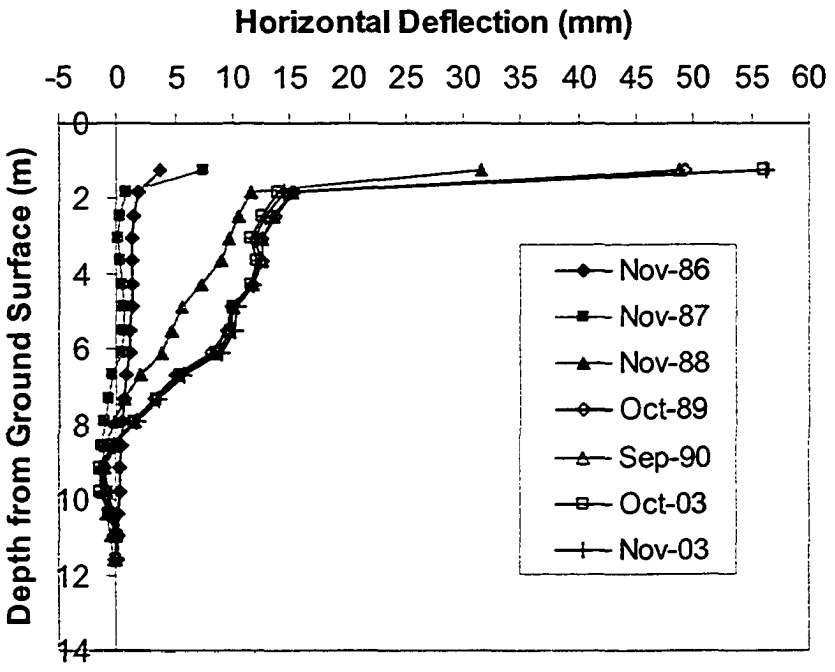

Figure 7. Horizontal deflection in "A" direction-Tensar at toe

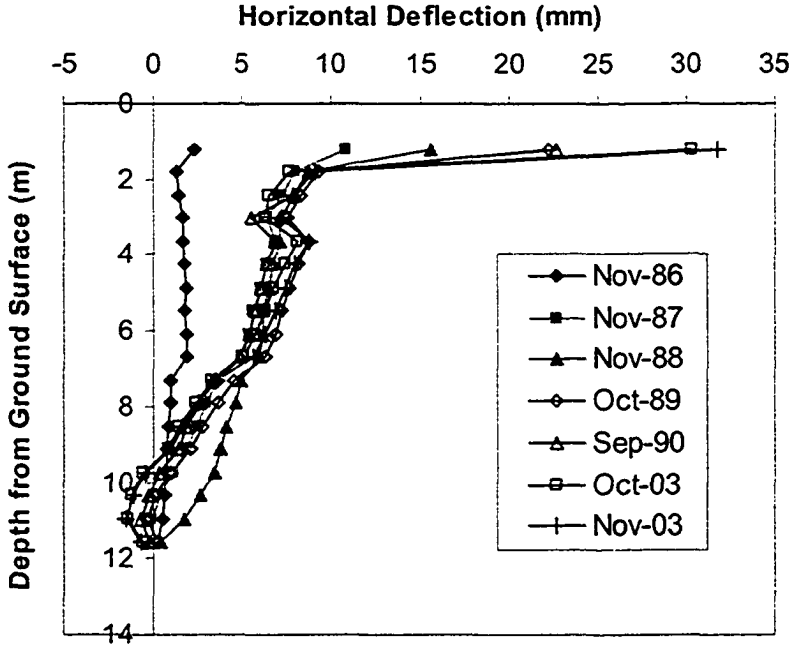

Figure 8. Horizontal deflection in "B" direction- Tensar at toe

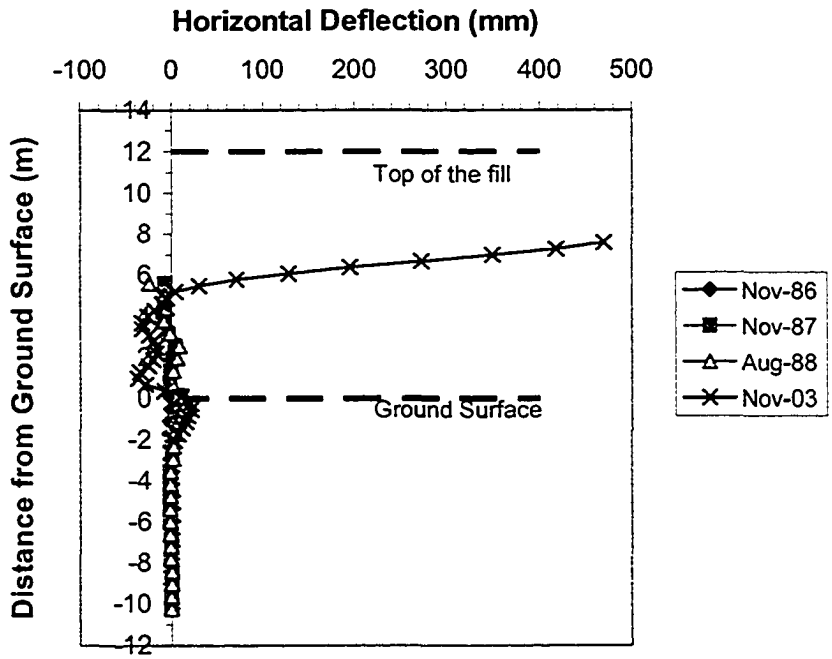

Figure 9. Horizontal deflection in "A" direction- Tensar at crest

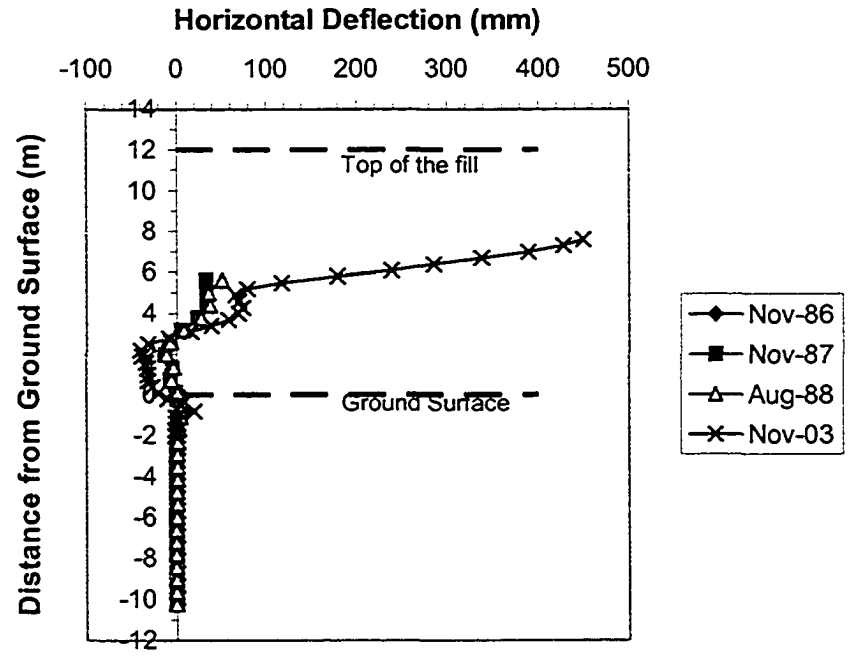

Figure 10. Horizontal deflection in "B" direction- Tensar at crest

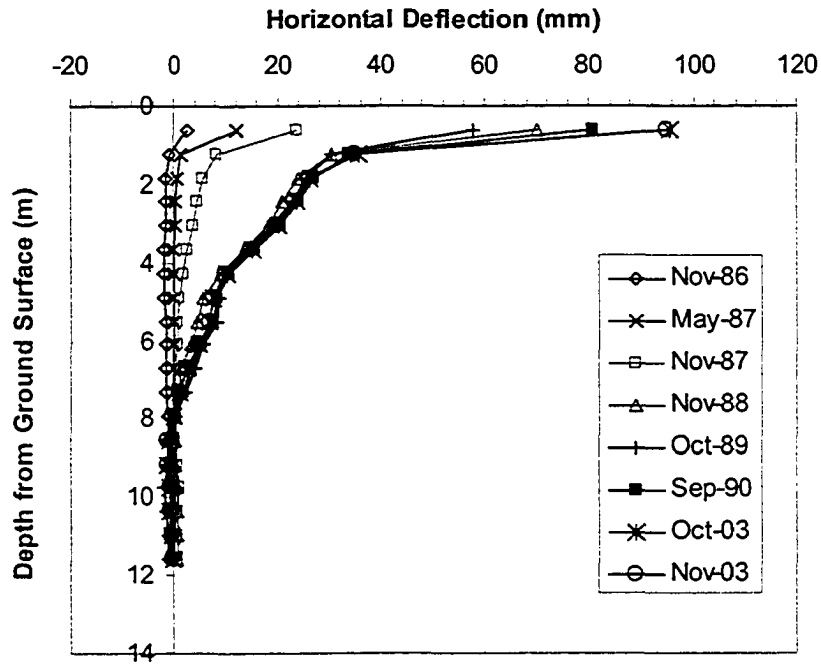

Figure 11. Horizontal deflection in "A" direction- Signode at toe

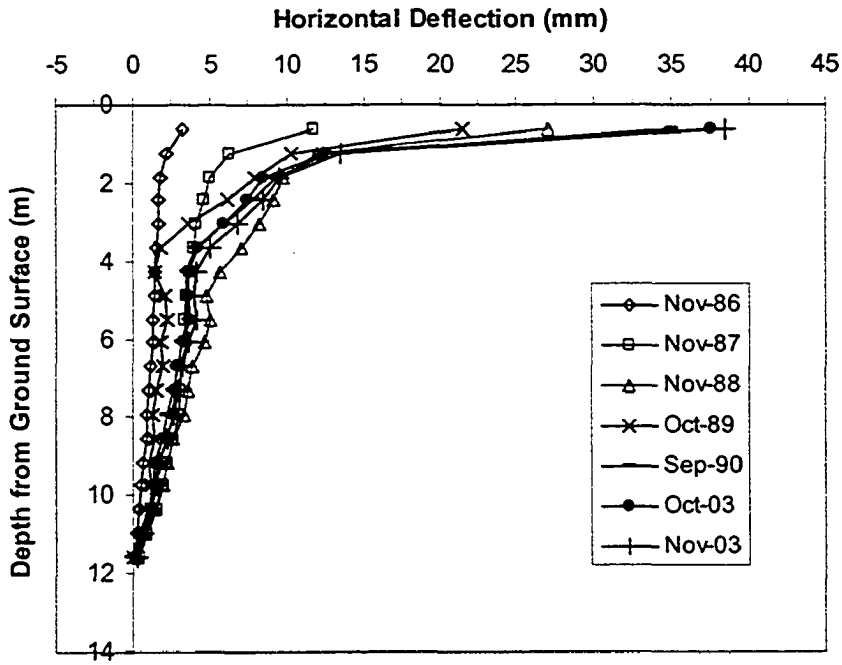

Figure 12. Horizontal deflection in "B" direction- Signode at toe

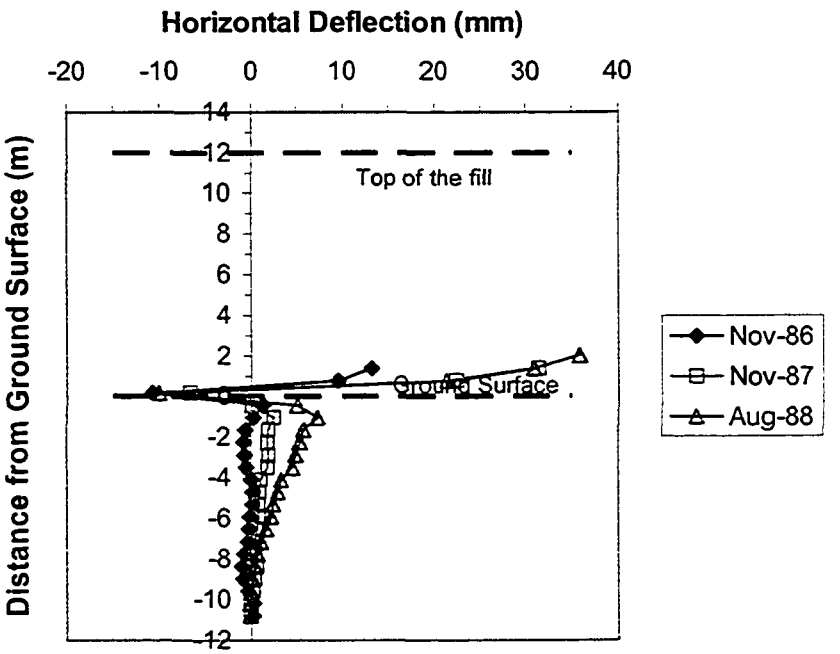

Figure 13. Horizontal deflection in "A" direction- Signode at crest

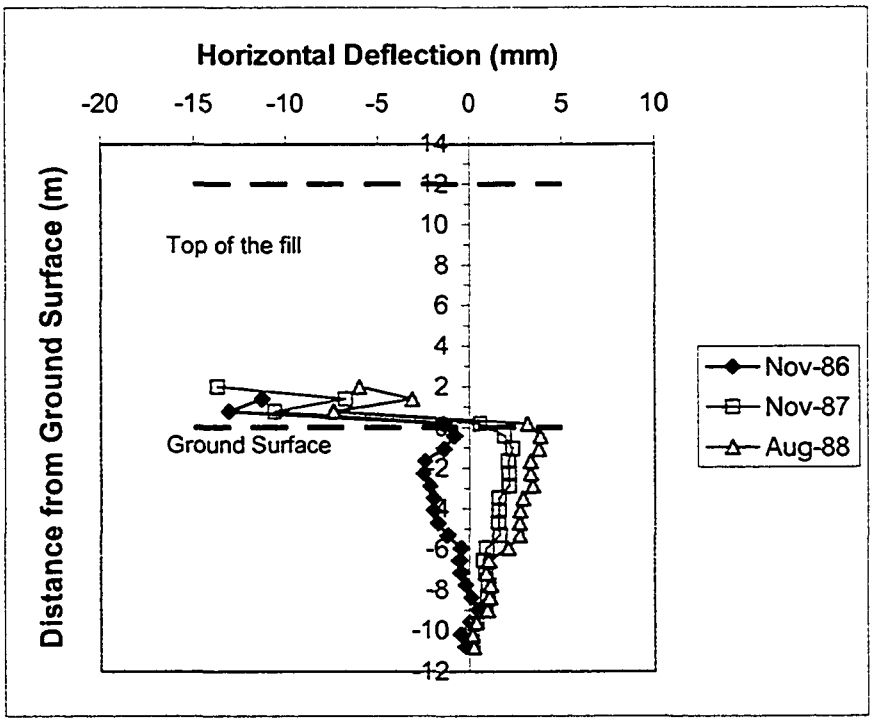

Figure 14. Horizontal deflection in "B" direction-Signode at crest

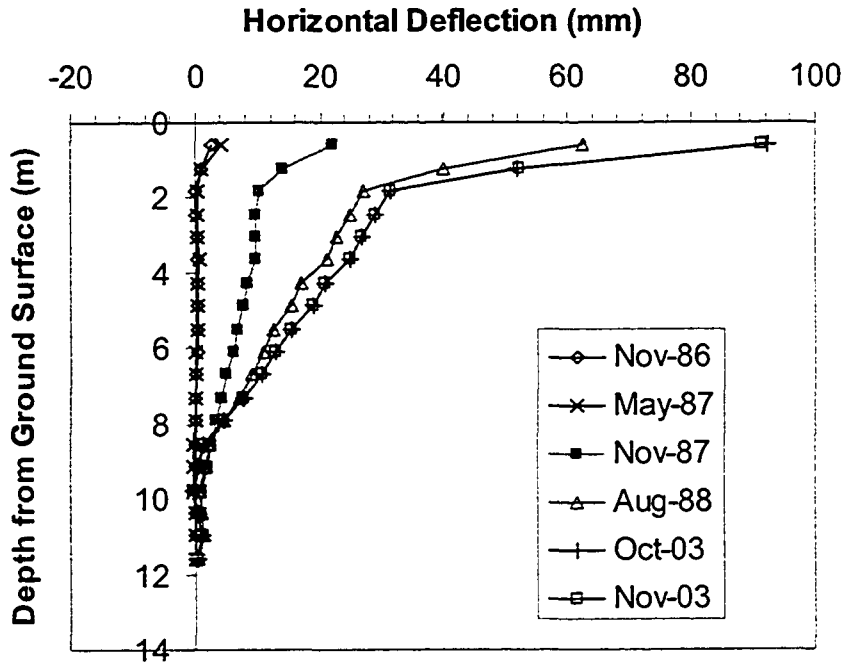

Figure 15. Horizontal deflection in "A" direction- Paragrid at toe

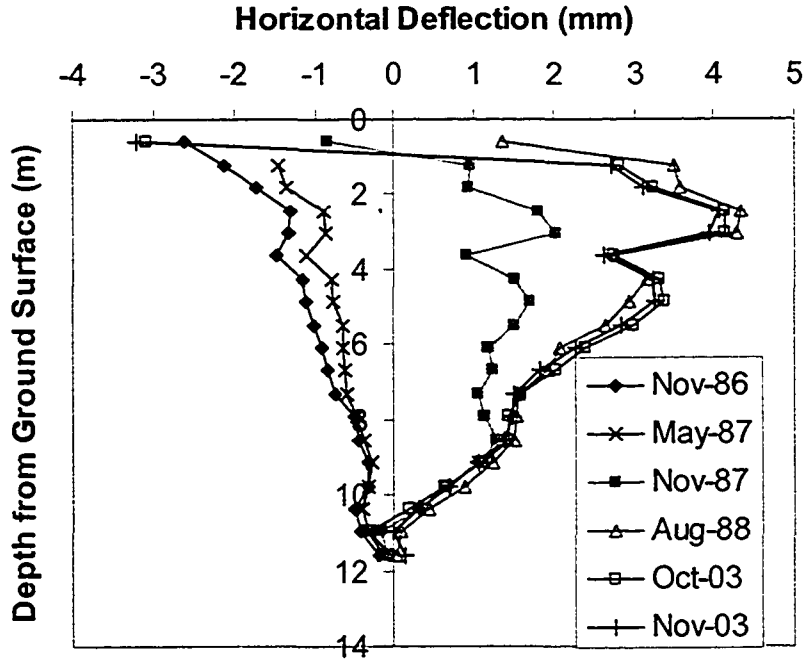

Figure 16. Horizontal deflection in "B" direction-Paragrid at toe

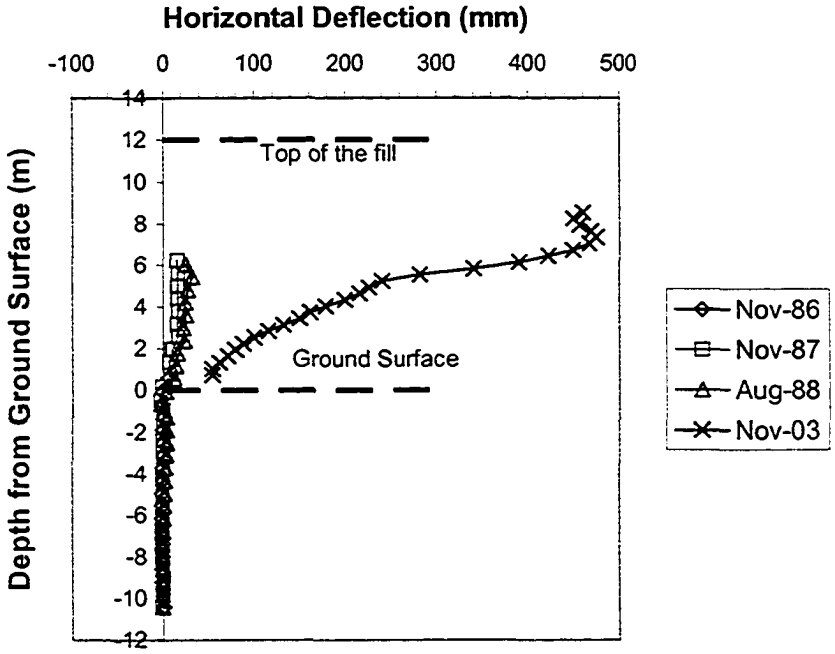

Figure 17. Horizontal deflection in "A" direction- Paragrid at crest

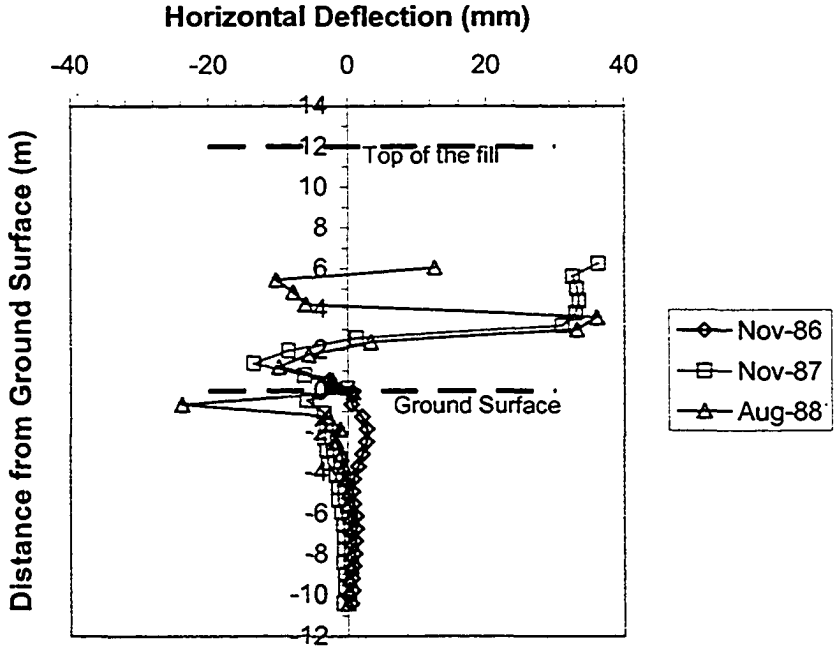

Figure 18. Horizontal deflection in "B" direction-Paragrid at crest

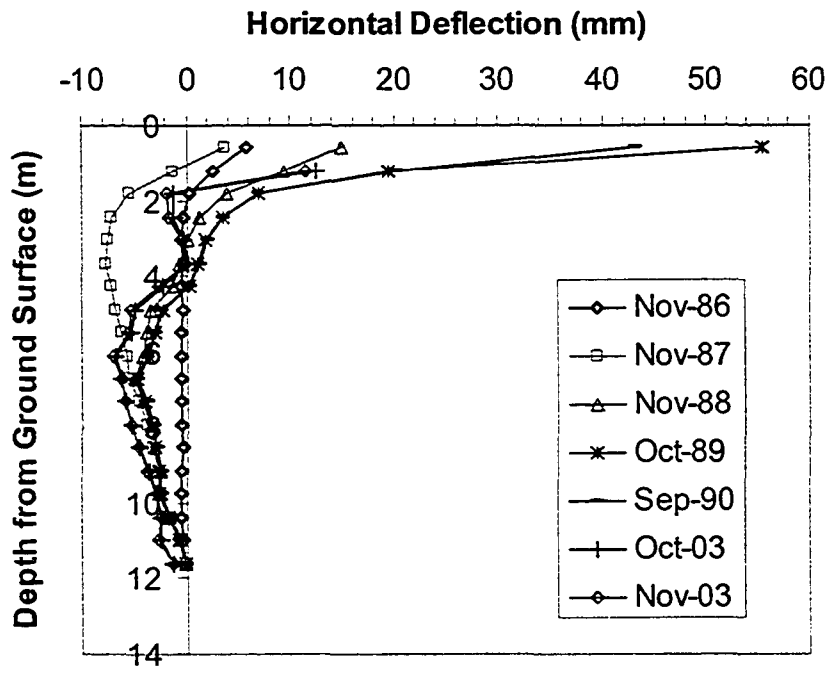

Figure 19. Horizontal deflection in "A" direction-Unreinforced at toe

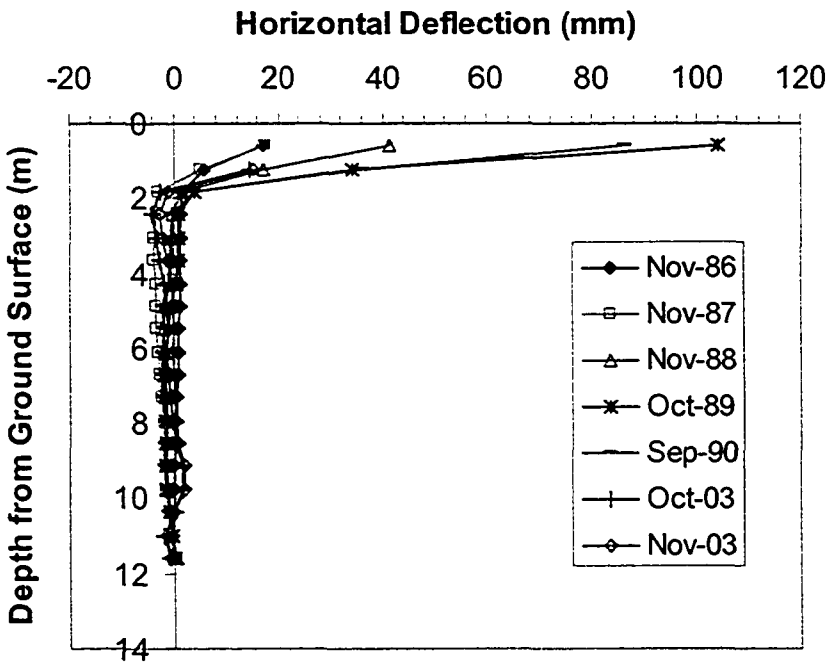

Figure 20. Horizontal deflection in "B" direction-Unreinforced at toe

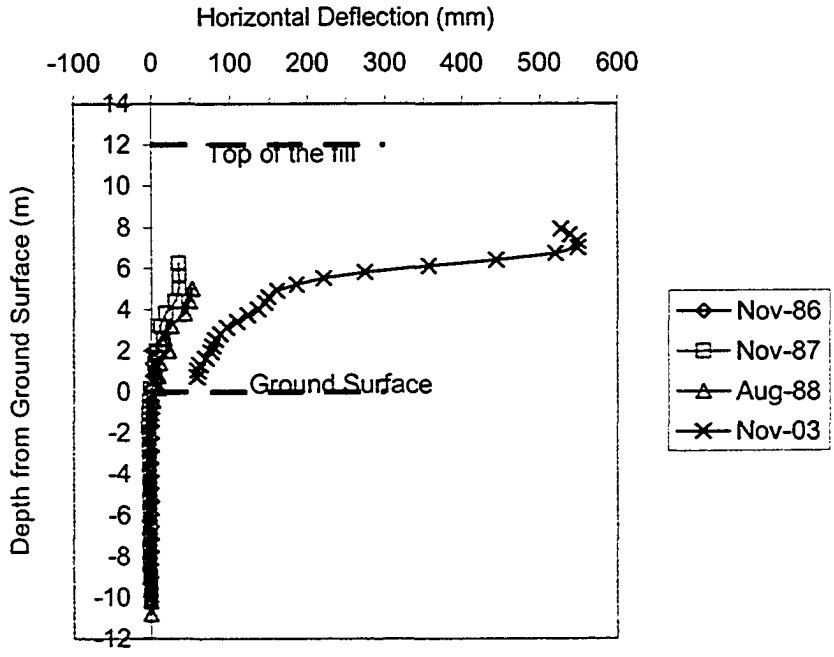

Figure 21. Horizontal deflection in "A" direction- Unreinforced at crest

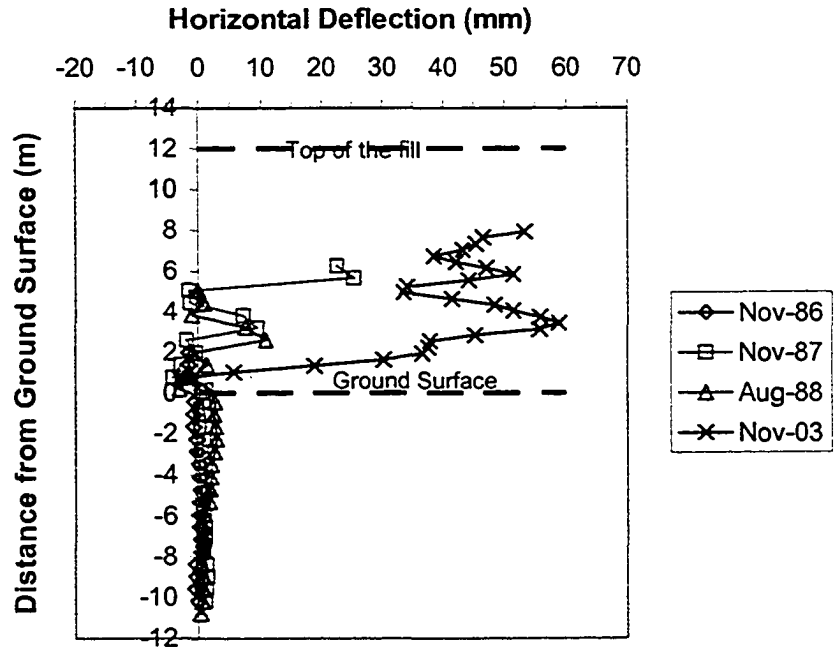

Figure 22. Horizontal deflection in "B" direction- Unreinforced at crest

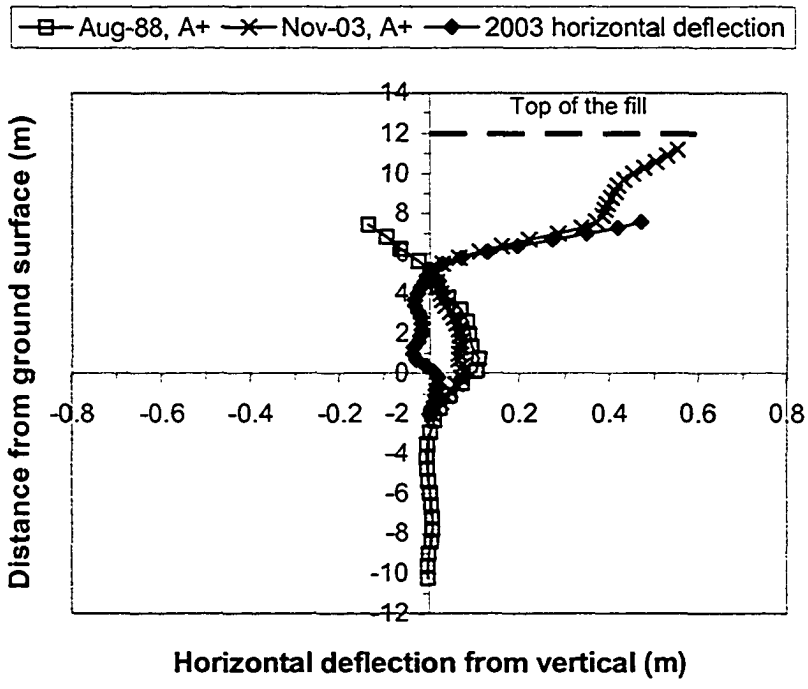

Figure 23. Horizontal deflection in "A" direction from vertical - Tensar at crest

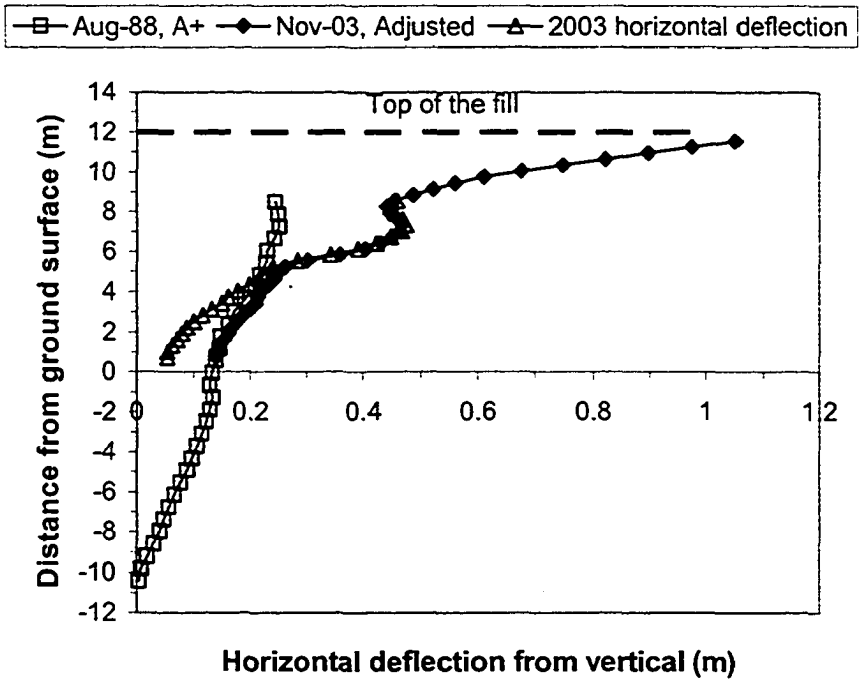

Figure 24. Horizontal deflection in "A" direction from vertical – Paragrid at crest

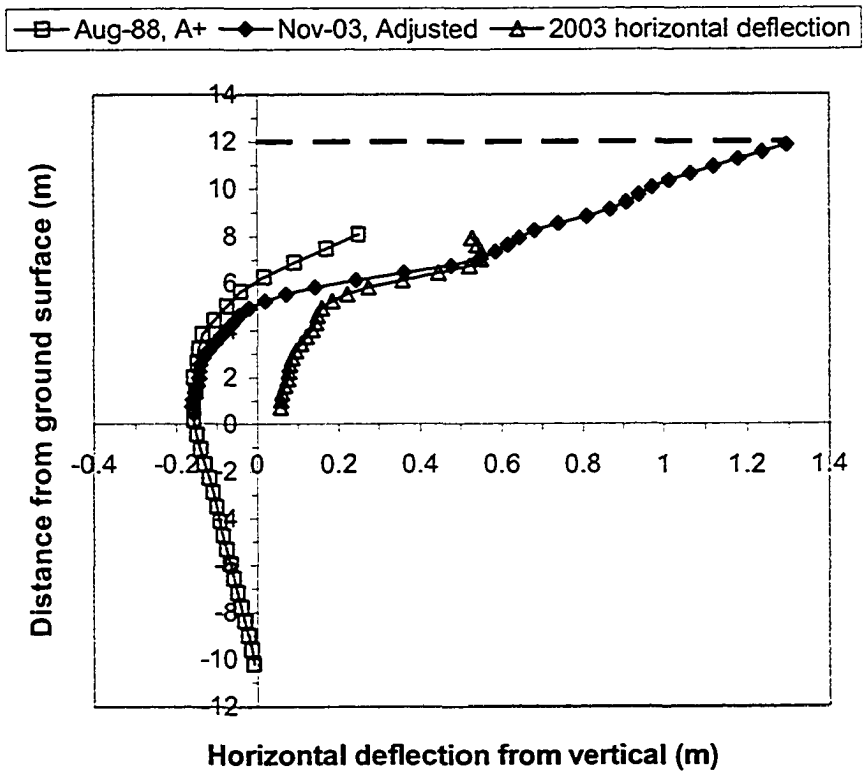

Figure 25. Horizontal deflection in "A" direction from vertical – unreinforced at crest

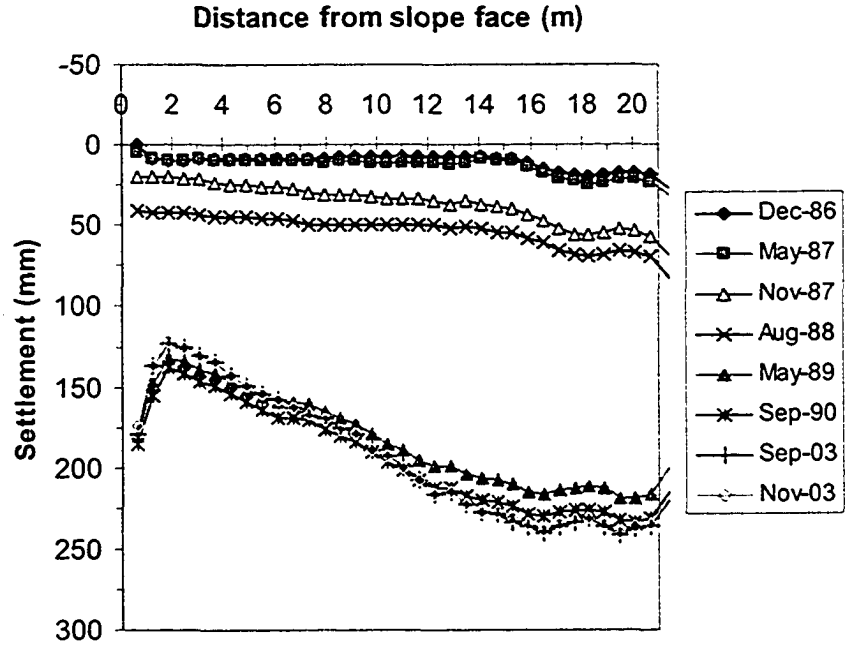

Figure 26. Settlement profile-Tensar section 0 m elevation from ground surface

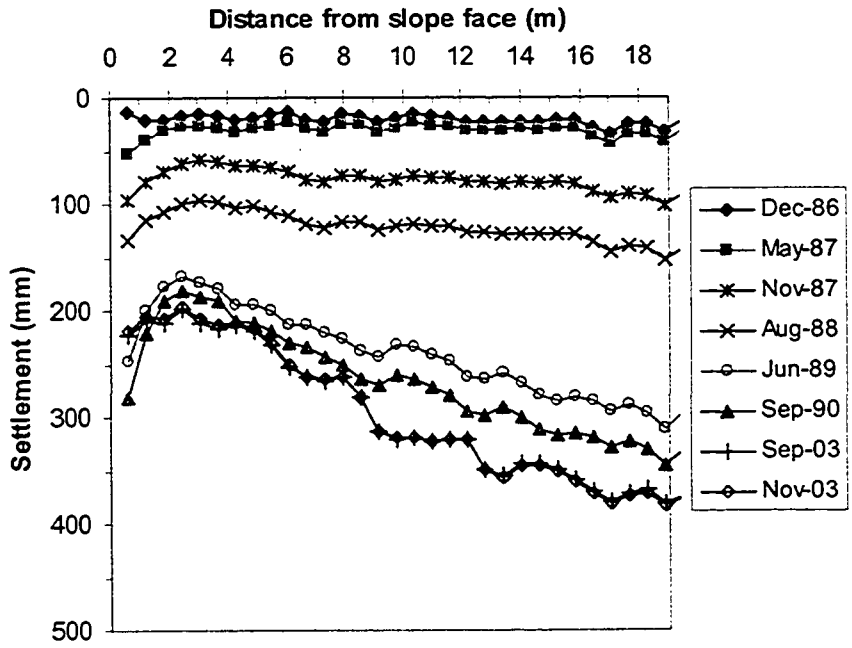

Figure 27. Settlement profile-Tensar section 2 m elevation from ground surface

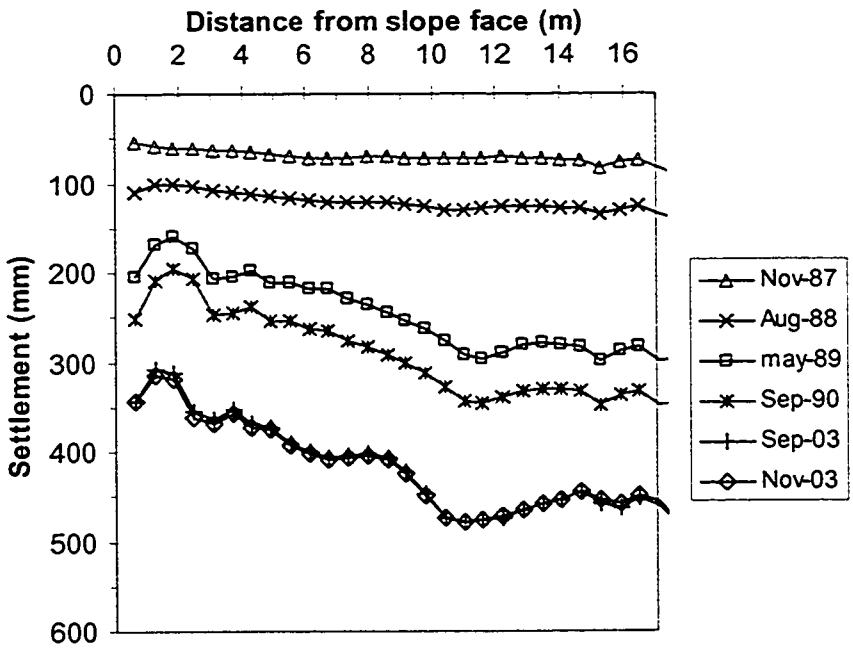

Figure 28. Settlement profile-Tensar section 4 m elevation from ground surface

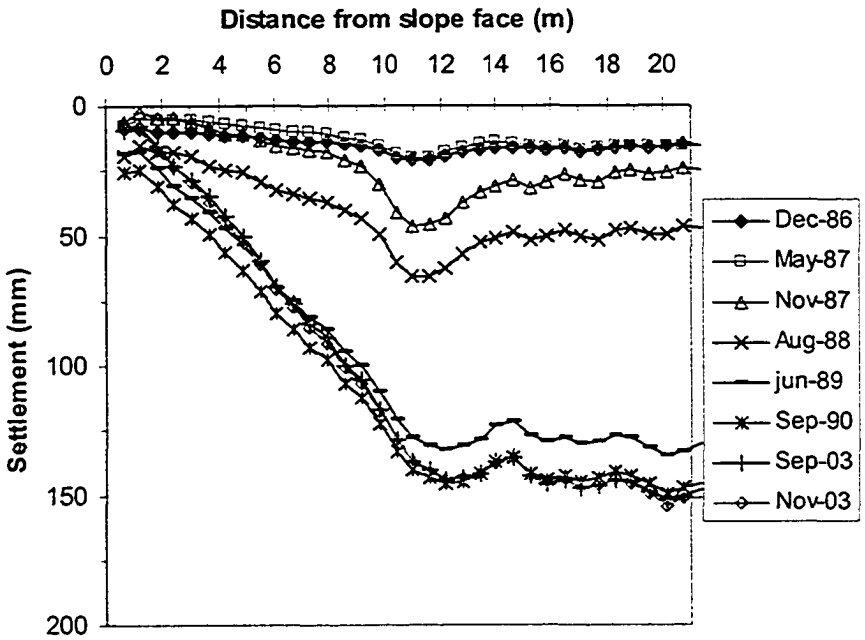

Figure 29. Settlement profile- Signode section 0 m elevation from ground surface

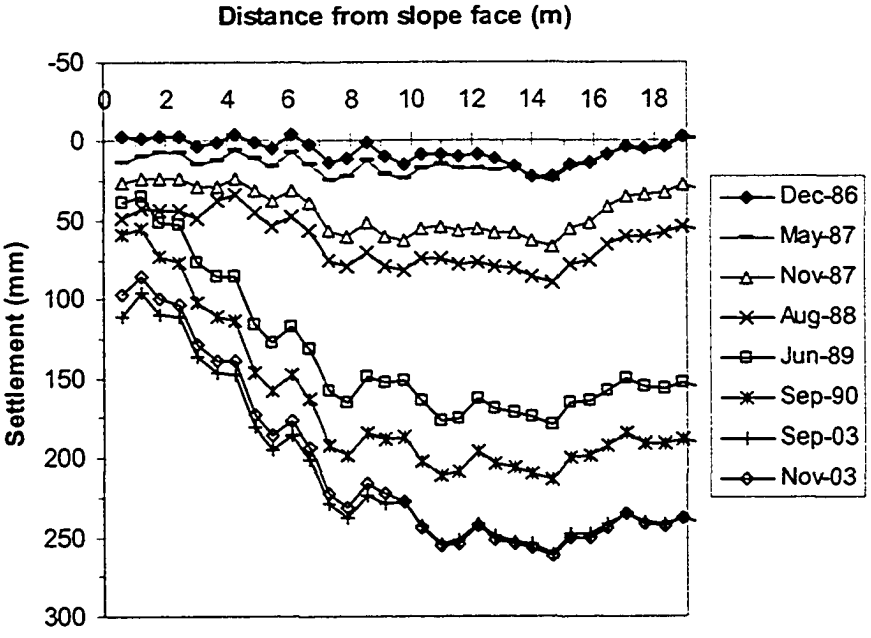

Figure 30. Settlement profile-Signode section 2 m elevation from the ground surface

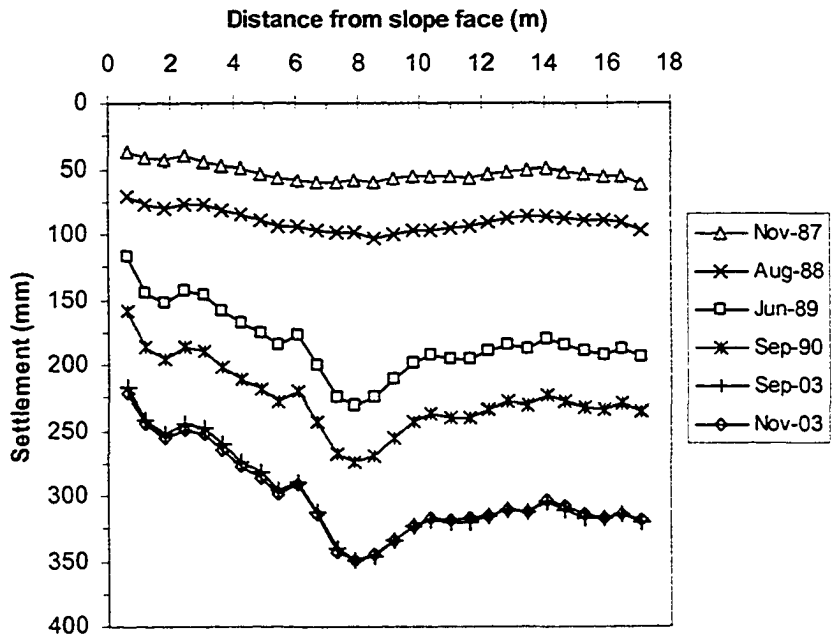

Figure 31. Settlement profile-Signode section 4 m elevation from the ground surface

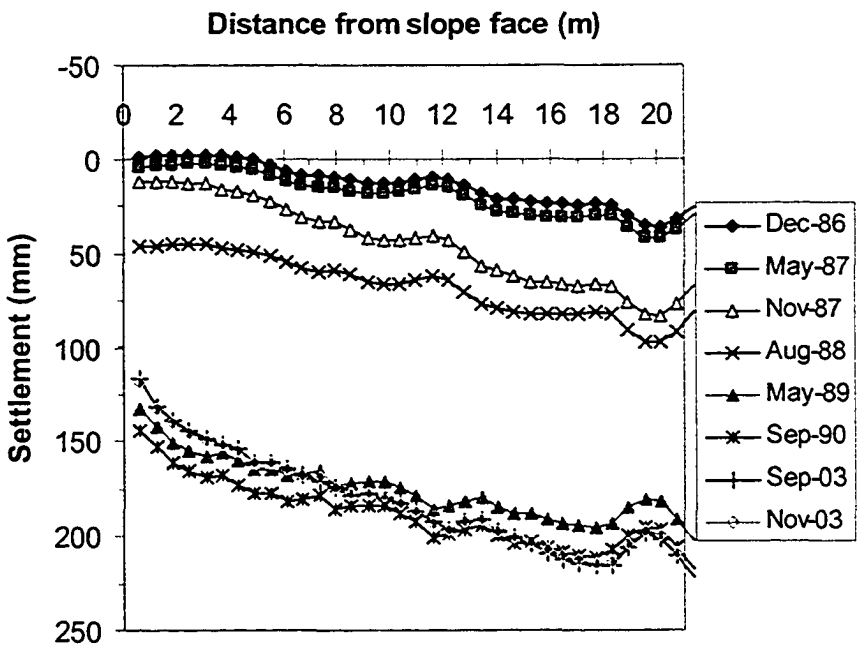

Figure 32. Settlement profile-Paragrid section at 0 m elevation from ground surface

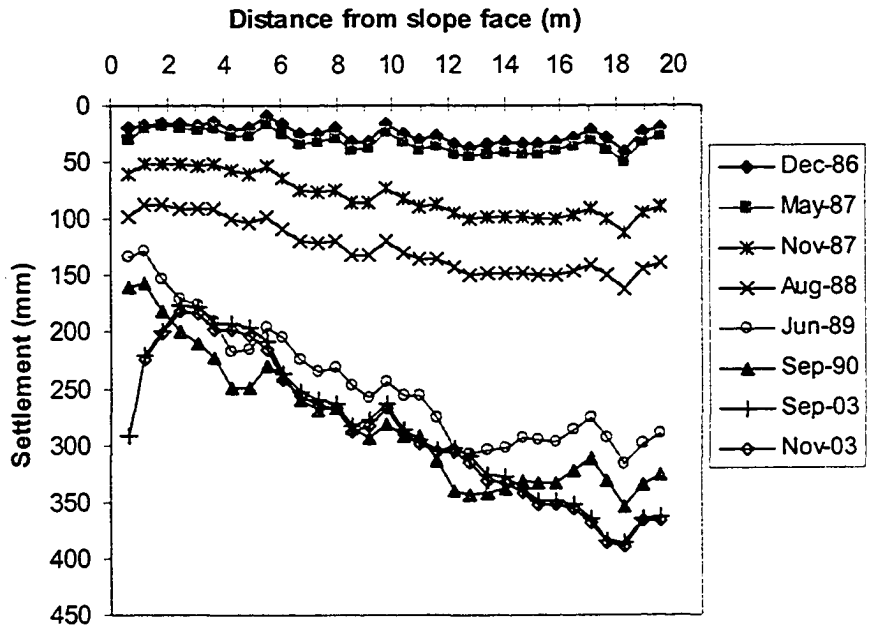

Figure 33. Settlement profile-Paragrid section at 2 m elevation from ground surface

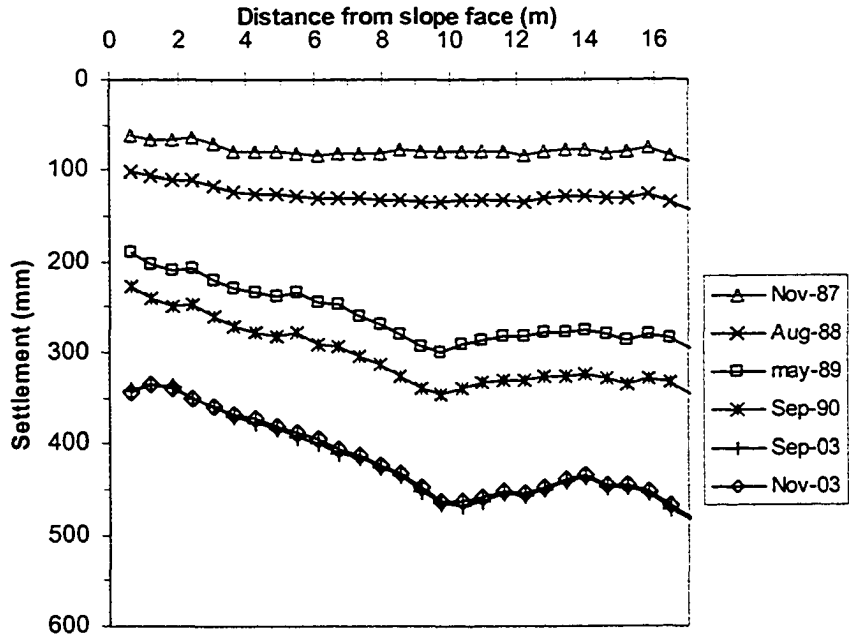

Figure 34. Settlement profile-Paragrid section at 4 m elevation from ground surface

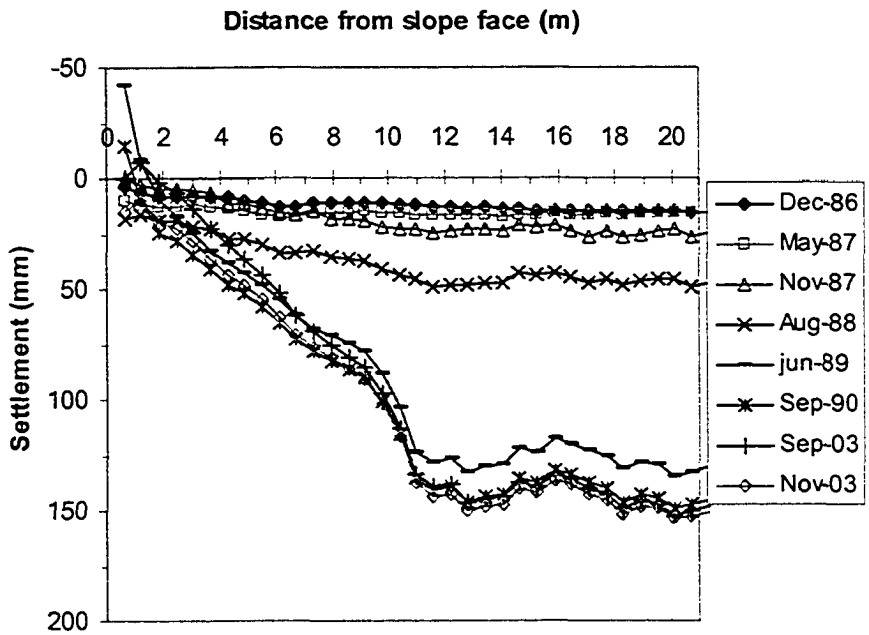

Figure 35. Settlement profile-Unreinforced section at 0 m elevation from ground surface

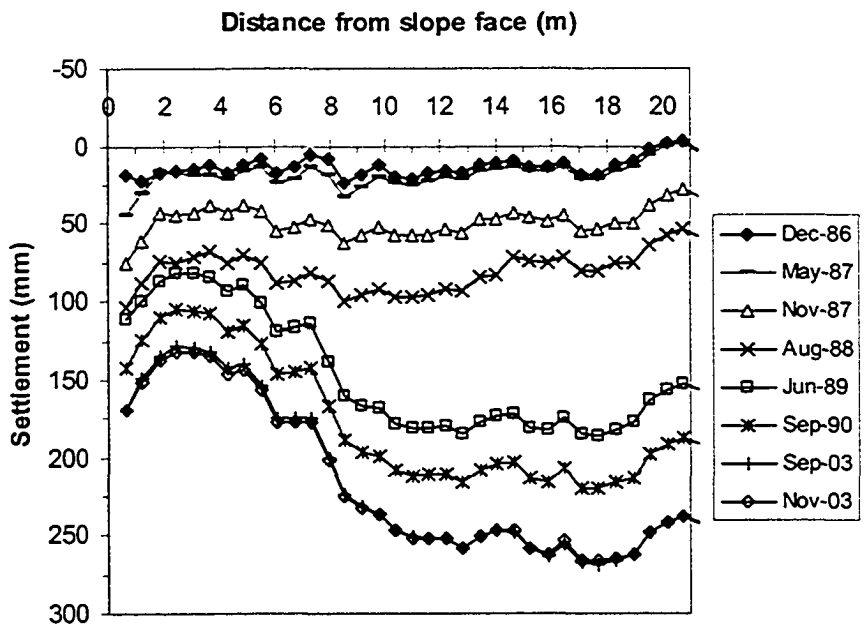

Figure 36. Settlement profile-Unreinforced section at 2 m elevation from ground surface

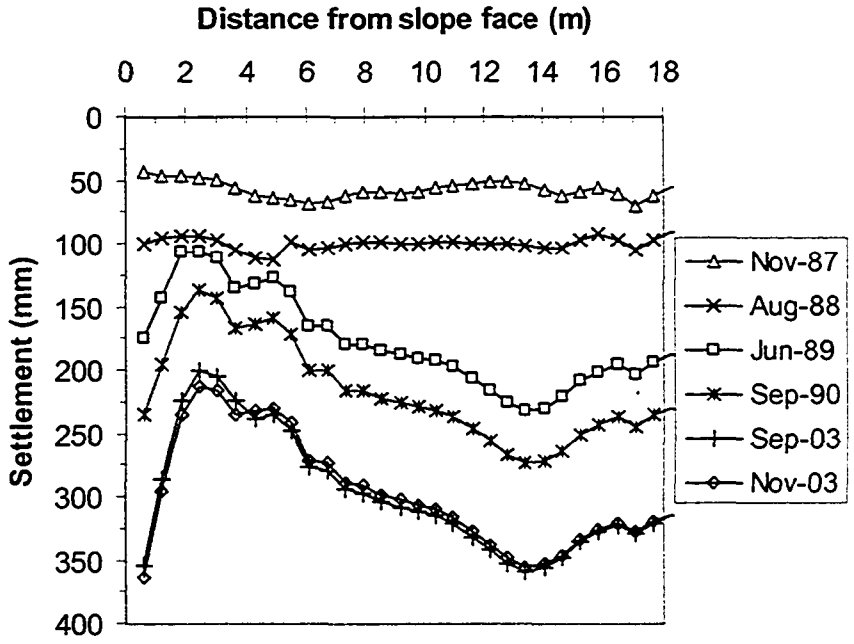

Figure 37. Settlement profile-Unreinforced section at 4 m elevation from the ground surface

Allen, T.M. and Bathurst, R.J. (2002). "Observed lomg-term performance of geosynthetic walls and implications for design", Geosynthetics International, Vol.9, Nos.5-6, pp.567-606.

Bathurst, R.J., Allen, T.M and Walters, D.L., (2002). "Short-term strain and deformation behaviour of geosynthetic walls at working stress conditions", Geosynthetics International, Vol.9, Nos.5-6, pp.451-482.

Bonaparte, R., Schmertmann, G.R., Chu, D. and Chouery-Curtis, V.E. (1989) " Reinforced Soil Buttress to Stabilize a High Natural Slope", Proceedings of the Twelfth international conference on soil mechanics and foundation engineering, Rio de Janeiro, 1989, Vol.2, pp.1227-1230.

Bartlett, S., Monley, G., Soderberg, A. and Palmer, A. (2001). "Instrumentation and Construction Performance Monitoring for I-15 Reconstruction Project in Salt Lake City, Utah", Transportation Research Record, No.1772, pp.40-47.

Christopher, B.R., Bonczkiewicz, C. and Holtz, R.D. (1994). "Design, construction and monitoring of full scale test of reinforced soil walls and slopes", Proceedings of the recent case histories of permanent geosynthetic-reinforced soil retaining walls conference, pp.45-60.

Liu, Y., (1992). "Performance of Geogrid Reinforced Clay Slopes." PhD. Thesis, University of Alberta: 406p.

Miyoshi, H., Kage, S., Suzuki, Y. and Sakamoto, M. (1992). "Design and construction of a geogrid-reinforced high embankment with high water content-volcanic cohesive soil: A case history", Earth reinforcement practice: Proceedings of the International Symposium on Earth Reinforcement Practice, Fukuoka, Kyushu, Japan, 11-13 November 1992, pp.275-280.

Yoo, C. and Lee, K. (2003). "Instrumentation of anchored segmental retaining wall", Geotechnical Testing Journal, Vol.26, No.4, December 2003, pp.382-389.

Chapter 6. Extensometers-Horizontal and Vertical

6.1 Introduction

Horizontal and vertical extensometers were installed in the Devon test embankment and vertical extensometers in the foundation soil in order to monitor the deformation pattern of the reinforced and unreinforced sections of the embankment. The long term performance of these instruments is discussed in this chapter by reviewing the measurements in 2003 and comparing them with the last set of measurements in 1989 and 1990, 1 to 2 years after the end of construction.

6.2 Literature review on horizontal and vertical extensometers used in reinforced soil structures

In November 1985 a steep reinforced soil embankment was constructed as a snow avalanche barrier at Andalsnes, on the west coast of Norway. The embankment is 6 m high, 55 m long and was constructed over a competent gravelly sand foundation (Hermann and Burd, 1988). The fill material used in the construction of the embankment was a free-draining cohesionless soil and was graded as a uniformly graded medium sand and non-frost susceptible. The fill material was reinforced with four layers of Tensar SR2 geogrid in order to stabilize the side slopes. The arrangement and spacing of the primary reinforcement was based on the limit equilibrium design method proposed by Jewell *et al.* The primary geogrid layers were spaced vertically at 1.5 m intervals and their length covered the whole width of the slope cross section which was 9 m at the base of embankment. Layers of Tensar SS1 geogrid were placed as secondary reinforcement near the surface of the slope to ensure local stability. The embankment slopes were constructed using the so-called wrap-around method in which the primary reinforcement also acts as

surface protection for the slope face. A fine-grade mesh was placed behind the Tensar geogrid on the face of the slope to prevent surface erosion of the fill.

Magnetic extensometers, consisting of a square PVC plate free to slide along a PVC tube, were used to measure soil displacement at 5 different elevations inside the fill at one half of the embankment (0.5, 1.5, 2.4, 3.35 and 3.85 m from the ground surface). Ring magnets attached to each plate allowed the positions to be measured by sliding a reed-relay through the horizontal PVC tube. The interface between the plate and the tube was well greased to minimize friction. Installation was made during construction and zero readings were taken immediately after placement and compaction of the surrounding soil. The initial positions of the magnetic extensometer plates were measured during construction in November 1985 and measurements were then taken in April and September 1986 to determine the subsequent soil movements. The September 1986 results show that at the 0.5 m level extensometer the soil strain started from a negative value at 0.5 m from the center of the slope and increased to its maximum of about 0.7% strain at 2.5 m from the slope center and then decreased. At 1.5 m elevation it started from zero and reached to about 0.5% at 1.5 m from the slope and then decreased. The general magnitude of the soil strains measured during the test is substantially less than had been anticipated and is of order of the measurement accuracy since the measured plate positions may be considered to be accurate, at best, to within ±1 mm which corresponds to a strain of approximately 0.1%. The magnetic extensometer results may only, therefore, be used to indicate the general magnitudes of the lateral soil strains; they were not sufficiently accurate to indicate with confidence the variations of soil strain occurring within the structure. In the final conclusion of this field study, it was mentioned that limit equilibrium

methods may give rise to excessive conservatism when used to design reinforced steep slopes.

Bartlett et.al (2001) discussed the instrumentation of geotextile reinforced embankments and walls that were used for a reconstruction project. High strength woven geotextile was used to improve the global stability of some embankment and wall systems during rapid, undrained loading conditions. In some locations as many as three layers of geotextile (730 kN/m ultimate strength; 292 kN/m allowable strength) were used to guard against development of shear failure in the foundation.

Vertical magnetic extensometers were used to measure the amount and rate of primary consolidation settlement at various levels within the profile. Approximately 20 vertical magnetic extensometers were installed inside the foundation soil and the reinforced embankments and walls. The devices consisted of 25-mm outside diameter PVC pipes placed inside a series of ring magnets, which were attached to the borehole side wall by protracting spider-like arms. Also five to six telescoping couplings each having a collapse range of 300 mm were included at joints in the PVC casing to accommodate settlement.

The installation of magnetic extensometers required special care and planning. Before installation, the ring magnets were positioned at predetermined depth intervals on the PVC casing so when deployed in the borehole, they would be positioned above and below the soil layer of interest so that the strain versus time in this layer could be calculated. When the magnets were properly positioned, a release cord was pulled, allowing the spider arms to release and lock the magnets in place. To finish the installation, a bentonite grout mix was tremied into the borehole between the PVC pipe and the borehole wall. A baseline survey was subsequently performed before fill placement by lowering a 22 mm

diameter magnet reed switch probe down the PVC casing to establish the initial depth of each magnet. The displacement ratio was defined as the ratio of the cumulative horizontal displacement at the critical depth divided by the cumulative settlement determined from an adjacent extensometer. Values of displacement ratio proved to be less sensitive to short term instrument reading errors and were the primary approach used to assess foundation stability for most of the project. Significant changes in displacement ratio with time can indicate when the foundation behavior is changing from a relatively stable condition associated with consolidation settlement to a state of excessive plastic deformation. The vertical magnetic extensometers and inclinometers were used in this project to successfully control the rate of embankment construction and to monitor foundation stability of embankments and MSE walls constructed on soft soils during staged construction.

In a paper by Irvin *et al.* (1990) the performance of reinforced trial embankments in London clay is reported. Four half-scale trial embankments were constructed using varying combinations of slope geometry and Netlon SR2 geogrid reinforcement. The response of the embankments to surcharge loading applied through hydraulic jacks was monitored by conventional instrumentation including magnetic plate extensometers.

The reinforced embankments were 3 m high with (a) a side slope of 1.0:1.5, containing two 1.5 m high geogrid envelopes, (b) a side slope of 1.0:0.5 with three 1 m high geogrid envelopes and (c) a side slope of 1.0:1.0 with three 1 m high geogrid envelopes. A control embankment was also constructed with height of 3 m and side slope of 1.0:1.5. A hydraulic loading system was used to achieve failure of the embankments. Internal deformations within the embankments were measured with magnetic plate extensometers which were arranged in a single vertical section 0.5 m from

the mid-length of the embankments. The spacing of the magnetic plates was approximately 1.5 m. Geogrid reinforced embankments had extensometers installed adjacent to, and midway between, reinforcement layers. This gave up to six horizontal instrumentation levels depending upon the geogrid configuration. Construction of the embankments was completed in four weeks. Over a further eight week period, prior to testing, instruments were read periodically to check that a reasonable level of consolidation had been achieved. Once this was confirmed, testing commenced.

Surcharge loading was divided into two phases, pre- and post-failure loading defined loosely by deformation rate. The third reinforced earth embankment did not fail sufficiently to justify detailed comment. In all embankments two distinct phases of internal displacement were apparent, separated by the onset of failure. In the control embankment displacements were relatively small-less than 20 mm- up to an applied load of 130 kPa. At loads greater than this, internal displacements increased rapidly, typically doubling in magnitude, and at least one distinct shear plane formed towards the rear of the slope. Outward face movements typically changed from approximately 1 mm per 15 kPa increase in applied load, to between 3 and 30 mm per 15 kPa load increment. Vertical displacements at the slope face showed little evidence of the failure occurring within the body of the embankment. The total vertical displacement of the loading frame at the onset of failure was 431 mm. The internal vertical displacements showed a gradual increase in displacement up to an applied load of between 115 and 130 kPa. At loads greater than 130 kPa the zone towards the rear of the slope showed a rapid increase in vertical displacements. During dismantling of the embankment, the shear planes were easily identified. Some indications were present to suggest two shear planes, one deep seated and passing through the embankment toe, the other passing through the face of the

slope at approximately mid-height. The locations of the shear planes agreed well with those deducted from the magnetic plate extensometers.

The effect of geogrid confinement was illustrated by the fact that the geogrid envelopes supplied sufficient confinement to the fill to allow the transfer of applied vertical load to the lower geogrid envelope. The results also indicate that the majority of the initial displacement, and a significant proportion of the failure load displacement, was contained within the uppermost geogrid envelope. This suggests that the geogrid prevented the transfer of horizontal displacements between the upper and lower envelopes. Significant horizontal displacements were not observed in the lower geogrid envelope until loads up to 250 kPa were applied. The applied vertical stress at the top of this envelope, at which significant horizontal movements occurred, was estimated to be approximately 100 kPa. The fill material in the base of the upper geogrid envelope moved out approximately 240 mm more than the fill material in the top of the underlying envelope. Despite the large difference between the displacements in the upper and lower envelopes there was no evidence to suggest shear between the base of the upper geogrid envelope and the top of the lower geogrid. From observations made during testing it was apparent that shear of the fill material was occurring above and adjacent to the base of the top geogrid envelope. The fill material moved outwards, causing a tensioning of the geogrid in the face of the embankment.

In the case of the reinforced embankment with a 1.0:0.5 side slopes, a similar but much more distinctive process occurred. Two distinct phases of internal displacement were apparent for loads up to 215 kPa. Onset of failure for all the geogrid envelopes occurred under an applied load of approximately 105 kPa. Initial movement was essentially uniform through the embankment. This was followed by a rapid sequential deformation of each of the geogrid envelopes. This can probably be explained by the

stress distribution induced in the embankment. The dispersal of vertical stress throughout the embankment is probably not as great as in the less steeply constructed embankment.

The information obtained during the sectioning of the embankments, together with the measured displacements, confirmed that the clay fill sheared adjacent to the geogrid layers. As the clay fill sheared, the material with in an individual geogrid envelope moved outward towards the face of the slope. The outward movement was eventually restrained by the geogrid wrapped around the slope face. Prior to the tensioning of the geogrid in the face of the slope, the maximum shear stress which could be transmitted through the fill to the geogrid was the shear strength of the clay fill. When the fill material displaced sufficiently to tension the face material, the geogrid was further loaded and the fill material constrained. The constraint of the fill material increased the strength of the structure as a whole. Further loading of the structure would then have been possible until the geogrid material ruptured.

6.3 Description of the instrument

Vertical and horizontal extensometers were used to monitor the vertical movements (settlements) and horizontal movements of the fill respectively and settlements in the foundation soils. During construction of the test embankment ring magnets made by the Department of Civil Engineering at University of Alberta, were placed in the foundation soils in a borehole and in the fill soil at locations where soil movements were to be monitored. A PVC central access tube was then placed in each installation and a spring loaded ring magnet with spider legs was installed at a specific depth inside the borehole. No record of the installation procedures were found in the documents. Based on the discussions with the technician involved during the installation of the instruments no grouting was used for

vertical extensometers. For the horizontal extensometers, a small trench was excavated at the location of the horizontal extensometer and then the magnets were installed along the access tube placed in the trench. Then the trench was backfilled with soil and was hand compacted. A lift of fill was placed on top of the instrument and then the fill was compacted. A sensing probe incorporating a reed switch traveled within the access tube and sensed the position of magnets along the outside of the tube. The reed switch closed on entering and leaving the magnet field, activating a buzzer at the surface where measurements were taken from. A steel measuring tape used to suspend the probe measured the distance from the collar of the access tube to each magnet. The accuracy of the steel measuring tape is ±1 mm. (Liu, 1992).

6.4 Location of extensometers

The vertical extensometers were installed at the toe and crest of each section of the embankment and the horizontal extensometers were placed at 0, 2, 4 and 6 m elevation above the base of the embankment at the instrumented sections at the center of the northern and southern parts of the embankment. The location and layout of the vertical and horizontal extensometers in the test embankment is illustrated in Figure 4 of Chapter 2.

For the vertical extensometers the bottom magnet used as a datum was placed 9 m or 12 m below the ground surface in the stiff till to ensure that it would not settle. For the horizontal extensometers the magnet installed at the center of the fill was used as a datum. It was assumed that the movement of this magnet relative to the adjacent magnets would be negligible and this assumption was confirmed during field measurements which showed very small horizontal movements at the magnets adjacent

to the center magnet relative to the overall observed horizontal movements.

6.5 State of instruments in 2003

The horizontal and vertical extensometers were almost at the same location as the horizontal and vertical inclinometers, hence the condition of the extensometers in 2003, sixteen years after the end of construction, were similar to inclinometers. All the access pipes were washed thoroughly and all the target magnets along the horizontal extensometers and vertical extensometers at the toe could be retrieved and read. For vertical extensometers at the crest of slopes the same problem as vertical inclinometers at the crest existed; the probe could not be lowered down the access pipe because of bending and deformation of the access pipes. In order to overcome this problem it was decided to make a smaller probe. The magnetic sensor inside the probe was taken out and the cable and the metallic measuring tape were connected to one end. A series of small plumb balls were attached to the other end of the sensor in order to add weight to the sensor to make it slide down inside the vertical access tubes. The concept and the system worked very well in three of the vertical extensometers at the crest of slopes but in the unreinforced section it was not possible to lower this small probe either, because of the severe deformed shape of the access tube in this section. By using this probe all the target magnets in the other 3 reinforced sections could be read.

6.6 Previous vertical extensometer readings

Vertical movements of the fill and foundation soil along vertical alignments beneath the toe and the crest of each test section were monitored using vertical extensometers. The extensometer measures distances between target magnets and datum magnets at the bottom of the access tubes.

The datum magnets were installed at locations 9 m or 12 m below the original ground surface in stiff till to ensure that they would not settle from the load of the test fill. Subtracting the original distances obtained during the first field readings, from the measured distances, the vertical displacements (settlements) of target magnets were determined.

The access tubes for vertical extensometers installed at the crest of all 4 sections of the test embankment were blocked during the 1988 construction season and no additional measurements could be made. The number of vertical extensometer measurements made during and after construction is summarized in Table 1 and initial field measurement dates for vertical extensometers are also indicated in Table 2. Because the magnets inside the fill were added when the fill was placed, the measured settlements indicated the displacement accumulated since the time of magnet installation. The detailed discussion of measurements and settlement development at each vertical extensometer location is presented by Liu (1992) but in general from the profiles obtained from vertical extensometers at the crest of slopes, it is observed that the settlement increased during the first construction season and kept developing but with a smaller magnitude, during subsequent consolidation. This process repeated during the second construction season and the following consolidation period. In the profiles also the settlement increased with elevation approximately linearly; the rate of the variation with elevation increased as more soil was placed on the test embankment. The foundation soil near the ground surface displaced much more than the soil lying underneath the layers near the surface. Some adjustments were made to magnets located 6 m below the ground surface for the vertical extensometers at the crest of slopes in all sections (Liu, 1992). Measured settlements at the -6 m location were considerably larger than at the upper magnet location. This phenomenon indicated extension deformation of the foundation soils between the two locations. This

extension seemed impossible. As mentioned in Chapter 2, the foundation soil between the two magnets is silty clay; the soils 6 m below the ground are stiff sandy clay and very dense sand. This measured displacement was apparently caused by buckling of the access tube. Therefore, the settlement at the -6 m location was adjusted based on the settlement measurements at the -6.5 m location beneath the toe of the slopes.

6.7 Previous horizontal extensometer readings

The two horizontal extensometer tubes installed at the 6 m elevation were damaged during the construction season in summer of 1988. The access tube at the 4 m level in the south part of the test embankment was also blocked during the summer of 1989 at a location 2 to 4 m from its west end. The number of horizontal extensometer measurements made during and after the construction is summarized in Table 1 and initial field measurement dates for vertical extensometers are also indicated in Table 3.

By traveling through the PVC central access tube at each instrumented level, the probe measures distances between the target magnets and the west end of the access tube. The field measurements are then converted into distances between target magnets and the center magnet. The center magnet was assumed not to move during the construction of the test fill. This assumption was justified by the field measurements that the induced error would be of little significance compared with the amount of measured displacements (Liu, 1992). By subtracting the initial distances between the target magnets and the center magnet from the measured distances, the horizontal displacements of the target magnets, relative to the center magnet, were determined. Moreover, by comparing horizontal displacements at adjacent magnets which were approximately 2 m apart, average horizontal strains of the soil were calculated. To be consistent

with the designation of the strain in the geogrids, extensive strain within the fill soil was designated as positive. Some adjustments to the field readings were made at some locations where highly localized compression and extension of soil was observed. This highly localized phenomenon appeared not to represent the overall behavior of the soil since only small height of fill was placed. To eliminate systematic errors, possibly caused by construction activities, the displacement of these magnets were adjusted to the average values of their adjacent magnets. The assumption of stationary center magnet was checked and confirmed for each horizontal extensometer. A detailed discussion of soil horizontal strain development at each level and each section of the embankment, adjustments and confirmation of stationary center magnet were presented by Liu, 1992.

6.8 2003 Readings

6.8.1 Vertical extensometer at the Toe-Tensar section

Four magnets were installed along the vertical extensometer at the toe of Tensar section. The datum magnet was installed at 9 m below the ground surface in the stiff till and the other three magnets were located at 6.5, 3.5 and 0.5 m below the ground surface in the foundation soil. Figure 1 illustrates the location of the target magnets along the access tube. Figure 2 presents the profile of settlement at different times along the access tube. During the 2003 field measurements the magnet at -3.5 m location showed inconsistent results and the settlement at this location increased suddenly to about 20 mm, much higher than the settlement above it. While comparing the 2003 settlement profile with the previous profiles, It was believed that the magnet at this location might have displaced and moved downwards so the settlement at this location was corrected based on the observed settlement profiles at previous dates. The adjusted settlement

profile is shown in Figure 3 and the data points shown by circles represent the adjusted locations. The development of settlement with time at different target magnet locations is presented in Figure 4.

The trends of settlement variation measured in 2003 are similar to the previous measurements but the amounts of settlements measured in 2003 are not consistent. The two measurements show a difference of about 5 mm close to the ground surface and about 1 mm at 6.5 m below the ground surface. The accuracy of the instrument was the accuracy of the measuring tape used to measure the distance between magnets which was ±1 mm. But indeed the variation in tension applied to the measuring tape and the straightness of the measuring tape inside the access tubes will increase inaccuracy. Any turning or twisting of the measuring tape around the cable of the instrument may cause some inaccuracy in measuring the distance between magnets. If an average of these 2003 measurements is considered, then since last measurements in 1989, the settlement at 0.5 m below the ground surface increased from 4.5 mm to 8.5 mm and at 6.5 m below the ground surface it increased from 0.8 mm to 1.4mm.

6.8.2 Vertical extensometer at the Crest-Tensar section

The target magnets along the vertical extensometer at the crest of Tensar reinforced section were located at 5.5, 4.5, 3.5, 2.5, 1.5 and 0.5 m above the ground level inside the fill and at -0.5, -2.5, -6 and -9 m in the foundation soil and the bottom magnet at -9 m was considered as the datum magnet. Figure 1 shows the magnet location at the crest of Tensar section. Two measurements were made in 2003 using the modified small probe. During the 2003 field measurements it was found that 2 other target magnets were installed at elevations above the +5.5 m location. But since there were no initial readings carried out for these two magnets after

their installation, their settlement since their installation could not be captured. Their distances with the adjacent magnets, based on 2003 measurements, are shown in Figure 1. The two sets of measurements in 2003 indicated similar distances. Figure 5 illustrates the settlement profiles measured at different times along this extensometer. Since all the vertical extensometer access tubes at the crest of slopes were damaged and blocked during the summer 1988 construction season, the last set of measurements were made in August 1988. The two measurements in 2003 are quite consistent and show a similar trend of settlement variation at different depths. There was a problem in settlement of the target magnet at 6 m below the ground surface from the first set of field measurements and all the settlement measurements at this location were corrected. Measured settlements at the -6 m location were considerably larger than at the upper magnet location. This phenomenon indicated extension deformation of the foundation soils between the two locations. This extension seemed impossible. As mentioned in Chapter 2, the foundation soil between the two magnets is silty clay; the soils 6 m below the ground are stiff sandy clay and very dense sand. This measured displacement was apparently caused by buckling of the access tube (Liu, 1992). Therefore, the settlement at the -6 m location was adjusted based on the settlement measurements at the -6.5 m location beneath the toe of the slope. The same adjustment was applied to this location during the 2003 field measurements. The profile in 2003 show that the settlement increased almost linearly from the target magnet at -2.5 m depth to the top target magnet at +5.5 m inside the fill and reached a maximum of about 465 mm at +5.5 m. This means that the settlement at this elevation increased about 293 mm since 1988 measurements. The settlement measurements by horizontal inclinometers (Chapter 5) also indicated that at the Tensar section, 4 m elevation, the settlement along the crest of the slope increased about 180 mm between August 1988 and September 1990 when reached about 300 mm. So it can be expected that some

additional settlement had also occurred at 5.5 m elevation (1.5 m higher that horizontal inclinometer) after the 1990 measurements which is captured by the vertical extensometer at the crest of the slope.

Figure 6 illustrates the development of settlement with time at the crest of Tensar section measured with vertical extensometer.

6.8.3 Vertical extensometer at the Toe-Signode section

The target magnets were installed at locations 1, 3.5, 6 and 9 m below the ground surface and the datum was the bottom magnet located at -12 m in the stiff foundation soil. The sketch of the magnet locations is illustrated in Figure 7. The settlement profiles of the foundation soil beneath the toe of the slope in the Signode section is shown in Figure 8. The two measurements in 2003 are quite consistent and the trend of settlement profile follows the trend of previous measurements. It also shows that since the last set of measurements in 1989, the settlement has increased about 2 mm in depths between 3.5 and 9 m below the ground surface and reached a maximum of about 7.5 mm. But at -1 m the settlement increased about 18 mm between 1989 and 2003 and reached 28 mm. The gradual increase in settlement at -1 depth was also captured during previous measurements. It indicates that the magnet at this location might have located in some soft soil pocket and is showing more settlement. Some additional soil sloughing since May 1989 collected at the toe of the slope or even additional loading during the excavation with backhoe might have caused the increase in settlement at this magnet which is close to the ground surface. The plot also indicates that some heave had occurred between depths -6 and -4 m which could not happen. The settlement profiles in most of the previous measurements at this extensometer also indicated this heave at these depths. Hence it implies that the magnet at -6 m depth might have slipped down and settled more than the real

settlement of the surrounding soil at that location. Therefore the settlements at -6 m depth were adjusted based on the observed settlement trend measured in May 1989 when no heave was measured. The adjusted plot is shown in Figure 9. The plot of settlement with time at different levels is presented in Appendix C.

6.8.4 Vertical Extensometer at the Crest-Signode section

Figure 7 illustrates the sketch of the target magnet location at the crest of slope in Signode reinforced section. The datum is located at -9 m below in the stiff foundation soil and the other target magnets were placed at -6, -3 and -1 m and at +0.5, +1.5, +2.5, +3.5, +5 and +5.5 m in the fill soil. During the 2003 field measurements it was found that 2 other target magnets were installed at elevations above the +5.5 m location. But since there were no initial readings carried out for these two magnets after their installation, their settlement since their installation could not be captured. Their distances with the adjacent magnets, based on 2003 measurements, are shown in Figure 7. Figure 10 presents the settlement profiles along the access tube of the vertical extensometer at the crest of Signode reinforced section. The two measurements in 2003 show consistent settlement profile. Again as discussed for Tensar section, some adjustments were made to the settlement of the target at 6 m below the ground surface as was applied to the previous measurement (Liu, 1992). No settlement profile was available after August 1988 due to the damage to the access tube at the crest of the slope. The 2003 measurements showed that the settlement increased almost linearly from -6 m to +5.5 m and reached a maximum of 440 mm at +5.5 m location. Before placement of the top 6 m of the fill during summer of 1988 the settlement at 5.5 m elevation above the ground surface was only about 140 mm which showed an increase of about 300 m from August 1988 (before placement

of the top 6 m fill) and 2003. The plot of settlement development with time at different levels is presented in Appendix C.

6.8.5 Vertical Extensometer at the Toe-Paragrid section

The target magnets at the toe of the Paragrid section were installed at 9, 6, 3.5 and 1.5 m below the ground surface and the datum magnet was installed 12 m deep in the stiff till. Figure 11 is a sketch of the location of the plate magnets installed along the vertical access tube at the toe of Paragrid reinforced section. The settlement profile of magnets at the toe of Paragrid section before any adjustment is presented in Figure 12. Again measured settlements in 2003 at 3.5 m below the ground surface were considerably larger than the settlement at the 1.5 m below the ground surface. This phenomenon indicated extension deformation of the foundation soil between the two locations. The magnet at -3.5 m depth might had been installed in a soft soil pocket and between September 1990 and 2003 this magnet have settled more than the other magnets above and below it. This extension seemed impossible and the settlement at this location was adjusted based on the previous settlement profiles. The adjusted settlement profile at the toe of Paragrid reinforced section is illustrated in Figure 13. The two measurements in 2003 are not quite consistent with each other and there is a difference in range of 2 to 4.5 mm between two measurements in 2003 but the trend is very similar to previous profiles. The accuracy of the instrument in an ideal situation as mentioned before is ±1 mm but there are some other factors during measuring the distance between magnets that will increase inaccuracy by couple of millimeters. Hence the difference in measurements in range of couple of millimeters could be expected as good agreement. Again if the average of these two measurements is considered, since the last set of measurements in 1990 the settlement increased between 2.5 and 7 mm at

different depths along the access tube. The development of settlement during different times is illustrated in a separate plot in Appendix C.

6.8.6 Vertical Extensometer at the crest-Paragrid section

The target magnets at the crest of Paragrid reinforced section were installed at -6, -3 and -1 m in the foundation soil and +0.5, +1.5, +2.5, +3.5, +5 and +5.5 m in the embankment soil. The datum magnet was located 12 m below the ground surface. The location of the magnets is illustrated in Figure 11. During the 2003 field measurements it was found that 2 other target magnets were installed at elevations above the +5.5 m location. But since there were no initial readings carried out for these two magnets after their installation, their settlement since their installation could not be captured. Their distances with the adjacent magnets, based on 2003 measurements, are shown in Figure 11. The settlement profile at the crest of Paragrid reinforced section is presented in Figure 14. The two sets of measurements made by the modified small probe gave consistent results and the settlement profile in 2003 increased as the elevation increased. It reached its maximum at +5.5 m when the settlement was about 513 mm in 2003. No measurements were available after placement of the top 6 m of the fill soil but the results show that between summer of 1988 and 2003, the settlement at 5.5 m above the ground surface increased from 238 mm to 513 mm. The settlement development during time at the crest of the Paragrid slope is presented in Appendix C.

6.8.7 Vertical Extensometer at the Toe-Unreinforced section

Figure 15 shows the location of the target magnets installed along the vertical access tube at the toe of the unreinforced section. The target magnets were placed at -6, -2.5 and -0.5 m and the datum magnet was installed at -9 m. Two measurements were made in 2003 and the results

before adjustments are illustrated in Figure 16. The previous measurements made during the construction till the last one in 1989 all showed that the foundation soil at the toe of unreinforced section settled very little (between 0 and 5 mm) but the measurements in 2003 showed that the soil had heaved since 1989. The two measurements in 2003 are consistent and show a similar behavior of the foundation heave. In reality this phenomenon could not happen and it indicates that the datum magnet has settled and some adjustment is required. If the settlement development at a higher magnet, -6 m depth, is reviewed it reveals that it had not experienced any significant settlement since its installation time. In fact its settlement ranged between -2 mm and 1 mm during its life time. So based on these observations the settlement at -6 m depth in 2003 are adjusted and as result the whole profile is adjusted by ignoring the settlement of the datum magnet. The adjusted plot is illustrated in Figure 17.

6.8.8 Vertical Extensometer at the crest-Unreinforced section

The target magnets along the vertical access tube at the crest of unreinforced section were installed at +6, +5, +4, +3, +2 and +1 m in the fill and -0.5, -3, -6 and -9 m in the foundation soil. Figure 15 illustrates the sketch of target magnet locations at the crest of unreinforced section. Unfortunately no measurements could be made in 2003 despite using the modified small extensometer probe. It showed that the deformation of the vertical extensometer access tube at this location was so severe that the small probe could not travel inside it. Figure 18 illustrates the settlement profiles measured during construction till August 1988.

6.9 Horizontal Extensometers

6.9.1 Tensar section

As mentioned before the horizontal extensometers were installed at different elevations inside the fill soil to monitor the soil horizontal strain at different locations inside the embankment. The magnet installed at the center of the fill was considered as datum and the other target magnets were placed about 2 m apart. The same probe was used to measure the distance between the target magnets and the datum magnet in order to minimize related errors. At the bottom level extensometer (0 m elevation) at the Tensar section, 10 target magnets were installed in addition to the datum magnet at the center of the fill. At 2 m elevation above the ground surface 9 target magnets, at 4 m elevation above the ground surface 8 target magnets and at 6 m elevation 7 target magnets were installed in addition to the central datum magnet.

Figure 19 presents the incremental soil horizontal strain variation at 0 m elevation in the Tensar reinforced section. Two measurements were made in 2003 and they show consistent strain profiles. The 2003 horizontal strain profiles also show that the horizontal strain in the soil at this elevation has not changed (variation is around 0.05%) since the last measurements in 1990. A detailed discussion of the soil horizontal strain variation at different stages of construction and consolidation is presented by Liu (1992). The profiles of total soil horizontal movement at the 0 m elevation in the Tensar section are shown in Figure 20. As the deformation profiles illustrate, the horizontal movement starts to increase from the center of the embankment towards the slope surface and reaches a maximum of about 76 mm at 3 m from the slope face.

The incremental soil horizontal strain variation at 2 m elevation in the Tensar reinforced section is presented in Figure 21. Again the two measurements in 2003 are quite consistent and also follow the similar trend of strain variation measured after the end of construction. The strain

profiles show similar trends as 1990 measurements and there is no soil horizontal strain development since then. The profiles of total soil horizontal movement at the 2 m elevation in the Tensar section are presented in Figure 22. The soil horizontal deformation increased from the center of the slope towards the slope surface and reached about 120 mm at the 1 m location from the slope face in 2003.

Figure 23 illustrates the profiles of incremental soil horizontal strain at +4 m elevation in the Tensar section. Since the access tube at this elevation was blocked and damaged in the 1988 construction season, no previous measurements were available after construction was complete. The measurements in 2003 show consistent profiles of soil horizontal strain but there are no measurements available after the end of construction to compare those with. The trend of the soil horizontal strain in 2003 follows the trend of the August 1988 measurements. The small peaks in the 1988 measurements were developed to high strain peaks at the 3 and 11 m locations from the slope face in the 2003 measurements. The profiles of total horizontal movement of the embankment soil at +4 m elevation in the Tensar section are presented in Figure 24. The maximum horizontal deformation in 2003 occurred at the 1 m location from the slope face and reached about 245 mm.

The plots for the development of the soil horizontal strains at the 0, 2 and 4 m elevation with time at different locations in the test embankment are presented in Appendix C.

6.9.2 Signode section

Figure 25 illustrates the soil horizontal strain profiles at 0 m level in the Signode reinforced section. The two sets of measurements in 2003 revealed consistent horizontal strain profiles with a maximum difference of

less than 0.1% strain between the two measurements. The profiles show that in 2003 within 5 m distance from the slope face the soil was compressed. The new measurements also showed that since the last measurements in 1990 the soil horizontal strain at this elevation has remained almost unchanged with variations in range of ±0.1% strain.

The soil horizontal strain variation at 2 m elevation above the ground surface is presented in Figure 26. The 2003 measurements revealed a similar horizontal strain profile to the previous measurements made after the end of construction. Again it seems that no additional horizontal strains were developed since 1990 in the fill soil at this elevation beside some small variations in strain which might have been due to measurement errors.

The profiles of soil horizontal strains at 4 m elevation above the ground surface are illustrated in Figure 27. A variation in strain in the range of ±0.25% was observed between the two sets of measurements in 2003. In general however the trend of strain variation was similar to the measurements made in 1990. No additional horizontal strain development was observed between 1990 and 2003.

The soil horizontal strain developments with time during different stages of construction and consolidation are presented in Appendix C. The amounts of horizontal deformation in the fill at the different elevations in the Signode section are also presented in Appendix C.

6.9.3 Paragrid section

The soil horizontal strain profiles at the 0 m elevation in the Paragrid reinforced section are presented in Figure 28. The two measurements made in 2003 show a similar strain variation along the extensometer axis

with minor variations (±0.1% strain). The measured strain profiles match with the previous measurements made after the end of construction. No significant horizontal soil strains developed since the 1990 field measurements. The 2003 measurements showed that the soil at this elevation did not undergo any additional horizontal movements.

Figure 29 illustrates the horizontal soil strain profiles at the 2 m elevation in the Paragrid reinforced section. The two measurements made in 2003 show a reasonable match and reveal consistent strain profiles. In general, no additional horizontal soil strains were developed at this elevation between 1990 and 2003.

At the 4 m elevation in the Paragrid section no measurements were made during and after the third construction stage due to the damage and blockage of the access tube. Hence the deformation response of the test embankment after placement of the top 6 m of fill was not monitored. In 2003 the access tube was washed and cleaned by pushing a stiff hose through the access pipe allowing the strain measurements to be made. The horizontal soil strain profiles at the 4 m elevation are illustrated in Figure 30. The two measurements in 2003 show consistent strain profiles with a high peak developed at 1 m distance from the slope face.

The plots of horizontal displacement versus distance inside the fill and the development of the soil horizontal strain with time are presented in Appendix C.

6.9.4 Unreinforced section

The profile of soil horizontal strain at the 0 m level in the unreinforced section of the test embankment is illustrated in Figure 31. Two sets of measurements were carried out in 2003 and show fairly consistent results.

Between 15 m and 19 m distance from the slope face the two measurements have a difference in the range of ±0.2% strain. No significant horizontal strain was developed at this elevation in the fill since the 1990 field measurements. The trend of horizontal strain in 2003 follows that in the 1990 field measurements.

Figure 32 illustrates the soil horizontal strain variation at the 2 m elevation in the unreinforced section. The two sets of measurements made in 2003 match each other with a ±0.1% strain difference. The trend of strain variation in the fill soil in 2003 is identical to the 1990 field measurements. It can be observed that no additional soil horizontal strain developed in the fill soil at this elevation since 1990.

Figure 33 presents the profiles of soil horizontal strains in the fill at the 4 m elevation. Again the two measurements made in 2003 show consistent results and the two profiles match each other perfectly. As was the case for the horizontal extensometers at 0 m and 2 m elevations, no additional soil horizontal strain was developed inside the soil fill since the 1990 field measurements but some contraction between 0.1% and 0.4% strain occurred within 5 m distance from the slope face.

The plots of horizontal displacement versus distance in the fill and the development of the soil horizontal strain with time are presented in Appendix C.

6.10 Long term performance of extensometers

6.10.1 Long term performance of vertical extensometers

The vertical extensometers at the toe of the slope sections were all washed and cleaned in order to make it possible to reach the bottom fixed

magnet and for all four access tubes at the toe of the slopes all target magnets and the fixed bottom magnet could be read during the 2003 field measurements, 13 years since the last field measurement. In the 3 reinforced sections the results showed that additional settlement in the range of 1 mm to about 17 mm occurred at the toe of the slopes between 1990 and 2003. In the Tensar reinforced section the settlement profiles measured in 2003 were the same but the magnitudes showed a small variation in the range of 1 to 5 mm along the vertical tube. The accuracy of the settlement measurements with vertical extensometers was ±1 mm which is the accuracy of the measuring tape. But during field measurements some factors could affect this accuracy and deteriorate its precision. The tension applied to the measuring tape while taking the readings or any turning or twisting of the measuring tape around the instrument cable can add inaccuracy to the measurements and decrease the accuracy to couple of millimeters. Hence the measurements with couple of millimeters could be considered reliable. By considering an average for the two measurements made in 2003, it shows that since the last set of field measurements in 1990, the foundation soil at the toe of Tensar reinforced section has settled more between 1 and 5 mm at different depths. The 2003 measurements showed that the magnet at -3.5 m depth had slipped down and settled more than its surrounding soil which in the plot showed some heave at that depth. Since this phenomenon could not take place and was not observed in the previous measurements, the settlement of the magnet was adjusted based on the previous measurements.

In the Signode reinforced section the two measurements made in 2003 were consistent and showed that since 1990 additional settlement of between 2 and 17 mm occurred along the extensometer at the toe of the slope. The measurements indicated that some heave had occurred between depths -6 and -4 m which could not happen. The settlement

profiles in most of the previous measurements at this extensometer also indicated this heave at these depths. Hence it implies that the magnet at -6 m depth might have slipped down and settled more than the real settlement of the surrounding soil at that location. Therefore the settlements at -6 m depth were adjusted based on the observed settlement trend measured in May 1989 when no heave was measured.

In the Paragrid section the trends of the two measurements made in 2003 were the same but the magnitudes of settlements were different in the range of 0 to 5 mm at different depths. With considering an average of the two measurements in 2003, it illustrated that since 1990 more settlement occurred along the vertical access tube at the toe of Paragrid reinforced slope. This additional settlement varied between 2 and 6 mm at different depths along the access tube. The magnet at -3.5 depth showed some heave taking place in the foundation soil which could not happen. The previous settlement measurements did not show such a behavior at this depth. It implied that this magnet had slipped down along the vertical access tube and hence showed more settlement than the upper magnet. This additional unreal settlement was adjusted based on the previous settlement profiles.

In the unreinforced section the two measurements in 2003 showed consistent results but again the settlement profiles in 2003 indicated some upward movement of the fill soil. This time the bottom magnet at -9 m depth seemed to have moved down ward. No other previous measurements showed such a behavior at this location. The upper magnet at -6 m depth had settled in range of ±2 mm during the whole life of the project and based on this observation the 2003 measurement were adjusted and the whole profile was modified. The final settlement profile illustrated consistent settlement profiles.

At the toe of all 4 sections of the test fill one magnet along the vertical extensometers showed erroneous results. In the Tensar section the magnet at the -3.5 m depth, in the Signode section the magnet at the -6 m depth, in the Paragrid the magnet at the -3.5 m depth and in the unreinforced section the datum magnet at the -9 m depth showed unrealistic settlement which was different from the actual settlement of the surrounding soil and the upper magnets. Al the measurements at these magnets were adjusted based on the upper and lower magnets and also the previous measurements. Beside the above mentioned instances, all the other magnets installed along the vertical extensometers functioned properly. These observations indicated that the long term performance of these instruments after 13 years since the last measurements were satisfactory.

All vertical extensometers at the crest of slopes were damaged and blocked during the third construction stage and additional measurements after August 1988 could not be taken. In 2003, by developing a smaller probe, it was possible to reach the fixed bottom magnet located at the 9 m depth in the 3 reinforced sections. Unfortunately it was not possible to lower the probe inside the vertical access tube at the crest of the unreinforced section. Two measurements were taken in 2003 at the vertical extensometers at the crest of the 3 reinforced sections. In all sections the two measurements showed quite consistent results and profiles. Since no previous measurements were made after the third construction stage in the fall of 1988, no settlement profile was available during or after the placement of the top 6 m of fill. The 2003 settlement measurements, therefore, show the combination of settlements due to the placement of the top 6 m of fill and due to the subsequent consolidation of the fill. All the target magnets along the access tubes were read during the 2003 field measurements. However, since no initial field measurements were available for the magnets installed in the upper parts of the fill, the

settlement profiles could not be determined for the upper portion of the fill. In all 3 reinforced sections the settlement increased almost linearly from -6 m to the highest target magnet. In the Tensar reinforced section the maximum settlement at the crest of slope reached 465 mm at +5.5 m. In the Signode reinforced section the maximum settlement reached 440 mm at +5.5 m. In the Paragrid reinforced section the maximum settlement at the crest of slope reached 513 mm at +5.5 m.

In general all the magnets installed along the vertical extensometers at the crest of slopes functioned properly except for the magnets at -6 m depth. At this depth in all 4 sections of the test embankments, the previous measurements had shown that the settlements at the magnet -6 m deep in the foundation soil were unrealistically large. In other words it showed that the magnet installed in the foundation soil displaced upwards as the fill soil was placed, which was obviously not the real behavior of the foundation soil. The same thing was observed during the 2003 field measurements. One possibility was that the magnet at -6 m depth along the access tube was not properly fixed and it was shifting and providing erroneous data. Another possibility could be the buckling of the access tubes. All the measured settlements at this location were therefore adjusted based on the settlement measurements at the same location beneath the toe of the slopes. Beside these magnets that were adjusted, all other magnets inside the fill and foundation soil along the vertical extensometers at the crest of slopes functioned satisfactorily.

6.10.2 Long term performance of horizontal extensometers

The horizontal extensometers installed at +6 m elevation were all damaged and blocked during the third construction stage and could not be retrieved in 2003. The other horizontal extensometers installed at 0, +2 and +4 m elevations were washed and cleaned in 2003 and all target

magnets could be read. It was assumed that the center magnet had remained stationary and in practice it appeared that the horizontal displacement of the center magnet was negligible in comparison to the amount of horizontal displacements of the target magnets. In almost all horizontal extensometers the two measurements in 2003 showed consistent results (with a maximum of ±0.2% variation) and the strain profiles were similar to the previous field measurements made in 1990. No significant additional soil horizontal strain developed at 0, +2 and +4 m elevations since September, 1990.

All the magnets installed along the horizontal extensometers inside the fill functioned properly and all the 2003 measurements revealed consistent results. In other words the long term performance of horizontal extensometers was reliable.

6.11 Summary and Conclusions

The vertical extensometers were installed at the toe and the crest of slopes of the Devon test embankment to monitor the settlement of the fill soil and foundation soil. The horizontal extensometers were installed in the test fill at 0, +2, +4 and +6 m elevations in order to measure the soil horizontal strains or displacements at these elevations in the fill. The horizontal extensometers at +6 m elevation were blocked during the 1988 construction season and no measurements could be taken during and after construction or in 2003.

The measurements made in 2003, fifteen years after the end of construction, and the last set of measurements in 1990, showed similar horizontal strains. Almost no significant soil horizontal strain was developed in the fill since 1990.

The vertical extensometers at the toe of the slopes showed some settlement as given in Table 4. The vertical extensometers at the crest of the slopes were read in 2003 by using a small modified probe that could travel inside the highly deformed vertical access tubes except for the vertical extensometer at the crest of the unreinforced section. No measurements were available during or after construction in 1988 at these vertical extensometers due to the damage and blockage of these access tubes. The consistent measurements in 2003 showed that the settlement of the fill and foundation soil increased almost linearly from -6 m to +5.5 m and reached the values summarized in Table 5.

Regarding the long term performance of the vertical extensometers installed at the toe of slopes in all 4 sections of the test fill one magnet along the vertical extensometers showed erroneous behavior. In the Tensar section the magnet at the -3.5 m depth, in the Signode section the magnet at the -6 m depth, in the Paragrid the magnet at the -3.5 m depth and in the unreinforced section the datum magnet at the -9 m depth showed unrealistic settlement which was different from the actual settlement of the surrounding soil and the upper magnets. Al the measurements at these magnets were adjusted based on the upper and lower magnets and also the previous measurements. Beside the above mentioned instances, all the other magnets installed along the vertical extensometers functioned properly. These observations indicated that the long term performance of these instruments after 13 years since the last measurements were satisfactory.

In general all the magnets installed along the vertical extensometers at the crest of slopes functioned properly except for the magnets at -6 m depth. At this depth in all 4 sections of the test embankments, the previous measurements had shown that the settlements at the magnet -6 m deep in the foundation soil were unrealistically large. In other words it showed that

the magnet installed in the foundation soil displaced upwards as the fill soil was placed, which was obviously not the real behavior of the foundation soil. The same thing was observed during the 2003 field measurements. One possibility was that the magnet at -6 m depth along the access tube was not properly fixed and it was shifting and providing erroneous data. Another possibility could be the buckling of the access tubes. All the measured settlements at this location were therefore adjusted based on the settlement measurements at the same location beneath the toe of the slopes. Beside these magnets that were adjusted, all other magnets inside the fill and foundation soil along the vertical extensometers at the crest of slopes functioned satisfactorily.

All the magnets installed along the horizontal extensometers inside the fill functioned properly and all the 2003 measurements revealed consistent results. In other words the long term performance of horizontal extensometers was reliable.

Table 1. Number of extensometer field measurements till 1990

Instrumentation		Tensar	Signode	Paragrid	Unreinforced
Horizontal Extensometer	0 m	15	17	15	17
	2m	14	15	14	15
	4m	6	12	6	12
	6m	2	3	2	3
Vertical Extensometer	Crest	11	10	11	10
	Toe	14	15	14	15

Table 2. Initial field measurement dates of vertical extensometers

Location	**Toe**	**Crest**
Tensar	14-Sep-86	13-Sep-86
Signode	12-Sep-86	12-Sep-86
Paragrid	12-Sep-86	12-Sep-86
Unreinforced	12-Sep-86	12-Sep-86

Table 3. Initial field measurement dates of horizontal extensometers

Location	**North section**	**South section**
0m	18-Sep-86	18-Sep-86
2m	20-Oct-86	20-Oct-86
4m	22-Sep-87	22-Sep-87

Table 4. Total foundation settlements in mm at the toe of the slopes from vertical extensometers

Settlement (mm)	Tensar		Signode		Paragrid		Unreinforced	
	1989	2003	1989	2003	1990	2003	1990	2003
-0.5 m	4	8	—		—		0	7
increase	**4**						**7**	
-1 m	—		8	28	—		—	
increase			**20**					
-1.5 m	—		—		23	28	—	
increase					**5**			
-2.5 m	—		—		—		2	6
increase							**4**	
-3.5 m	5	9	3	7	9	15	—	
increase	**4**		**4**		**6**			
-6 m	—		4	7	9	15	-2	1
increase			**3**		**6**		**3**	
-6.5 m	1	2	—		—		—	
increase	**1**							
-9 m	Datum		-6	-1	6	8	Datum	
increase			**5**		**2**			
-12 m	—		Datum		Datum		—	
increase								

Table 5. Total embankment and foundation settlements in mm below the crest of the slopes from vertical extensometers

Settlement (mm)	Tensar		Signode		Paragrid		Unreinforced	
	1988	2003	1988	2003	1988	2003	1988	2003
5.5 m	172	464	141	440	238	514	—	
increase	292		299		276			
5 m	—		128	400	187	426	144	—
increase			272		239		—	
4.5 m	169	424	—		—		—	
increase	255							
4 m	—		—		—		126	—
increase							—	
3.5 m	161	385	110	323	141	344	—	
increase	224		213		203			
3 m	—		—		—		97	—
increase							—	
2.5 m	142	343	90	256	104	290	—	
increase	201		166		186			
2 m	—		—		—		84	—
increase							—	
1.5 m	126	297	68	201	71	212	—	
increase	171		133		141			
1 m	—		—		—		63	—
increase							—	
0.5 m	101	242	52	159	52	161	—	
increase	141		107		109			

Table 5 (continued). Total embankment and foundation settlements in mm below the crest of the slopes from vertical extensometers

Settlement (mm)	Tensar		Signode		Paragrid		Unreinforced	
	1988	2003	1988	2003	1988	2003	1988	2003
-0.5 m	72	190	—		—		34	—
increase	118						—	
-1 m	—		28	116	33	125	—	
increase			88		92			
-2.5 m	22	95	—		—		—	
increase	73							
-3 m	—		22	89	22	95	31	—
increase			67		73		—	
-6 m	12	16	9	16	12	17	10	—
increase	4		7		5		—	
-9 m	Datum		Datum		Datum		Datum	
increase								

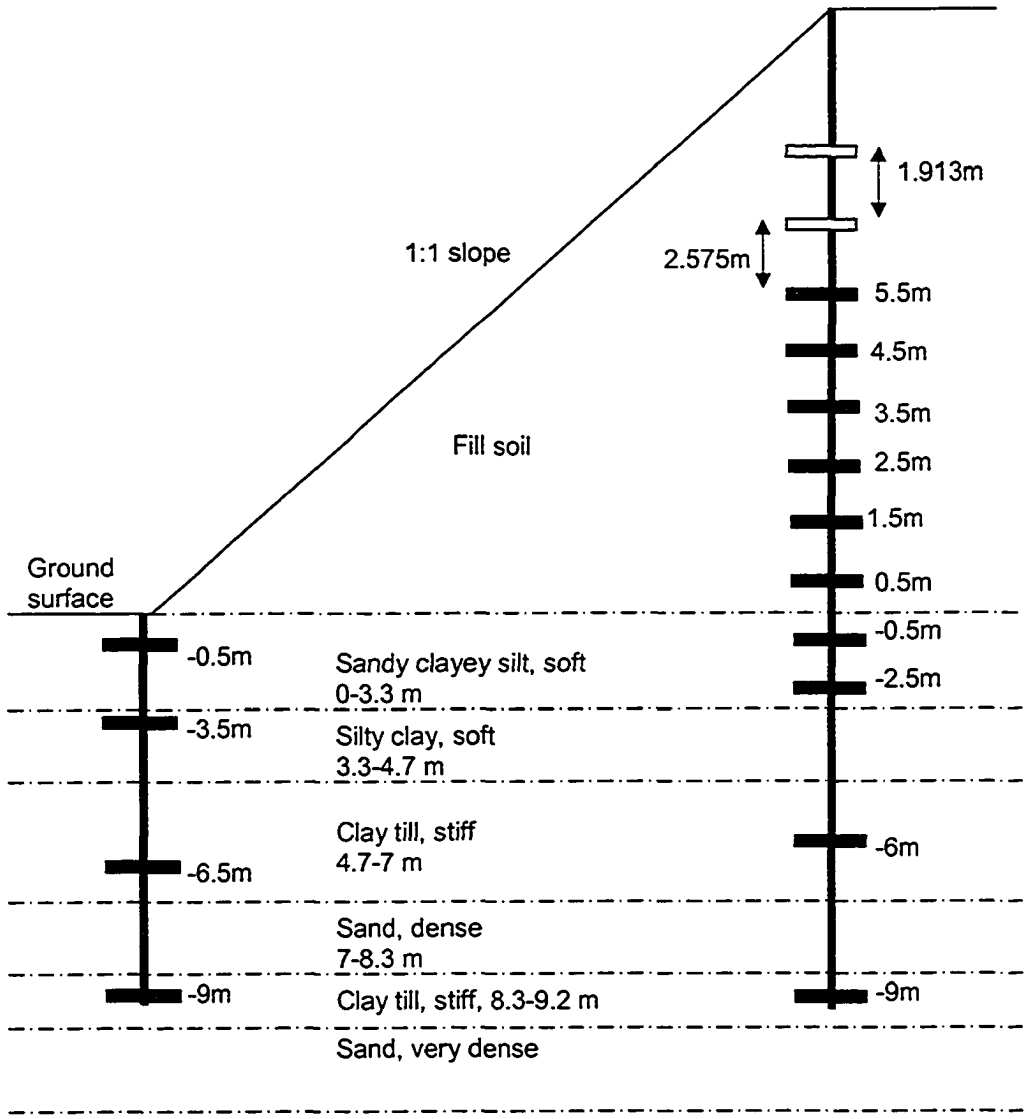

Figure 1. Target magnet locations along the vertical extensometers at the Tensar section

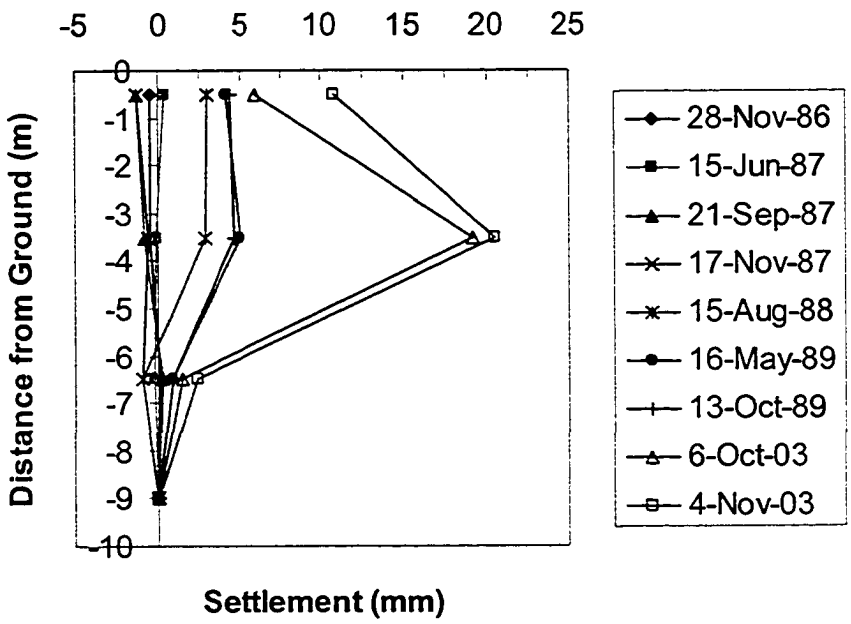

Figure 2. Settlement profile at the toe of Tensar section – before adjustment

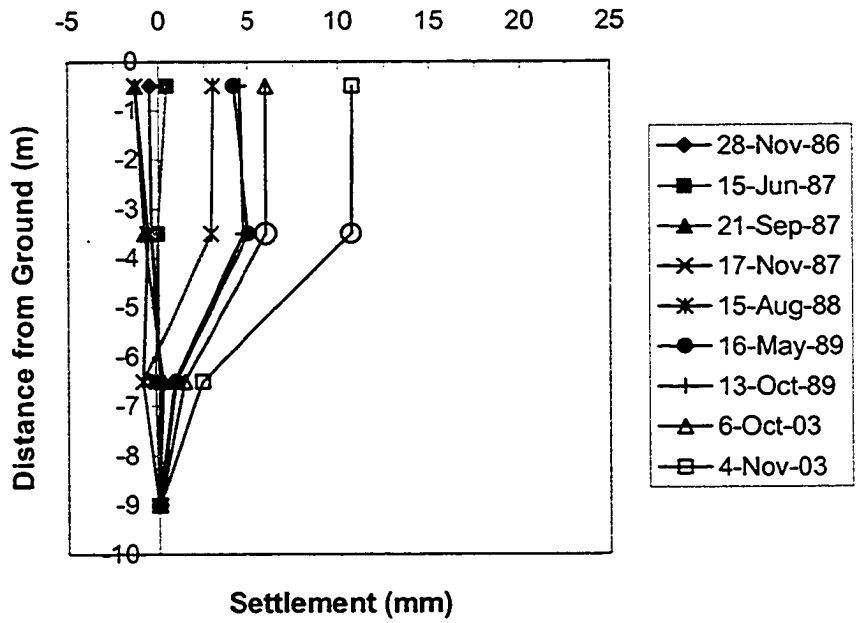

Figure 3. Settlement profile at the toe of Tensar section – after adjustment

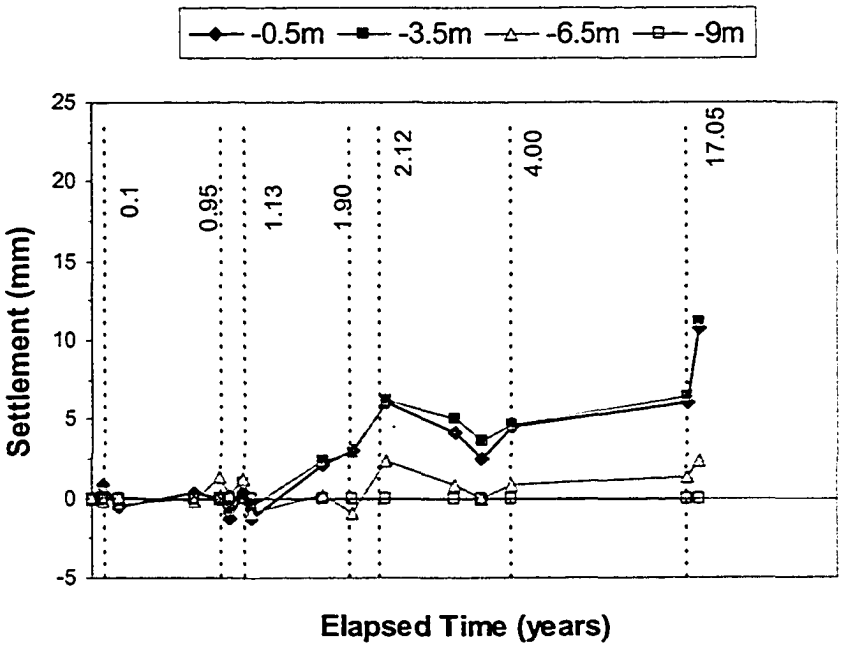

Figure 4. Settlement profile development with time-Tensar at toe after adjustment

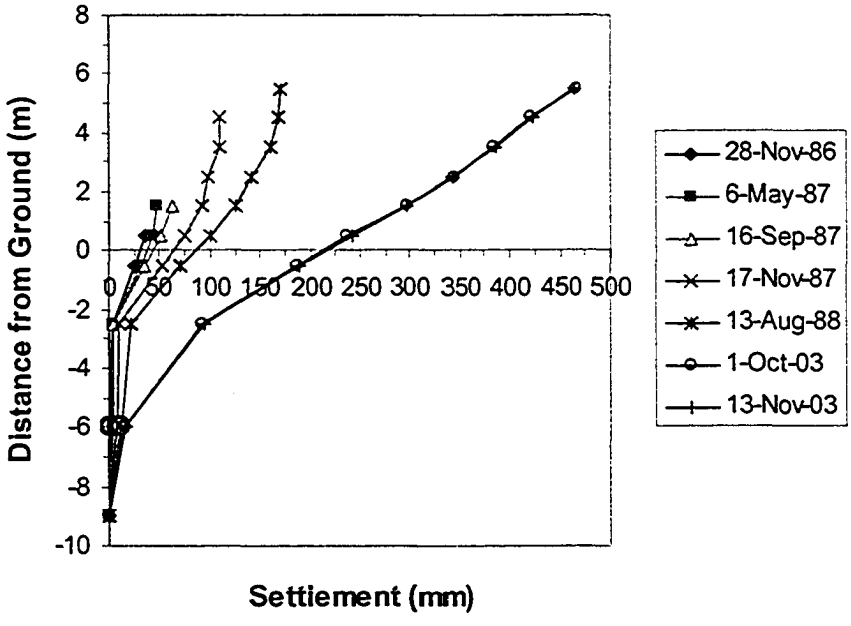

Figure 5. Settlement profile at the crest of Tensar section

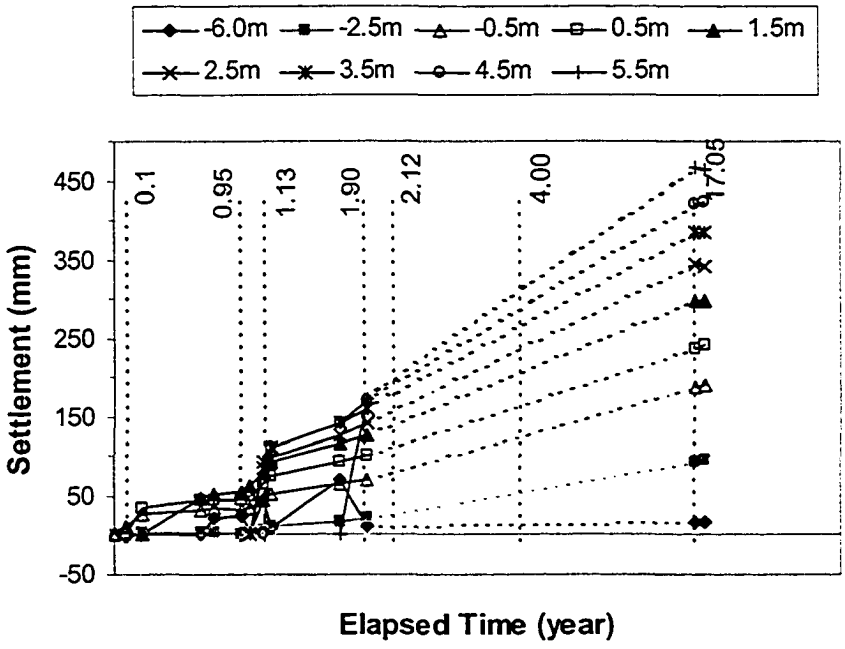

Figure 6. Settlement profile development at the crest of Tensar section

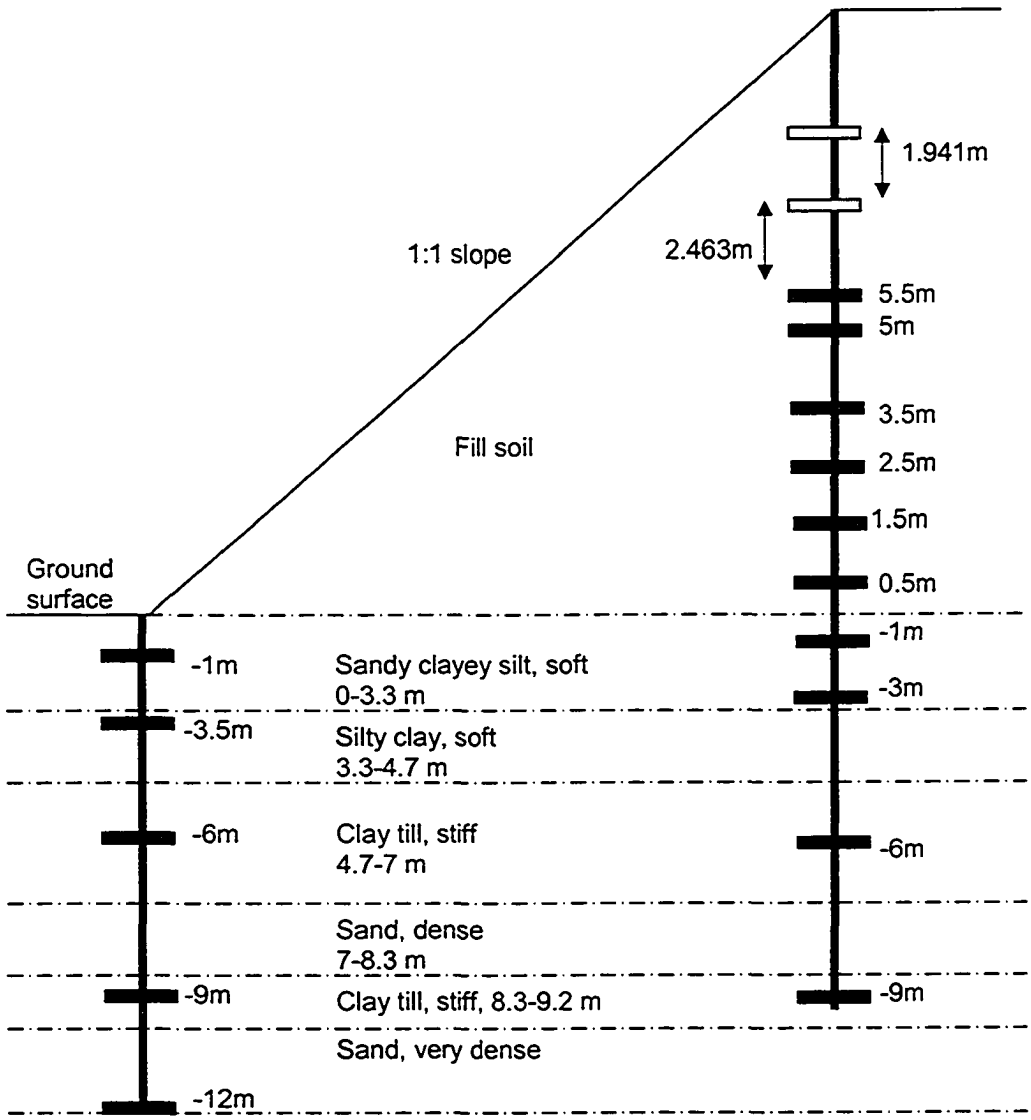

Figure 7. Target magnet locations along the vertical extensometer at the Signode section

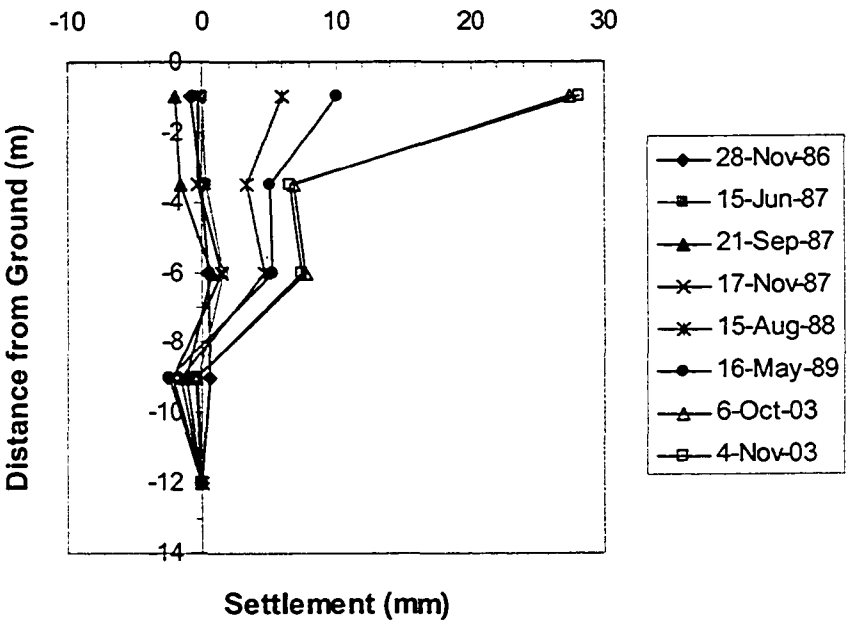

Figure 8. Settlement profile at the toe of Signode section-before adjustment

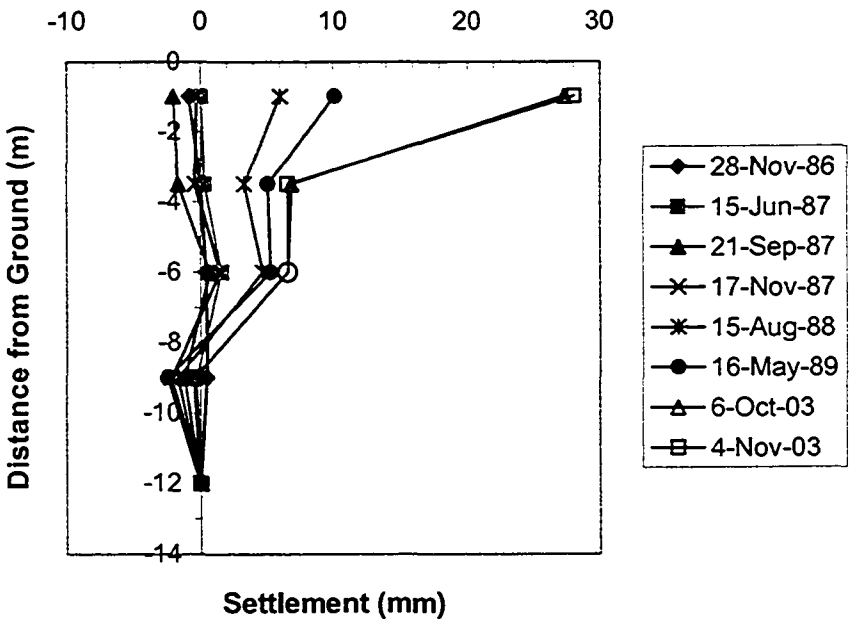

Figure 9. Settlement profile at the toe of Signode section-after adjustment

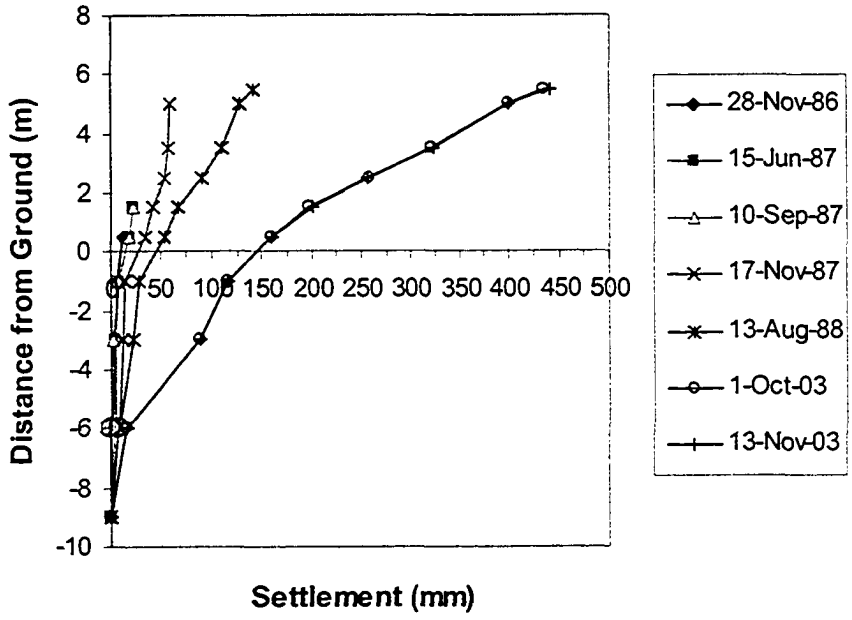

Figure 10. Settlement profile at the crest of Signode section

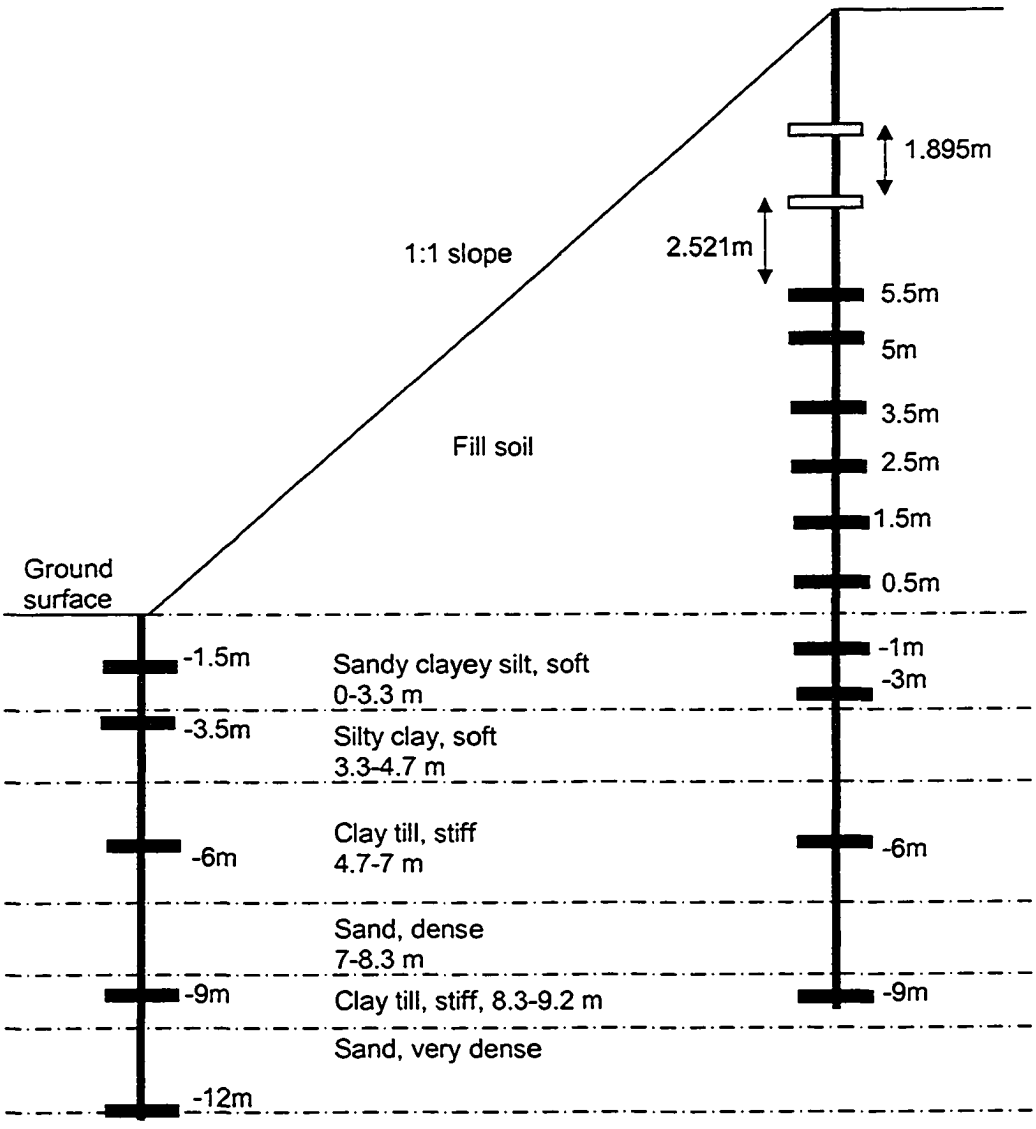

Figure 11. Target magnet locations along the vertical extensometer at the Paragrid section

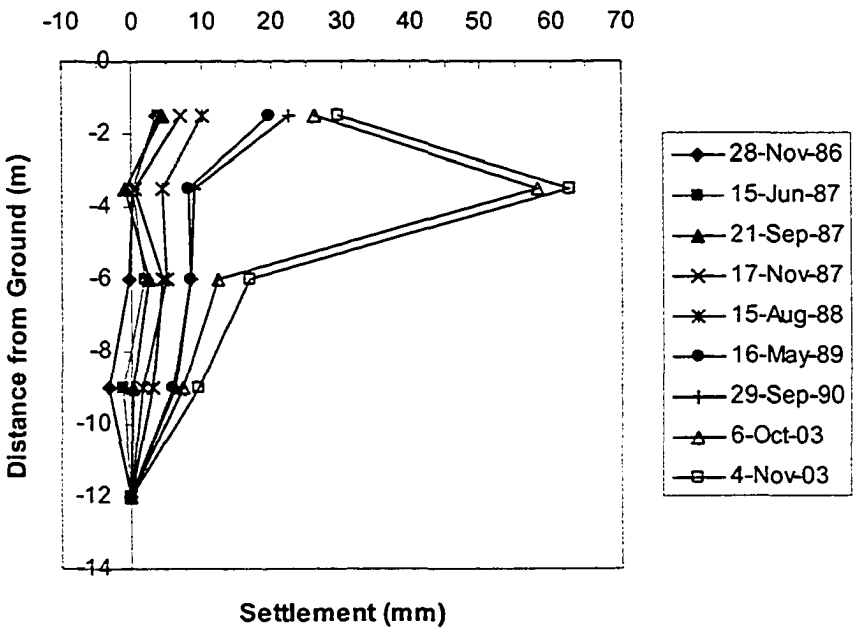

Figure 12. Settlement profile at the toe of Paragrid section-before adjustment

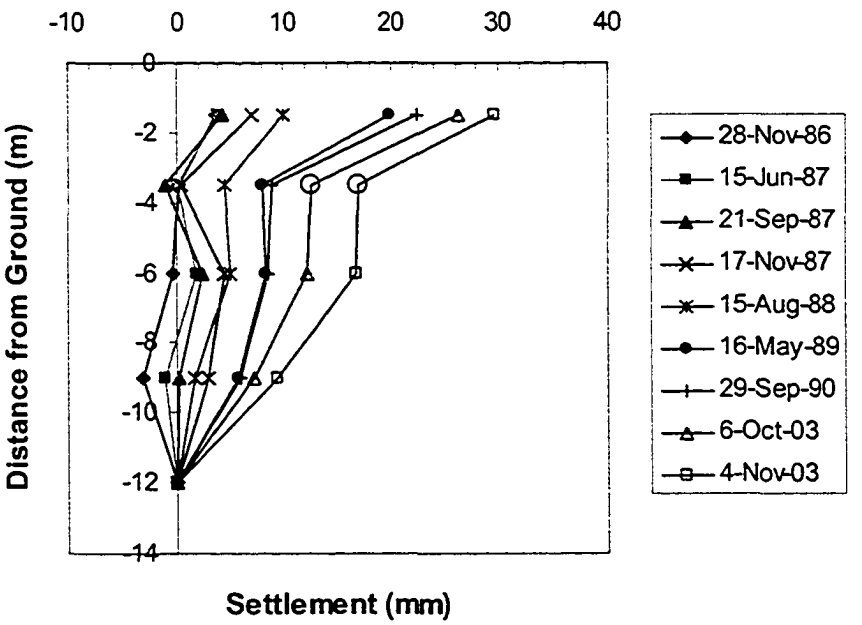

Figure 13. Settlement profile at the toe of Paragrid section-after adjustment

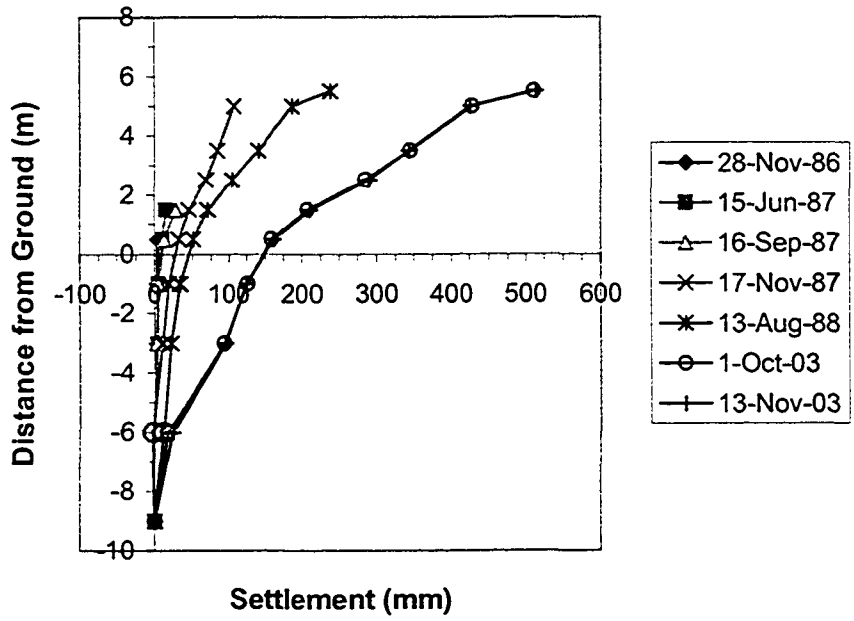

Figure 14. Settlement profile at the crest of Paragrid section

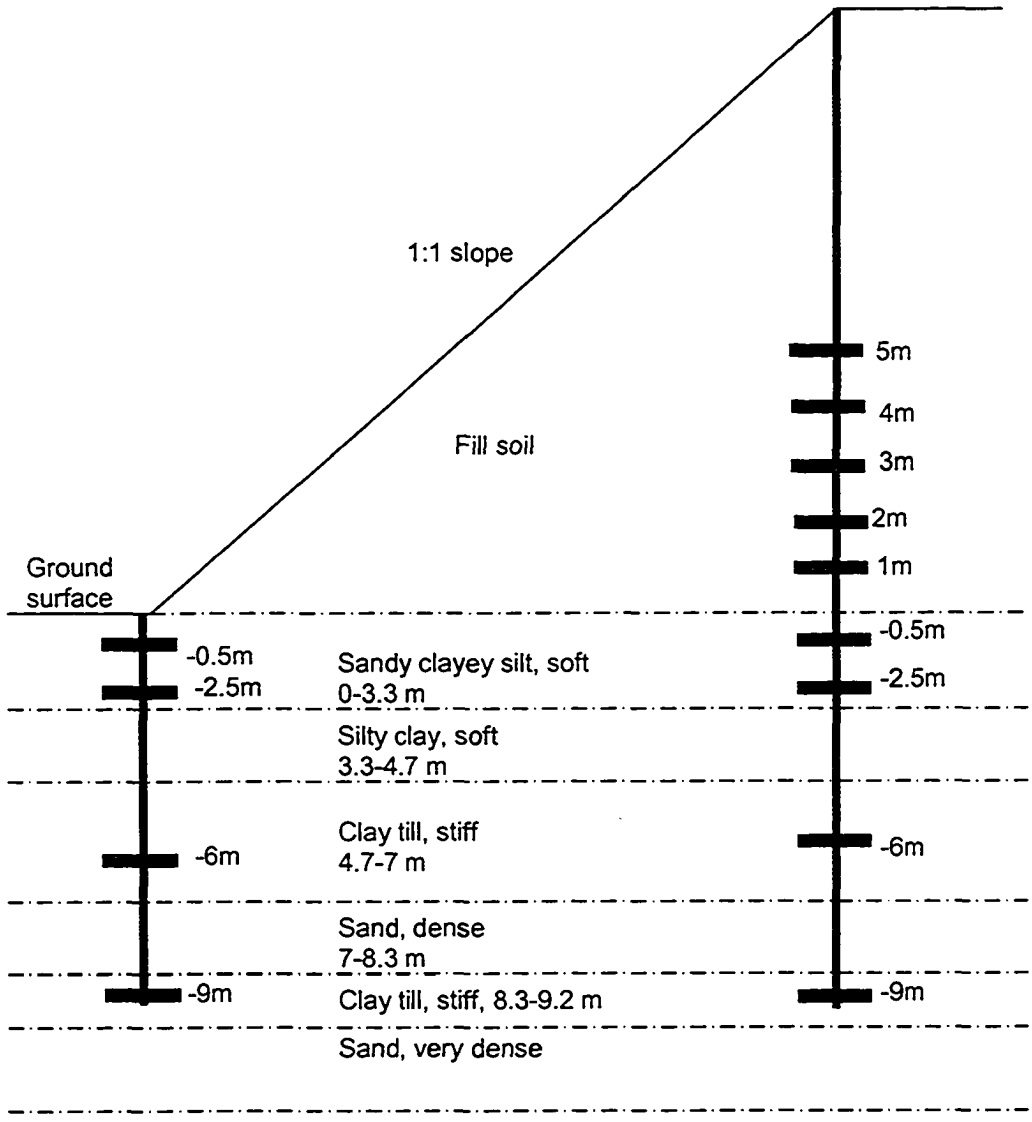

Figure 15. Target magnet locations along the vertical extensometer at the unreinforced section

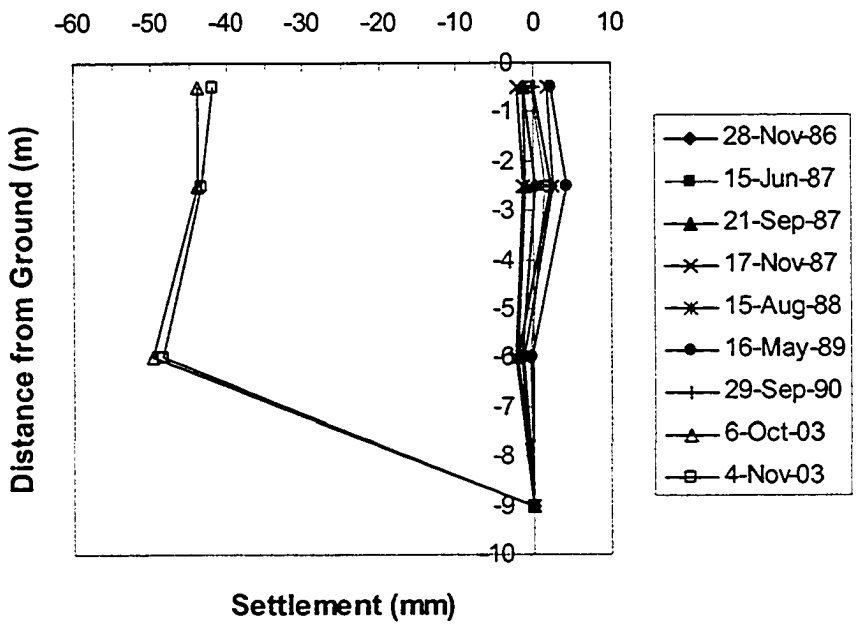

Figure 16. Settlement profile at the toe of unreinforced section-before adjustment

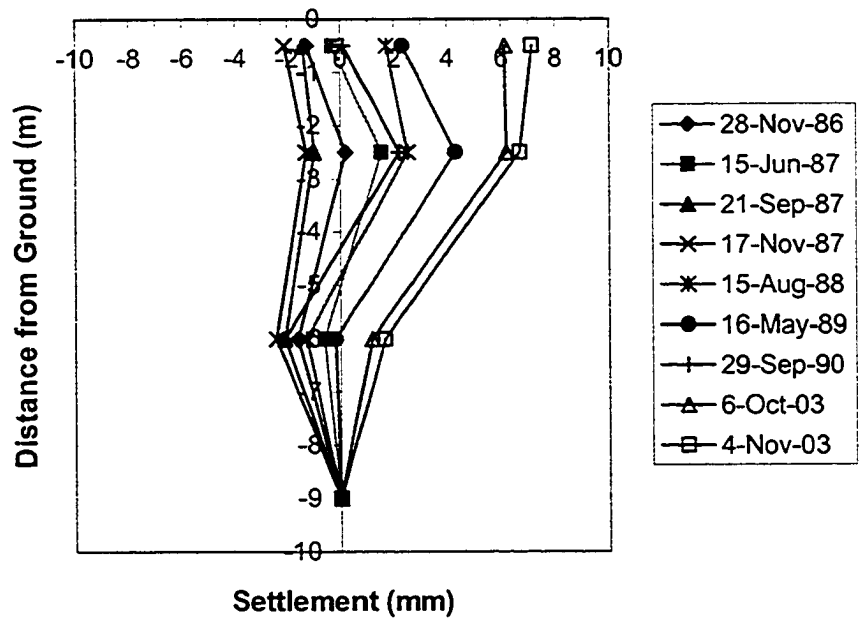

Figure 17. Settlement profile at the toe of unreinforced section-after adjustment

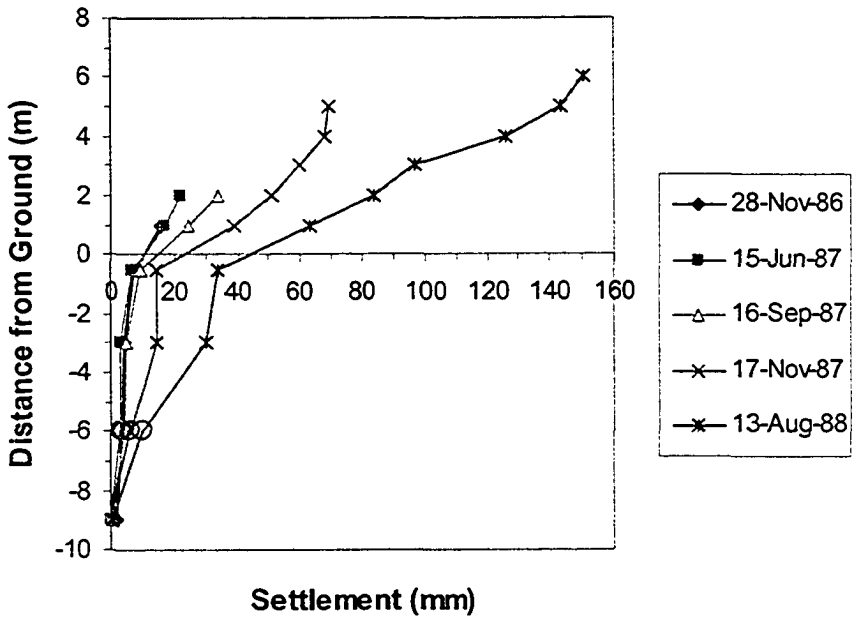

Figure 18. Settlement profile at the crest of unreinforced section

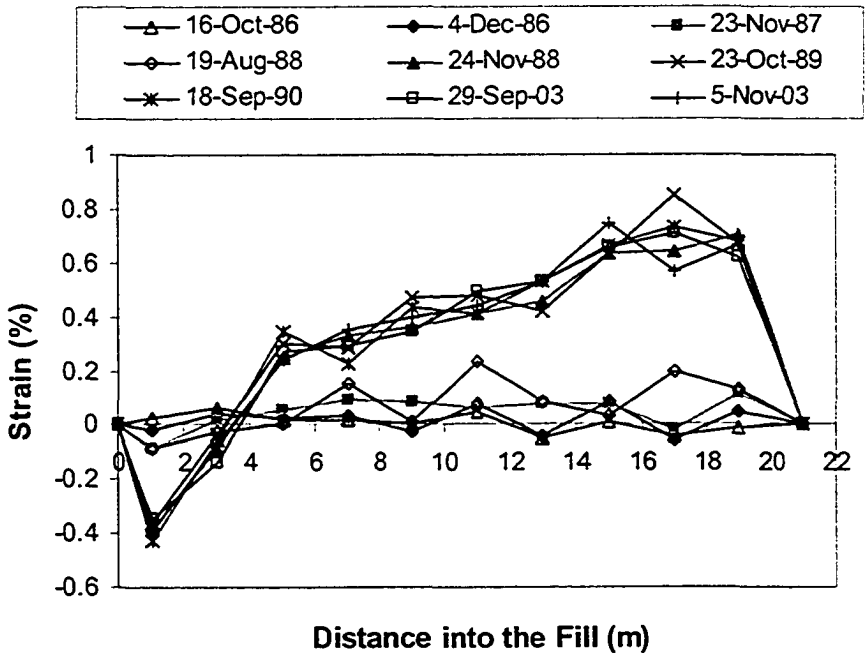

Figure 19. Soil horizontal strain profile at Tensar section, 0 m elevation

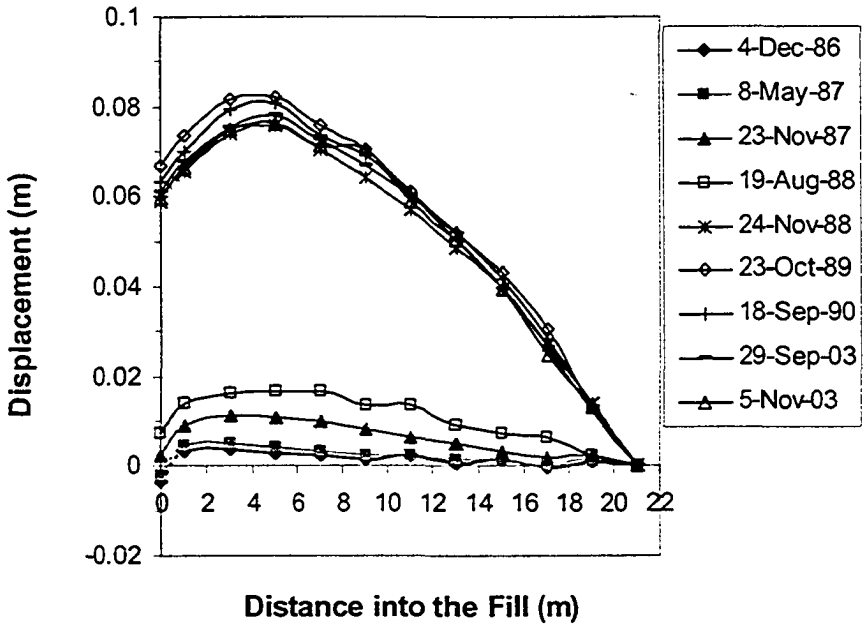

Figure 20. Soil horizontal movement at Tensar section, 0 m elevation

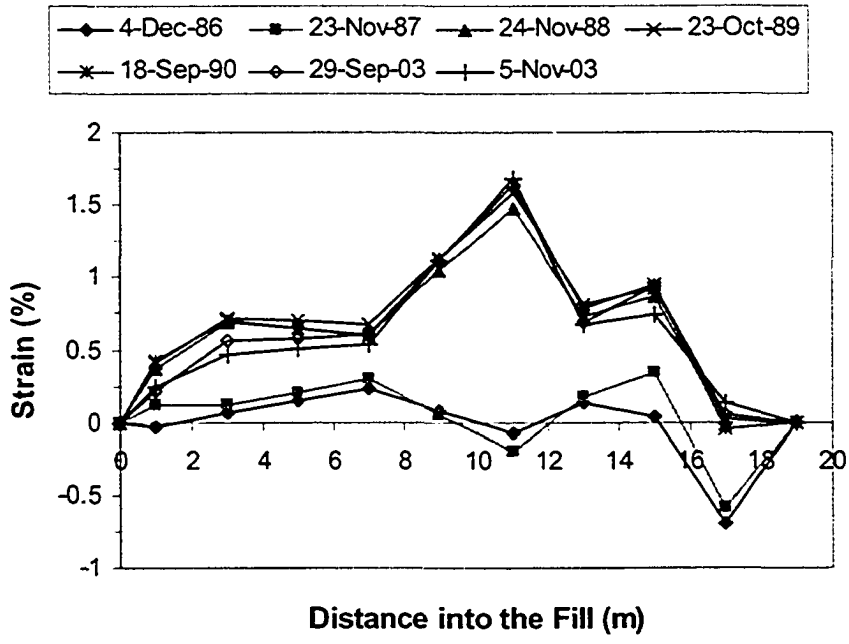

Figure 21. Soil horizontal strain profile at Tensar section, 2 m elevation

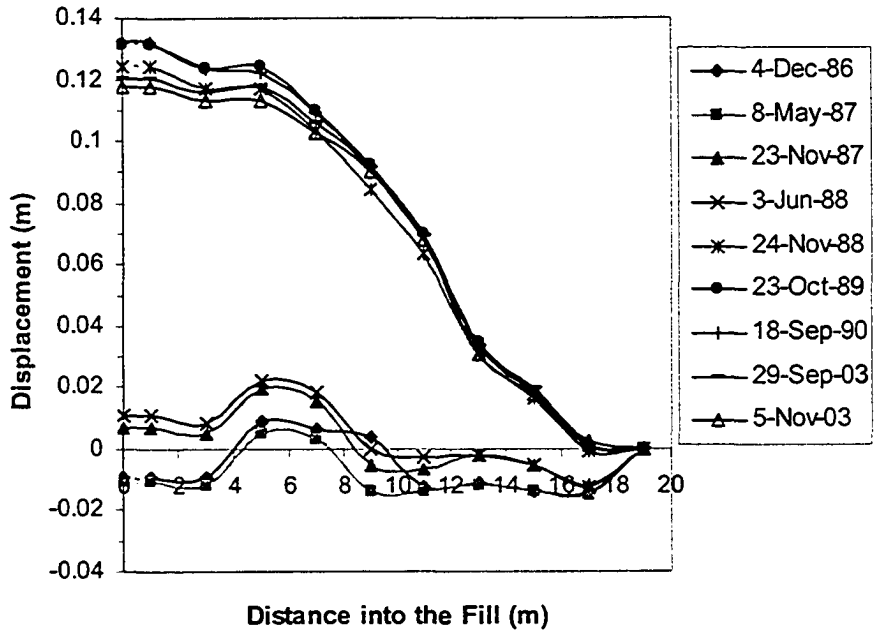

Figure 22. Soil horizontal movement at Tensar section, 2 m elevation

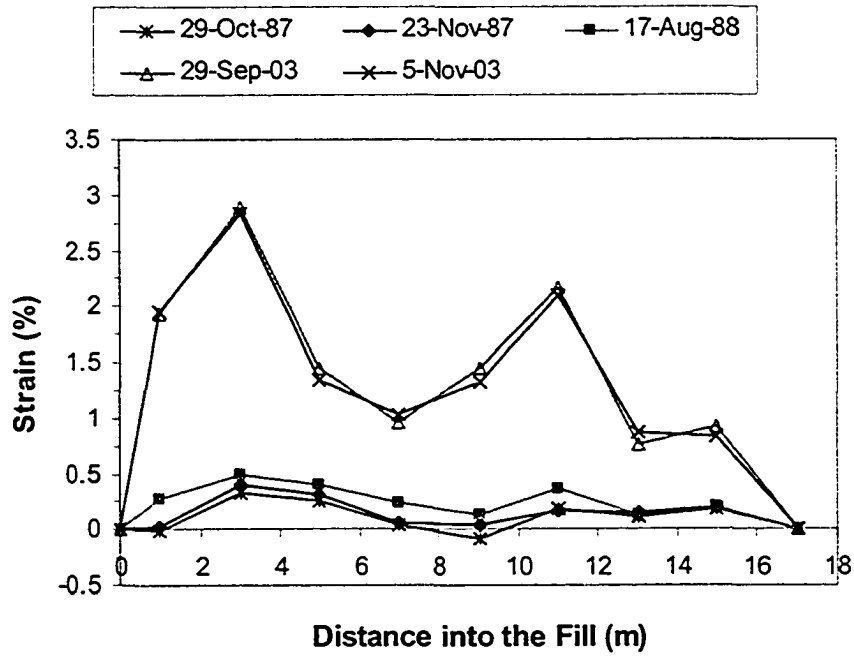

Figure 23. Soil horizontal strain profile at Tensar section, 4 m elevation

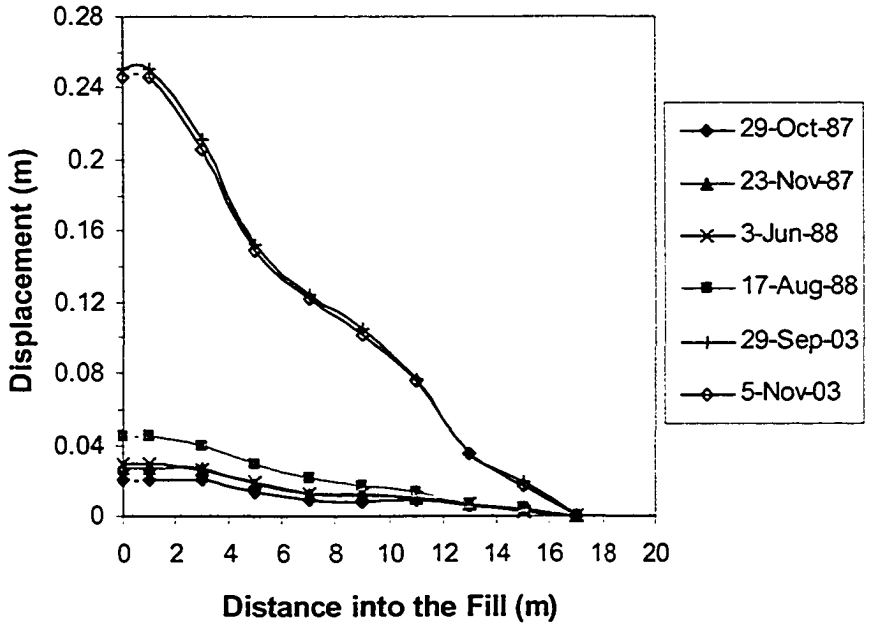

Figure 24. Soil horizontal movement at Tensar section, 4 m elevation

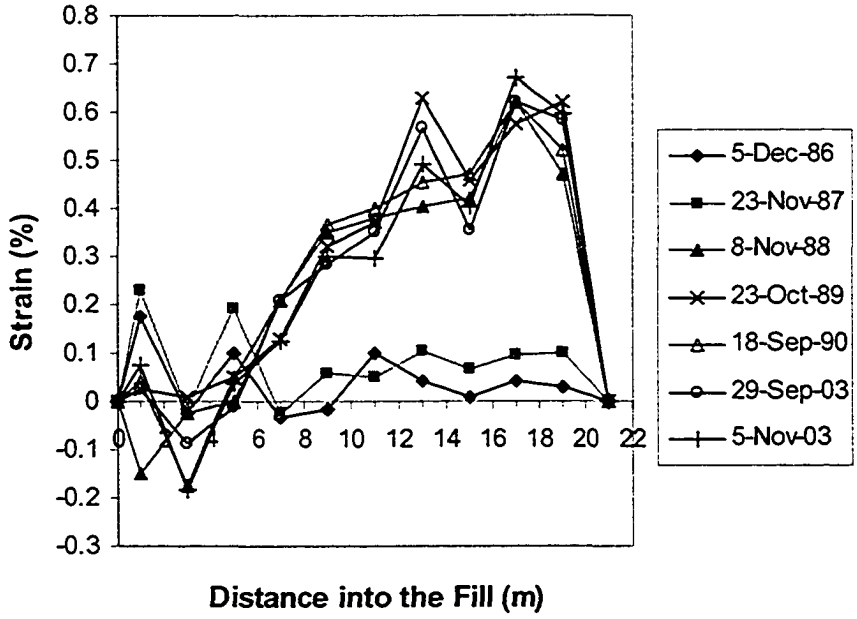

Figure 25. Soil horizontal strain profile at Signode section, 0 m elevation

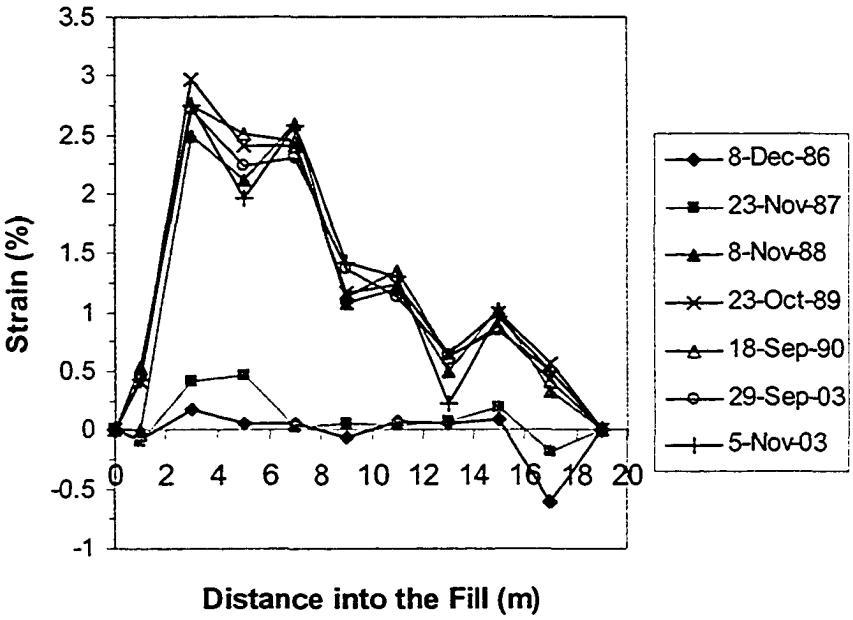

Figure 26. Soil horizontal strain profile at Signode section, 2 m elevation

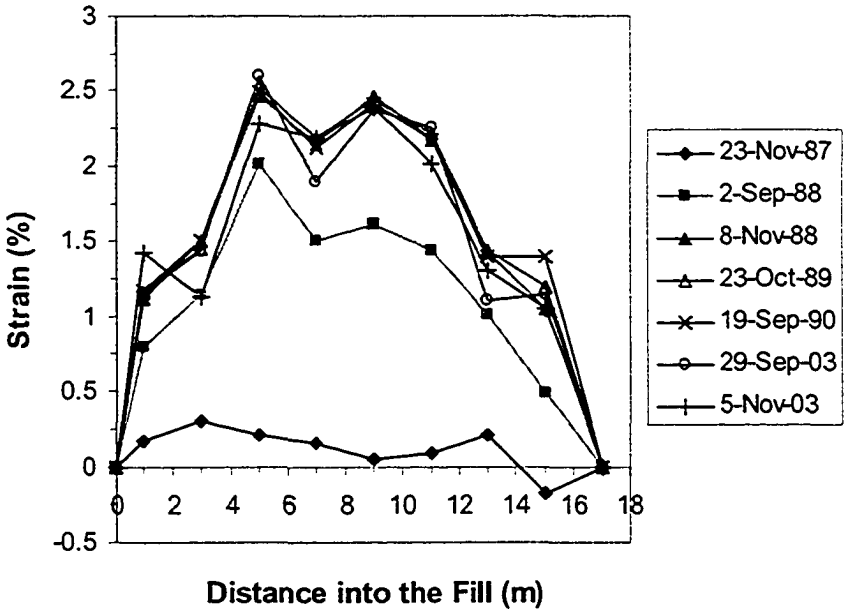

Figure 27. Soil horizontal strain profile at Signode section, 4 m elevation

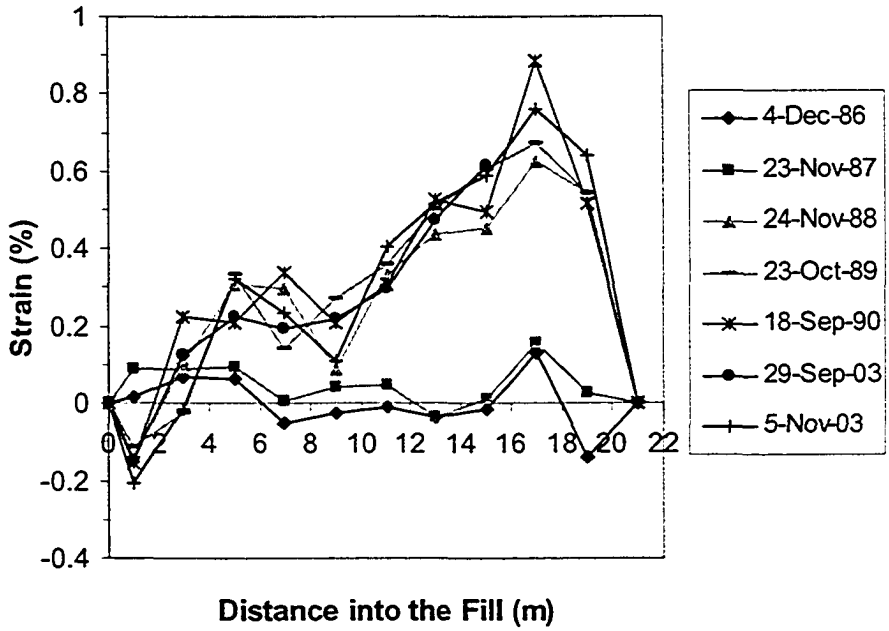

Figure 28. Soil horizontal strain profile at Paragrid section, 0 m elevation

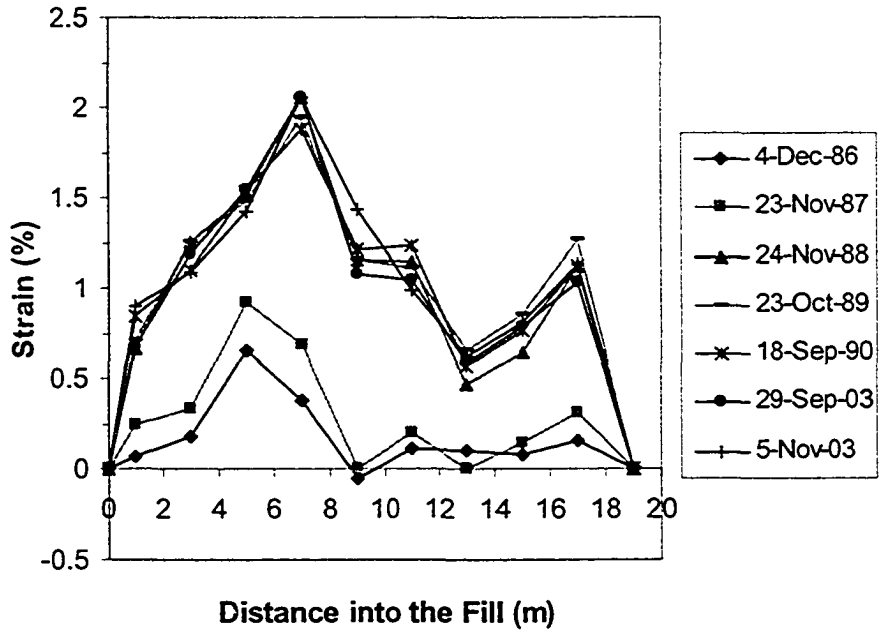

Figure 29. Soil horizontal strain profile at Paragrid section, 2 m elevation

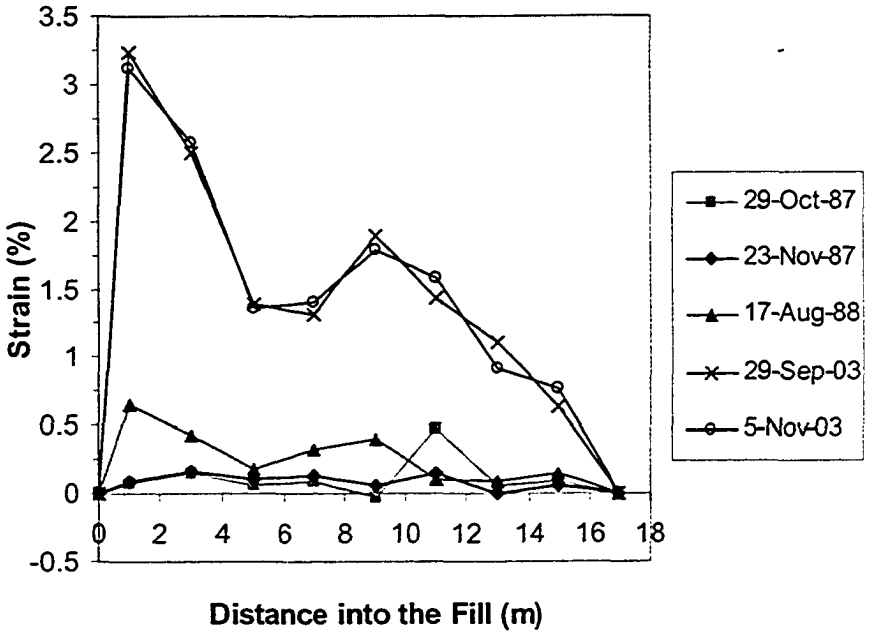

Figure 30. Soil horizontal strain profile at Paragrid section, 4 m elevation

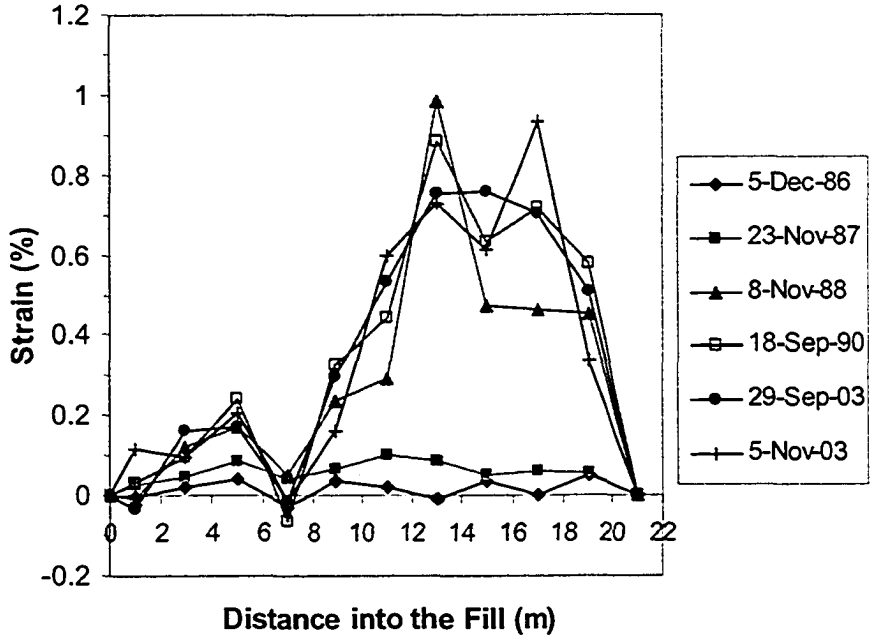

Figure 31. Soil horizontal strain profile at unreinforced section, 0 m elevation

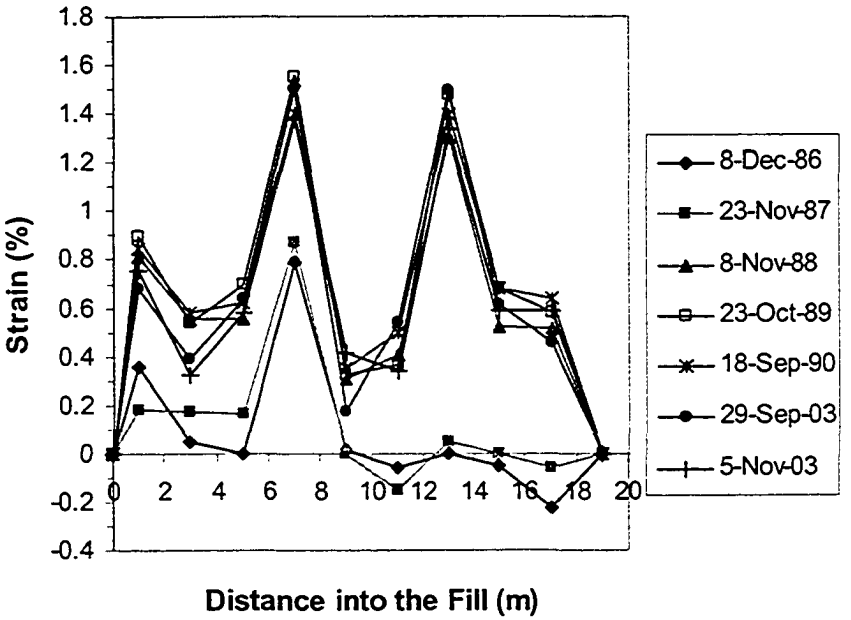

Figure 32. Soil horizontal strain profile at unreinforced section, 2 m elevation

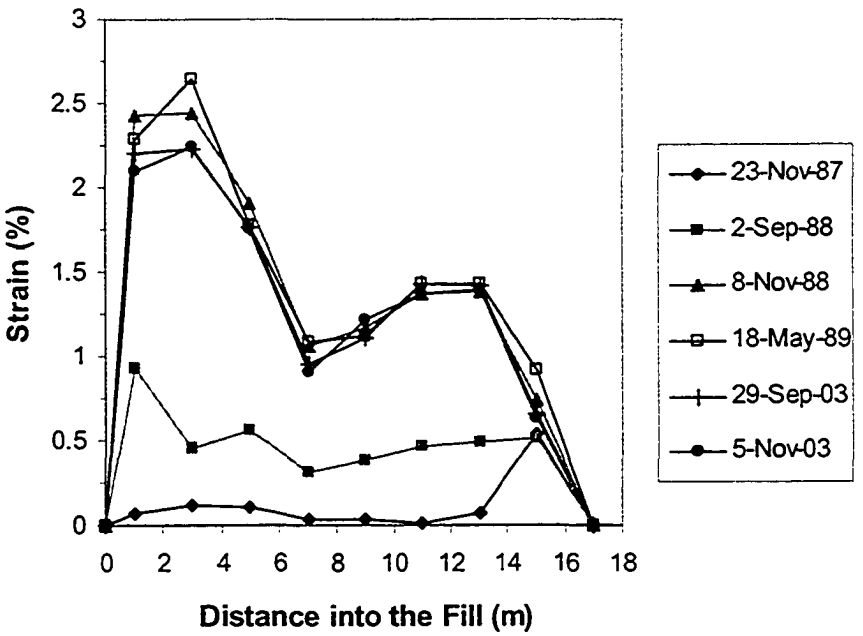

Figure 33. Soil horizontal strain profile at unreinforced section, 4 m elevation

Bartlett, S., Monley, G., Soderberg, A. and Palmer, A. (2001). "Instrumentation and Construction Performance Monitoring for I-15 Reconstruction Project in Salt Lake City, Utah", Transportation Research Record, No.1772, pp.40-47.

Hermann, S. and Burd, H.J. (1988). "An instrumented steep reinforced soil embankment at Andalsnes, Norway", Geotextiles and Geomembranes, Vol.7, No.4, pp.293-308.

Irvin, R.A., Farmer, I.W. and Snowdon, R.A. (1990). " Performance of reinforced trial embankments in London clay – Undrained loading", Proceedings of the Performance of reinforced soil structures conference, British Geotechnical Society, 1990, pp.119-125.

Jewell, R.A., Paine, N. and Woods, R.I. (1984). "Design methods for steep reinforced embankments", Proceedings of Polymer Grid Reinforcement, ICE, London, Paper No.3.1.

Liu, Y., (1992). "Performance of Geogrid Reinforced Clay Slopes." PhD. Thesis, University of Alberta: 406p.

Chapter 7. Piezometers

7.1 Introduction

Pore pressures within the test embankment and in the foundation soil were monitored during and after construction of the Devon test embankment. Fifty-five Pneumatic piezometers were installed inside the fill and foundation soil to measure the pore pressure response at different stages of construction and the consolidation of the embankment. In 2003, after retrieving the access tubes of the piezometers, pore pressure measurements were taken to see how they had changed since 1990.

7.2 Description of the instrument

Pneumatic piezometers are generally used to measure pore water pressure in saturated soils. Their application includes monitoring pore pressures to determine slope stability, to determine safe rates of fill or excavation, in earth fill dam and embankment construction, etc. At the Devon test embankment, pore pressure transducers, model 51417, made by Sinco Slope Indicator Co., as shown in Figure 1, were used. This kind of pneumatic piezometer employs a simple and reliable transducer that is inherently free from drift. Long term performance of these piezometers is enhanced by corrosion resistance plastic construction, polyethylene tubing and inline filters in all connectors (Slope Indicator Technical Notes, 2000). The tubing carries gas to and from the piezometer tip and these piezometers use twin tubing. A typical connection of twin tubes to the piezometer tip is shown in Figure 2. A portable pneumatic indicator, model C-6300, made by Terra Technology Corp. was employed as the readout terminal. The indicator has a self-contained air-pressure tank and its resolution is ±1 kPa.

The piezometer contains a flexible rubber diaphragm. As shown in the diagram of Figure 3, water pressure acts on one side of the diaphragm and gas pressure acts on the other. When a reading is required, a pneumatic indicator is connected to the terminal or directly to the tubing. Compressed nitrogen gas from the indicator flows down the input tube to increase gas pressure on the diaphragm. When the gas pressure exceeds the water pressure, the diaphragm is forced away from the vent tube, allowing excess gas to escape via the vent tube. When the return flow of gas is detected at the surface, the gas supply is shut off. Gas pressure in the piezometer decreases until water pressure forces the diaphragm to its original position, preventing further escape of gas through the vent tube. At this point, gas pressure equals water pressure, and the reading can be obtained from the pressure gauge on the indicator (Hanna, 1985).

Some pneumatic piezometers were installed inside the test fill soil and the others were installed in the foundation soil beneath the embankment. The filter of the piezometers inside the fill was in direct contact with soil and they were placed in preformed holes. The tubing was protected at the top and bottom with hand-compacted layers of embankment materials and use of heavy vibratory rollers was avoided until there was a lift of about 0.5 m above the tubing. Tight bending was also avoided in the tubing. The piezometers inside the foundation soil were installed in boreholes. The piezometer was lowered inside a borehole to its intended depth and some tremie sand was placed around the piezometer tip in the intake zone. A seal was placed above the intake zone and the bore hole was backfilled.

7.3 Location of Piezometers

Figure 4 illustrates the layout of the 27 piezometers in the northern section of the test embankment and foundation soil. The same layout applies to the southern section of the embankment. The N-1 piezometer was

installed at the center of the fill along the centerline. Two piezometers were installed at each instrumented level at each test section of the embankment, 3 and 6 m below the ground surface in the foundation soil and 1, 3, 5 and 8 m above the ground surface. Seven piezometers were also placed in the test fill and the foundation soils in the center plane of the test embankment. The identification letters in Figure 4 stand for: NW is north-west section inside the fill, NE is north east section inside the fill, N is the center of the fill, NW-T is north west section along the toe of the slope in the foundation soil, NW-C is north west section along the crest of the slope in the foundation soil, N-C is in the foundation soil beneath the centerline of the fill, NE-C is north east section along the crest of the slope in the foundation soil and NE-T is north east section along the toe of the slope in the foundation soil.

7.4 Previous readings

Pore pressures were measured by using a pneumatic readout device with a resolution of 1 kPa. In order to limit the error due to head loss in the tubes, a low flow rate was maintained throughout the monitoring period. The development and variation of pore pressures were plotted versus time. In total during the construction of the embankment until the 1990 field measurements, a maximum of 21 field measurements were carried out. The detailed results and discussions of the pore pressure variation during this time are presented by Liu (1992) but in general the correspondence of the pore pressure development with respect to the construction activities could be clearly observed. Pore pressures in the fill soil built up during the construction stages and dissipated during the subsequent no construction periods. The rate of the dissipation was generally smaller in the later periods than during the first period, possibly due to consolidation of the soil structure. The closer to the center of the embankment, the higher the pore pressure built up during construction.

The pore pressures at different locations however tended to equilibrate as the pore water migrated within the fill soil during the consolidation periods. The induced pore pressure at each individual location, however, depended predominantly upon the degree of saturation of the fill soil at that location. No pore pressure measurements were obtained within the upper 6 m of the fill soil due to the damage to the piezometers at 8 m elevation during the construction activities. The variation of the pore pressure in the foundation soils did respond to construction activities, but it was complicated by other factors such as groundwater table fluctuation.

7.5 State of piezometer instrumentation in 2003

As mentioned in previous chapters, due to soil slough and surface soil movements along the slopes most of the terminal boxes and access tubes were buried beneath debris. The terminal boxes for the piezometers were completely buried deep below the debris and during the clean up activities with the backhoe most of the piezometer tubes were damaged. In total, 29 out of the 55 piezometers could be identified and functioned properly. All the connection ends of the tubes were washed to remove the soil inside the connectors. The first set of field measurements in 2003 were carried out by using the existing connectors at the end of the tubes, but in 2004 all the connectors were removed and the tube ends were trimmed and new connectors were installed at the end of all tubes and a new set of pore pressure measurements was made.

7.6 2003 and 2004 Measurements

As mentioned above, two sets of measurements were carried out, one in 2003 and the other in 2004 after changing the end connectors of the tubes. Both measurements were carried out during summer time, 30.Jul.03 and 27.Aug.04. Based on the Environment Canada climate data,

the precipitation between 23rd and 30th of July 2003 was about 42 mm and between 20th and 26th of August 2004 was about 34 mm which occurred several days before taking each piezometer measurement. The two readings are presented in the same plot. Figure 5 illustrates the pore pressure variation at 6 m below the ground surface in the foundation soil beneath the northern half of the embankment and Figure 6 shows the same results in the southern half of the embankment.

In the northern section, 6 m below the ground surface (Figure 5), only 2 piezometers, NW-T-6 AND NW-C-6, out of the 5 piezometers could be identified and read. The measurements in 1989 show a slight increase in pore pressures since the end of construction in 1988 with an increase from 7 to 8 kPa and from 1 to 2.5 kPa at the above mentioned piezometers respectively. The recent measurements at these locations also showed an increasing trend in pore pressures where they increased from 8 to about 9.5 kPa and from 2.5 to 3.5 kPa respectively.

In the southern section, 6 m below the ground surface (Figure 6), 2 out of 6 piezometers could be read. Both SE-T-6 and S-C-6 piezometers at this elevation also show an increase in pore pressure since the end of construction. The pore pressure increased from 1.5 to 8.5 kPa and from 6 to 8.5 kPa at these piezometers respectively, almost to the same pore pressure.

Figures 7 and 8 illustrate the pore pressure variation at 3 m elevation below the ground surface at the northern and southern halves of the test embankment respectively. In the northern section (Figure 7) again 2 piezometers out of 5 functioned properly and the results show that the pore pressure at these two piezometers increased from 2 kPa to 8 kPa at NE-C-3 and to 11 kPa at NE-T-3, between 1989 and 2003. However, in

2004, the pore pressures decreased almost the same amount of 4 kPa and reached 4 and 7 kPa respectively.

In the southern section, 3 m below the ground surface (Figure 8), again 2 out of 5 piezometers were identified and gave good results. Both piezometers showed almost no change in pore pressure since the end of construction till 1989, but in 2003 both of them reached 5 kPa. The 2004 measurements indicated that the pore pressure in both piezometers increased from 5 to about 8.5 kPa. These slight fluctuations are probably due to ground water table increases.

Figures 9 and 10 illustrate the pore water variation at 1 m above the ground surface inside the fill soil in the northern and southern sections of the embankment respectively. In the northern section, 3 out of 5 piezometers functioned properly. As shown in Figure 9, the pore water pressures at the end of construction were different at these 3 locations. But the measurements in 1989, one year after the end of construction, showed that all 3 piezometers had reached a stable state with the same value of about 14 kPa. The measurements in 2003 and 2004 also showed consistent results for these 3 piezometers. There was a slight reduction in pore pressure where it decreased from 14 to about 8 kPa in 2003 and remained almost the same in 2004.

In the southern section of the embankment at 1 m elevation above the ground surface (Figure 10) 3 out of 5 piezometers gave acceptable results. S-1 and SE-2 piezometers both showed a reduction in pore pressure since the end of construction in 1988 as the pore pressures dropped from about 55 kPa to about 26 and 18 kPa respectively. The trend of decrease in pore pressure was continued with a slight decrease between 1989 and 2003. The 2003 measurements showed that the pore pressure dropped from 26 to 3.5 kPa and from 18 to 12 kPa at the above

piezometers. The SE-3 piezometer was not read after the end of the third construction stage but the measurements in 2003 showed that the pore pressure at this piezometer remained high only dropping from 98 kPa during the third construction stage to about 84 kPa in 2003. This high reading is suspect.

Figure 11 and 12 illustrate the pore pressure changes in the northern and southern halves of the embankment at 3 m elevation above the ground surface respectively. In the northern section (Figure 11) all 4 piezometers were identified and all of them gave reasonable readings. All the piezometers showed a decrease in pore pressure values after the end of construction. In 1989 the average pore pressure at this section of the embankment was about 26 kPa with a range of 9 kPa to 38 kPa. In 2003 the average pore pressure at these piezometers was about 7.5 kPa and in 2004 they reduced more to about 3 kPa in average.

In the southern section (Figure 12) only 1 of the 4 piezometers functioned. The pore pressure at this piezometer was about 24 kPa at the beginning of the third construction stage and then in 1989, one year after the end of construction, it dropped to 18 kPa and the measurements in 2003 showed a reduction to 5.5 kPa and the measurements in 2004 showed a pore pressure of 3.5 kPa.

The pore water pressure changes at 5 m elevation above the ground surface in the two halves of the test embankment are illustrated in Figures 13 and 14. All 5 piezometers at the northern section of the embankment at this elevation functioned properly, as shown in Figure 13. The same trend of pore pressure reduction after the end of construction is also observed. The average pore pressure of 38 kPa in 1989, one year after the end of construction, decreased to about 10 kPa in 2003 and then dropped to

about 5 kPa in average in 2004. The reduction trend was similar and consistent for all 5 piezometers.

In the southern section of the test embankment (Figure 14) the measurements also show that since the last set of measurements in 1989, the pore pressures dropped to the same value of about 4 kPa at the 3 functioning piezometers out of five. The 2004 measurements showed a slight increase in pore pressure at these 3 piezometers to about 8 kPa.

None of the piezometers at the 8 m elevation above the ground surface functioned during the 2003/2004 field measurements and no readings were available from previous field measurements.

7.7 Long term performance of pneumatic piezometers – Summary and Conclusions

- During the 2003/2004 field measurements, 15 years after the end of construction, 53% of the 55 pneumatic piezometers installed in the foundation and fill soils of the Devon test embankment could be identified and functioned properly. Most of the damage to the piezometers happened during the cleanup activities with the backhoe in 2003 when the debris from sloughing was removed from the terminal boxes. During the excavation most of the piezometer plastic tubes were damaged and disconnected. Some piezometers, which had remained undamaged, had no identification tags and in total about 5 fell in this category. The results of these piezometers were not considered in this chapter due to uncertainty about their location.

- The same readout box was used during the 2003/2004 field measurements as in the 1986 to 1990 period in order to minimize

any error induced by using different types of readout boxes. The functioning piezometers in 2003/2004 in the foundation soil did not show any reduction in pore pressure after the end of construction and instead most of them illustrated some increase in the pore pressure values.

- Table 1 summarizes the measurement of pore pressure at different times and elevations inside the test fill and foundation soils. These results also show that inside the fill soil the pore pressure change is different from the foundation soil and the pore pressures decreased since the last set of measurements in 1989, one year after the end of construction. This decrease clearly reflects the consolidation taking place in the embankment. In the foundation soil the pore pressures appear to have been affected by water table fluctuations, that is, changes in the regional groundwater regime. In general, the correspondence of the pore pressure development with respect to the construction activities could be clearly observed. Pore pressures in the fill soil build up during the construction stages and dissipated during the subsequent no-construction periods. The rate of the dissipation was generally smaller in the later no-construction periods than during the first period, probably due to consolidation of the soil structure. The closer to the center of the embankment, the higher the pore pressure built up during construction. The pore pressures at different locations however tended to equilibrate as the pore water migrated within the embankment after the construction periods. The induced pore pressure at each individual location in the embankment, however, was influenced by the initial degree of saturation of the fill soil at that location.

- In total 55 pneumatic piezometers were installed in the test embankment and the foundation soil. Twenty in the foundation soil

and 35 in the fill soil at different elevations. In the embankment soil 21 out of 35 piezometers were identified and functioned properly. In the foundation soil, 8 out of 20 piezometers could be identified and functioned properly. In total there were 5 functioning piezometers in the embankment soil which had no label and could not be identified and 3 more unidentified functioning piezometers were found in the foundation soil. The other remaining piezometers suffered severe damage to their access tubes and could not be read.

Table 1. Average pore pressure measured by functioning piezometers

Elevation	Pore pressure, kPa		
	1988	**1990**	**2003/2004**
N 5m	45	39	7.5
S 5m	26	34	7
N 3m	25	25	7
S 3m	23	18	4.5
N 1m	30	14	8
S 1m	54	22	8
N -3m	1.5	2	7.5
S -3m	5	4.5	6.5
N -6m	4	5	6.5
S -6m	4.5	4	10.5

Figure 1.A view of pneumatic piezometer

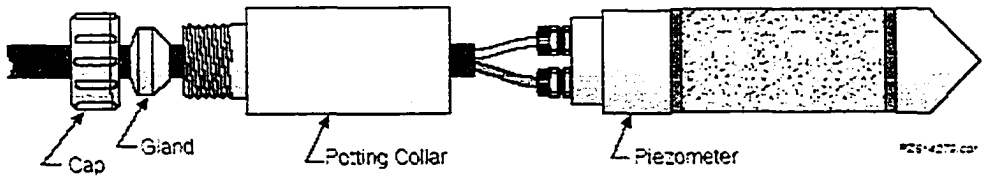

Figure 2. Sketch of the pneumatic piezometer tip and tubing connections

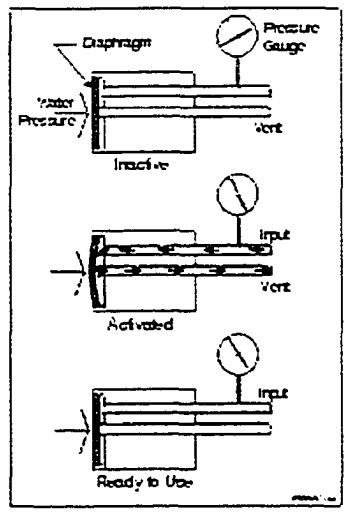

Figure 3. Schematic working diagram of the pneumatic piezometer

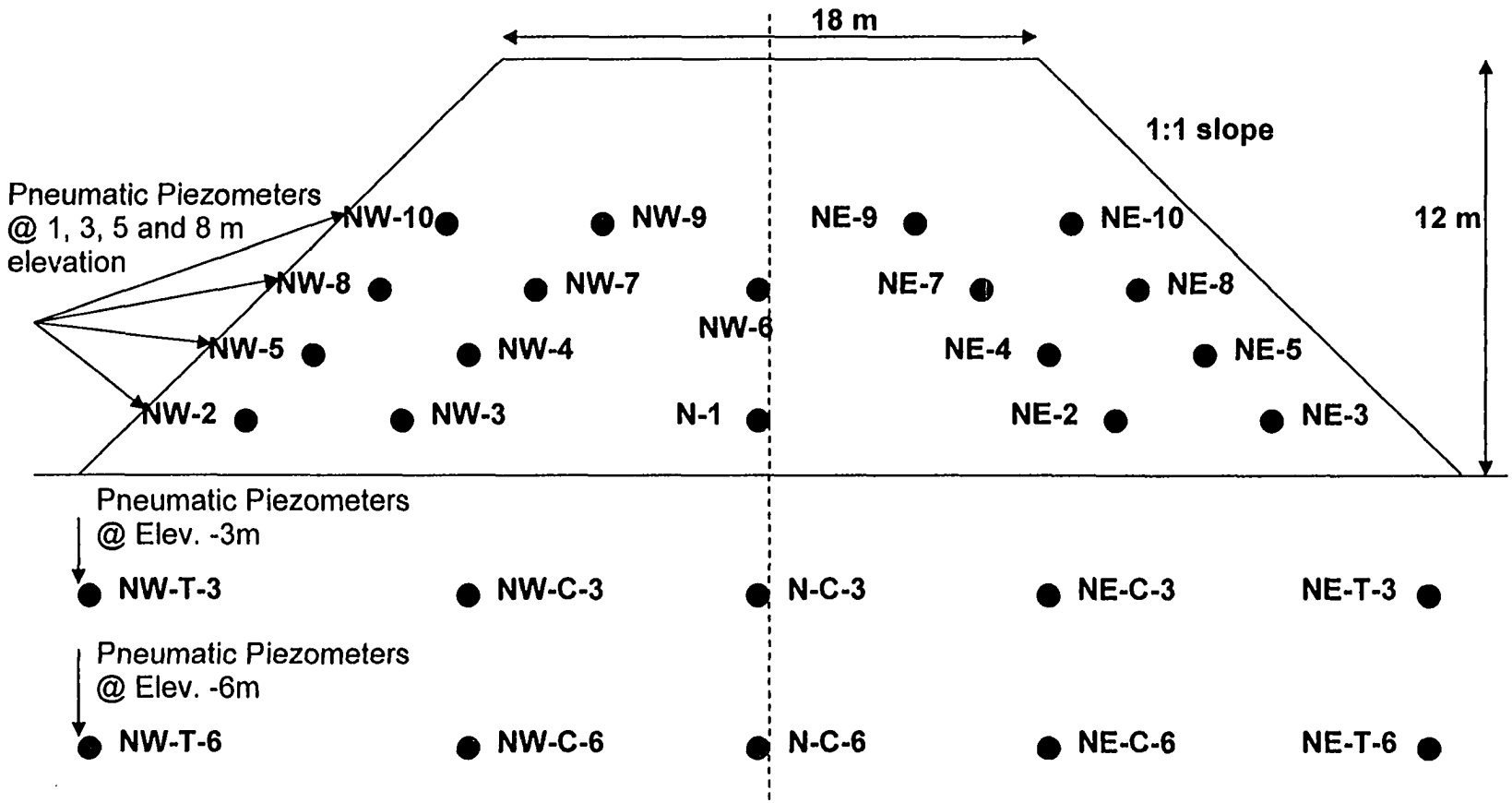

Figure 4. Lay out of pneumatic piezometers in the northern half of the test embankment (not to scale)

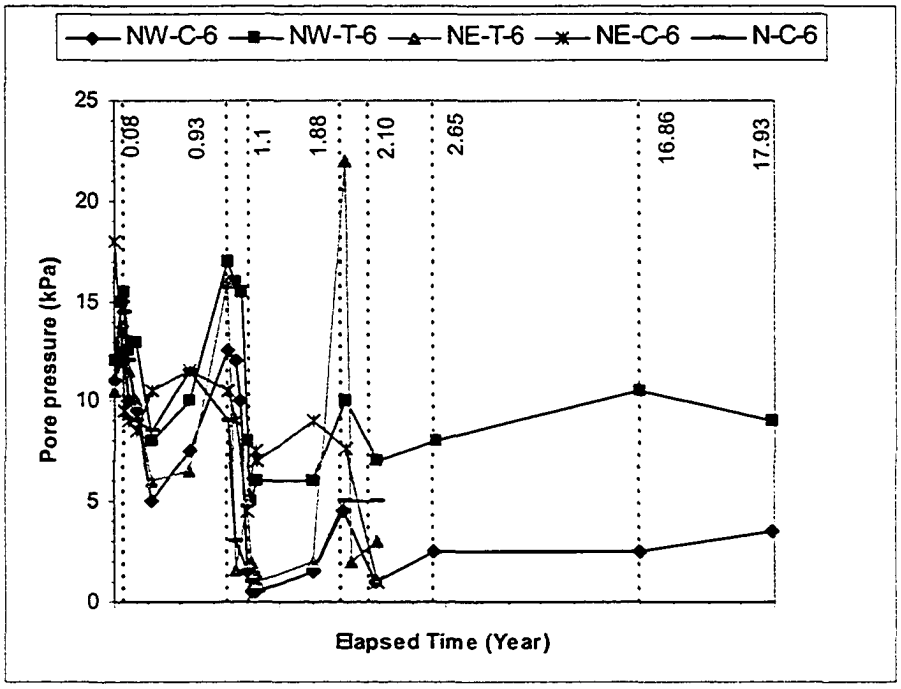

Figure 5. Pore pressure variation at 6 m below the ground surface- North half of the test embankment

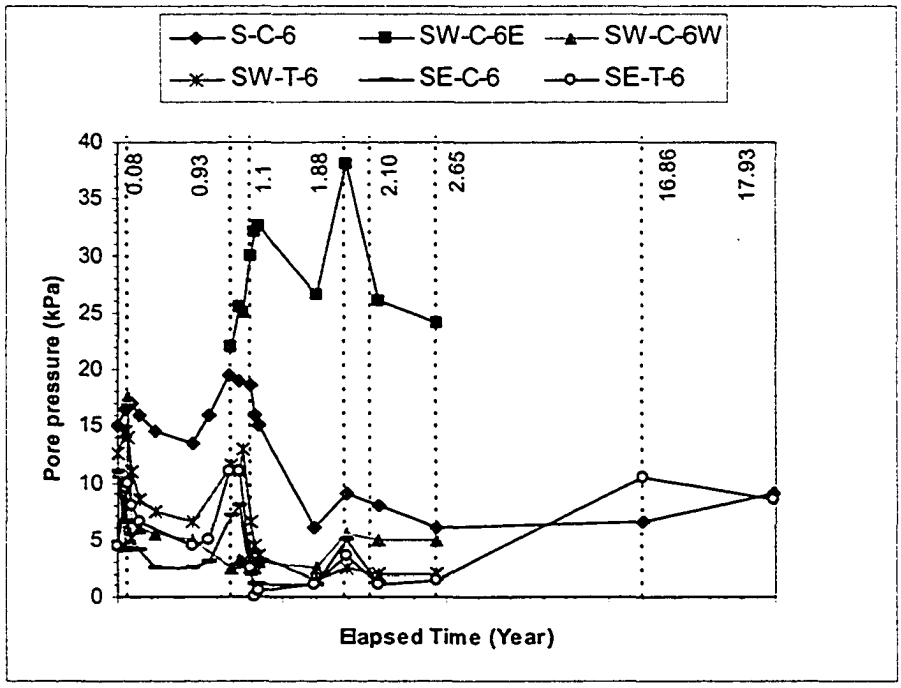

Figure 6. Pore pressure variation at 6 m below the ground surface- South half of the test embankment

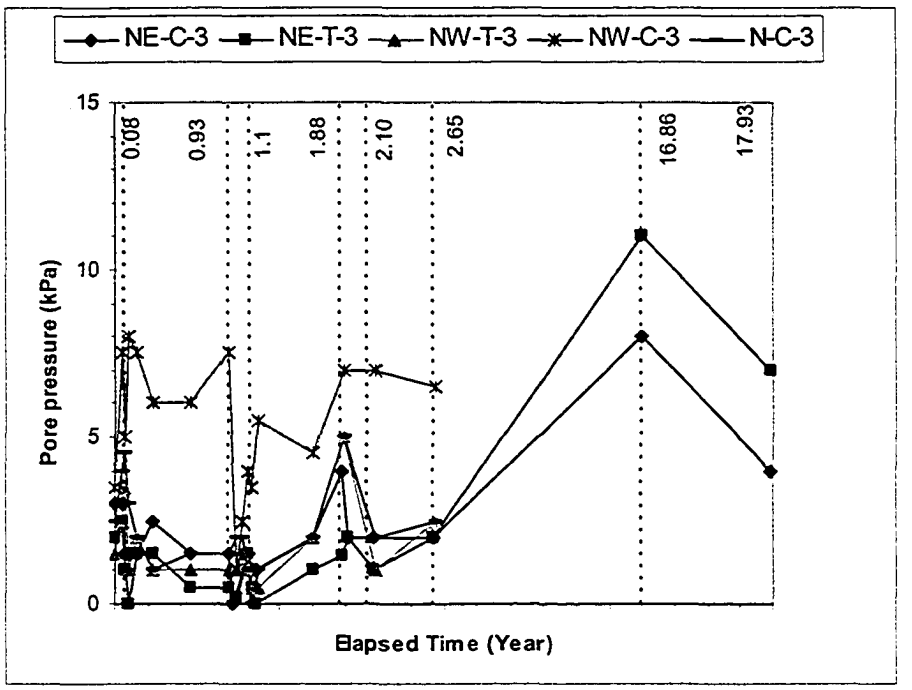

Figure 7. Pore pressure variation at 3 m below the ground surface-North half of the test embankment

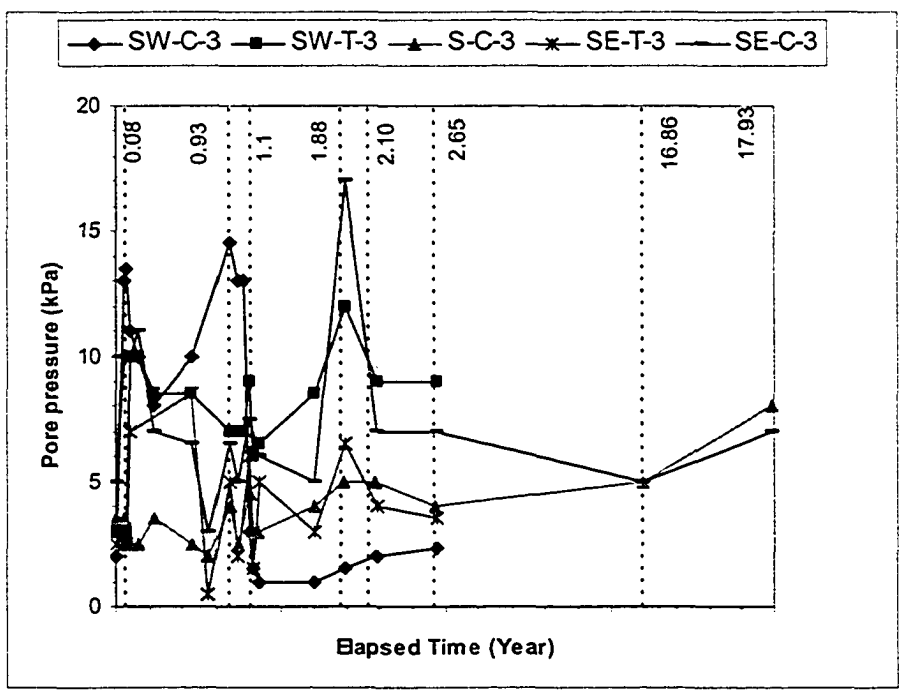

Figure 8. Pore pressure variation at 3 m below the ground surface-South half of the test embankment

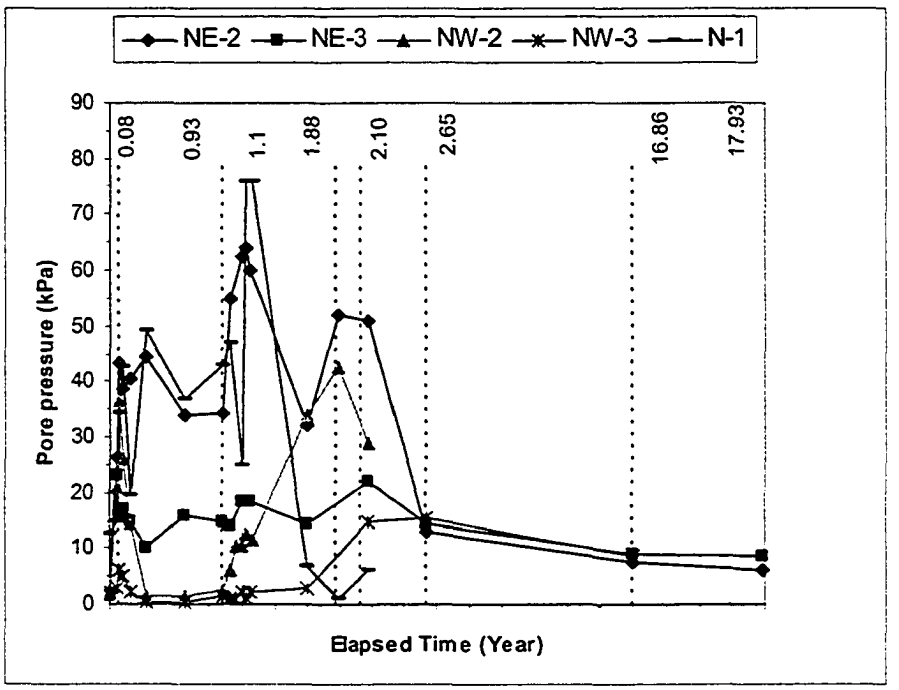

Figure 9. Pore pressure variation at 1 m above the ground surface-North half of the test embankment

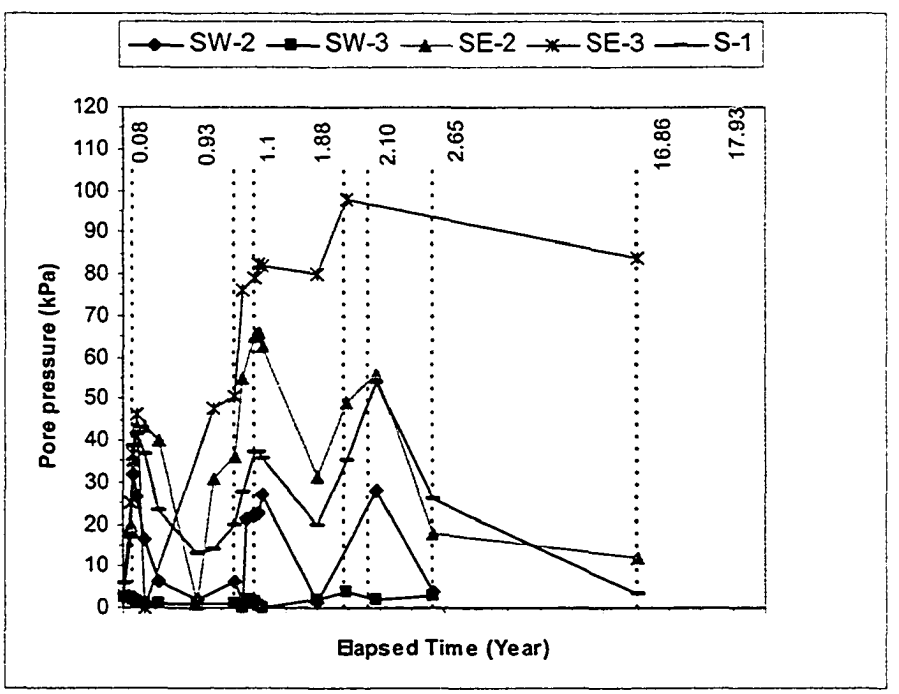

Figure 10. Pore pressure variation at 1 m above the ground surface-South half of the test embankment

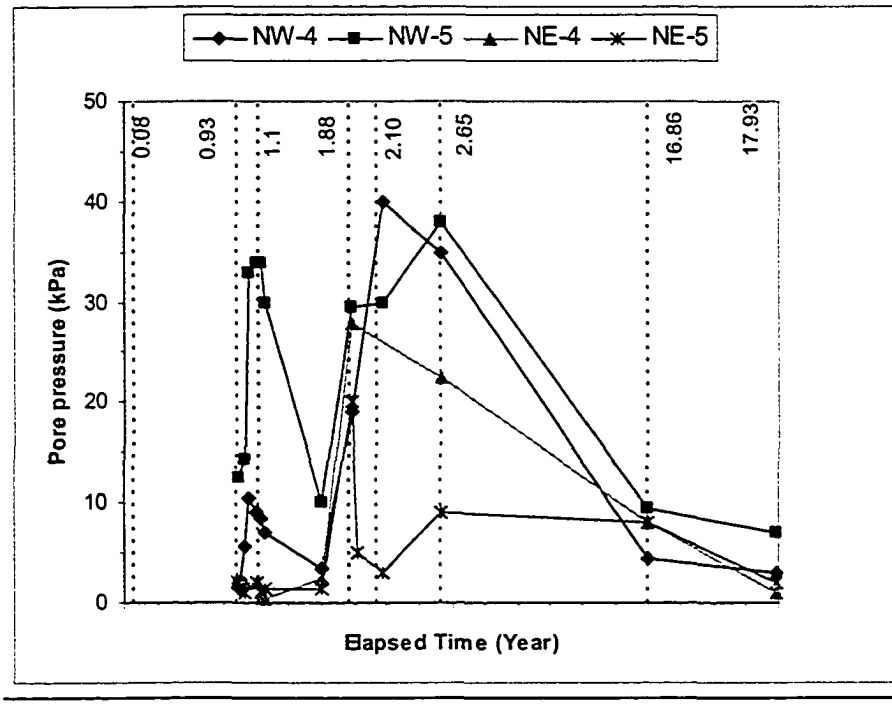

Figure 11. Pore pressure variation at 3 m above the ground surface-North half of the test embankment

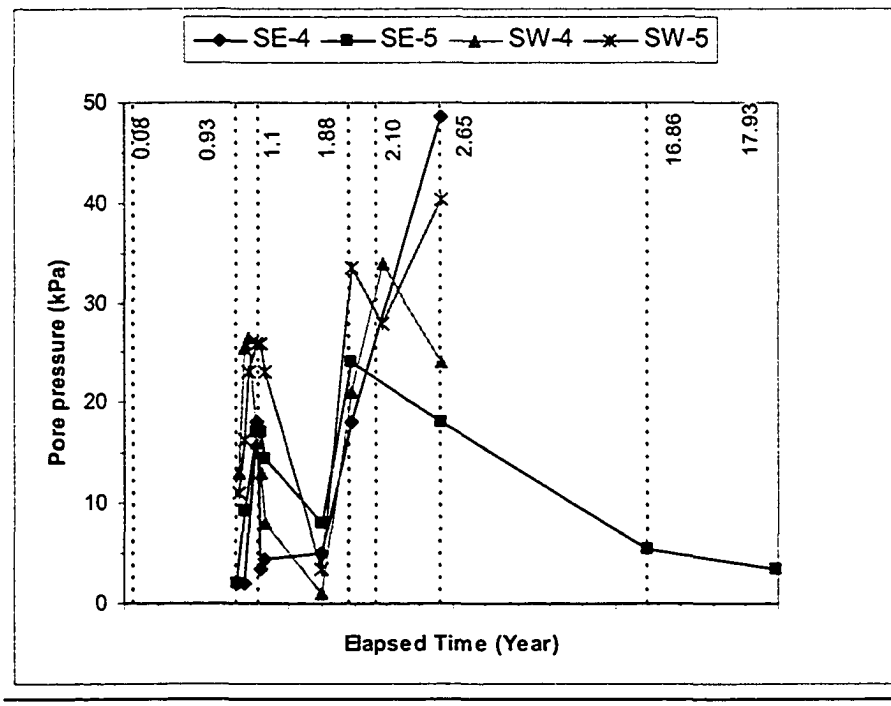

Figure 12. Pore pressure variation at 3 m above the ground surface-South half of the test embankment

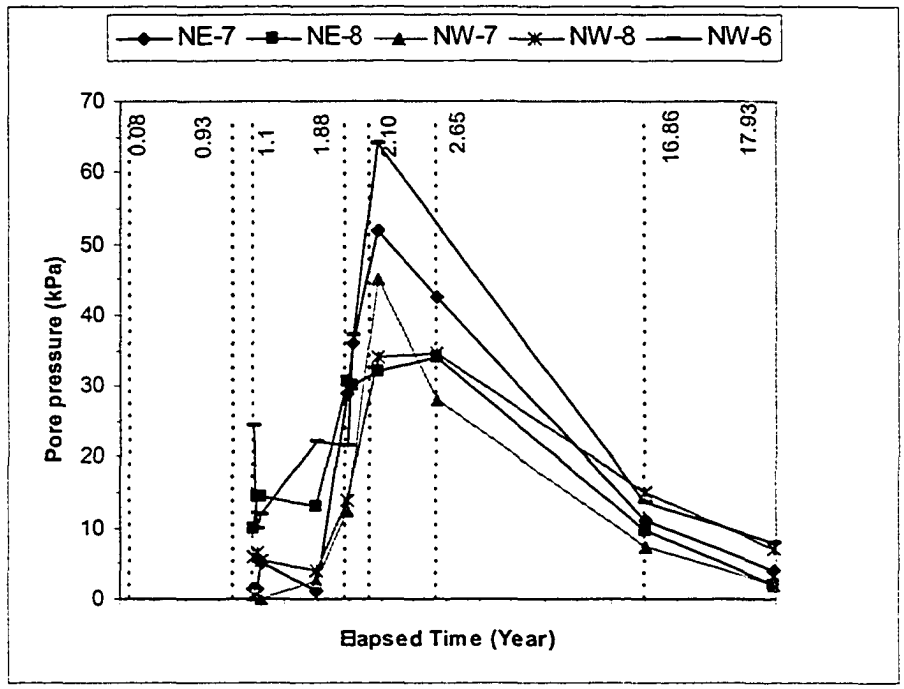

Figure 13. Pore pressure variation at 5 m above the ground surface- North half of the test embankment

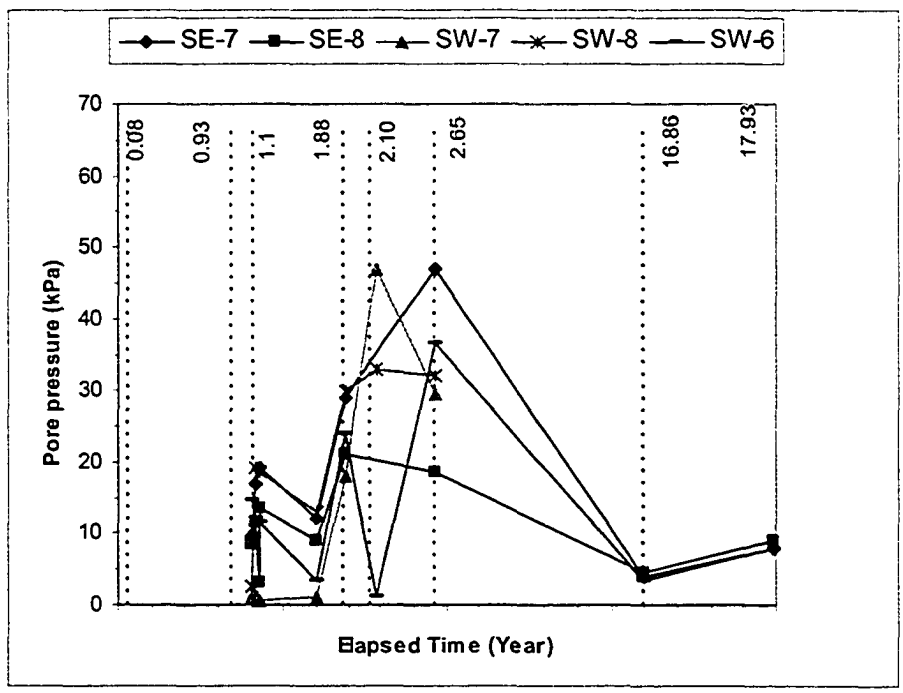

Figure 14. Pore pressure variation at 5 m above the ground surface- South half of the test embankment

Hanna, T.H., (1985). Field Instrumentation in Geotechnical Engineering, Series on Rock and Soil Mechanics, Vol.10, 1985

Liu, Y., (1992). "Performance of Geogrid Reinforced Clay Slopes." PhD. Thesis, University of Alberta: 406p.

Slope Indicator Technical Notes, (2000). "Pneumatic Piezometer", Slope indicator Company

Chapter 8. Comparison between different measurements

8.1 Introduction

As presented in previous chapters, the results of different instruments installed in the Devon test embankment were reviewed separately and the measurements in 2003, fifteen years after the end of construction, were presented. The new sets of measurements for each instrument were reviewed and compared with the previous measurements in order to check the consistency and relevancy of the new measurements with the previous measurements made thirteen years before. In this chapter different measurements which can be categorized under a same group of behavior will be compared. These comparisons will include: 1) soil horizontal strains with geogrid strains, 2) soil horizontal movements measured by horizontal extensometers and vertical inclinometers, and 3) soil vertical deformations measured by vertical extensometers and horizontal inclinometers and the elevation surveys.

8.2 Soil horizontal strains and geogrid strains

As discussed in previous chapters, the horizontal extensometers which measured the lateral soil deformation were installed 1 m above and below each geogrid layer. This provided the possibility of measuring the soil horizontal strains 1 m above and below each geogrid layer and by measuring the geogrid strains with EWR strain gauges along the geogrid layers, a general comparison can be made between the horizontal strains in the geogrid and in a 2 m thick soil band surrounding the geogrids. In order to do this comparison however too many assumptions have to be made which include, different initial dates for the EWR strain gauges and the two horizontal extensometers above and below the grid layers, different elevations of instruments with 1 m vertical spacing between them and different soil properties in the fill as discussed in Chapter 2. In addition to

these, the EWR strain measurements are all local strain values and a temperature correction has been applied to them. In order to make a comparison between soil and geogrid strains the global strain values must be used. As discussed in Chapter 4 the correlations between local and global strains obtained from field measurements had a wide scatter hence these correlations are in doubt. In Figures 43, 44 and 45 of Chapter 4, in the correlation between local and global strains, the global strains can vary by ±1% strain. Hence the differences between grid and soil horizontal strains can be entirely experimental error. Because of all of the assumptions involved, such a comparison has not been made in this thesis.

8.2.1 Comparison of geogrid strains

Figures 1, 2 and 3 illustrate a comparison between the local strains measured in 2003 at different types of geogrids installed at different elevation inside the embankment. As it can be seen at Signode section in contrast with the Tensar section, the large strain zones are located slightly deeper. This is possibly due to the difference in the tensile stiffness between the two grids. When a slope is reinforced with a stiffer grid (Signode) large reinforcement forces are mobilized in the material during the fill placement. Since the Paragrid had some manufacturing defects at the grid joints, its performance can not be compared with other geogrids. All these presented strains are local strain values measured by EWR strain gauges and they are also corrected for temperature induced strains. Global strain values would be different from these local strain values for different geogrids except for the Signode which the lab test results and the field correlation between local and global strains showed similar results.

8.2.2 Comparison of soil horizontal strains

Figures 4, 5 and 6 present comparison between the soil horizontal strains at 0 m, 2 m and 4 m elevations above the ground surface in all 4 sections of

the test embankment measured in 2003. There are two distinct phases in the development of the deformations in the slopes. During the first and second stages of construction when only 6 m of fill was placed, the deformations in all slopes were relatively small and were distributed smoothly except for some rather small localization in the unreinforced slope. The slopes deformed significantly after the 1988 construction stage when the top 6 m of the fill was placed. As shown in Figure 4, the soil horizontal strains at 0 m elevation or at the ground surface in all 4 test sections are fairly small and similar. But at 2 m and 4 m in the fill (Figures 5 and 6) the difference between the horizontal soil strain variations between different sections are considerable. It should also be kept in mind that as discussed in section 2.3.2, the fill soil had a very large variation in moisture content and density and hence the stress-strain behavior of the fill soil had varied dramatically at different locations and elevations inside the fill. Therefore comparing the soil horizontal strains at different reinforced sections with the unreinforced section could not be a quantitative comparison. The horizontal soil strains in the reinforced sections seem to be slightly higher than the strains in the unreinforced slope (Figures 5 and 6). This is likely because of weak bonding between the soil and the geogrids. The additional horizontal strains might also come from some differential vertical movements which were transferred to the horizontal soil strains through the reinforcing geogrid. This may also raise a doubt in someone's mind that what had been the effect of geogrid installation if it soil horizontal strains in the unreinforced section are smaller than the reinforced sections. In reality understanding the different mechanisms for slope stability and failure at different sections of the embankment and the real observations may help to clarify it.

8.2.3 Comparison of Unreinforced Section to Reinforced Sections

Complete slope stability analysis was done by Liu (1992) and the following discussions relate his conclusions to the observed behavior of the

reinforced and reinforced sections in the test embankment. Failure mode of the unreinforced embankment slope was determined to be rotational with a circular shaped slip surface. Localization of excessive vertical deflections (measured by horizontal inclinometers) and locations of large horizontal deformation zones (measured by horizontal extensometers) were also close to the predicted slip surface using Spenser's method. Also some tension cracks were found parallel to the crest on the top surface of the test fill at 2 to 3 m from the crest in unreinforced section as shown in Figures 7, 8 and 9 taken in 2004. Another potential failure mode, not predicted by theoretical stability analysis, actually existed in the unreinforced section and it intersected the slope surface at about 2 to 3 m deep. This instability progressed during and after the construction. Excessive horizontal deformations (Extensometer at 4m and inclinometer at the crest) and excessive vertical deflections at 4 m level (inclinometer at 4 m) plus blocked access tube of horizontal extensometer at 4 and 6 m elevation at a location 3 to 4 m from the slope surface all indicated large differential vertical displacements related to this shallow slope instability. Also scarps were observed about 2 m below the crest of the slope demonstrating the occurrence of this instability. This instability is most likely related to poor compaction adjacent to the slope surface, weakening of the surface soil due to freeze-thaw cycles and heavy rain activities during the summers. In the unreinforced section two large deformation zones one at 7 m location of the 2 m level and the other at the location 2 to 3 m from the slope face at the 4 m level were closely related to the possible deep and shallow rotational slip surfaces. But on the other hand, in the reinforced slopes in the test embankment, other than for some shallow (<0.5 m) surface soil movements likely caused by cyclic freeze-thaw, there were no indications of instability. Hence the location of peak tensile strains at each geogrid layer and localization of the vertical deformations were a good indication of the location of the developing slip surface. The locations of peak horizontal strains in soil, however, might not be necessarily related to the slip surface. When the soil strains down the slope, the geogrid layers prevent or reduce

the horizontal soil movement by transferring the load from the over-stressed zones to under-stressed soil deeper within the slope. As a result, the horizontal strain of the soil deep in the slope (so called resistant zone) may increase while the horizontal strain of the soil around the slip surface may decrease. As the grid layers are being heavily tensioned at the peak locations, they transfer the horizontal loads to the soil deep in the slope and develop maximum horizontal strains in the soil at depths beyond the potential slip surface. The reinforcing layers reduce the localized vertical deflections and hence the resulting settlement profiles in the Tensar section were fairly smooth. This indicated that the tension in the geogrid, which is mobilized by the horizontal soil strain and differential vertical displacements transfers horizontal loads generated by the upper soil, from the soil around the failure surface to the soil deep with in the slope. In other words the strength in a much larger volume of soil is mobilized through the reinforcing layers to reduce localized deformations as well as to maintain stability.

In Tensar section the failure mode was analyzed to be rotational and the slip surface passed through four locations of measured large deformation and the toe of the slope. Similar to the unreinforced slope, there was a possibility of shallow failure mechanism. This slip surface was indicated by the locations of large vertical deflections at the 4 and 6 m levels and the peak strain in the top geogrid layer at the 5 m level. The size of the shallow failure was similar to that in the unreinforced slope but there was no visual indication in the field showing the potential failure. This fact implies that the secondary grid layers did reduce the possibility of this shallow failure.

In Signode section Bishop modified and Spencer modified methods gave an identical circular slip surface. In contrast with the Tensar section, the large strain and displacement zones were located slightly deeper than the predicted most critical slip surface. This was possibly due to the difference in the tensile stiffness between the two grids. When a slope is reinforced with a stiffer grid (Signode) large reinforcement forces are mobilized in the

material during the fill placement. To reach the limit equilibrium condition with the minimum factor of safety, a larger disturbing force is required. Therefore, the most critical slip surface moves deeper into the slope. In Signode section the load transfer function was not as obvious as in Tensar section. The locations of the large horizontal soil strains appeared to be in the active zone and therefore the typical load transfer mechanism was not applicable. However comparing the profiles of horizontal soil strains in Signode section with the profiles in unreinforced section, it was found that the zone of large horizontal soil deformation in Signode section was much wider and the distribution was smoother than in the unreinforced section. Again comparing to the unreinforced slope, the strength in a larger volume of the soil in the reinforced slope was mobilized through the tension in the grid layers against localized deformation and instability of the slope. As discussed in Chapter 2, the variation in moisture content at different elevation inside the fill and the effect of moisture content change on the unconfined shear strength makes the fill soil such heterogeneous material that comparing the soil horizontal strains at different elevations inside the fill would not be a valid comparison. However, with the reinforcing layers, not only were the localization of the vertical deflections reduced, but also the distributions of the horizontal soil strains were less localized. Loads were transferred from over-stressed zones to under-stressed zones in the soil mass and the resistance of a larger volume of the soil was mobilized by the tension in the geogrids to prevent or reduce stress and displacement localizations.

8.3 Comparison between soil horizontal deformation

Soil horizontal deformation was measured with horizontal extensometers installed at 0 m, +2 m, +4 m and +6 m and vertical inclinometers at the crest of slopes. Table 1, 2, 3 and 4 summarize the amount of horizontal deformation at the location of vertical inclinometers at each elevation inside the test fill in Tensar, Signode, Paragrid and unreinforced sections

respectively. In the Tensar section the vertical access tube for the inclinometer at the crest of slope seemed to be very deformed and due to two dimensional soil movement the tube was compressed and most portions of the tube was pushed towards inside of the fill. This can be seen from the values in Table 1 as well that the vertical access tube in Tensar section was bent towards inside of the fill and this might have shown some unrealistic deformation pattern for this access tube at the lower elevations inside the fill.

In the Signode section unfortunately no measurements of vertical inclinometer at the crest could be made in 2003, so no comparison could be made for this section.

In the Paragrid section, Table 3, the horizontal extensometer and the vertical inclinometer at the crest of slope at +2 m have reasonable agreement for soil horizontal deformations but at +4 m, the inclinometer readings are higher than horizontal extensometers. Possibly the construction activities and equipment caused more outward movement of the vertical inclinometer access tube, as discussed in Chapter 5. As it can be seen there is a good match between the August 1988 measurements by vertical inclinometers and horizontal extensometers. The horizontal deflection measured by vertical inclinometer at the crest of the Paragrid section is calculated assuming that the horizontal movement at the ground surface measured by the vertical inclinometer was equal to the horizontal extensometer measurement. In the unreinforced section, Table 4, also it is shown that usually the vertical inclinometer measurements are larger than the measurements by horizontal extensometer, considering the assumption of equal horizontal deformation at the ground surface measured by the horizontal extensometer and the vertical inclinometer. But again in the early stages of the measurements there was a good agreement between two measurements by horizontal extensometer and vertical inclinometer.

8.4 Comparison between soil vertical deformation

Settlement inside the embankment and the fill material were measured with vertical extensometers installed at the crest of slopes and also the horizontal inclinometers placed inside the embankment at 0, +2 m, +4 m and +6 m. Inclinometers give the deformed shape of the access pipe, or in other words the pattern of settlement at the inclinometer elevation but in order to determine the exact amount of settlement in the fill, some reference points should be considered at the horizontal inclinometer location in order to measure the absolute amount of settlement at that reference point and then by considering that settlement the settlement pattern for the whole inclinometer access tube can be defined. As discussed in inclinometers chapter, the absolute amount of settlements were determined by vertical extensometer settlements during the 2003 field measurements. So generally the amount of settlement shown by horizontal inclinometers match exactly with the amount of settlement shown by vertical extensometers at the crossing point of vertical extensometers and horizontal inclinometers. But leveling of the access tube end points were also carried out in addition to the leveling of the concrete monuments at each test section. The locations of concrete monuments and deep bench mark are shown in Figure 10. These concrete monuments were constructed along the center of each test section. Based on the surveying notes in the archives of the project, and based on the assumption that the deep bench mark has not moved, two sets of elevation survey were done for all instrument access tube ends and the concrete monuments. Based on the old surveying notes, the elevation of the deep bench mark was considered to be 100.543 and Table 5 summarizes the elevation survey of the concrete monuments. The cap of the north east monument at Paragrid test section was damaged during attempting to remove the cap and no surveying was carried out based on this concrete monument. This table shows that all 3 concrete monuments have moved upward between 9 to 12.5 mm since their last surveying assuming that the deep bench mark remained fixed.

The two sets of elevation survey carried out in 2003 were done by establishing 13 turning points around the test embankment and the surveying loop in each case was closed with ±2 mm resolution. Table 6 summarizes the elevation survey of horizontal inclinometer access tube ends at all elevations and different test sections. According to the survey notes 100.000 m in local elevation survey system equals to 702.471 m in the global elevation survey system. By considering this conversion the elevation of the horizontal inclinometer access tube ends in the global system were calculated. Since one set of elevation survey was carried out when the site was covered with snow, it might had affected the elevation survey as it can be seen that there are some differences (maximum of 15 mm) between two sets of surveying. Determining the initial elevations of the end of the horizontal inclinometer access tubes was carried out based on the electronic data files available from Liu. Tables 7 and 8 summarize the difference between the elevation of the horizontal inclinometer access tube ends based on surveying and the vertical extensometer measurements in 2003 for the west ends and east ends respectively. As it is shown, the elevation survey does not have any consistency and does not reflect the real settlement profiles of the test embankment. In different sections of the embankment for example, the settlement in the north-east and south-east sections of the embankment decreased from 0 m elevation to 2 m elevation. Hence due to these discrepancies the settlements measured from vertical extensometers at the crest of slopes were used to determine the amount of absolute settlement for horizontal inclinometers installed at different elevations. These comparisons also show that since there was not sufficient confidence in the initial pipe end elevation measurements through surveying and also the elevation of the deep bench mark could not be confirmed by any other reference point, hence the elevation survey could not be trusted to be used for elevation determination of the horizontal inclinometers.

Table 1. Soil horizontal deformation comparison - Tensar section

Horizontal Deformation (mm)	0 m elevation				2 m elevation				4 m elevation	
	Aug-1988	Oct-1989	Sep-1990	2003	Aug-1988	Oct-1989	Sep-1990	2003	Aug-1988	2003
Horizontal Extensometer	12	55	55	53	0	80	80	80	20	110
Vertical Inclinometer	0	---	---	-6	6	---	---	-40	-5	31

Table 2. Soil horizontal deformation comparison - Signode section

Horizontal Deformation (mm)	0 m elevation				2 m elevation				4 m elevation	
	Aug-1988	Oct-1989	Sep-1990	2003	Aug-1988	Oct-1989	Sep-1990	2003	Sep-1988	2003
Horizontal Extensometer	8	48	46	47	25	97	97	97	105	157
Vertical Inclinometer	-10	---	---	---	36	---	---	---	---	---

Table 3. Soil horizontal deformation comparison - Paragrid section

Horizontal Deformation (mm)	0 m elevation				2 m elevation				4 m elevation	
	Aug-1988	Oct-1989	Sep-1990	2003	Aug-1988	Oct-1989	Sep-1990	2003	Aug-1988	2003
Horizontal Extensometer	8	50	52	54	30	90	96	90	20	110
Vertical Inclinometer	10	---	---	*54*	20	---	---	80	25	178

Table 4. Soil horizontal deformation comparison - Unreinforced section

Horizontal Deformation (mm)	0 m elevation				2 m elevation				4 m elevation	
	Aug-1988	Oct-1989	Sep-1990	2003	Aug-1988	Oct-1989	Sep-1990	2003	Sep-1988	2003
Horizontal Extensometer	6	58	60	58	---	58	61	57	40	105
Vertical Inclinometer	9	---	---	*58*	15	---	---	76	42	135

Table 5. Summary of elevation survey of concrete monument

	NW Monument	SW Monument	SE Monument
2003 (1)	100.957	101.118	100.658
2003 (2)	100.957	101.117	100.655
Average	**100.957**	**101.1175**	**100.6565**
Initial from notes (1)	100.946	101.104	100.642
Initial from notes (2)	100.948	101.106	100.653
Average	**100.947**	**101.105**	**100.6475**
Difference (mm)	**10**	**12.5**	**9**

Table 6. Elevation survey summary of horizontal inclinometers access tube ends at different elevations and sections

	2003 (1)	2003 (2)	Initial
SE-SI-0m	701.242	701.242	---
SE-SI-2m	702.93	702.928	703.25
SE-SI-4m	705.004	705.009	705.192

	2003 (1)	2003 (2)	Initial
SW-SI-0m	701.545	701.534	---
SW-SI-2m	703.023	703.013	703.148
SW-SI-4m	704.8	---	705.124

NE-SI-0m	701.473	701.476	---
NE-SI-2m	702.832	702.840	703.192
NE-SI-4m	704.861	704.876	705.157

NW-SI-0m	701.282	701.283	701.436
NW-SI-2m	703.063	703.063	703.186
NW-SI-4m	704.895	704.896	705.134

Table 7. Horizontal inclinometers west end settlements in 2003 based on extensometer measurements and elevation survey

	Northern half of embankment		**Southern** half of embankment	
Settlement in **mm**	**West** End Deflection Based on West Side Extensometer	**West** End Deflection Based on Survey	**West** End Deflection Based on East Side Extensometer	**West** End Deflection Based on Survey
0 m Elevation	176	154	14	—
2 m Elevation	220	123	169	130
4 m Elevation	343	239	360	324

Table 8. Horizontal inclinometers east end settlements in 2003 based on extensometer measurements and elevation survey

	Northern half of embankment		**Southern** half of embankment	
Settlement in **mm**	**East** End Deflection Based on West Side Extensometer	**East** End Deflection Based on Survey	**East** End Deflection Based on East Side Extensometer	**East** End Deflection Based on Survey
0 m Elevation	118	—	9	—
2 m Elevation	257	356	100	321
4 m Elevation	343	290	218	186

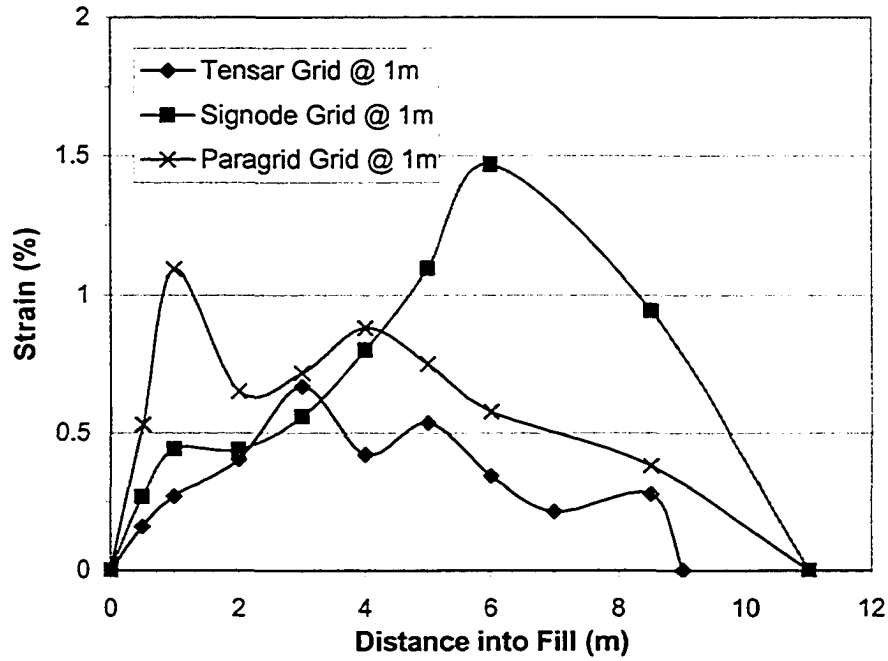

Figure 1. Comparison of different grid strains measured with EWR strain gauges in 2003- 1 m elevation

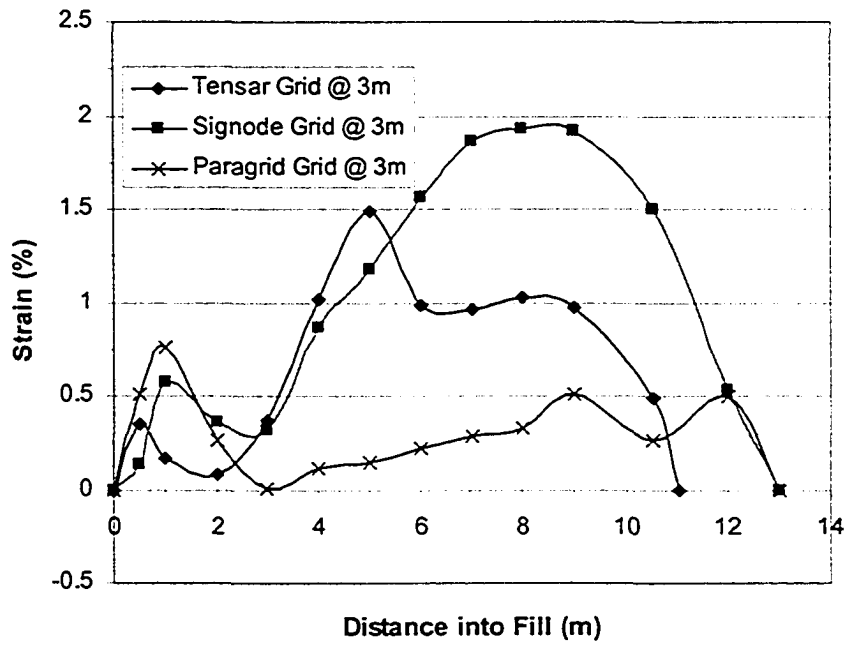

Figure 2. Comparison of different grid strains measured with EWR strain gauges in 2003- 3 m elevation

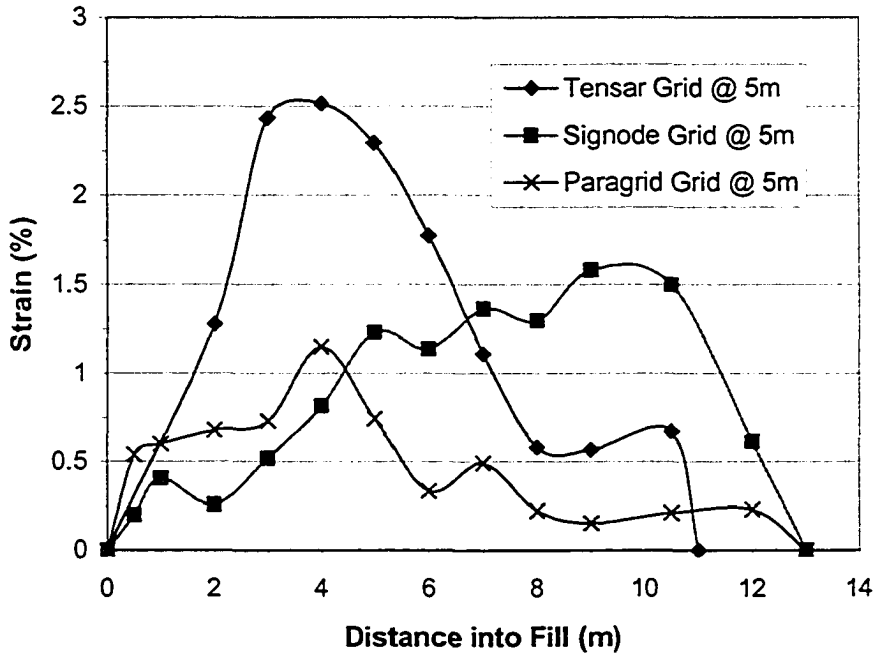

Figure 3. Comparison of different grid strains measured with EWR strain gauges in 2003- 5 m elevation

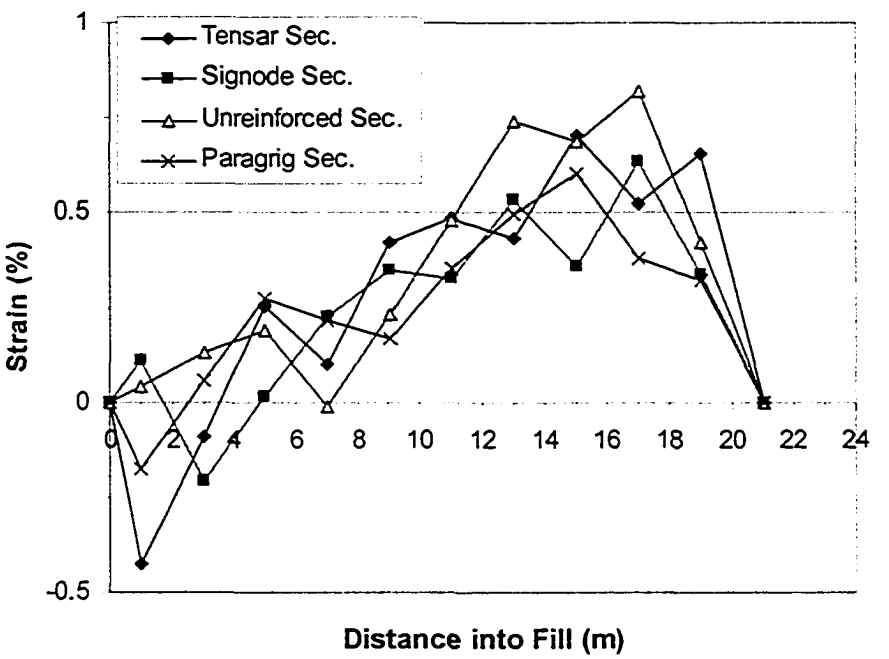

Figure 4. Soil horizontal strains at different sections – 0 m elevation

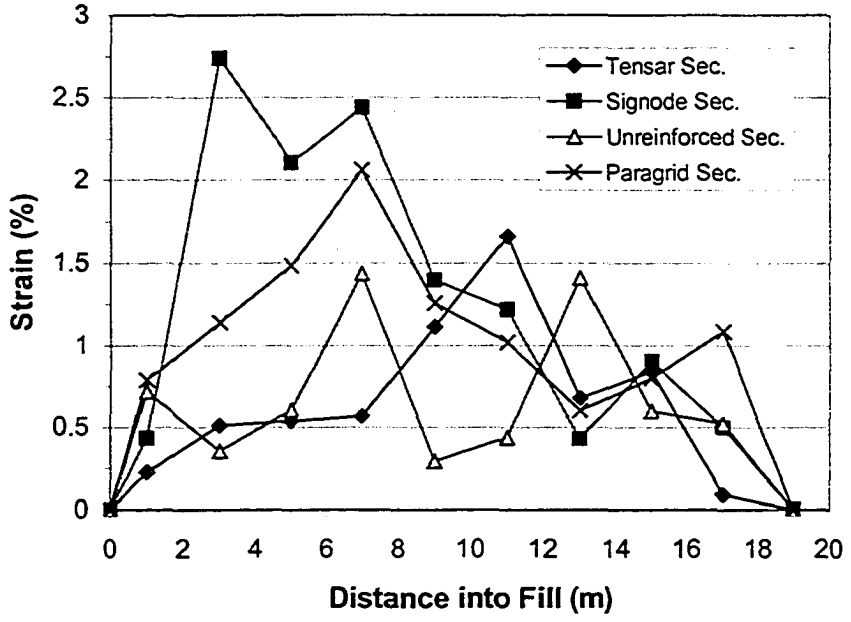

Figure 5. Soil horizontal strains at different sections –2 m elevation

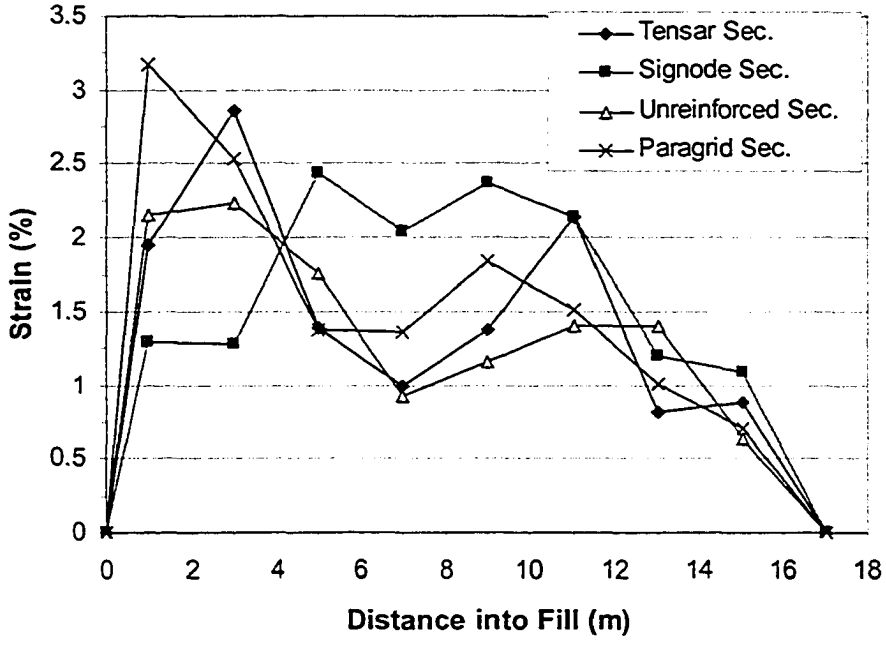

Figure 6. Soil horizontal strains at different sections – 4 m elevation

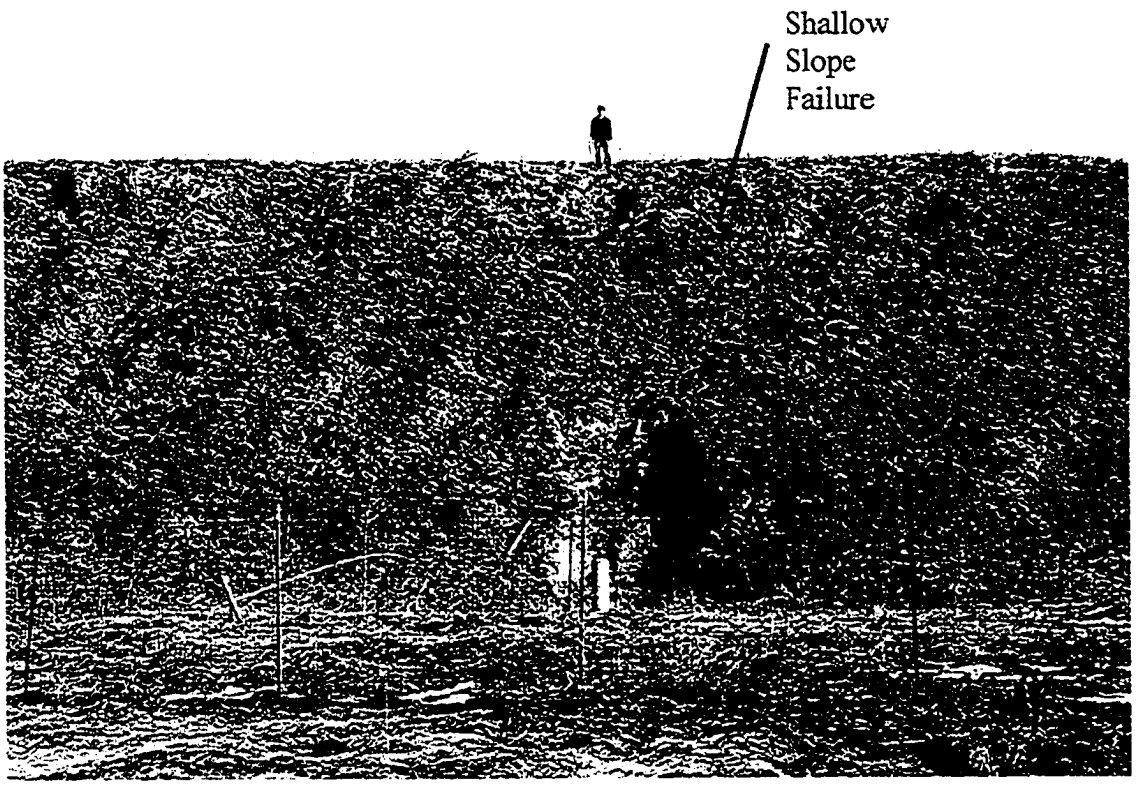

Figure 7. Unreinforced Section-Shallow slope failure, picture taken in 2004

Figure 8. Unreinforced Section-Scarps at the back of the crest plus crest failure, picture taken in 2004

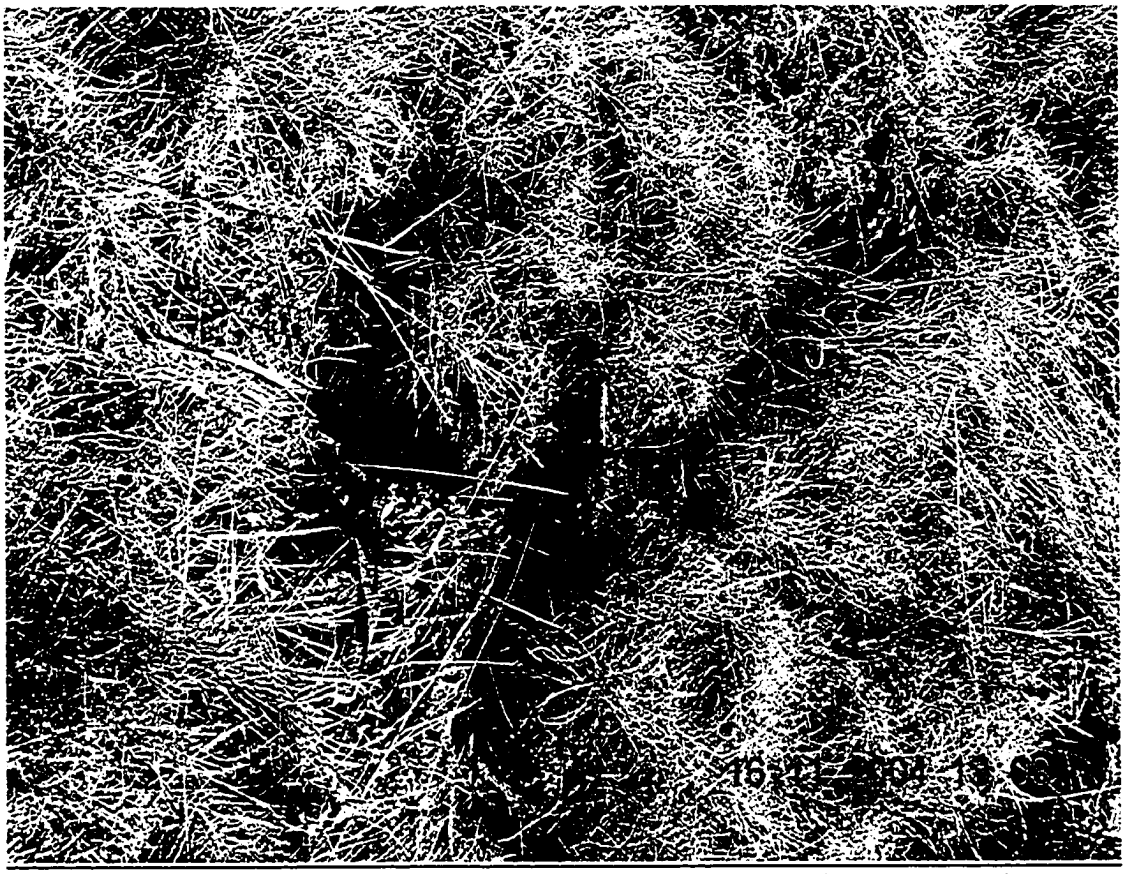

Figure 9. Unreinforced Section-Scarps at the back of the crest, picture taken in 2004

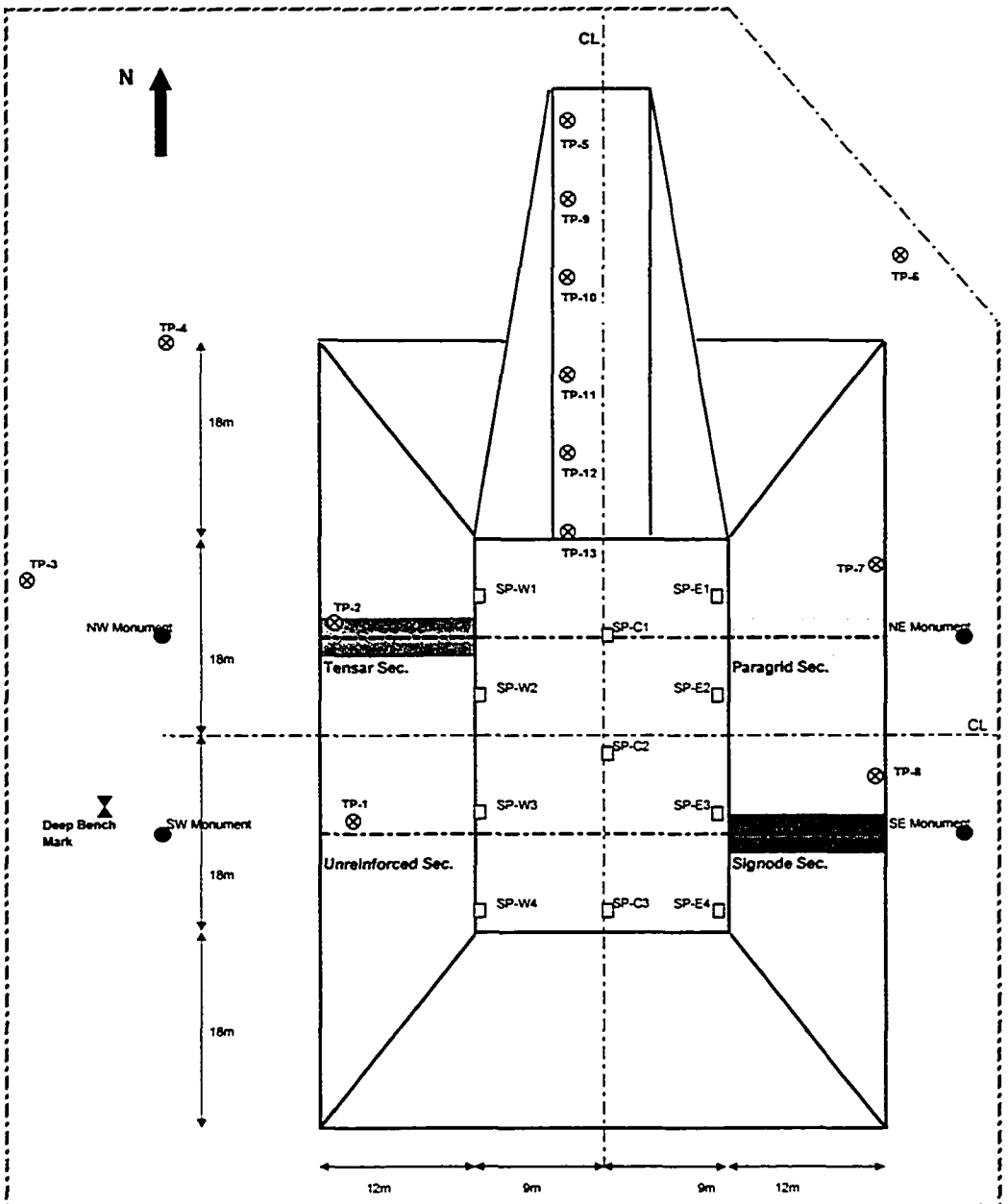

Figure 10. The location plan of concrete monuments and deep bench mark

Chalaturnyk, R.J., (1988). "The behavior of a reinforced soil slope", MSc. Thesis, Department of civil engineering, University of Alberta, Edmonton, Alberta, 320p.

Hanna, T.H., (1985). Field Instrumentation in Geotechnical Engineering, Series on Rock and Soil Mechanics, Vol.10, 1985

Liu, Y., (1992). "Performance of Geogrid Reinforced Clay Slopes." PhD. Thesis, University of Alberta: 406p.

Slope Indicator Technical Notes, (2000). "Pneumatic Piezometer", Slope indicatorCompany

Chapter 9. Summary and conclusions

9.1 Summary

The first objective of the thesis research was to perform field work to locate and refurbish the instruments about 13 years after the last set of field measurements. The second objective of the thesis was to read all the instruments still functioning to determine the deformation patterns in the soil and the geogrids 16 years after the end of construction. The third objective was to evaluate the long-term performance of the soil instrumentation and geogrid instrumentation in the test embankment. The various soil and geogrid instruments, which had been installed 18 years earlier, were refurbished and new sets of measurements were taken for each instrument. The past readings up to 1990 were available and by comparing them to the new sets of readings, an evaluation of the long-term performance and reliability of the instruments was obtained. The fourth objective of the research was to collect the previous and new data from the instrumentation and document it for a case history, now in its 16th year of service life. All the previous measurements were also calculated again in order to compare them with previous results and check the consistency of selecting the same initial reading date and following the same procedure. Also the same measuring probes and readout devices were used during the 2003 field measurements in order to minimize the error induced by using a different device. The results of the long term performance investigation for each instrument and the deformation patterns in the soil and geogrid are summarized separately as followings:

9.2 Conclusions

9.2.1 Embankment soil properties:

- The variation of moisture content and dry density of the compacted soil in the embankment from field density tests taken during construction was analyzed for the first time. The analyses show a large scatter in properties and indicate that the fill soil would have a large variation in stress-strain properties. The range of moisture contents indicate that the undrained strength would vary from less than 20 kPa to over 200 kPa. Such a large variation in soil properties would have a significant influence on soil and geogrid strains.

9.2.2 Thermocouples:

- The readout device, connection boxes and thermocouples all have functioned properly since their installation time. Only two thermocouples out of 97 failed which gives a survival rate of about 98% and shows that the installation procedure for these thermocouples was successful.

- As the distance into the slope increases the maximum variation of temperature along the geogrid layer decreases. A 4°C to 5°C maximum temperature variation is observed from about 6 m from the slope face up to 12 m from the slope face.

9.2.3 Electrical wire resistance strain gauges:

- The EWR gauges were installed on geogrid longitudinal members to measure the strains developed in geogrids at different times during and after the embankment construction. The last set of

strain measurements was carried out in 1990. All the electrical connection boxes were cleaned up during 2003 field work and recalibration of the readout box was confirmed. The same readout box was used for 2003 measurements that was used for measurements before 1990. In the 2003 field measurements, 46 strain gauges out of 198 active EWR strain gauges installed on primary geogrids had failed with 16 of them failing between field measurements in 1990 and 2003.

- In total 54 dummy EWR strain gauges were installed on pieces of geogrid following the same procedures as used on the instrumented reinforcement and installed in the fill in the same manner in order to study the effect of environment on the strain measurements. Fifty-three of these gauges functioned properly during the 2003 field measurements.

- The dummy EWR strain gauge measurements show that before applying any temperature correction to eliminate the temperature induced strain from the measured strains, the strain variation in all dummy gauges are in a range of ±0.15% strain during the service life of the project, but when the temperature correction is applied the variations are more scattered and they are in a range of ±0.3% strain. It is argued that if no slippage occurred between the soil and grids, the geogrids confined with soil would not undergo thermal expansion or contraction from temperature changes. So instead of temperature induced strains, thermal stress or thermal force will occur in the geogrids with the magnitude depending on the elastic properties, temperature change and linear coefficient of thermal expansion. Therefore the application of temperature correction for eliminating temperature-induced strains from the

measured strains used for this project has underestimated or overestimated the final strains.

- The active EWR strain gauge measurements in 2003 illustrate that the profiles of strain variation along the geogrids are almost identical to the last sets of measurements in 1990 after the end of construction.

- Analyses of laboratory strain gauge calibration tests reported in the 1986 files were performed to evaluate and compare the global strains in the geogrids to the local EWR strain measurements. For the Tensar grid, different tests gave completely different correlations between local EWR strain measurements and global grid strains. At one EWR strain gauge location at the middle of the rib the local strain was four times the global strains. At the EWR strain gauge location at the node, the local strain was one-half the global strain. No record exists for the actual location of the EWR gauges on the Tensar ribs except for a sketch that indicates the gauges were between the middle of the rib and the node. It had to be concluded that the location of the EWR gauges on the Tensar grids is not known at the present time and a correlation between local EWR strain measurements and global grid strains cannot be determined for the Tensar geogrids. Previous analyses by other researchers of EWR strain measurements never considered the difference between local strains and global strains for the Tensar grids.

- The Signode laboratory tests indicated that the local EWR strain measurements were the same as the global strains in this geogrid. No laboratory measurements on the Paragrid geogrid were found. As this geogrid had a number of weakened joints, it

must be expected that the global grid strains would be considerably larger than the local EWR strain measurements.

- Bison inductance coil strain gauges were installed on all the geogrids to measure global strains and these were read to 1990. In 2003 the readout instrument did not work and a replacement readout device could not be found so no readings of these instruments were made during this research. Previous readings between August 1986 to September 1990 show a good survival rate with 77 of the 87 inductance coil strain gauges still working.

- Correlations were developed between the local EWR strain measurements and the global Bison strain measurements using measurements in 1987, 1988 and 1989. All correlations had a fairly wide scatter but average values for the Signode geogrid indicated that the local EWR strains and global grid strains were similar. For the Paragrid geogrids, the global strains were about 2.5 the local EWR strains. For the Tensar geogrid, the local and global strains were similar which is a completely different result from the laboratory tests in the 1986 files.

9.2.4 Vertical inclinometers at toe:

- The vertical inclinometers installed at the toe of the slopes measured the horizontal movement of the foundation soil below the toe of slopes. The two sets of measurements in 2003 revealed consistent results and showed that no considerable amount of horizontal deformation had occurred since 1990. The difference in horizontal deflection between 1990 and 2003 near the ground surface was 1 mm to 5 mm out of 15 mm to 30 mm total horizontal deflection. At 0.5 m depth, 7 mm to 18 mm additional

horizontal deflection between 1990 and 2003 occurred for a total deflection of 56 mm to 92 mm.

9.2.5 Vertical inclinometers at crest:

- The last previous readings at these inclinometers were taken 12 August, 1986 before the final 6 m of fill were placed. Damage to these inclinometer tubes during the August-October, 1986 fill construction prevented further readings. In 2003, a small length probe was obtained and inclinometer readings were taken for the first time showing the horizontal deflection of the embankment resulting from the top 6 m fill load.

- Measurements for the Signode section could not be made because the probe became stuck inside the access tube and could not be retrieved. The measured horizontal deformation pattern in the slope direction in 2003 showed that above the +5.2 m elevation, the horizontal deformation increased very dramatically such that in the Tensar section it increased from 58 mm at the +5.2 m elevation to 635 mm at the +7.2 m elevation, in the Paragrid section it increased from 190 mm at the +5.2 m elevation to 434 mm at the +7.2 m elevation and finally in the unreinforced section it increased from 135 mm at the +5.2 m elevation to 500 mm at the +7.2 m elevation. In other words after the placement of the top 6 m of fill the top 7 m of each slope section underwent a substantial amount of horizontal deformation which caused critical bends and deformations in the vertical access tubes of the inclinometers at the crest of slopes. Substantial horizontal deformations also occurred at the base of the fill which bent the inclinometer tubes so much that even the

short probe could not pass this depth in the Paragrid and unreinforced sections.

9.2.6 Horizontal inclinometers:

- The two sets of measurements made in 2003 are quite consistent with each other and the settlement profiles measured in 2003 at all sections show that the trend followed the settlement trend measured in the 1990 field measurements, except at the Paragrid reinforced section at the +2 m elevation where there is slight change in the settlement profile since 1990. The absolute amount of settlements measured by vertical extensometers at the crest of slopes was used in order to locate the elevation of the horizontal inclinometers inside of the fill.

- At the ground surface only about 6 mm additional settlement occurred in the foundation soil in the locations close to the center line of the fill in all sections of the fill between 1990 and 2003. At 2 m elevation above the ground surface all sections showed a similar amount of increase in settlement since 1990, in the range of 46 to 54 mm but the increase of settlement at 4 m elevation was different for the northern and southern sections. The maximum settlement in the northern sections increased about 135 mm since the 1990 measurements but the southern sections experienced an increase in maximum settlement of about 78 mm. The measurements also showed that the maximum amount of settlement at the 0 m, +2 m and +4 m elevations in the northern sections were higher than the maximum settlement at the southern sections which might have been due to having different moisture contents or compaction effort during the construction of the embankment and a difference in foundation soil properties.

The access tubes for the inclinometers at the 6 m elevation were blocked and were not accessible due to damage during the third construction stage.

9.2.7 Vertical extensometers at toe:

- The vertical extensometers at the toe of the slopes showed some additional settlement at the different test sections in the range of 1 to 13 mm at different depths in the foundation soil between 1990 and 2003.

9.2.8 Vertical extensometer at crest:

- The last previous readings at these extensometers were taken 12 August, 1986 before the final 6 m of fill were placed. Damage to these extensometer tubes during the August-October, 1986 fill construction prevented further readings. In 2003, a small size probe was modified and extensometer readings were taken for the first time showing the settlement of the embankment resulting from the top 6 m fill load.

- Two consistent measurements in 2003 showed that the settlement of the fill and foundation soil increased almost linearly from a depth of -6 m to +5.5 m and reached values between 440 and 514 mm at +5.5 m elevation. The increase in settlement at +5.5 m from the top 6 m fill load varied from 276 mm to 299 mm.

9.2.9 Horizontal extensometers:

- Horizontal extensometers were installed inside the test fill at 0 m, +2 m, +4 m and +6 m elevation above the ground surface in order

to measure the soil horizontal strains or displacements. The horizontal extensometers at 6 m elevation were blocked during the 1988 construction season and no measurements could be taken in 2003 as well.

- The measurements made in 2003 at the other three elevations, fifteen years after the end of construction, and the last set of measurements in 1990, showed that the soil horizontal strains follow a pattern of variation similar to the previous measurements and almost no significant soil horizontal strain was developed in the fill since 1990.

9.2.10 Pneumatic piezometers:

- In the 2003/2004 field measurements, 21 out of the 35 piezometers in the embankment could be identified and functioned properly and 8 of the 20 piezometers in the foundation could be identified and functioned properly for a total of 29 or 53% of the 55 installed.

- The embankment piezometers had pore pressures between 14 kPa and 39 kPa in 1990 and consolidation reduced their pore pressures to between 5 kPa and 8 kPa in 2003/2004. The foundation piezometers had pore pressures between 2 kPa and 5 kPa in 1990 and these increased to between 6 kPa and 10 kPa in 2003/2004, probably from a rise in the ground water table below the embankment.

- Most of the damage to the piezometers happened during the clean-up activities with the backhoe in 2003 when the debris from

soil sloughing was excavated from around the terminal boxes and the piezometers plastic tubes were damaged and disconnected.

9.2.11 Comparison between measurements:

- The soil horizontal strains at 0 m elevation or at the ground surface in all 4 test sections were fairly small and similar. But at 2 m and 4 m in the fill the difference between the horizontal soil strain variations between different sections was considerable. The fill soil had a very large variation in moisture content and density and hence the stress-strain behavior of the fill soil varied significantly at different locations and elevations inside the fill. Therefore comparing the soil horizontal strains at different reinforced sections with the unreinforced section could only be done on a qualitative basis.

- The failure mode of the unreinforced embankment slope was determined to be rotational with a circular shaped slip surface. Some tension cracks were found parallel to the crest on the top surface of the test fill at 2 to 3 m from the crest in unreinforced section. Also scarps were observed about 2 m below the crest of the slope demonstrating the occurrence of slope instability below the crest. In the reinforced slopes in the test embankment, other than for some shallow (<0.5 m) surface soil movements likely caused by cyclic freeze-thaw, there were no indications of instability.

- There is a good match between the horizontal movement of the soil measured by vertical inclinometers and horizontal extensometers in August 1988, but there is not a good agreement between the measurements in 2003.

- The absolute amounts of settlements for horizontal inclinometers were determined by vertical extensometer settlements during the 2003 field measurements. Therefore the amount of settlement shown by horizontal inclinometers match exactly with the amount of settlement shown by vertical extensometers at the crossing point of the vertical extensometers and the horizontal inclinometers. Leveling survey data could not be used due to incomplete data on the initial levels of the access tube ends. Also it was not possible to reconfirm the elevation of the deep bench mark.

9.3 Recommendations for the future research:

- In order to better understand the relation between the local and global strains in different geogrids, a Bison strain gauge readout device should be obtained and new sets of measurements taken on the inductance coil strain gauges to establish an updated field correlation between the local and global strains.
- Sections of geogrids, with the EWR and Bison strain gauges attached to them, should be cut out and tensile tests carried out to measure any difference in grid properties and to measure a correlation between local and global strains.
- Soil sampling can also be done and samples from different depths of the test sections can be taken for laboratory determination of the present soil properties. The change in strength parameters and consolidation of the fill soil can be evaluated with these tests.
- Field pullout tests on the geogrids, is another test that can be done in the field for further research on the pullout behavior under field conditions.

- Surcharging of the test fill and possibly loading it to failure can be another aspect of future work at the Devon test embankment.

Appendix A

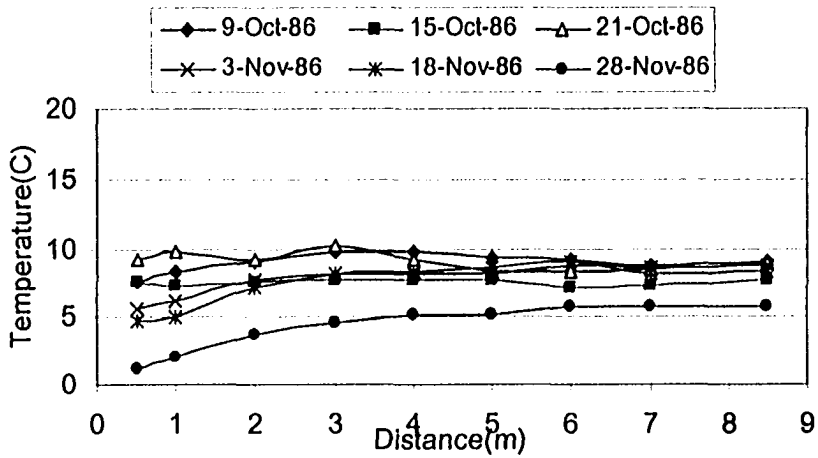

Figure 1. Temperature variation, Tensar bottom layer, 1986

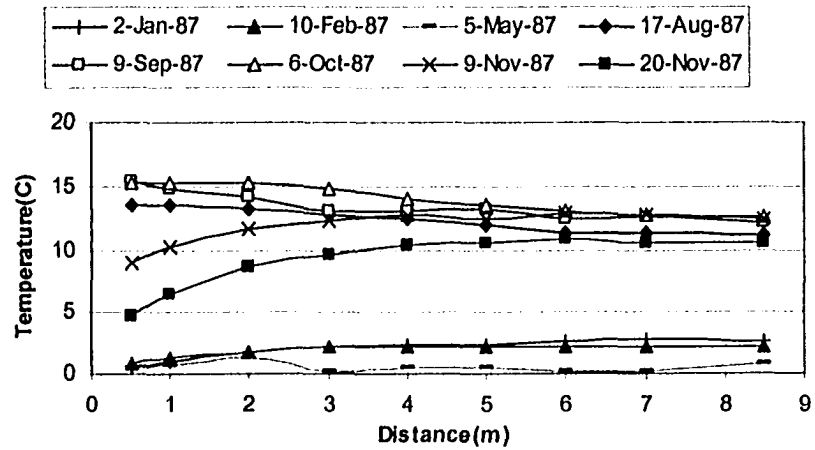

Figure 2. Temperature variation, Tensar bottom layer, 1987

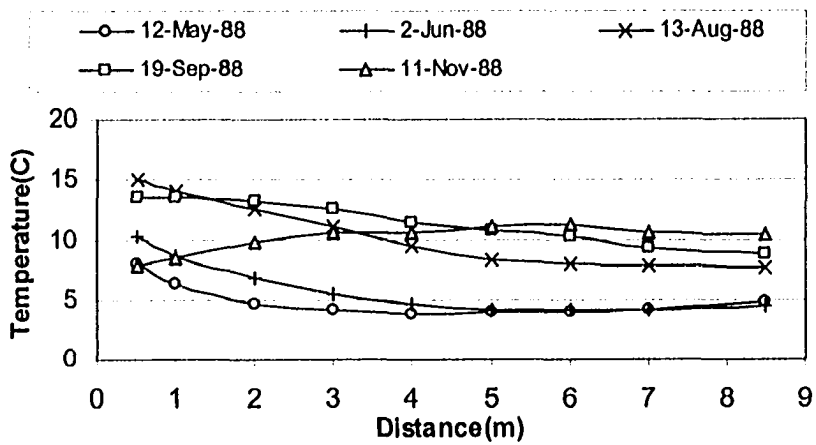

Figure 3. Temperature variation, Tensar bottom layer, 1988

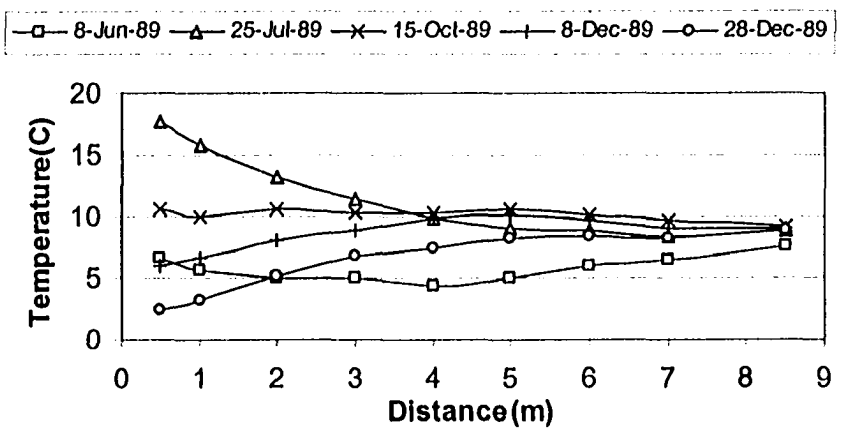

Figure 4. Temperature variation, Tensar bottom layer, 1989

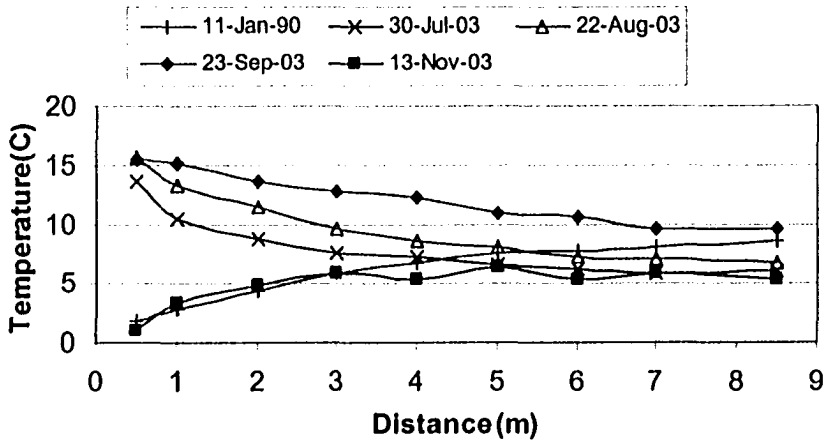

Figure 5. Temperature variation, Tensar bottom layer, 1990 & 2003

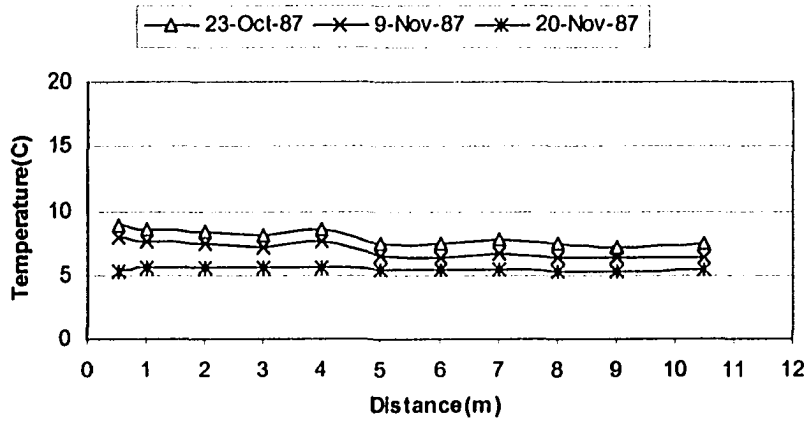

Figure 6. Temperature variation, Tensar top layer, 1987

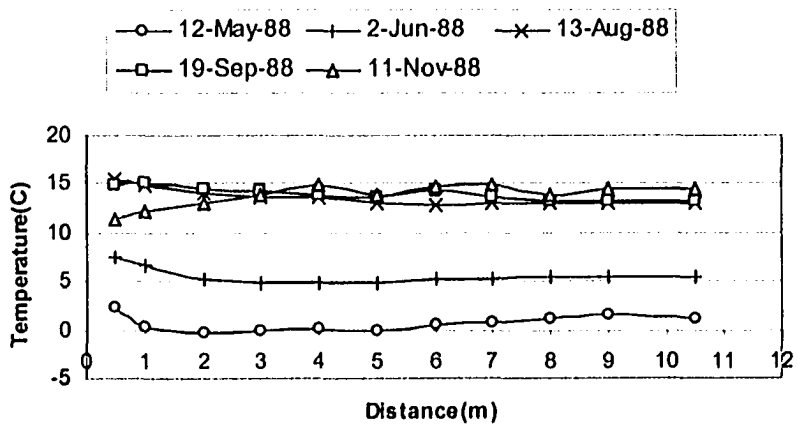

Figure 7. Temperature variation, Tensar top layer, 1988

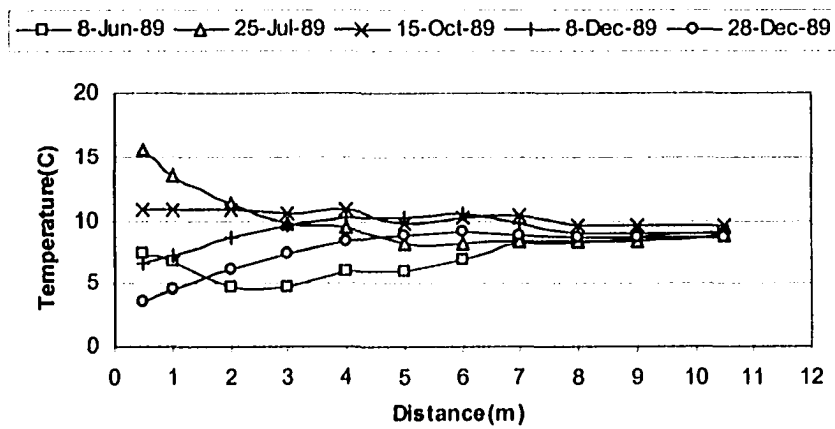

Figure 8. Temperature variation, Tensar top layer, 1989

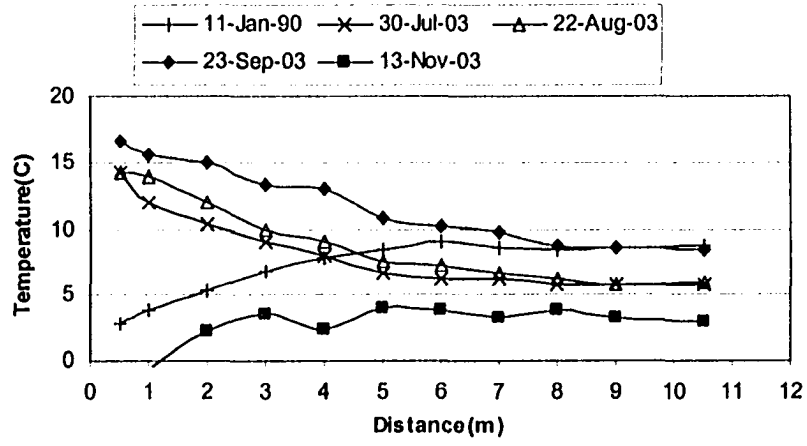

Figure 9. Temperature variation, Tensar top layer, 1990 & 2003

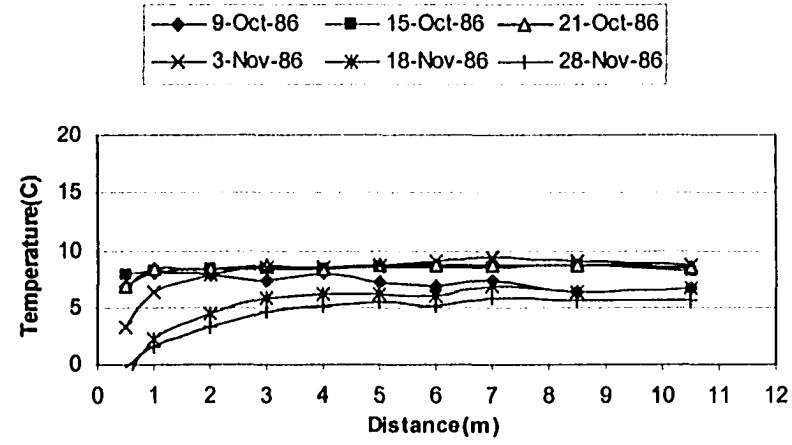

Figure 10. Temperature variation, Signode bottom layer, 1986

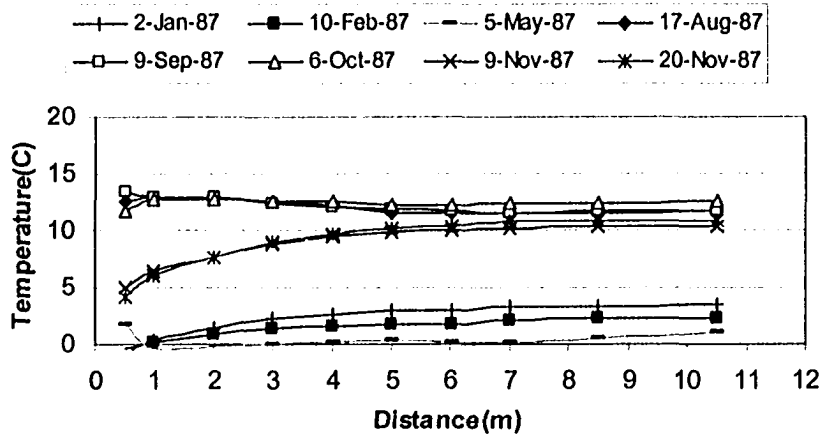

Figure 11. Temperature variation, Signode bottom layer, 1987

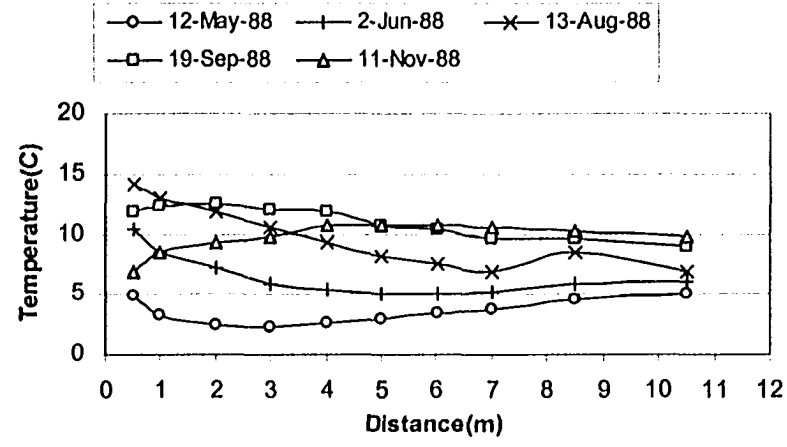

Figure 12. Temperature variation, Signode bottom layer, 1988

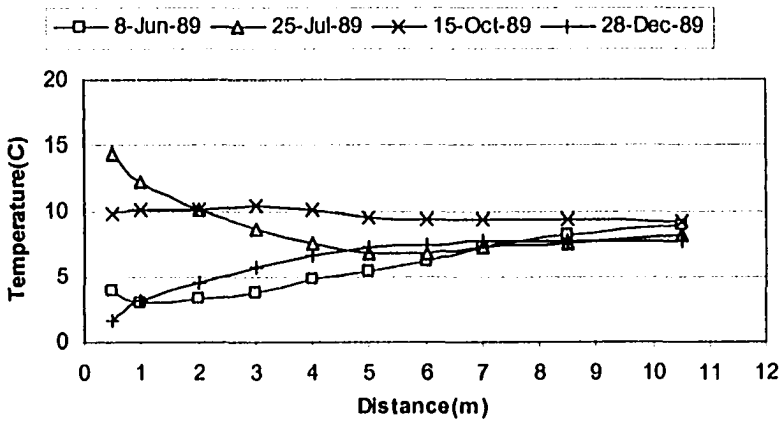

Figure 13. Temperature variation, Signode bottom layer, 1989

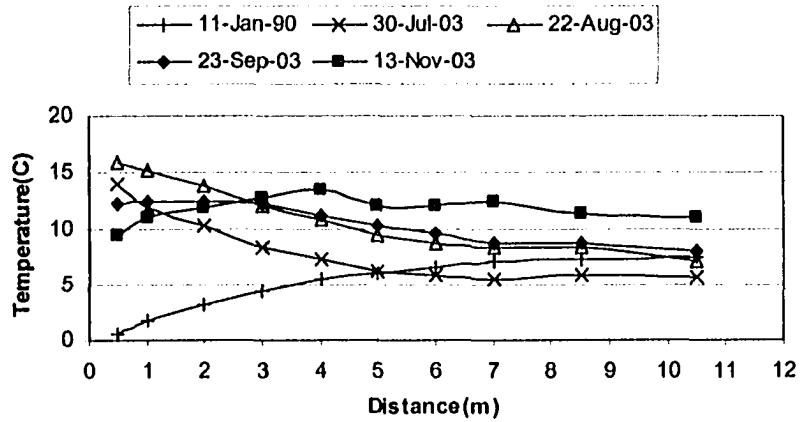

Figure 14. Temperature variation, Signode bottom layer, 1990 & 2003

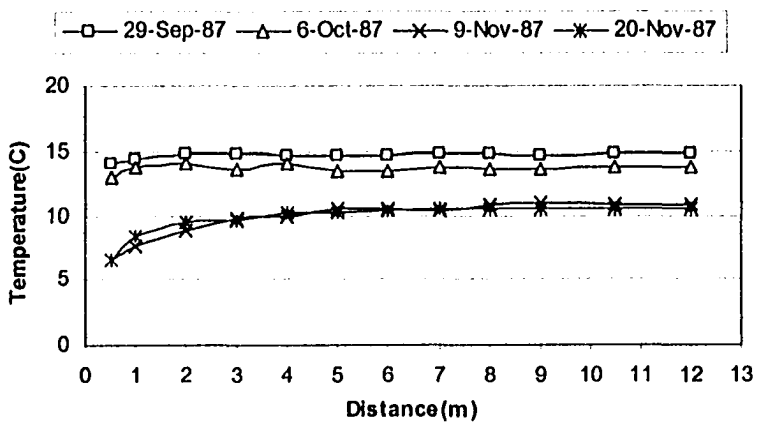

Figure 15. Temperature variation, Signode middle layer, 1987

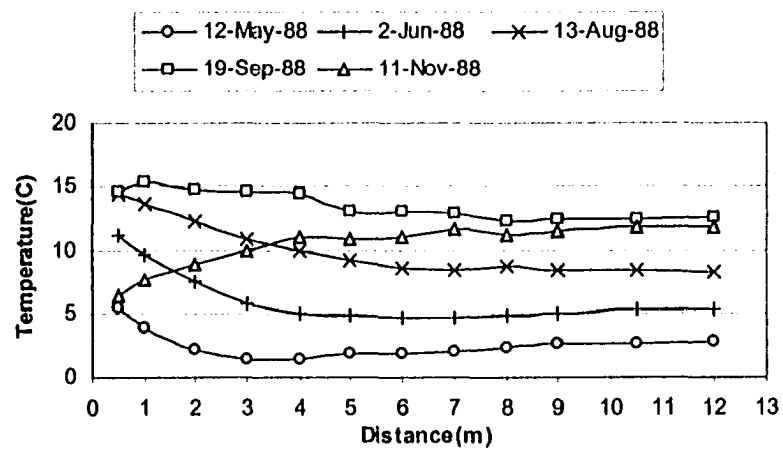

Figure 16. Temperature variation, Signode middle layer, 1988

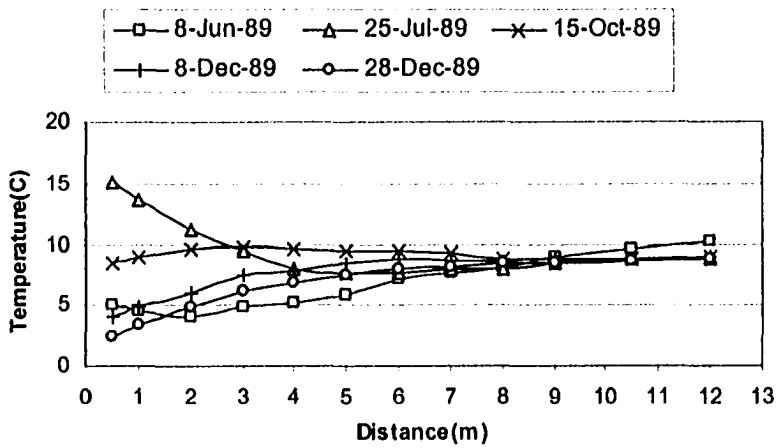

Figure 17. Temperature variation, Signode middle layer, 1989

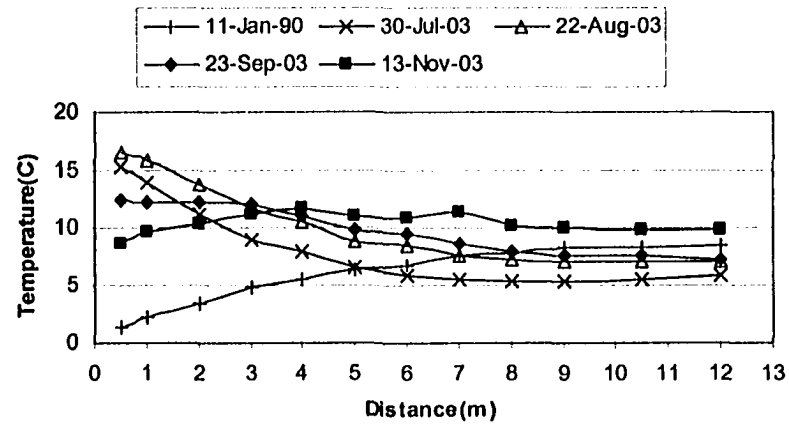

Figure 18. Temperature variation, Signode middle layer, 1990 & 2003

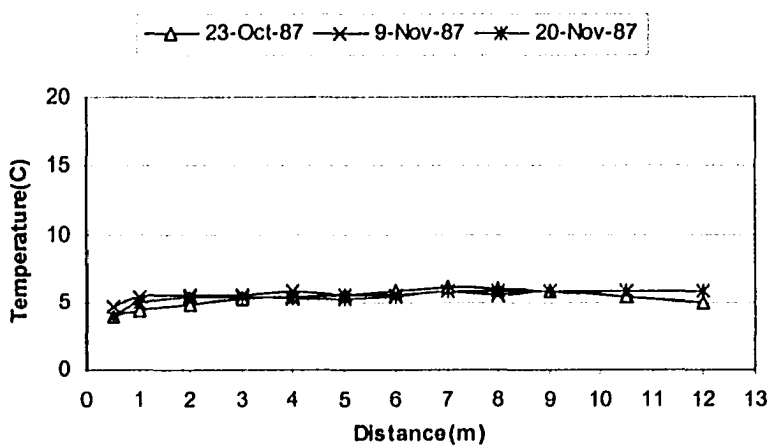

Figure 19. Temperature variation, Signode top layer, 1987

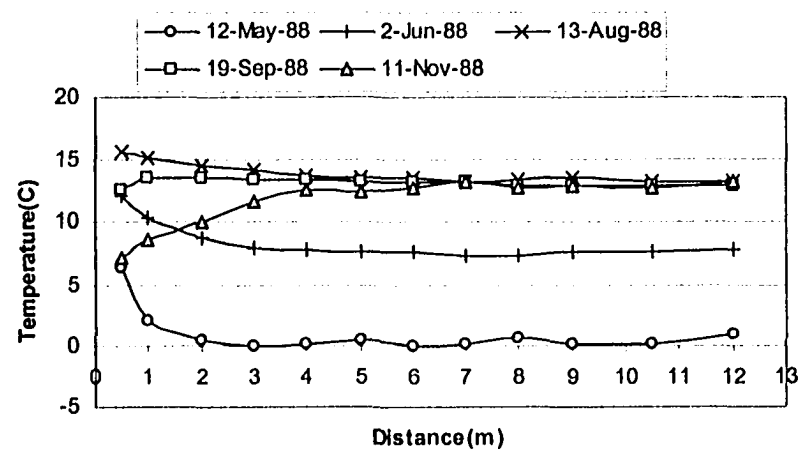

Figure 18. Temperature variation, Signode top layer, 1988

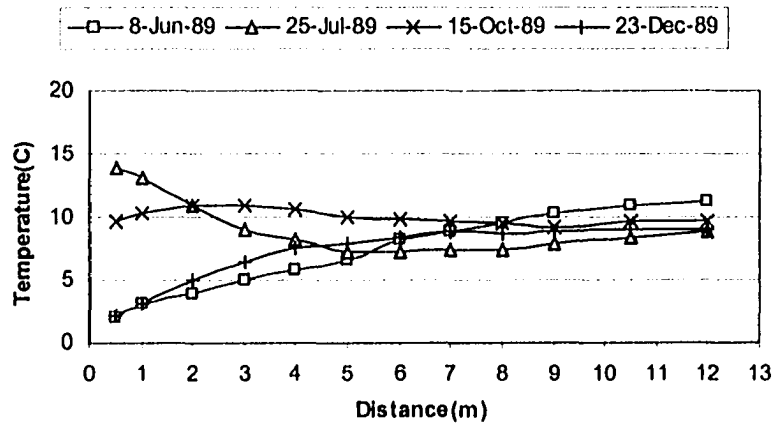

Figure 21. Temperature variation, Signode top layer, 1989

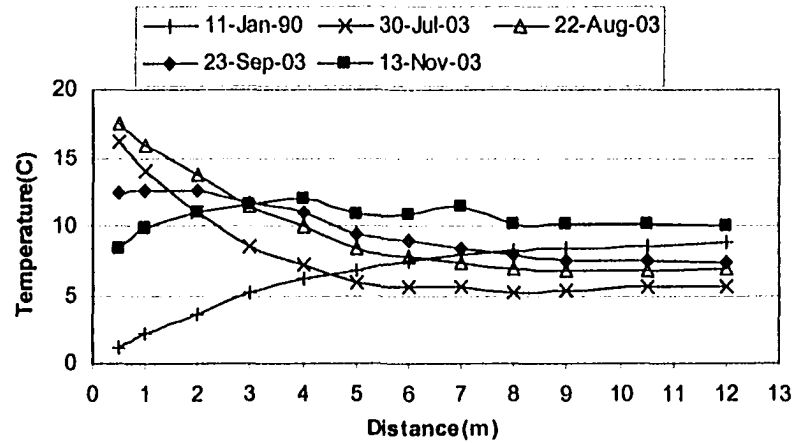

Figure 22. Temperature variation, Signode top layer, 1990 & 2003

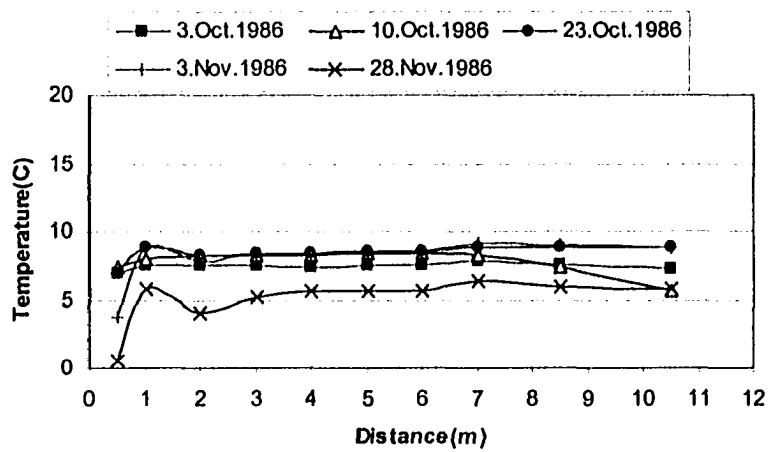

Figure 23. Temperature variation, Paragrid bottom layer, 1986

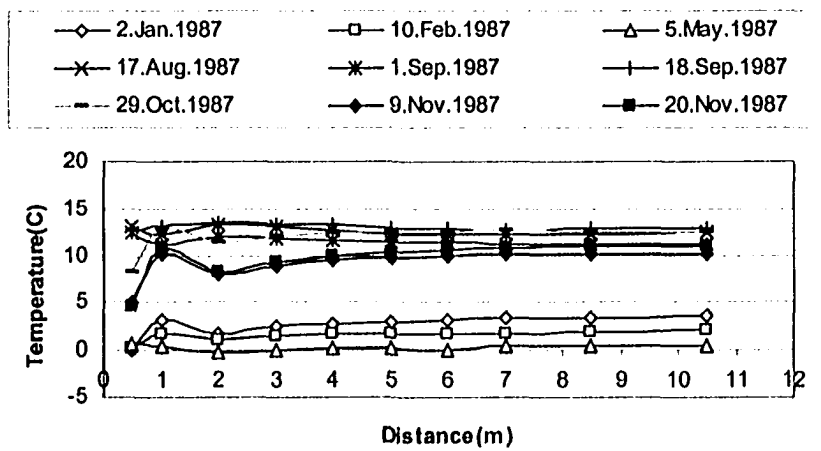

Figure 24. Temperature variation, Paragrid bottom layer, 1987

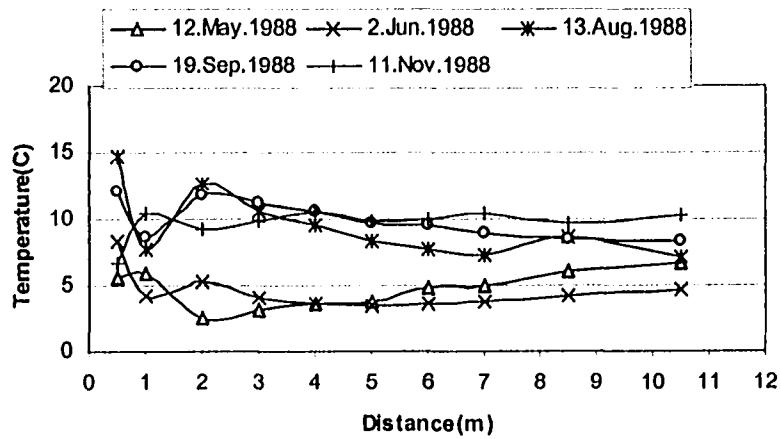

Figure 25. Temperature variation, Paragrid bottom layer, 1988

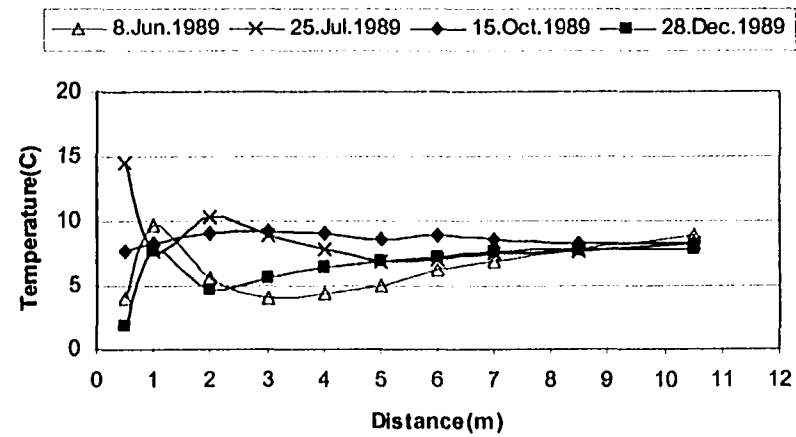

Figure 26. Temperature variation, Paragrid bottom layer, 1989

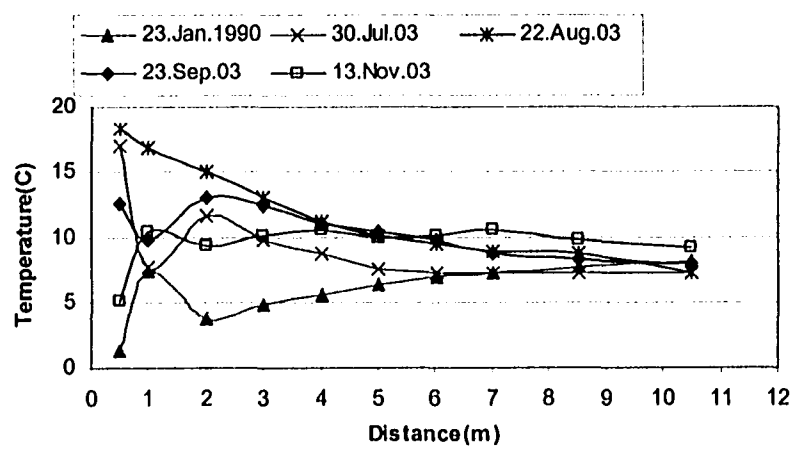

Figure 27. Temperature variation, Paragrid bottom layer, 1990 & 2003

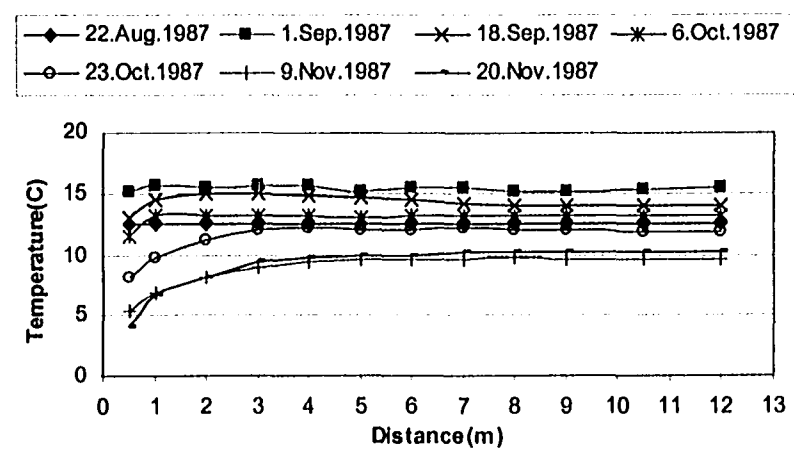

Figure 28. Temperature variation, Paragrid middle layer, 1987

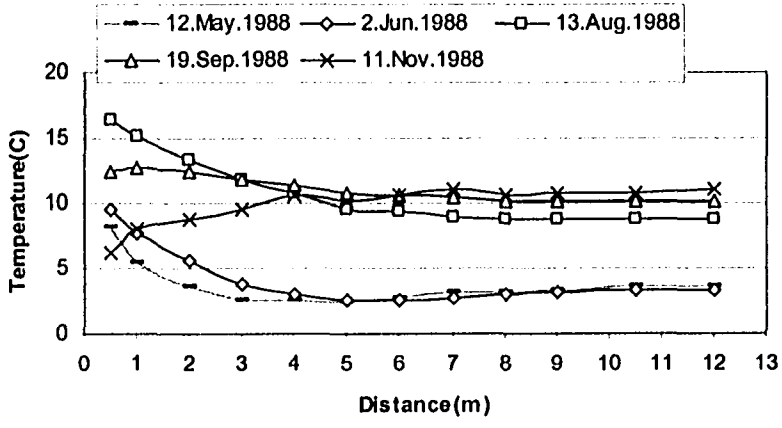

Figure 29. Temperature variation, Paragrid middle layer, 1988

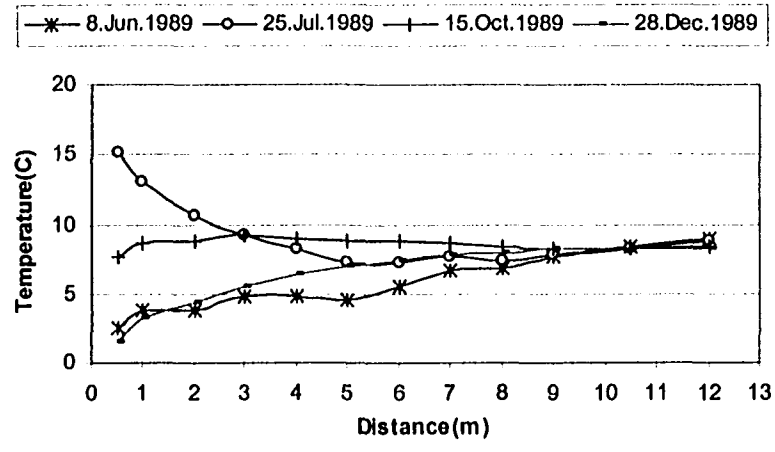

Figure 30. Temperature variation, Paragrid middle layer, 1989

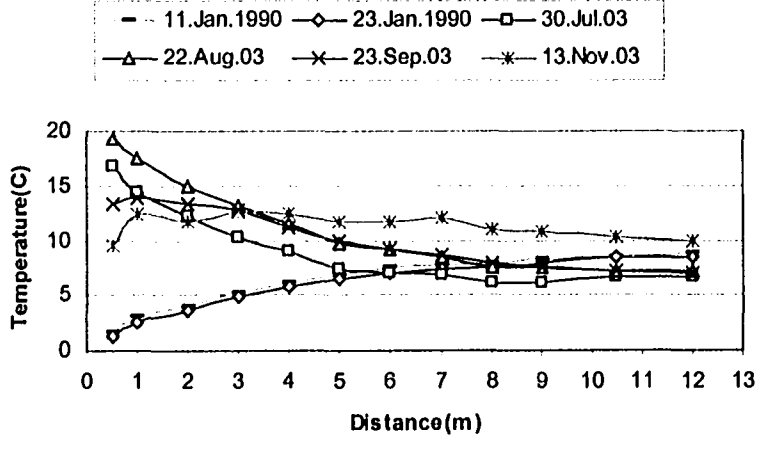

Figure 31. Temperature variation, Paragrid middle layer, 1990 & 2003

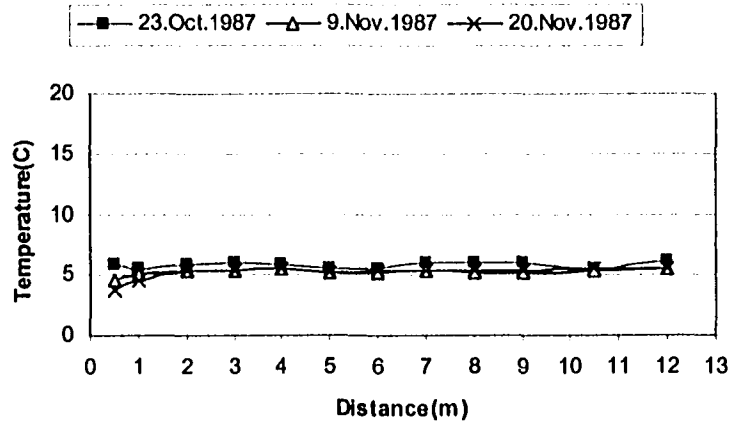

Figure 32. Temperature variation, Paragrid top layer, 1987

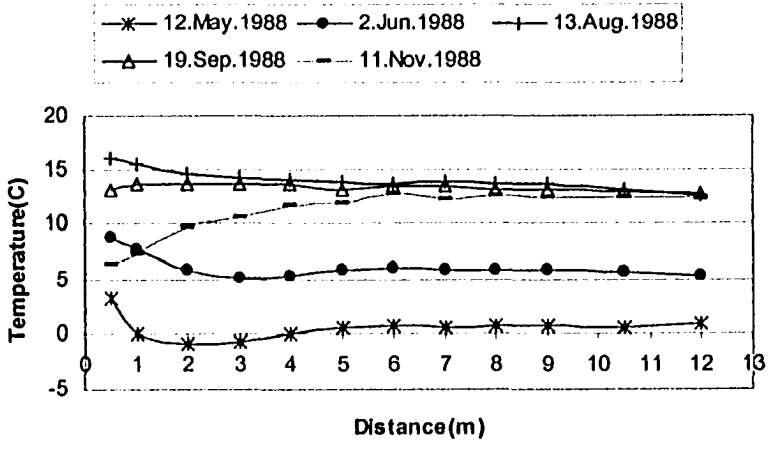

Figure 33. Temperature variation, Paragrid top layer,1988

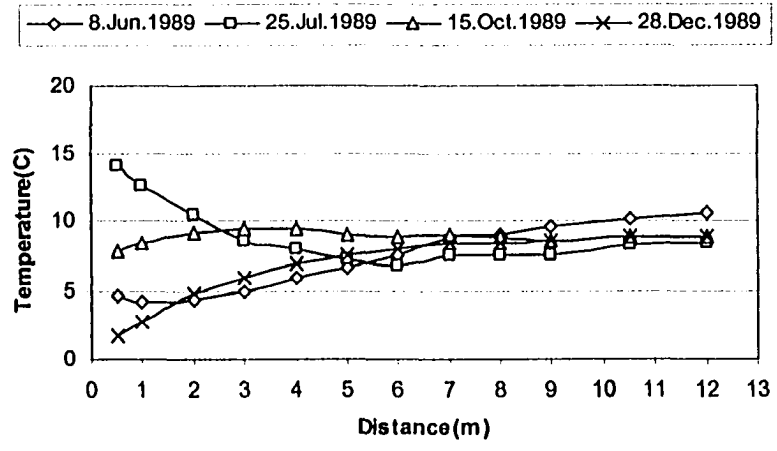

Figure 34. Temperature variation, Paragrid top layer, 1989

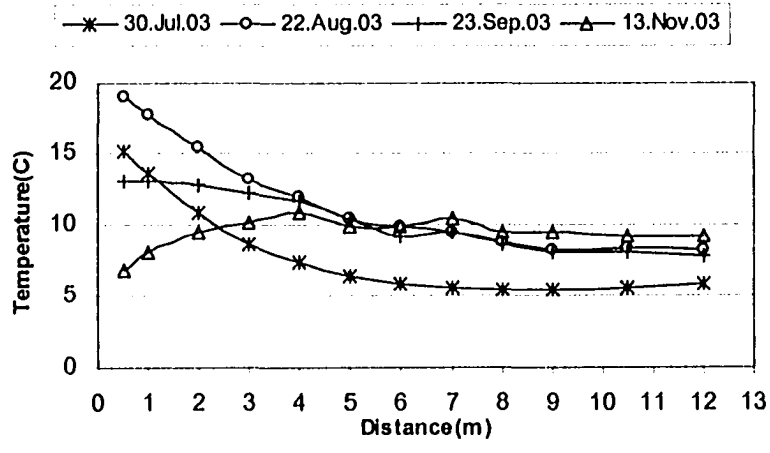

Figure 35. Temperature variation, Paragrid top layer, 1990 & 2003

Appendix B

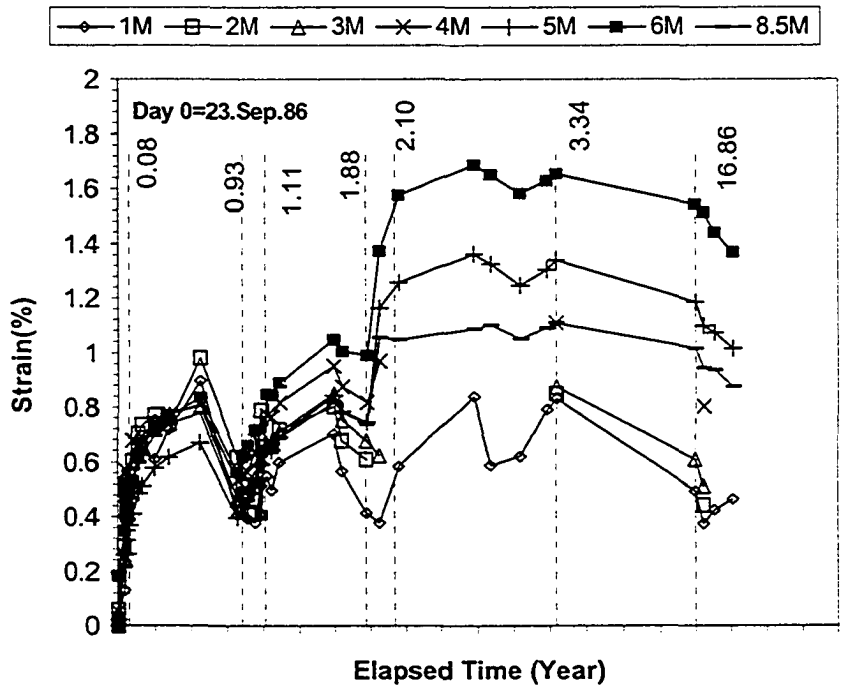

Figure 1. EWR strain gauge variation including 2003 measurements- Signode bottom layer

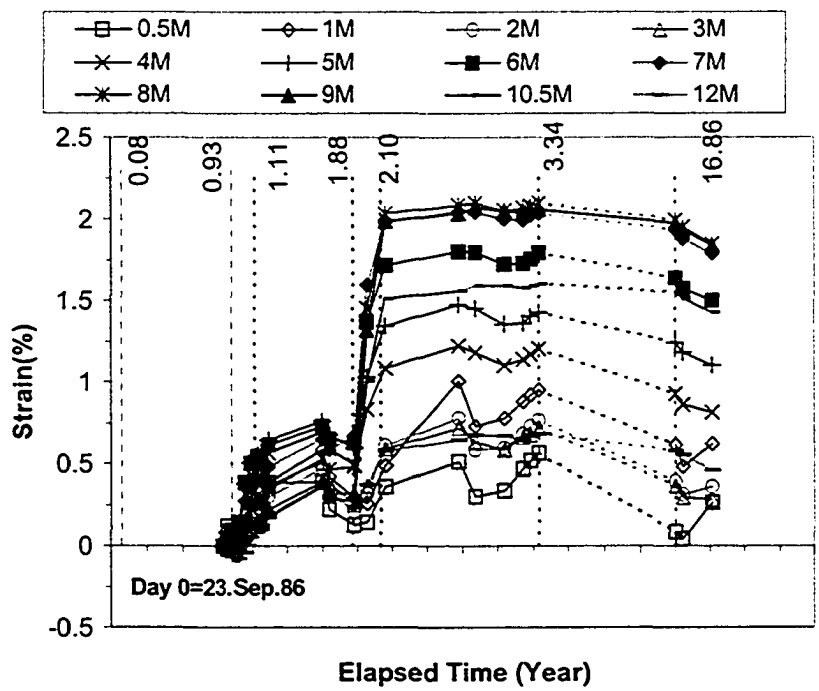

Figure 2. EWR strain gauge variation including 2003 measurements- Signode middle layer

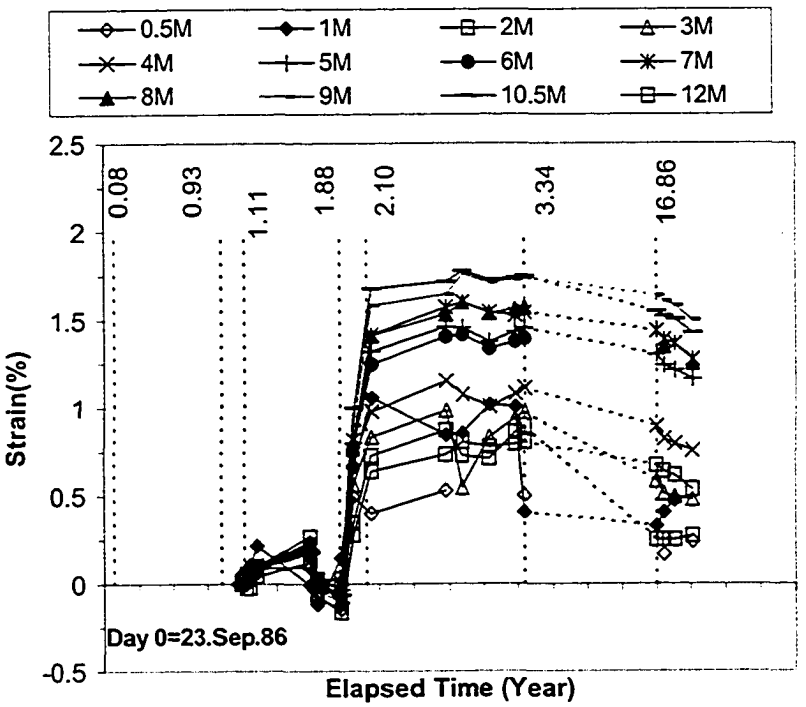

Figure 3. EWR strain gauge variation including 2003 measurements-Signode top layer

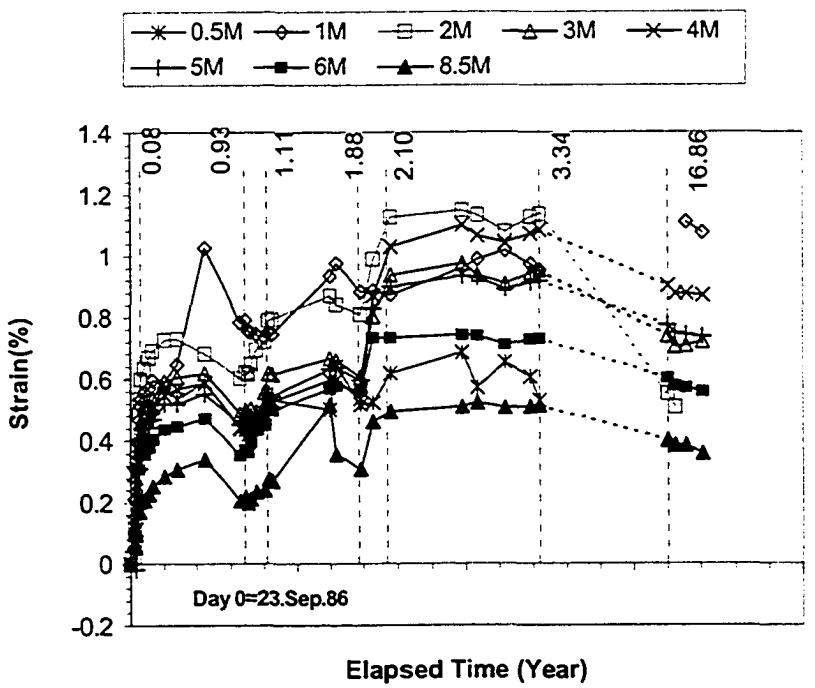

Figure 4. EWR strain gauge variation including 2003 measurements-Paragrid bottom layer

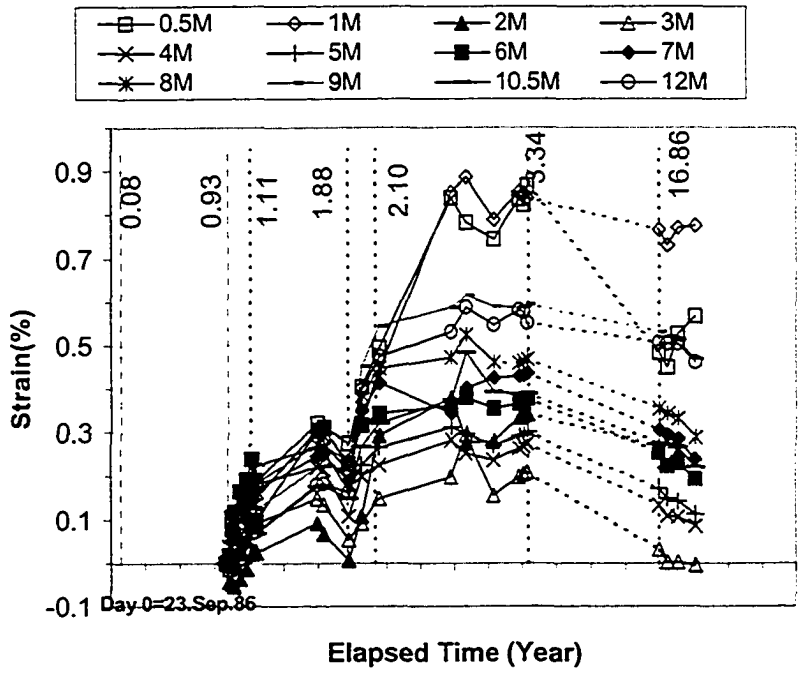

Figure 5. EWR strain gauge variation including 2003 measurements- Paragrid middle layer

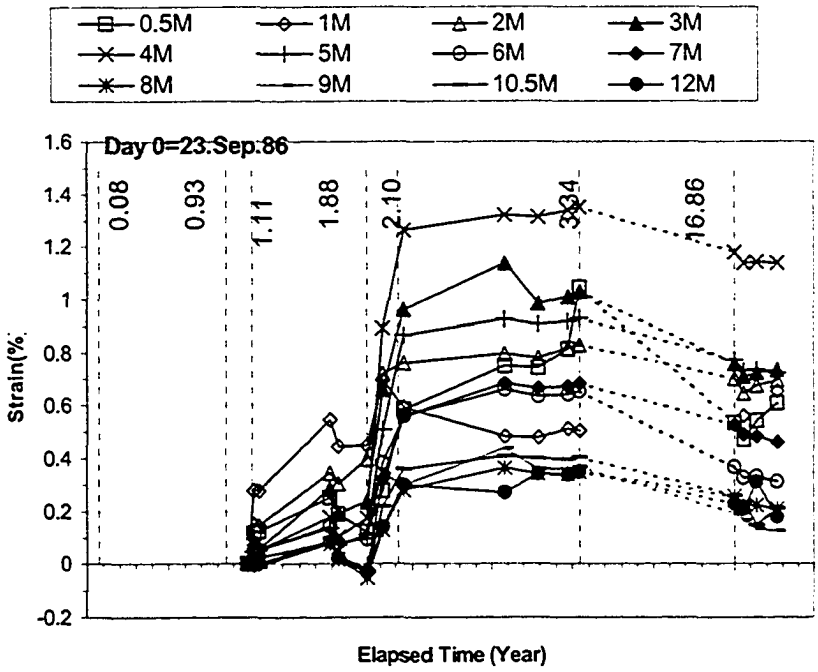

Figure 6. EWR strain gauge variation including 2003 measurements- Paragrid top layer

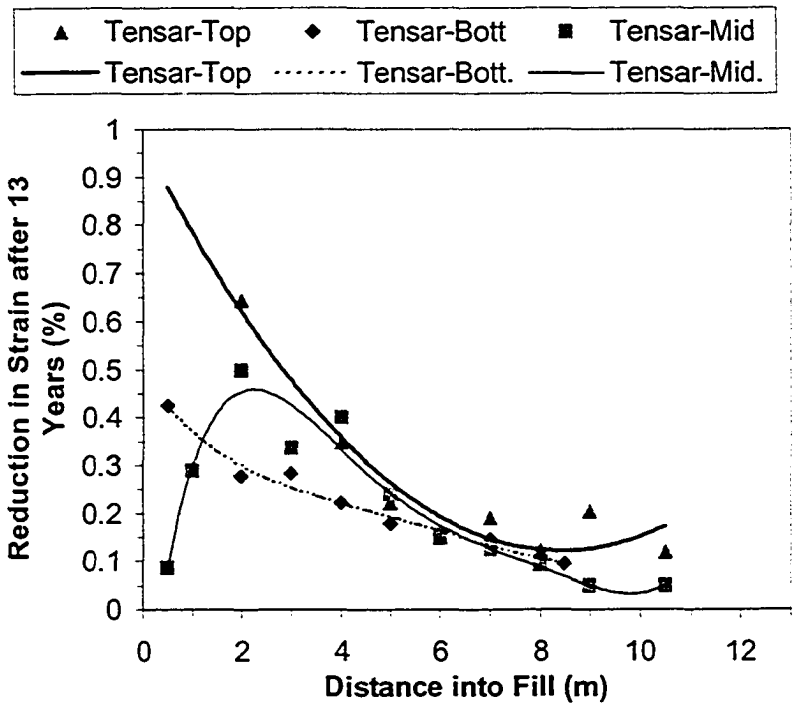

Figure 7. Reduction in strain between 1990 and 2003 field measurements - Tensar section

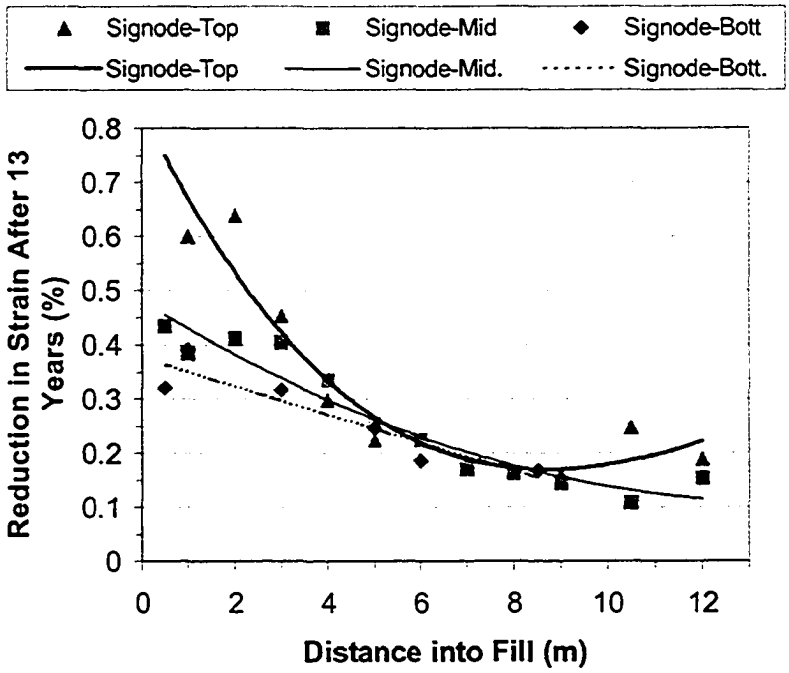

Figure 8. Reduction in strain between 1990 and 2003 field measurements - Signode section

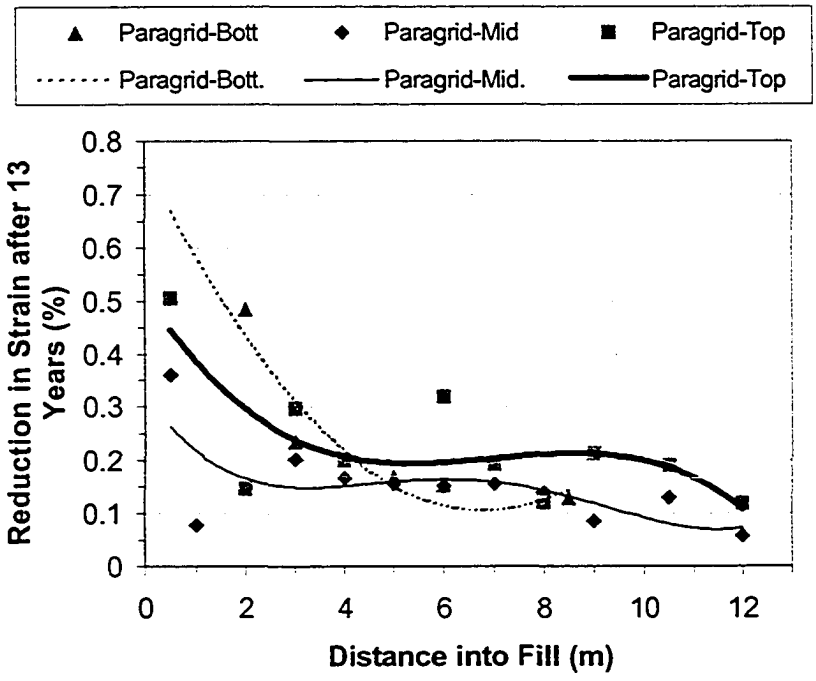

Figure 9. Reduction in strain between 1990 and 2003 field measurements - Paragrid section

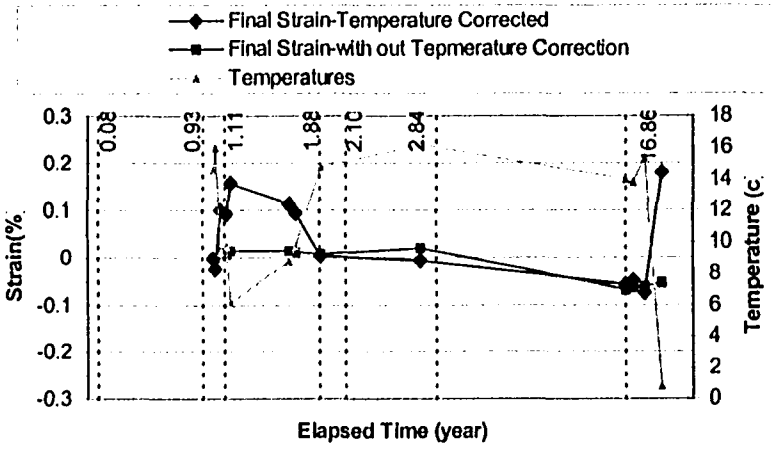

Figure10. Dummy EWR gauge strain variation-Tensar mid.-0.5m

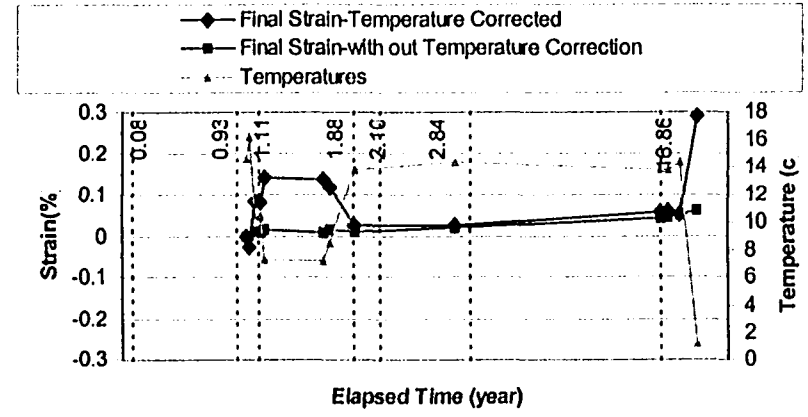

Figure11. Dummy EWR gauge strain variation-Tensar mid.-1m

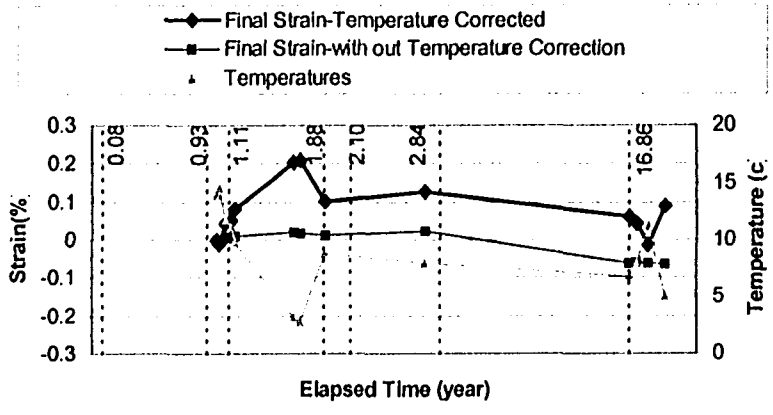

Figure12. Dummy EWR gauge strain variation-Tensar mid.-5m

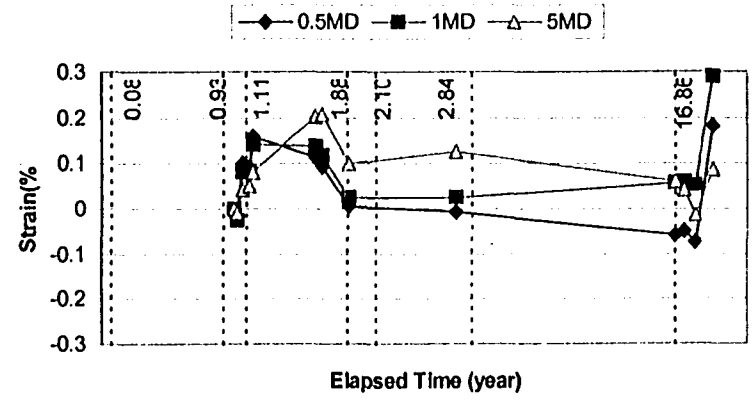

Figure13. Dummy EWR gauge strain variation-Tensar mid.

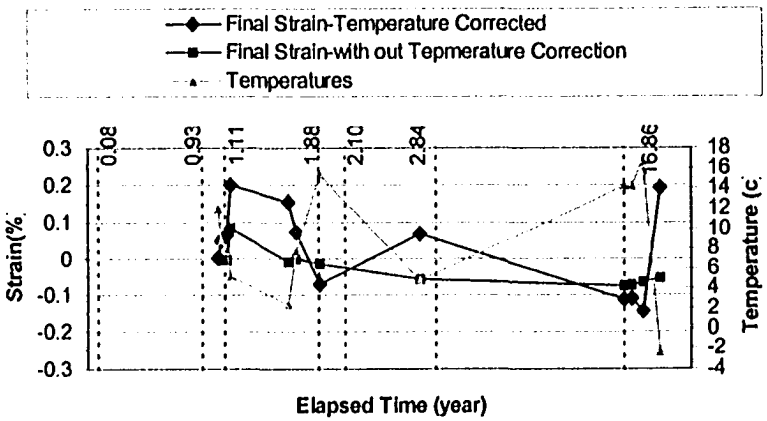

Figure14. Dummy EWR gauge strain variation-Tensar top.-0.5m

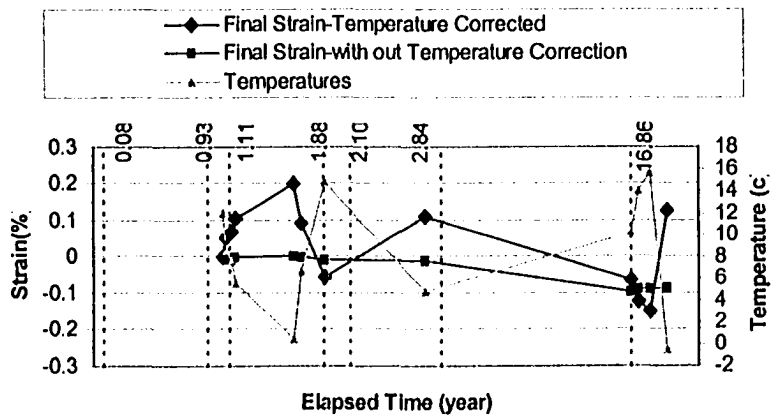

Figure15. Dummy EWR gauge strain variation-Tensar top-1m

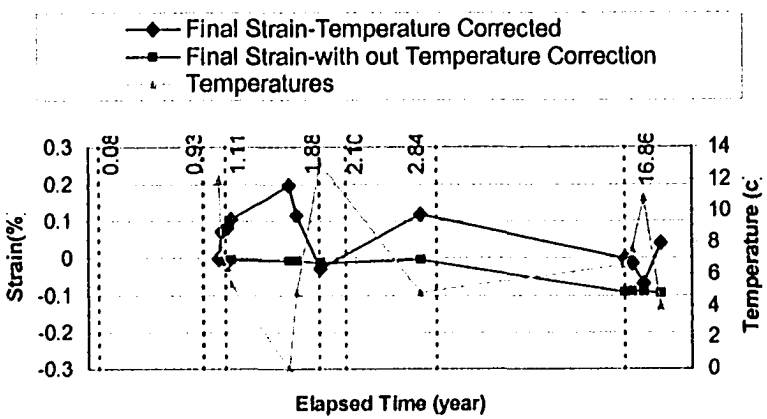

Figure16. Dummy EWR gauge strain variation-Tensar top-5m

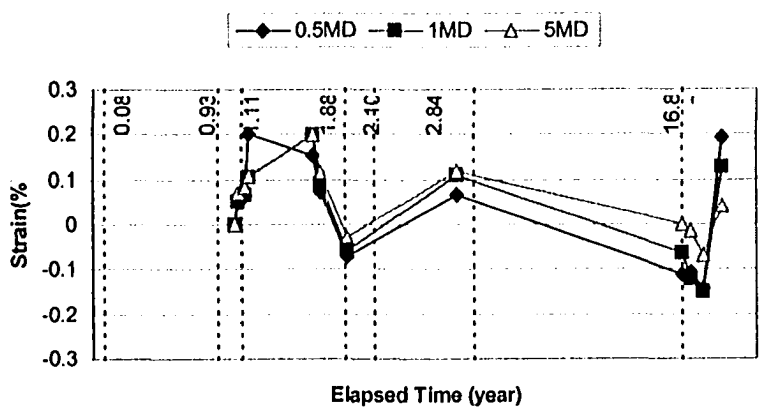

Figure17. Dummy EWR gauge strain variation-Tensar top.

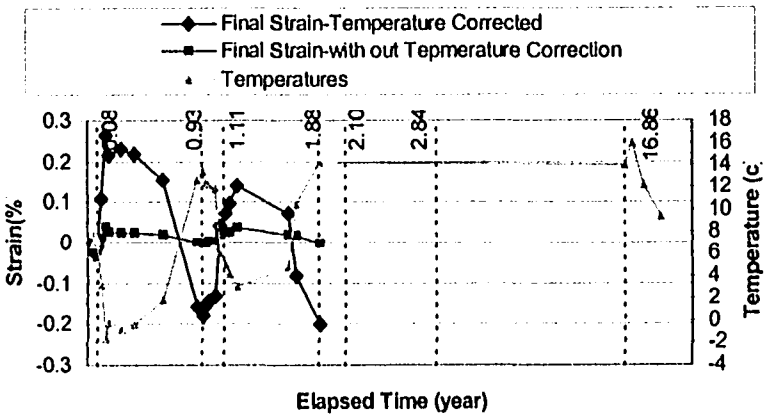

Figure18. Dummy EWR gauge strain variation-Signode bot.-0.5m

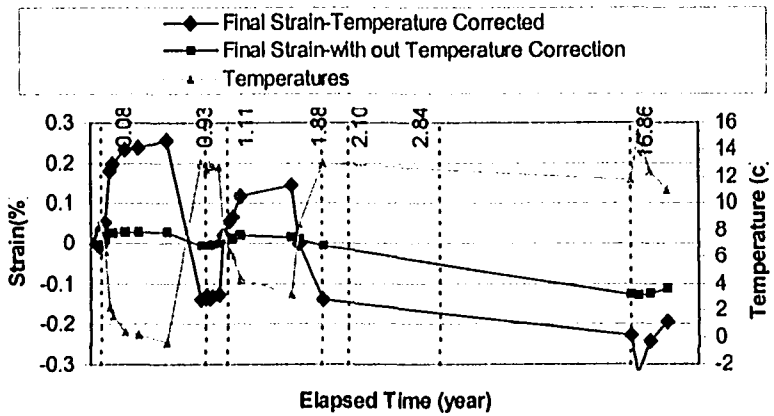

Figure19. Dummy EWR gauge strain variation-Signode bot.-1m

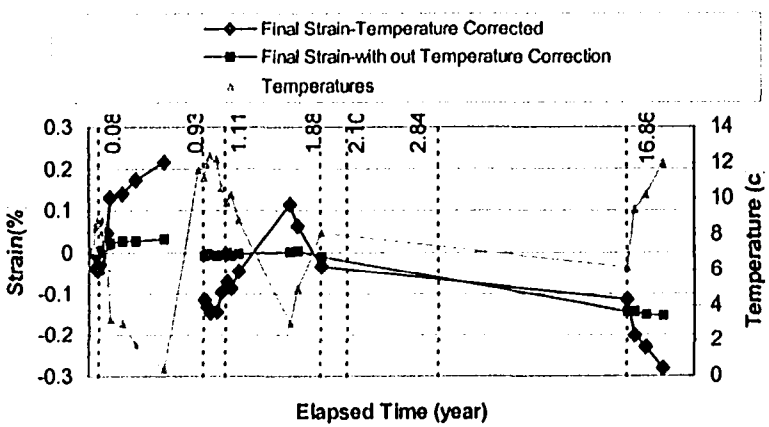

Figure20. Dummy EWR gauge strain variation-Signode bot.-5m

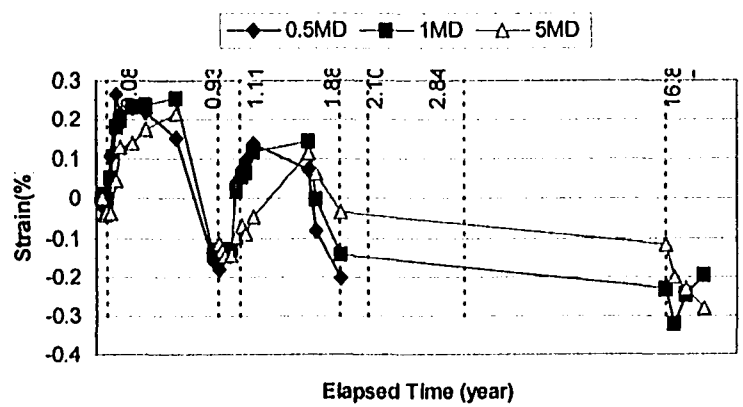

Figure 21. Dummy EWR gauge strain variation-Signode bot.

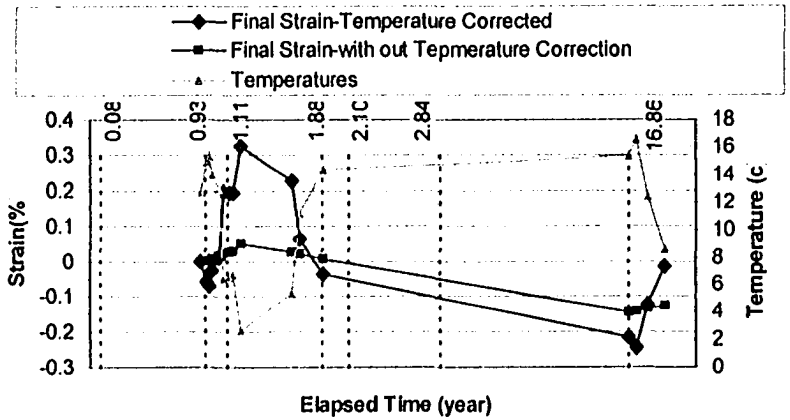

Figure22. Dummy EWR gauge strain variation-Signode mid.-0.5m

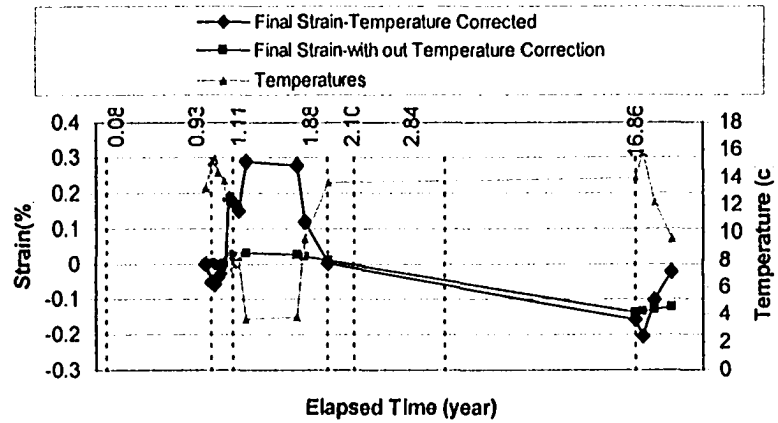

Figure 23. Dummy EWR gauge strain variation-Signode mid.-1m

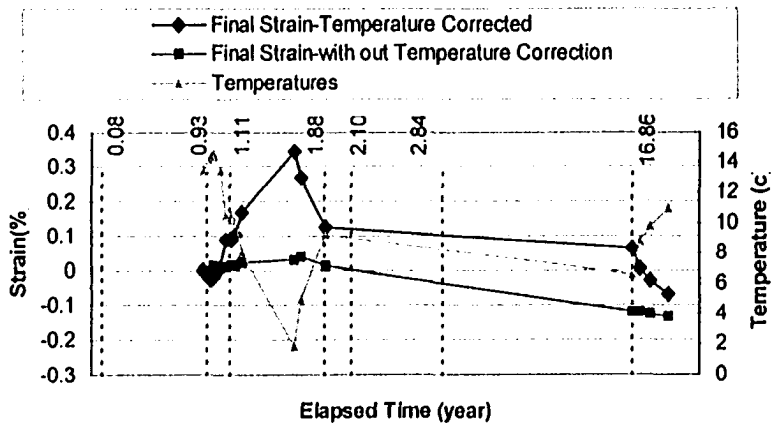

Figure24. Dummy EWR gauge strain variation-Signode mid.-5m

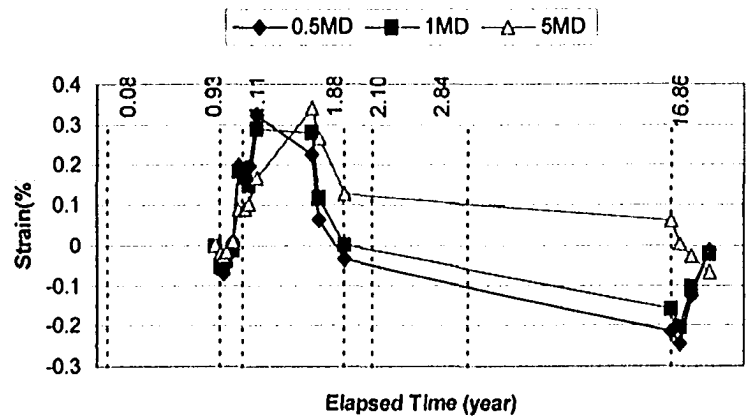

Figure 25. Dummy EWR gauge strain variation-Signode mid.

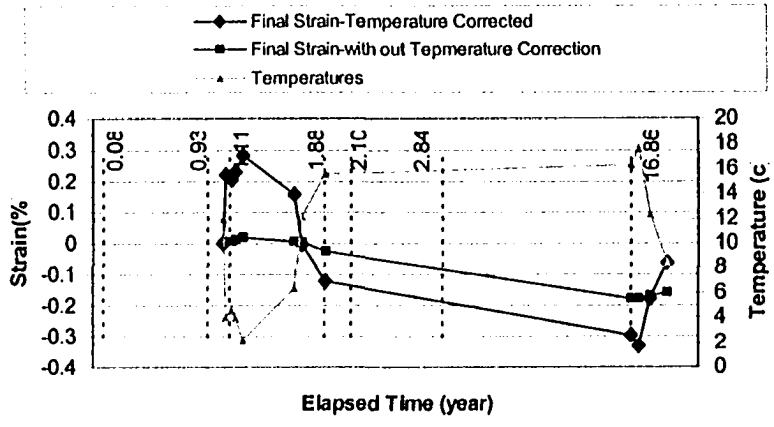

Figure26. Dummy EWR gauge strain variation-Signode top-0.5m

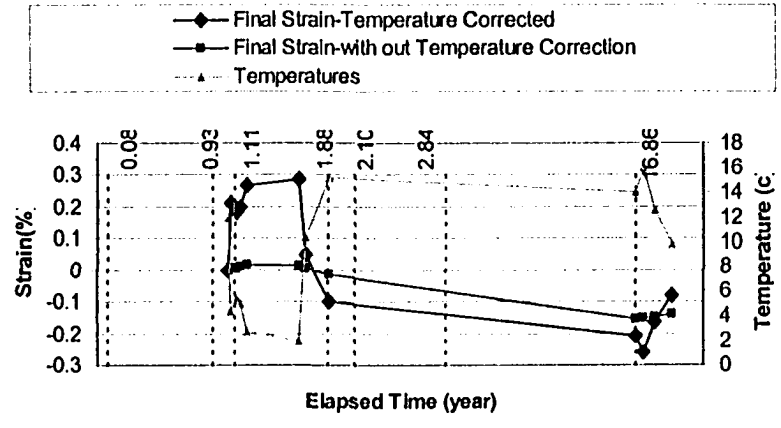

Figure 27. Dummy EWR gauge strain variation-Signode top-1m

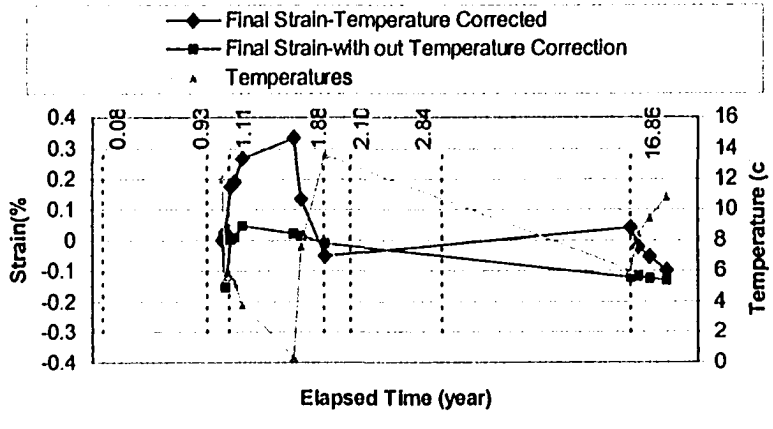

Figure28. Dummy EWR gauge strain variation-Signode top-5m

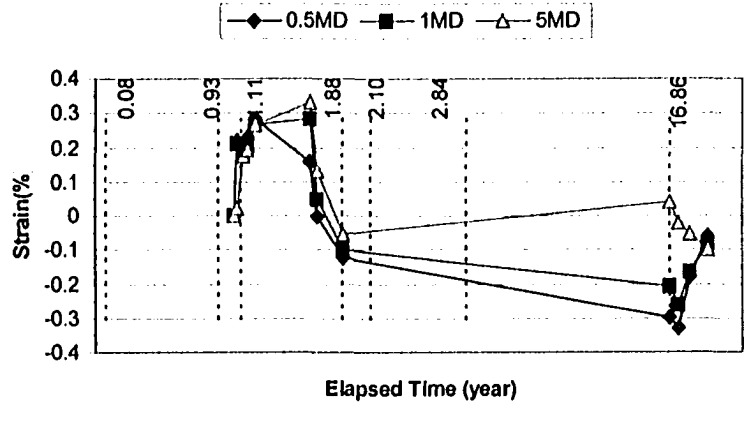

Figure 29. Dummy EWR gauge strain variation-Signode top

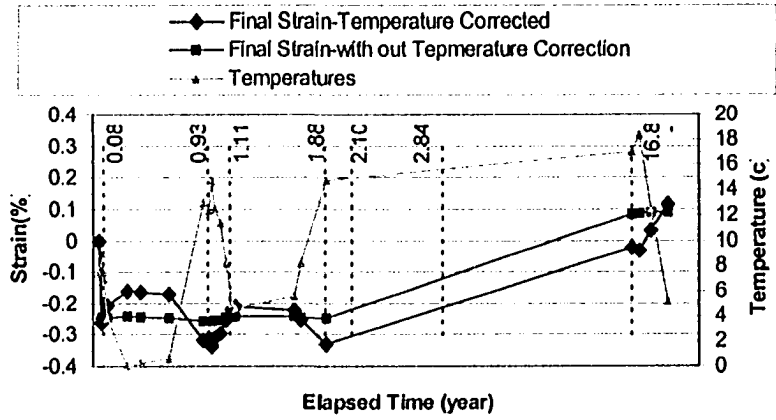

Figure 30. Dummy EWR gauge strain variation-Paragrid bott.-0.5m

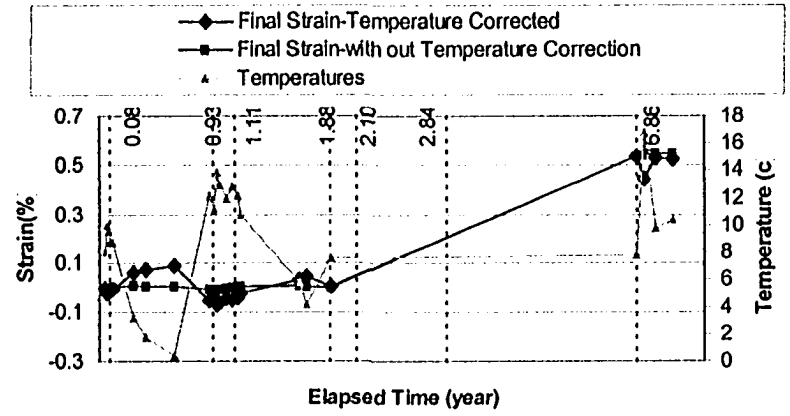

Figure 31. Dummy EWR gauge strain variation-Paragrid bott.-1m

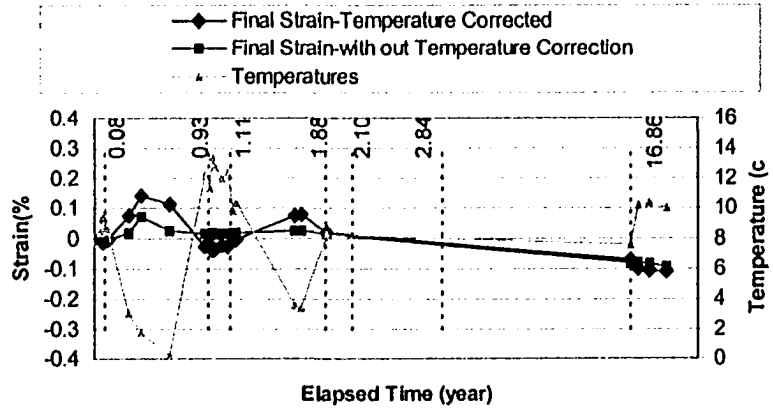

Figure 32. Dummy EWR gauge strain variation-Paragrid bott.-5m

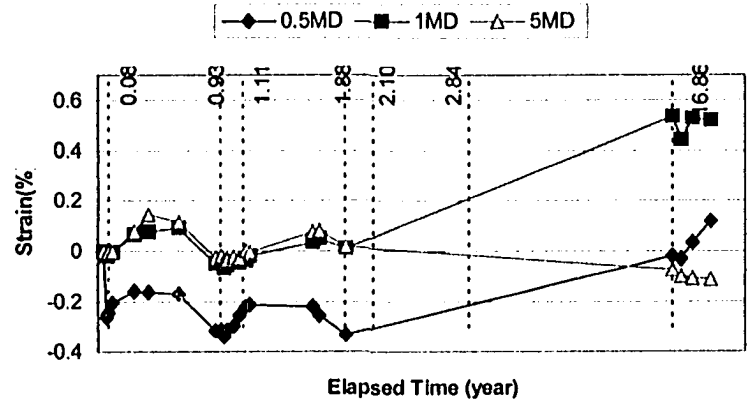

Figure 33. Dummy EWR gauge strain variation-Paragrid bott.

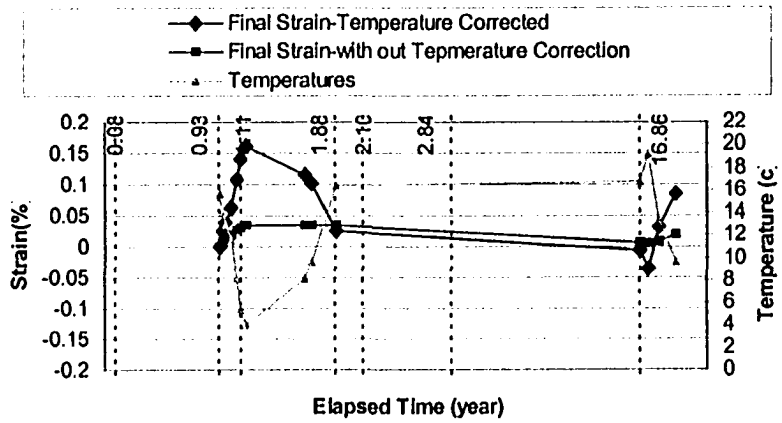

Figure 34. Dummy EWR gauge strain variation-Paragrid mid.-0.5m

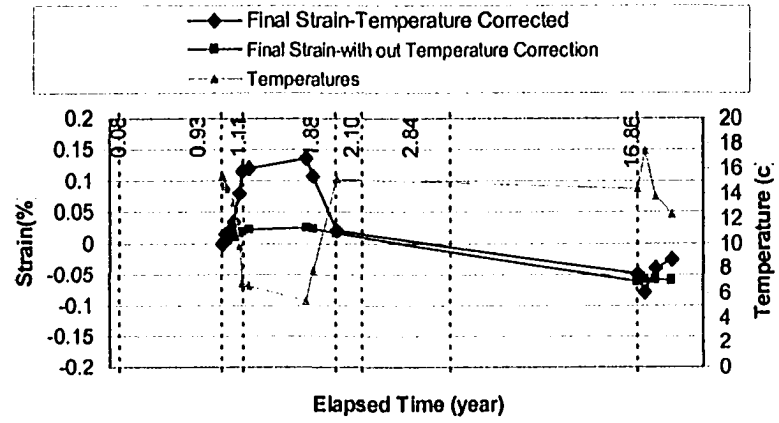

Figure 35. Dummy EWR gauge strain variation-Paragrid mid.-1m

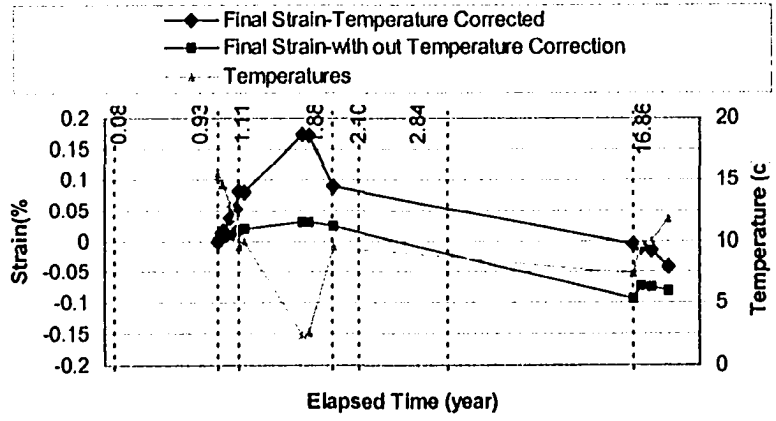

Figure 36. Dummy EWR gauge strain variation-Paragrid mid.-5m

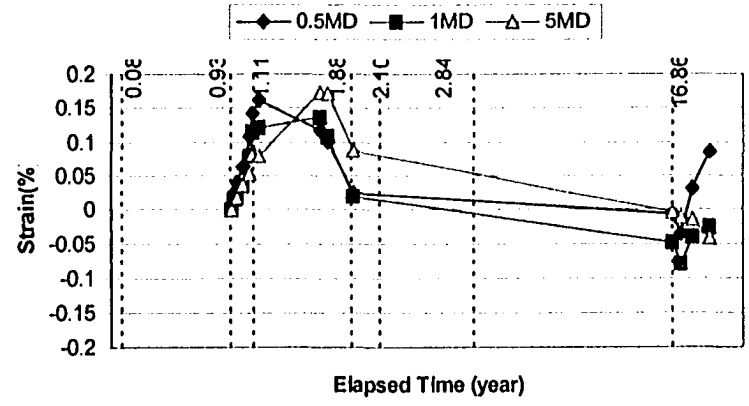

Figure 37. Dummy EWR gauge strain variation-Paragrid mid

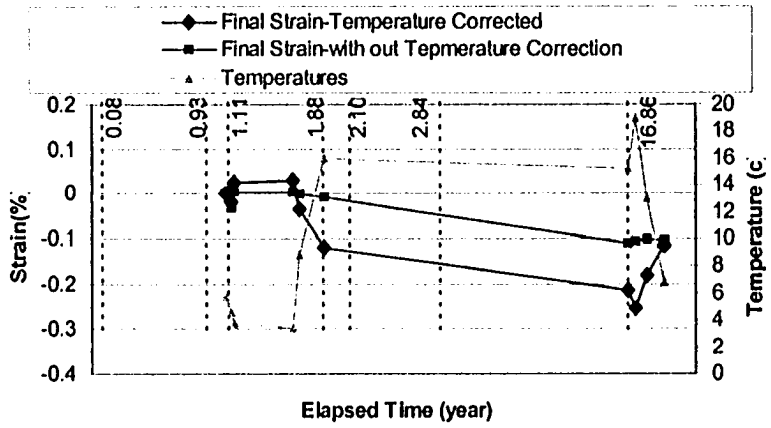

Figure 38. Dummy EWR gauge strain variation-Paragrid top-0.5m

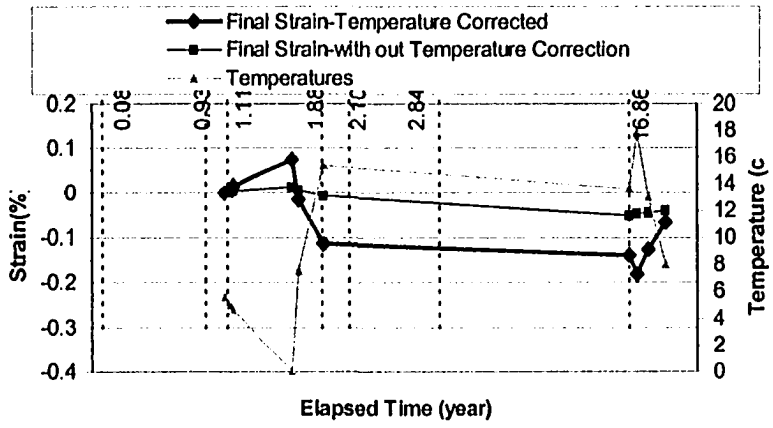

Figure 39. Dummy EWR gauge strain variation-Paragrid top-1m

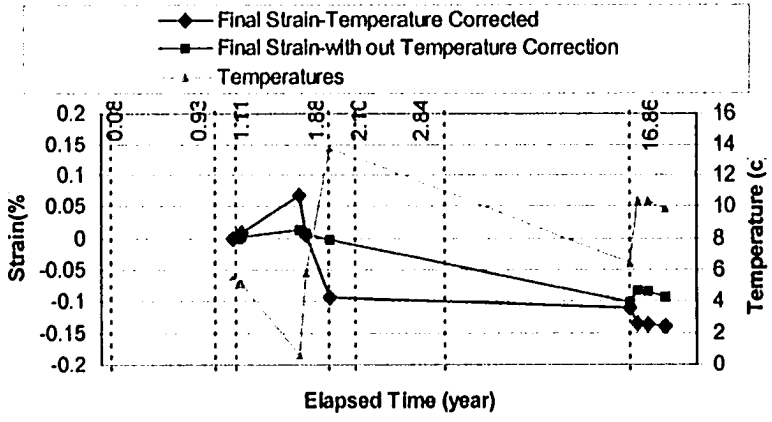

Figure 40. Dummy EWR gauge strain variation-Paragrid top-5m

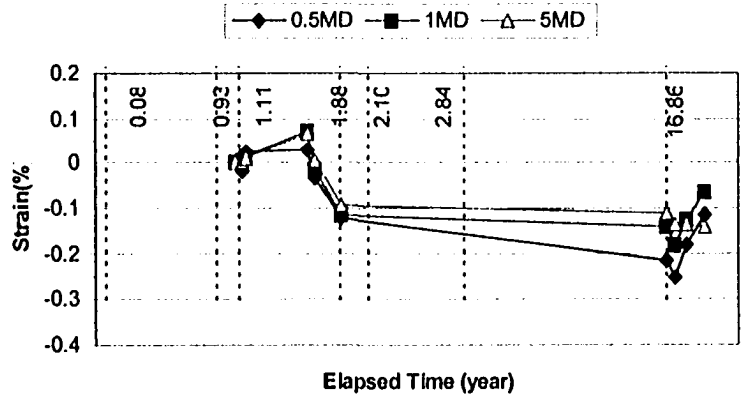

Figure 41. Dummy EWR gauge strain variation-Paragrid top

Appendix C

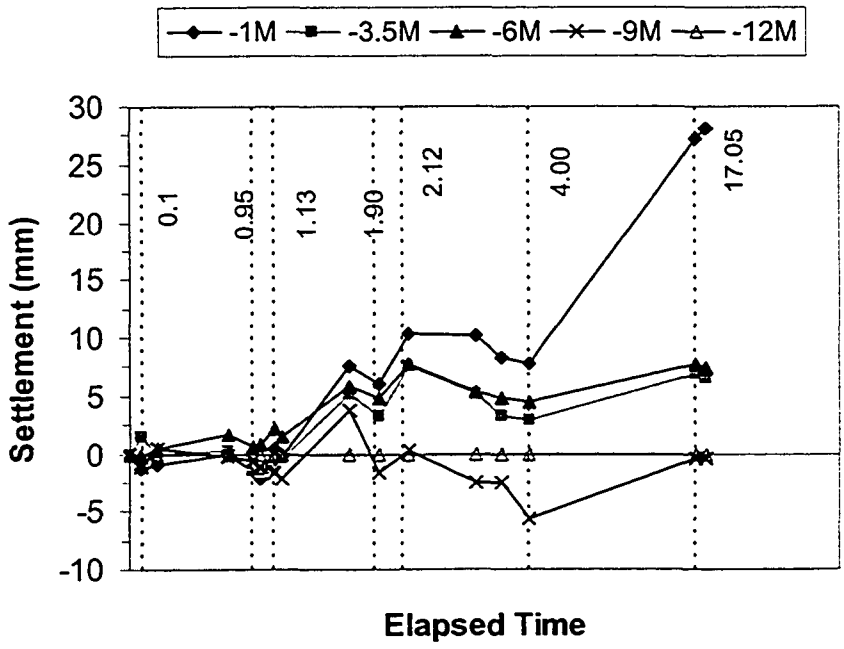

Figure 1. Settlement development with time-Tensar section at toe-before adjustment

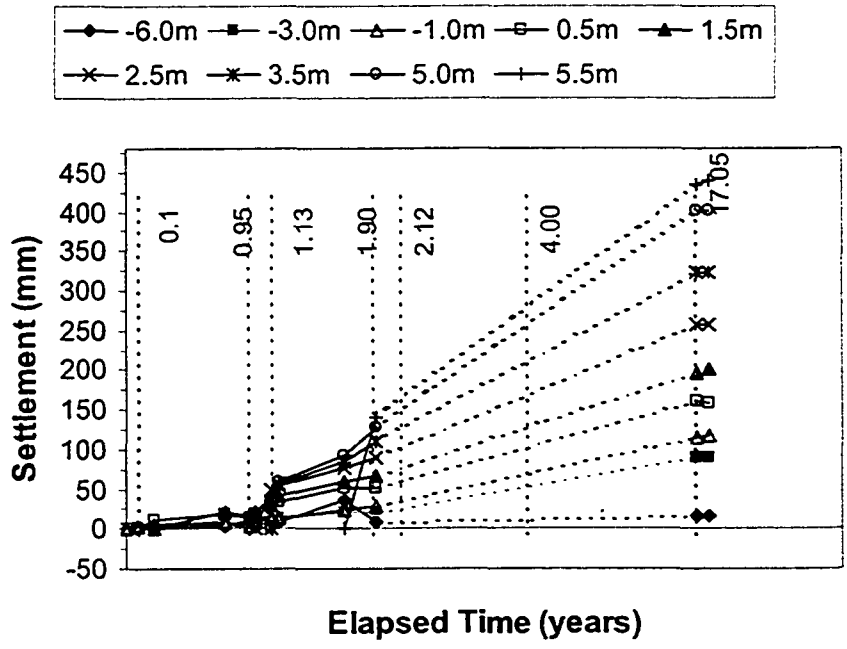

Figure 2. Settlement development with time-Tensar section at crest

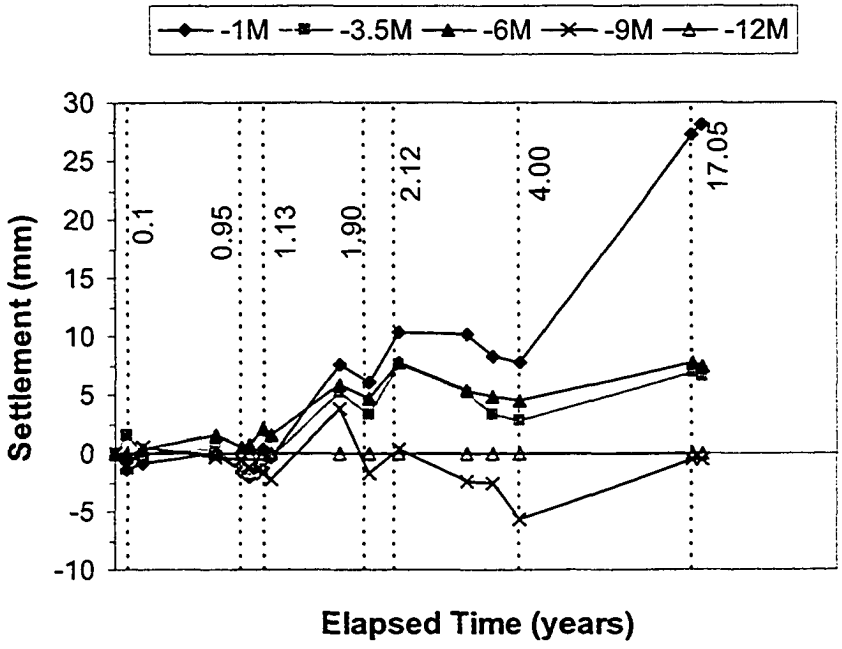

Figure 3. Settlement development with time-Signode section at toe

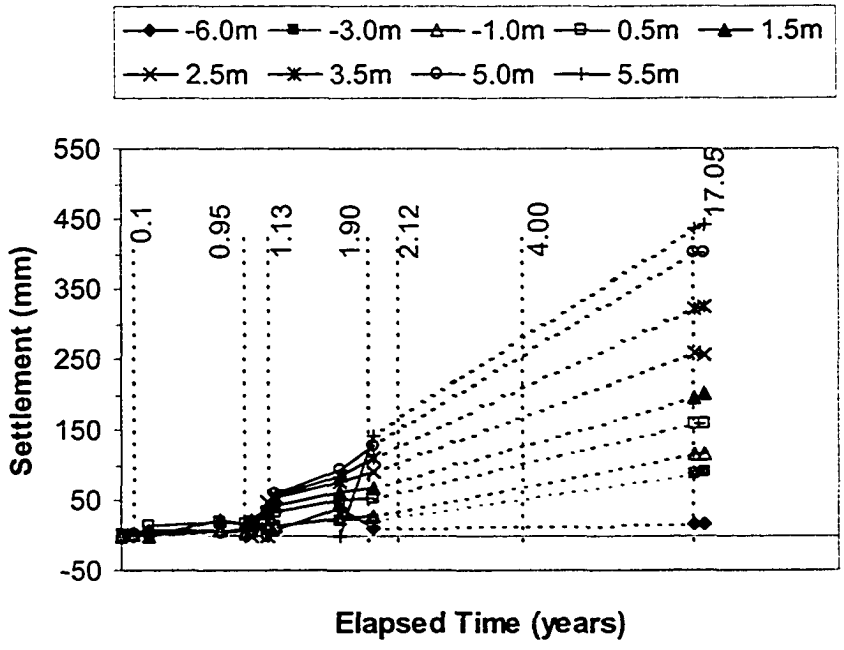

Figure 4. Settlement development with time-Signode section at crest

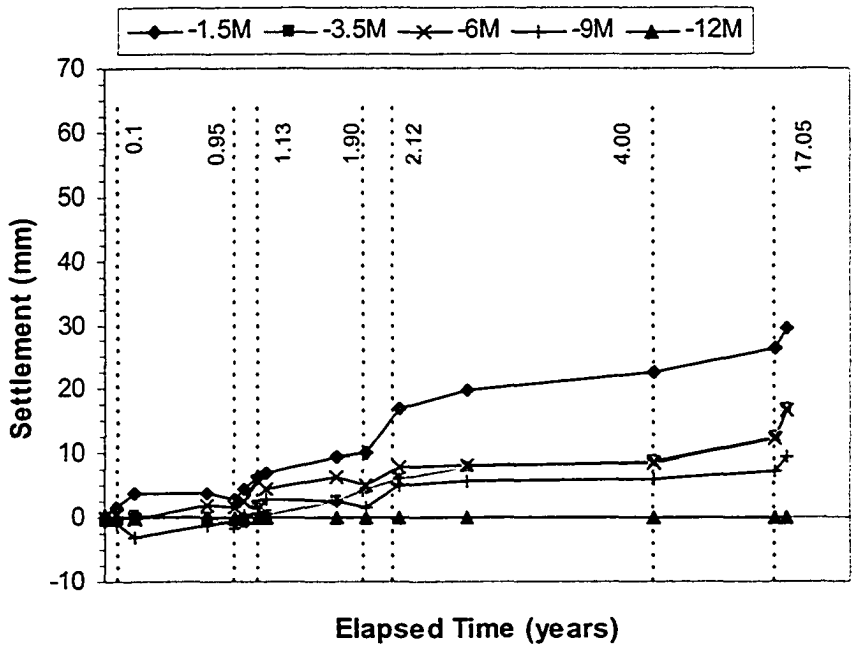

Figure 5. Settlement development with time-Paragrid section at toe

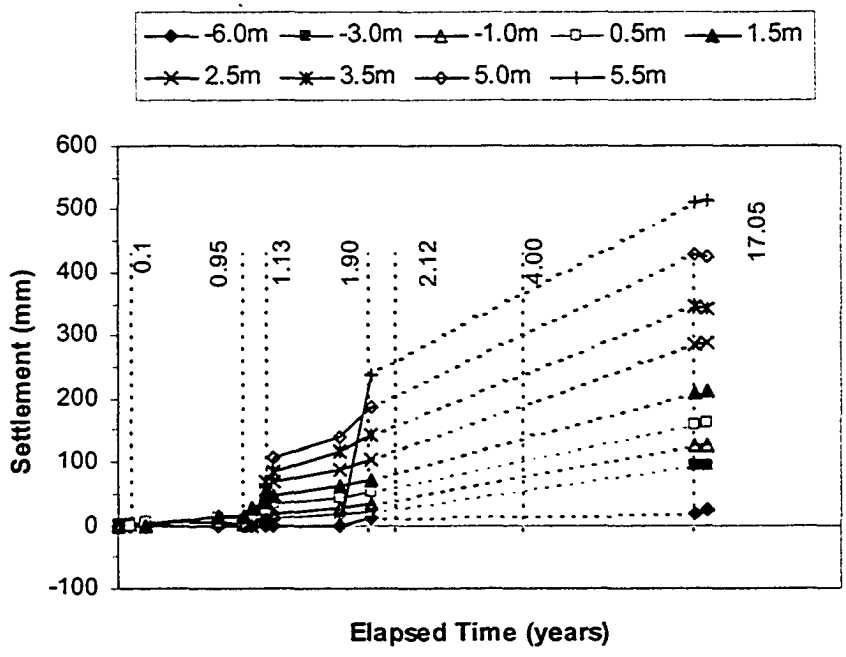

Figure 6. Settlement development with time-Paragrid section at crest

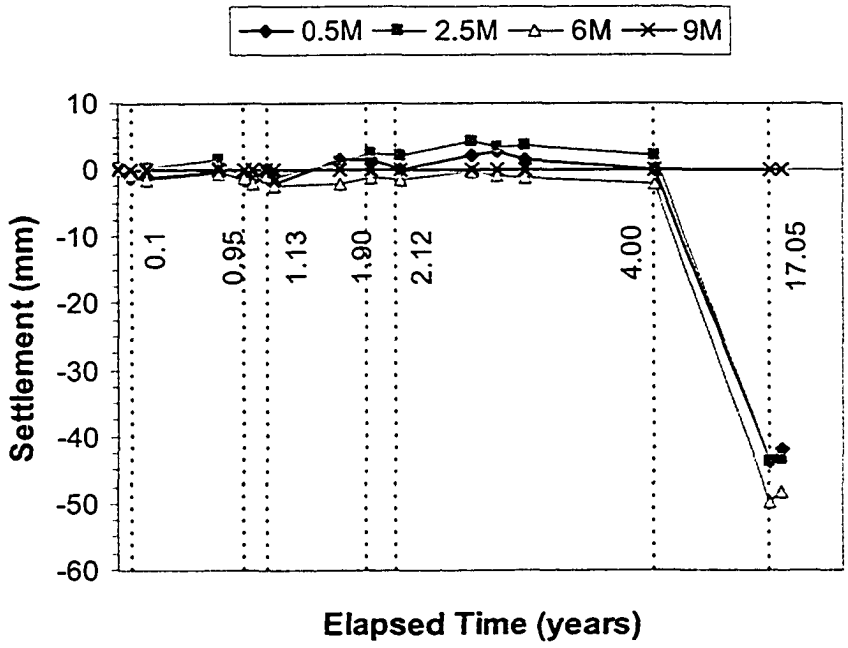

Figure 7. Settlement development with time-Unreinforced section at toe

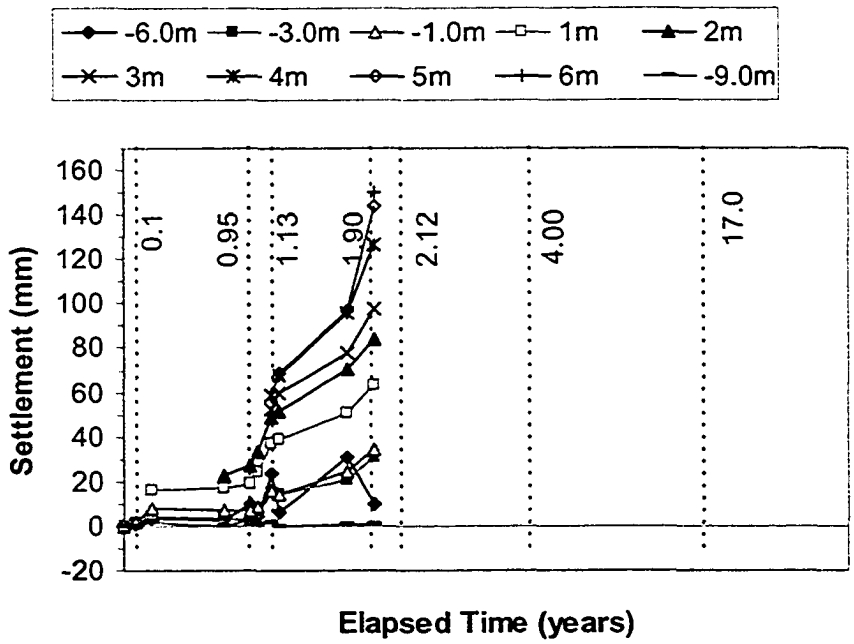

Figure 8. Settlement development with time-Unreinforced section at crest

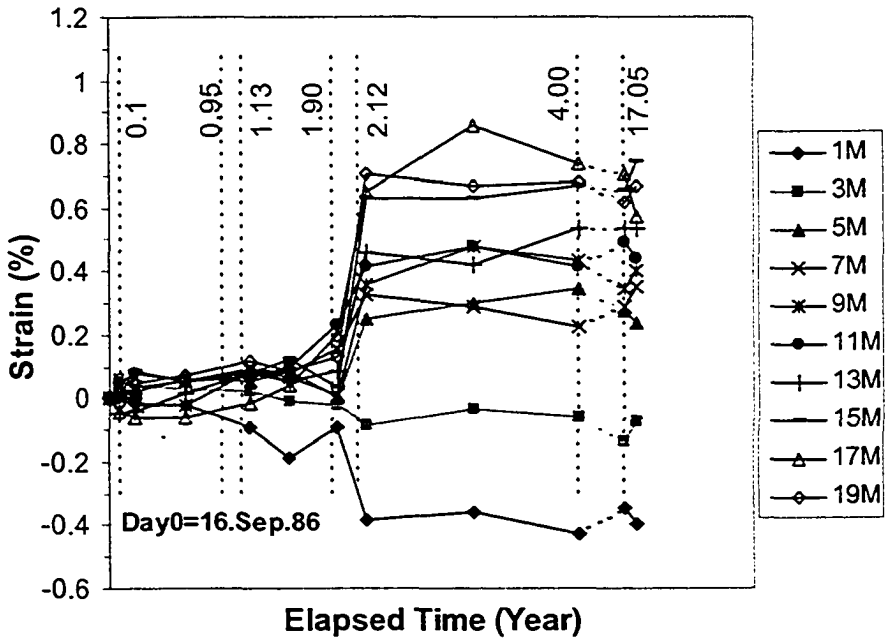

Figure 9. Horizontal soil strain development with time-Tensar section at 0 m elevation

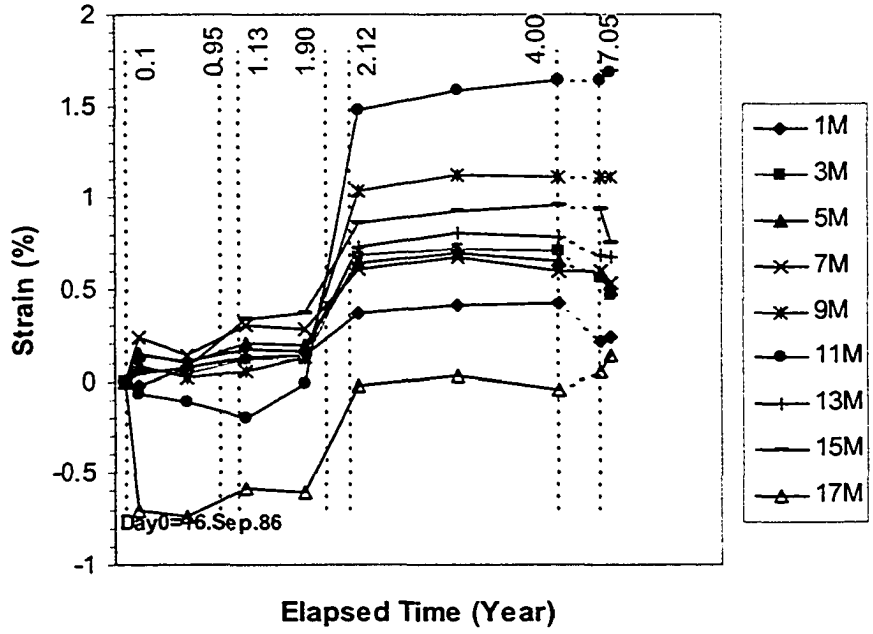

Figure 10. Horizontal soil strain development with time-Tensar section at 2 m elevation

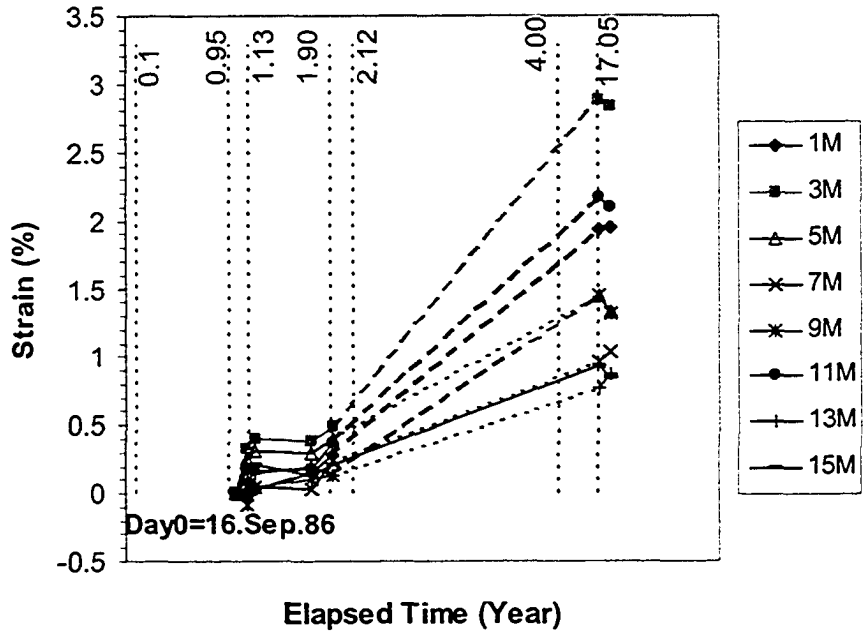

Figure 11. Horizontal soil strain development with time-Tensar section at 4 m elevation

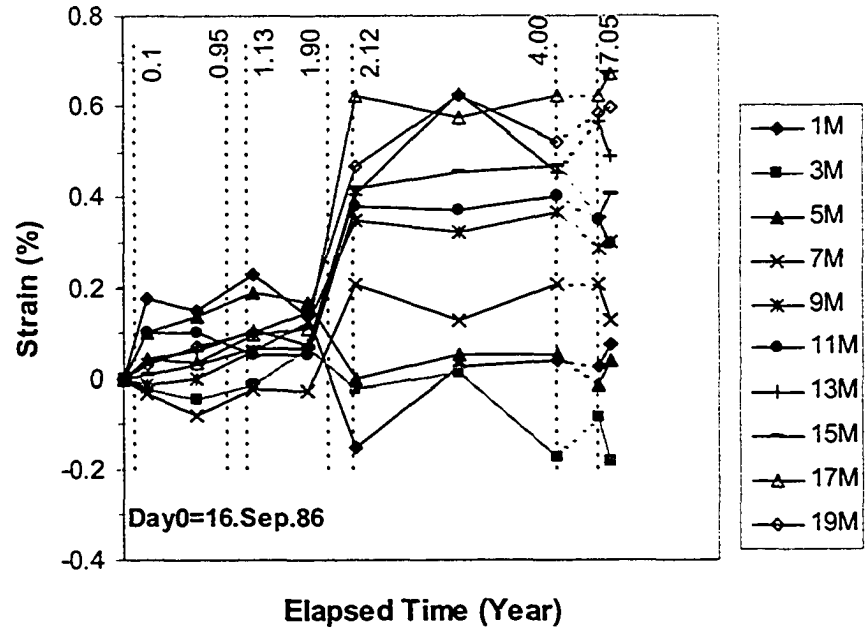

Figure 12. Horizontal soil strain development with time-Signode section at 0 m elevation

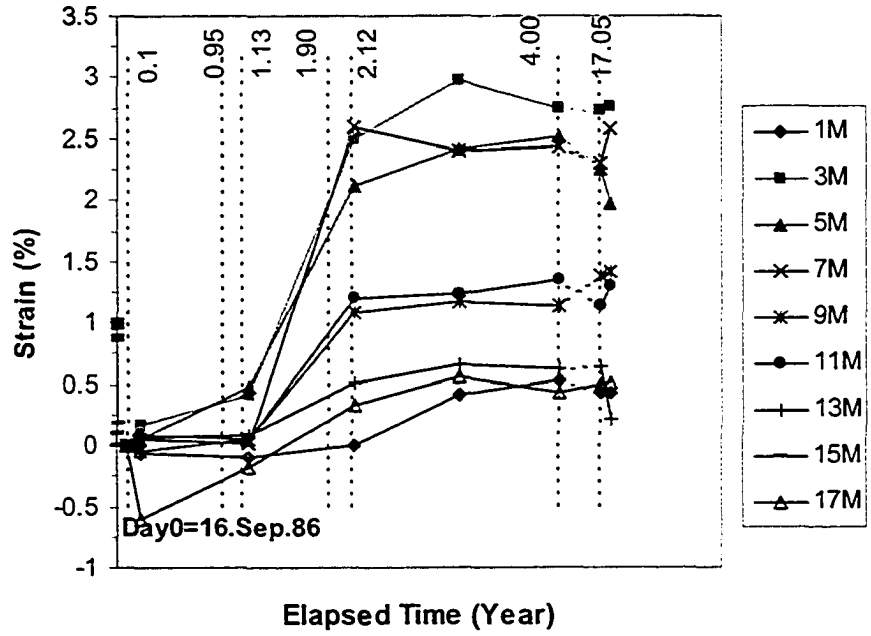

Figure 13. Horizontal soil strain development with time-Signode section at 2 m elevation

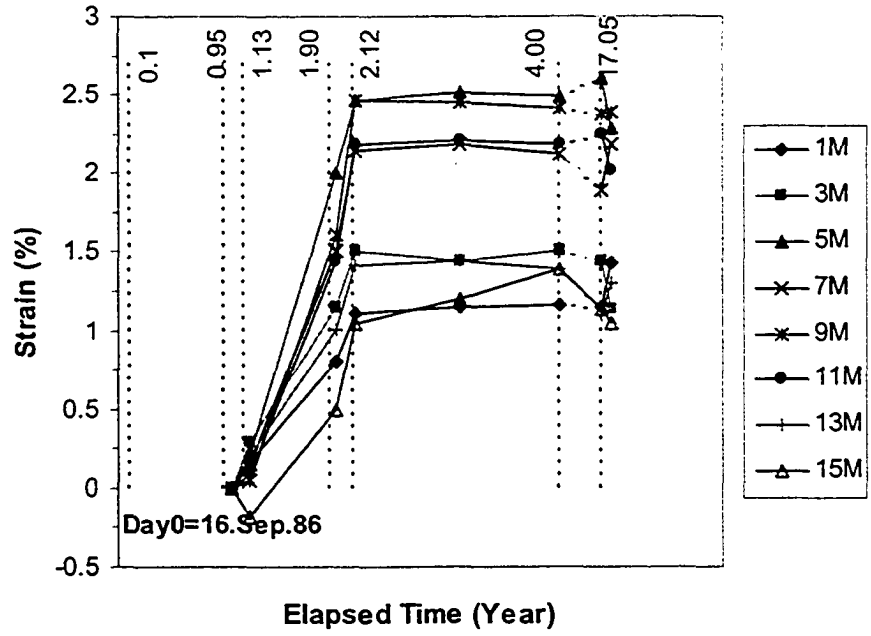

Figure 14. Horizontal soil strain development with time-Signode section at 4 m elevation

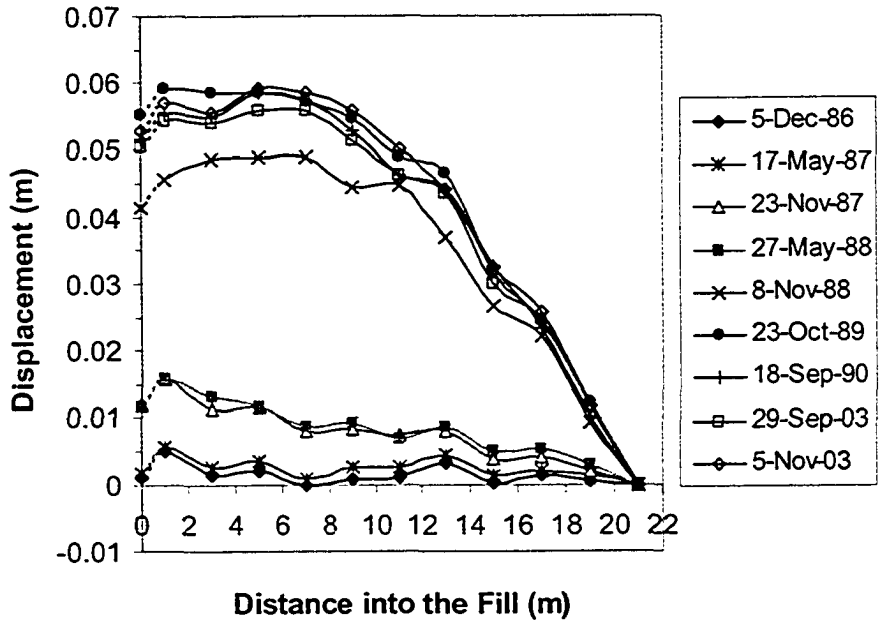

Figure 15. Horizontal displacement profile-Signode section at 0 m elevation

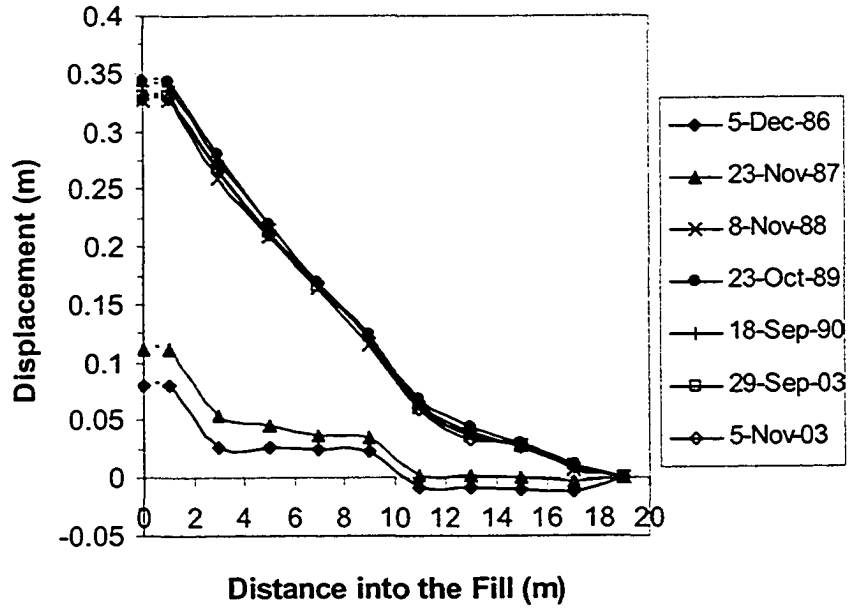

Figure 16. Horizontal displacement profile-Signode section at 2 m elevation

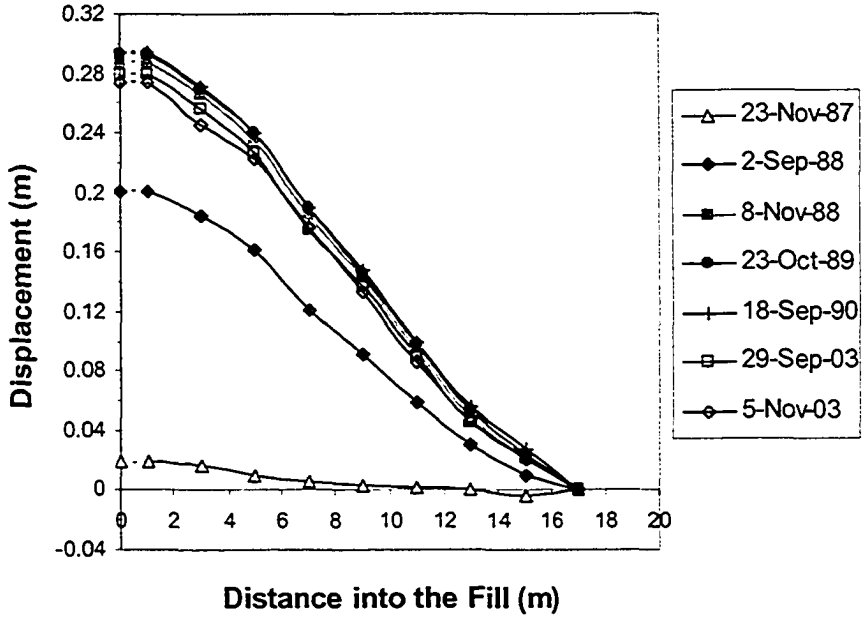

Figure 17. Horizontal displacement profile-Signode section at 4 m elevation

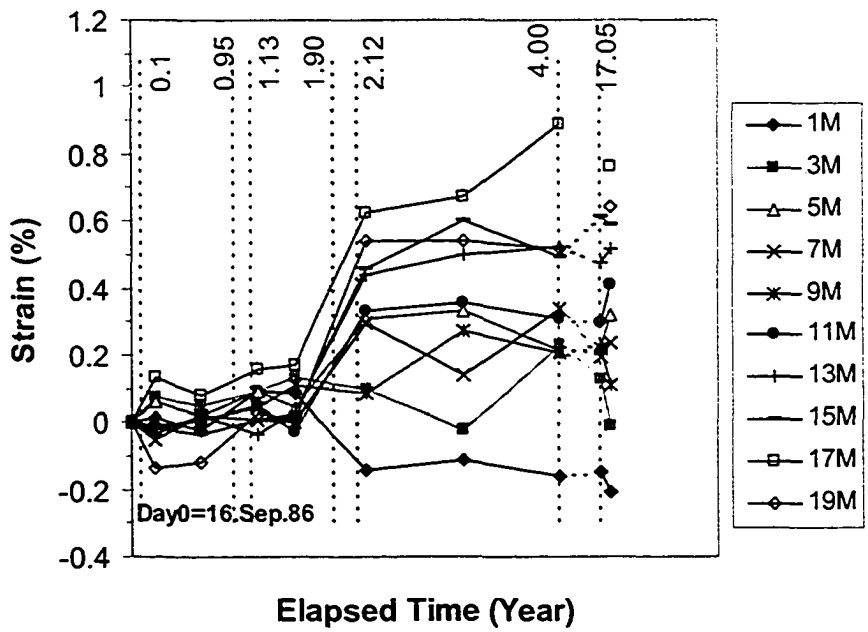

Figure 18. Horizontal soil strain development with time-Paragrid section at 0 m elevation

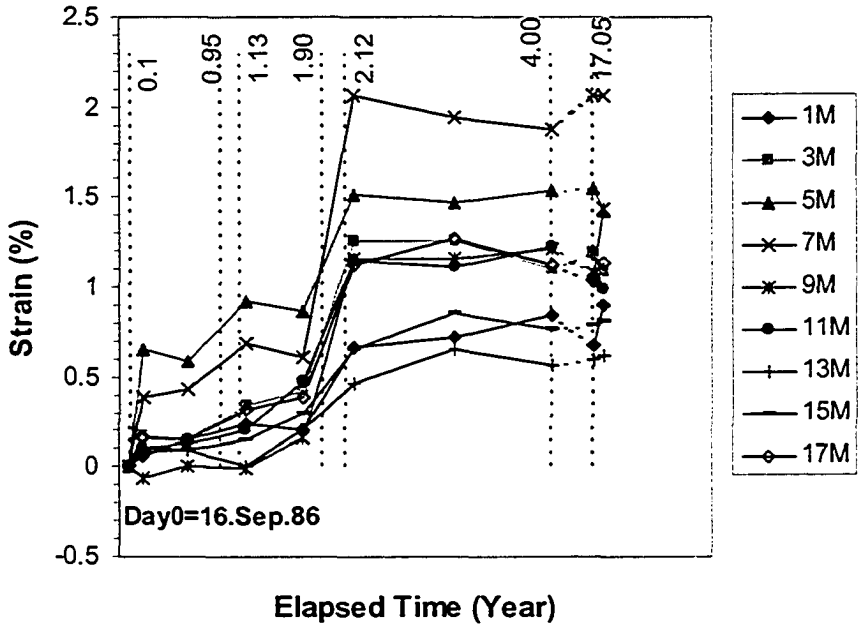

Figure 19. Horizontal soil strain development with time-Paragrid section at 2 m elevation

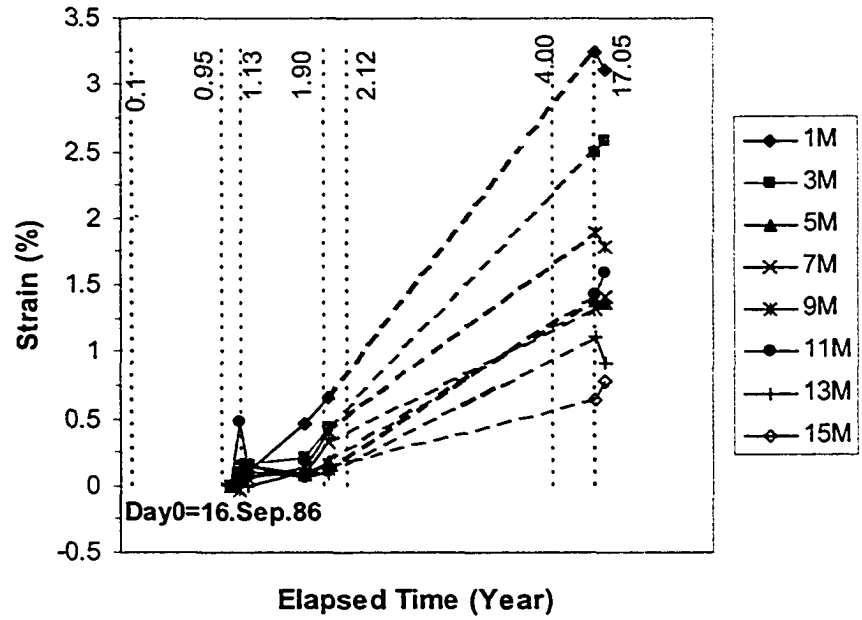

Figure 20. Horizontal soil strain development with time-Paragrid section at 4 m elevation

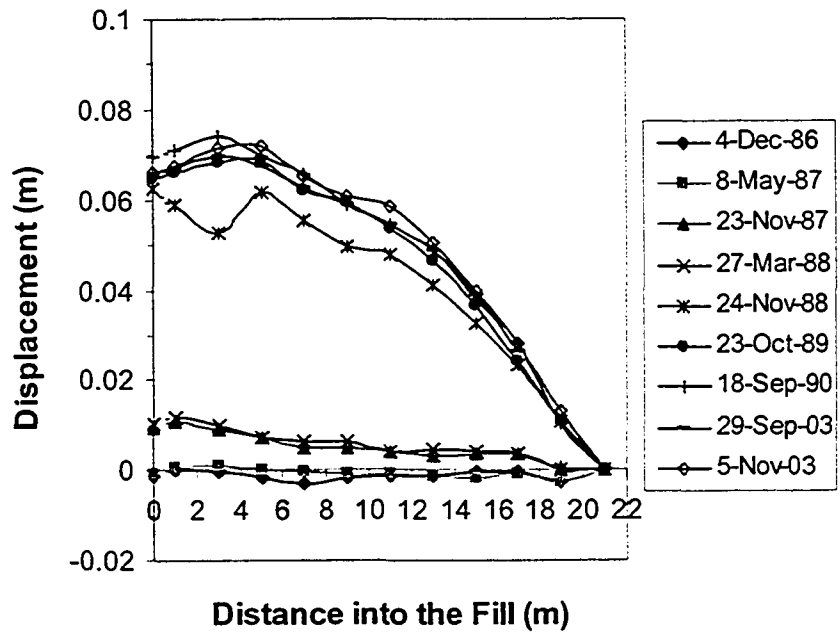

Figure 21. Horizontal displacement profile-Paragrid section at 0 m elevation

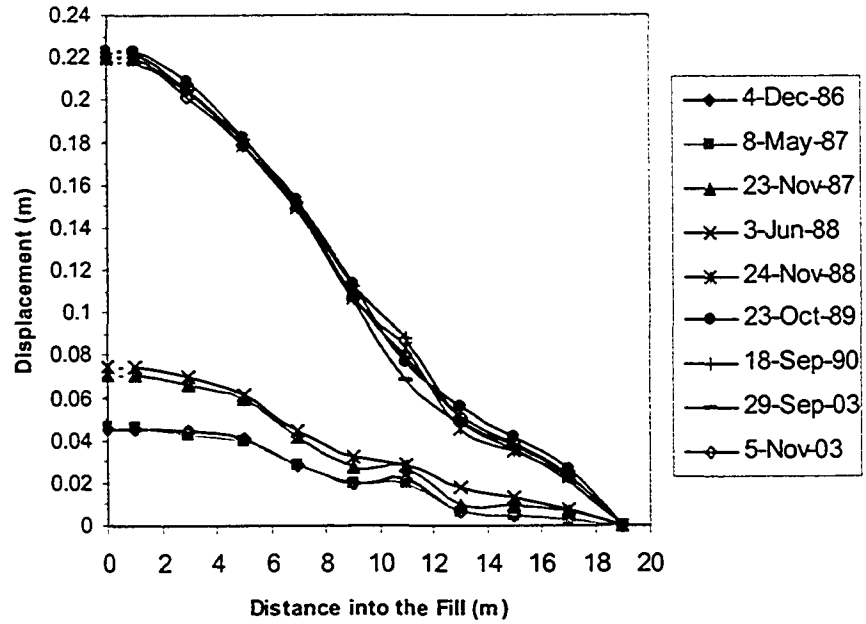

Figure 22. Horizontal displacement profile-Paragrid section at 2 m elevation

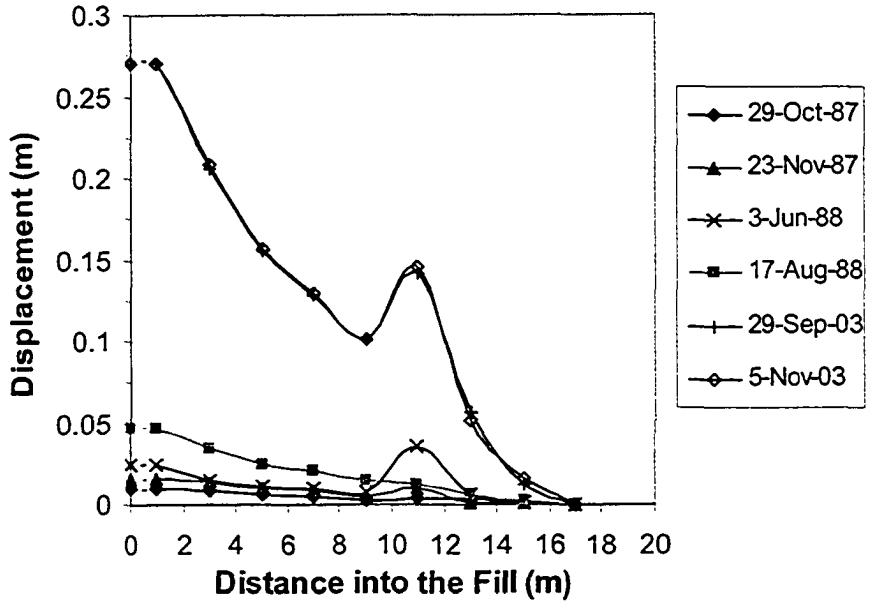

Figure 23. Horizontal displacement profile-Paragrid section at 4 m elevation

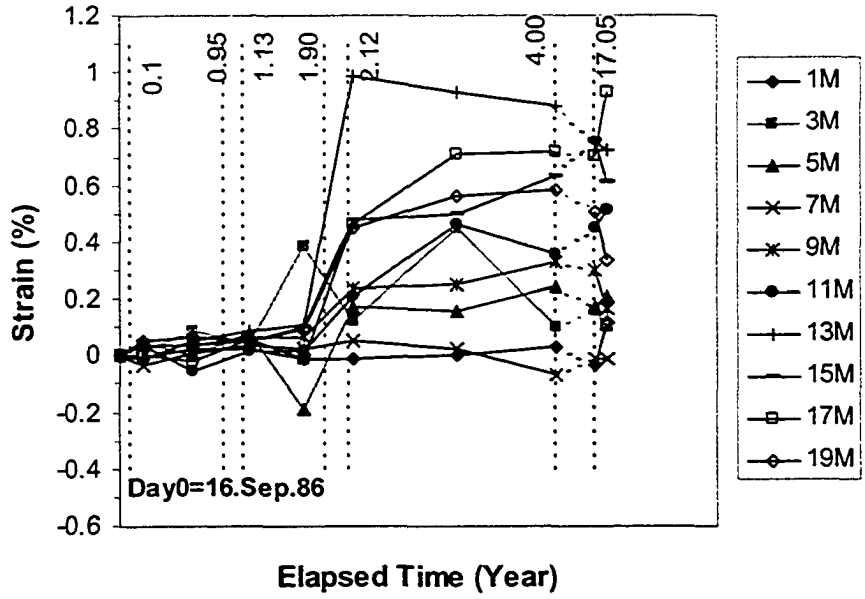

Figure 24. Horizontal soil strain development with time-Unreinforced section at 0 m elevation

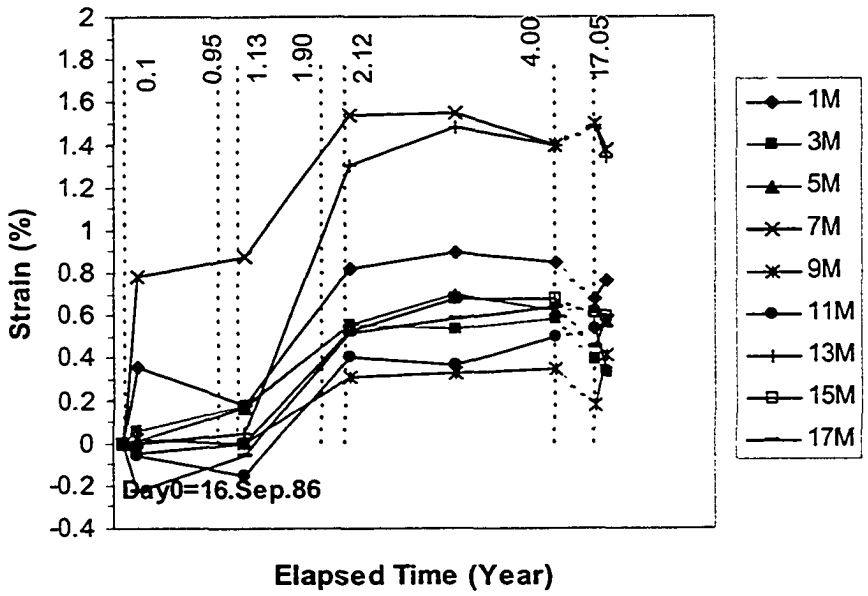

Figure 25. Horizontal soil strain development with time-Unreinforced section at 2 m elevation

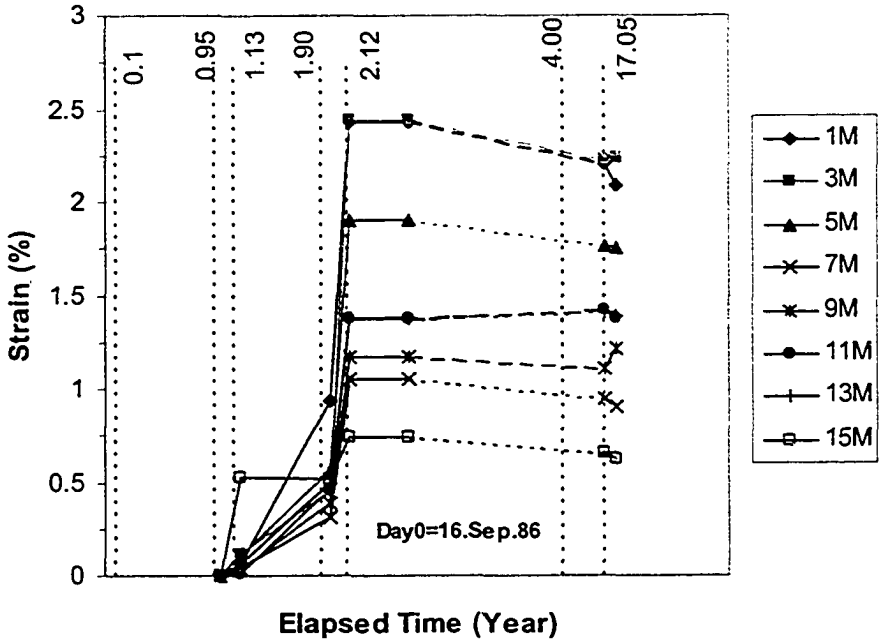

Figure 26. Horizontal soil strain development with time-Unreinforced section at 4 m elevation

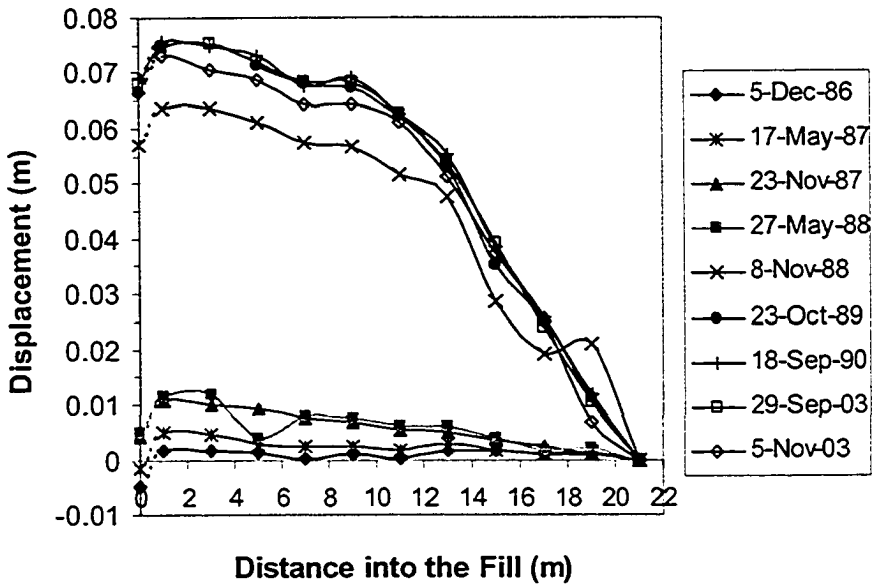

Figure 27. Horizontal displacement profile-Unreinforced section at 0 m elevation

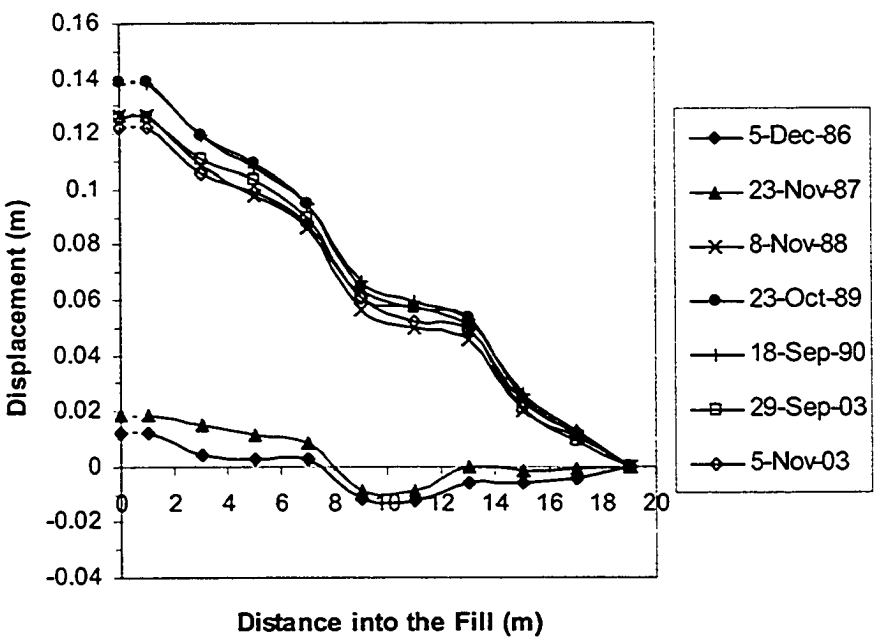

Figure 28. Horizontal displacement profile-Unreinforced section at 2 m elevation

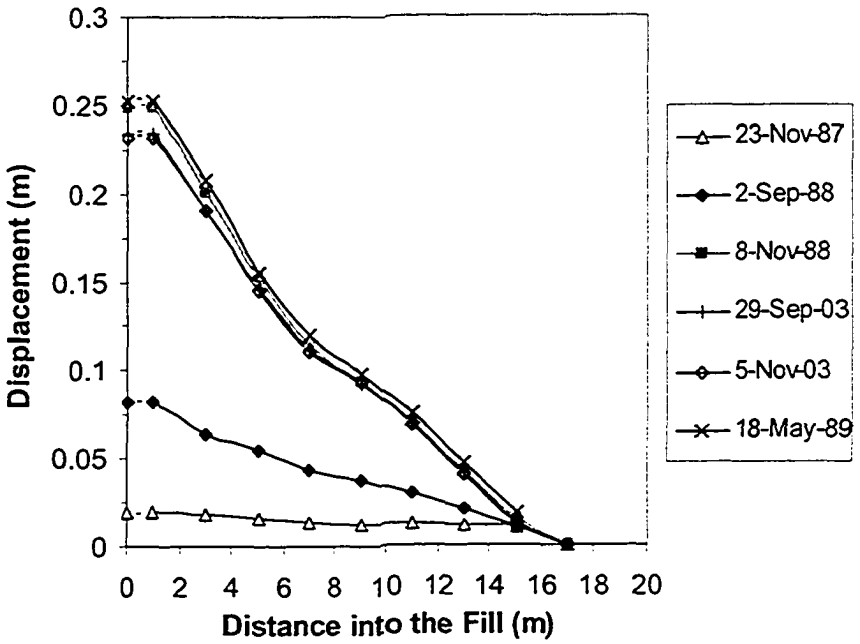

Figure 29. Horizontal displacement profile-Unreinforced section at 4 m elevation